

INFORMATION TO USERS

This was produced from a copy of a document sent to us for microfilming. While the most advanced technological means to photograph and reproduce this document have been used, the quality is heavily dependent upon the quality of the material submitted.

The following explanation of techniques is provided to help you understand markings or notations which may appear on this reproduction.

1. The sign or "target" for pages apparently lacking from the document photographed is "Missing Page(s)". If it was possible to obtain the missing page(s) or section, they are spliced into the film along with adjacent pages. This may have necessitated cutting through an image and duplicating adjacent pages to assure you of complete continuity.
2. When an image on the film is obliterated with a round black mark it is an indication that the film inspector noticed either blurred copy because of movement during exposure, or duplicate copy. Unless we meant to delete copyrighted materials that should not have been filmed, you will find a good image of the page in the adjacent frame. If copyrighted materials were deleted you will find a target note listing the pages in the adjacent frame.
3. When a map, drawing or chart, etc., is part of the material being photographed the photographer has followed a definite method in "sectioning" the material. It is customary to begin filming at the upper left hand corner of a large sheet and to continue from left to right in equal sections with small overlaps. If necessary, sectioning is continued again—beginning below the first row and continuing on until complete.
4. For any illustrations that cannot be reproduced satisfactorily by xerography, photographic prints can be purchased at additional cost and tipped into your xerographic copy. Requests can be made to our Dissertations Customer Services Department.
5. Some pages in any document may have indistinct print. In all cases we have filmed the best available copy.

University
Microfilms
International

300 N. ZEEB RD., ANN ARBOR, MI 48106

8211179

Gilkey, Robert Harding

**MOLECULAR PSYCHOPHYSICS AND MODELS OF AUDITORY SIGNAL
DETECTABILITY**

Indiana University

PH.D. 1981

**University
Microfilms
International** 300 N. Zeeb Road, Ann Arbor, MI 48106

**Molecular Psychophysics and Models of
Auditory Signal Detectability**

Robert H. Gilkey

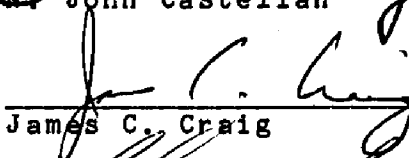
**Submitted to the Faculty of the Graduate School
in partial fulfillment of the requirements
for the degree Doctor of Philosophy
in the Department of Psychology
Indiana University
November, 1981**

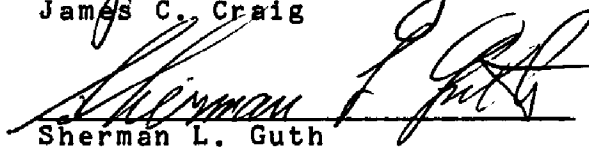
We accept the dissertation of Robert H. Gilkey in final form.

November, 1981


Donald E. Robinson, Chairman


John Castellan


James C. Craig


Sherman L. Guth


Conrad G. Mueller


Richard M. Shiffrin

This dissertation is dedicated to the memory of my father,
Harding W. Gilkey

Table of Contents

	Page
Abstract	
Acknowledgements	
Chapter 1: Introduction	1
Chapter 2: Methods	26
Chapter 3: Results	32
Chapter 4: Discussion--Models	39
Chapter 5: Summary and Conclusions	56
References	65
Appendix 1	
Appendix 2	
Vita	

Acknowledgments

It is with true appreciation that I thank the members of my committee, Donald Robinson, John Castellan, James Craig, Lee Guth, Conrad Mueller, and Richard Shiffrin, for their continued interest, support, and guidance not only during the last year, but throughout my graduate career. In particular, thanks are due to my friend and mentor Don Robinson. My relationship with him has been rewarding on all levels: "a good impedance match."

A number of other people have been instrumental in the production of this dissertation. First, for thousands of button-pushes above and beyond the call of duty, I would like to thank my subjects, Steve Gamblin, Carol Voigt, Tom Wolfe, and Julane Miller. I would also like to thank the people in the shop, Dick Martin, Don Baker, Eunice King, and Mike Bailey, who promptly and cheerfully built and maintained much of the electronic equipment. I would also like to thank Lori Sappington, Katie Kennedy, and Harriet Rairdon for help with typing, figures, and details. I would also like to thank Amanda Walley, the "ideal" proofreader. Finally, and most importantly, I would like to thank Amy Wilson, without whose many hours of help and friendship this thesis would still be a collection of unintelligible scrawl on yellow pads of paper.

Alan Frank, Tom Hanna, Tom Carrell, and Jan Weisenberger have been invaluable as both friends and colleagues. Tom Hanna, in particular, has spent countless valuable hours exchanging ideas and trying to make me understand mathematics.

My family and friends have supported me throughout my graduate career. My mother, Marion Gilkey, and Noel Fleming have provided financial support without hesitation whenever it was needed. More importantly, my mother has been an understanding voice in the most trying

times. Tom Carrell has always been "a good man to go to the well with." Jan Weisenberger has lived with me throughout many painful periods, and has always been there when I needed her. I thank her for her confidence in me, even when I had none in myself.

I would like to thank Computing Services at Indiana University-Purdue University at Indianapolis, Wrubel Computing Center at Indiana University Bloomington, and the Quantum Chemistry Program Exchange, Indiana University Bloomington, for computing assistance. This research was supported by Grants NSF-BNS-77-17-308 and PHS-S07-7031 to Dr. Robinson, and a Doctoral Research Grant-in-Aid from Indiana University.

Chapter 1

INTRODUCTION

Green (1964) distinguished between two methods of psychophysical analysis: molar and molecular. Molar psychophysics is the technique which has been most frequently applied to the study of auditory processing. Within molar psychophysics the stimulus is typically defined by its statistical properties (e.g., its average power). The performance of human subjects is also specified by its statistical properties (e.g., the average probability of a correct response). When models are fit to the data the outputs of the models are described by their distributional properties. The fit is therefore a fit of the average performance of a model to the average performance of a subject. No attempt is made to use the model to predict the trial-by-trial fluctuations in the responses of the subjects.

In contrast, within molecular psychophysics the stimulus can be specified exactly on any given trial. Similarly, the responses of subjects are considered on a trial-by-trial basis. When fitting models to the data, the output of the models are specified exactly for each stimulus. The fit is specified by comparing the output of the model to the response of the subject for each individual stimulus.

The present thesis employs data collected within a molecular experiment to evaluate a number of models of auditory detection. In this chapter, four models will be described which have been of traditional importance in psychoacoustics. Although each of these models has been investigated in some detail on the molar level, only one of them has received thorough consideration on the molecular level.

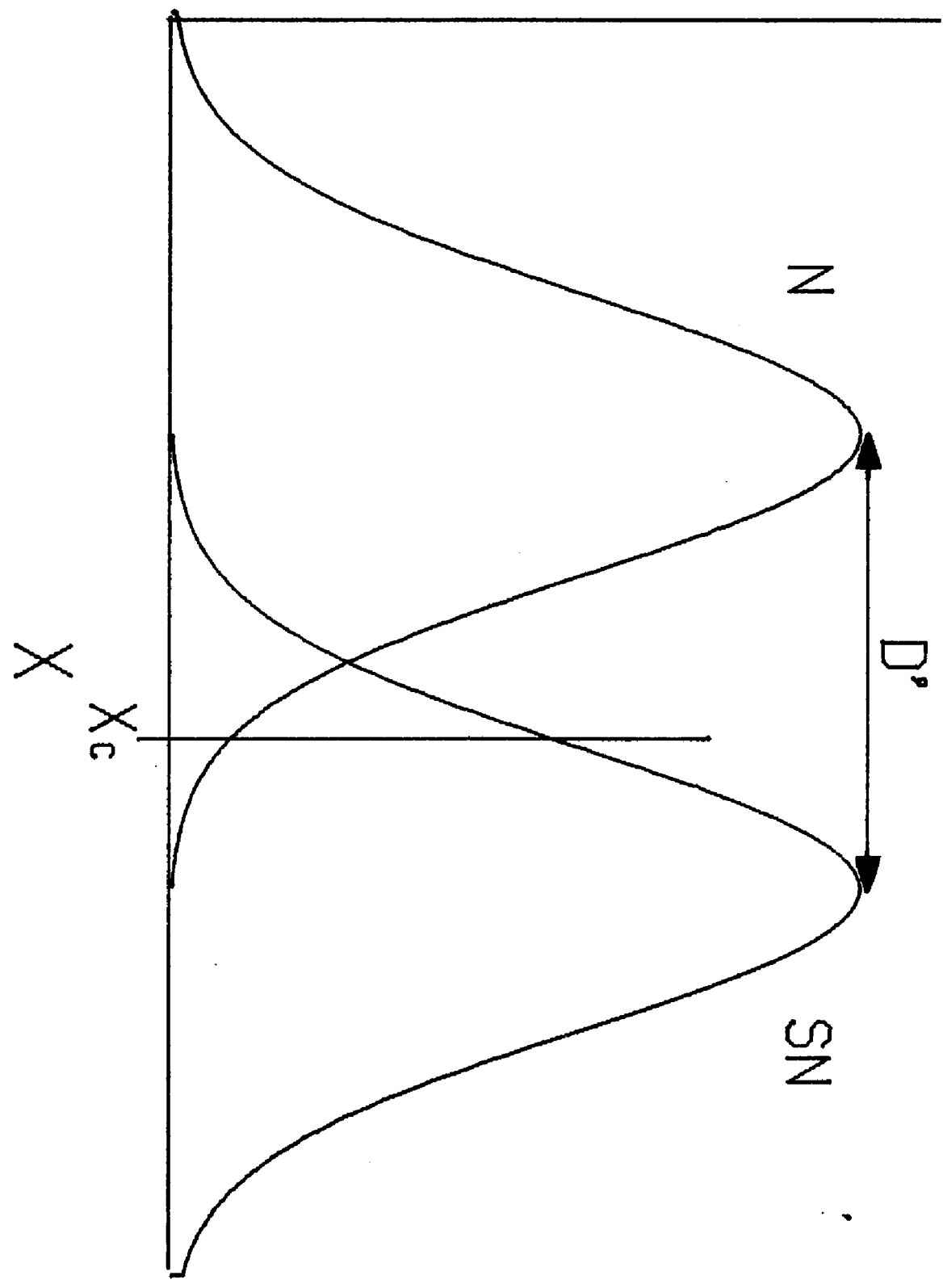
The Theory of Signal Detectability as a starting point

The Theory of Signal Detectability (TSD) is composed of two theories: a decision theory and a detection theory. The development within this thesis, as well as within most of the studies reviewed here, assumes that the decision processes used by the subject in the detection task are well summarized by the decision theory of TSD.

In outlining the Theory of Signal Detectability, Peterson, Birdsall and Fox (1954) considered the decision problem faced by an observer who must decide whether a waveform received during a particular observation interval came from a population of noise-alone waveforms or a population of signal-plus-noise waveforms. They assumed that the decision of such an observer is based on the value of some decision variable, X , which, because of the random nature of noise, fluctuates across observation intervals that contain noise-alone waveforms. Similarly, the value of X varies across observation intervals that contain signal-plus-noise waveforms. The resultant distributions of values of X are shown in Figure 1.1. The distribution labeled N shows the probability density associated with each value of X on trials during which a sample from the population of noise-alone waveforms is presented. The distribution labeled SN shows the probability density associated with each value of X on trials during which a sample from the population of signal-plus-noise waveforms is presented. The observer establishes a criterion X_c along the decision axis. On any given trial, the observer reports the presence of a signal (i.e., responds "Yes") if the observed value of the decision variable, X_j , is greater than X_c . If X_j is less than X_c , the subject reports that no signal was presented (i.e., responds "No"). The probability that the observer will report the presence of a signal during an observation interval in which a signal was presented, $P(y/SN)$, is equal to the area

Figure 1.1. Theoretical distributions of the subject's decision variable, X , for noise-alone (N) and signal-plus-noise (SN) trials.

DENSITY



under the SN curve to the right of X_c . The probability that the observer will report the presence of a signal during an observation interval in which no signal was presented, $P(y/N)$, is equal to the area under the N curve to the right of X_c . The normalized distance between the means of the N and SN distributions, dz (Note 1), has been widely used as a measure of sensitivity for both models and humans. It can readily be computed from $P(y/SN)$ and $P(y/N)$. A measure of the subject's bias, Beta, can also be calculated from the obtained hit and false-alarm rates. Beta is equal to the ratio of the ordinate of the SN distribution to the ordinate of the N distribution at X_c .

Although the development of TSD by Peterson, et al. was oriented towards radar applications, the structure of their theory proved to be more generally applicable. In 1954, Tanner and Swets applied TSD to the study of human psychophysics. Since that time, the structure of TSD has become more and more widely accepted as a good initial description of the decision processes underlying human performance in many psychophysical tasks.

Two assumptions that underlie the application of TSD to the study of human observers are of particular importance to the development here. First, TSD assumes that the human observer is always operating in a noise background. Even in an environment that is relatively free from "external" noise sources, the observer introduces "internal" noise. As a result, measurement terms such as absolute threshold or quiet threshold are misnomers and have no particular importance to the models considered here. TSD also assumes that the dimension depicted by X is continuous. There are no discontinuities or quantal jumps in perception, as would be predicted by various threshold theories. The outputs of all of the models we will consider are continuous functions of the parameters of the input stimuli.

If one accepts the decision theory of TSD as a description of the decision process of the human observer, then it remains for the psychophysicist to determine the decision variable used by the subject. That is, the psychophysicist must specify a set of transformations by which external stimuli are changed into values of X . Thus, the present thesis will attempt to specify such a set of transformations for the case in which the task of the subject is to detect a tonal signal in a noise background.

Molar psychophysics

Although the output of a model of detectability is typically assumed to be monotonic with the decision variable, X , when comparing the output of a model to the molar performance of a human observer, one cannot directly measure the decision variable of the human observer. It is therefore necessary to transform the output of the model into a measure of performance. This is accomplished by producing distributions of the output of the model for the noise-alone and signal-plus-noise cases. Once the distributions for a particular stimulus situation have been obtained, a "dz-like" measure can be computed. Further, by calculating dz as a function of signal-to-noise ratio, a psychometric function for the model is obtained. It is also possible to compute the Receiver Operating Characteristic (ROC) for a model from these distributions. Although most models do not specify the mechanism by which a particular criterion is established, it is possible to move a hypothetical criterion along the decision axis and compute the expected hit and false-alarm probabilities at each point. By plotting the hit rate as a function of the false-alarm rate, the ROC for the model is obtained.

The decision theory of TSD, which was reviewed in the previous section, has been widely applied in psychoacoustics. A detection theory, ideal detector analysis, has also been of great importance. This type of analysis allows one to describe the most effective detection strategy for an observer to adopt, given a specified amount of a priori information about the stimulus. Two of the models that will be considered here have their origin in ideal detector analysis.

If the signal is completely specified to the observer before the observation interval, that is, the parameters of signal are known exactly (SKE), the optimal strategy is to cross-correlate the known representation of the signal with the input waveform (Peterson, et al., 1954). Peterson, et al. were also able to show that the N and SN distributions on the decision axis have equal variances and are normal in form. Further, the expected d' for the Cross-Correlation observer is equal to the square root of $2E/N_0$, where E is the energy of the signal and N_0 is the spectrum level of the masking noise.

Ideal detector analysis was introduced to human psychophysics by Tanner and Birdsall (1958). Although the performance of the human observer is always much worse than that of the ideal observer, they argue that ideal detectors are useful as normative models because systematic differences between the performance of the human and the ideal suggest what information is processed by the ideal that is either not received or not processed by the human observer.

Green (1960) found that the psychometric function for the Cross-Correlator differed from that of the human in two important respects. First, the psychometric function of the ideal observer showed considerably higher sensitivity than that of the human. Second, the slope of the psychometric function was much shallower for the ideal than for

the human. Green went on to show that the psychometric function for the ideal becomes steeper and moves toward the human psychometric function if the task of the ideal is to detect a signal which may be any one of M orthogonal signals. For the case thus far considered, M has been equal to 1. The slope of the ideal detector's psychometric function for M equal to 64 corresponded well to that of the human for an M equal to 1 task. However, the absolute sensitivity of the ideal observer was still 10 dB greater than that of the human observer. One possible interpretation of this remaining discrepancy in sensitivity is that the human observer operates in the presence of some form of "internal" noise. The effective signal-to-noise ratio for the human is therefore less than the measured signal-to-noise ratio and less than the effective signal-to-noise ratio for the ideal observer.

The argument that the human observer is operating like the ideal observer, but with greater uncertainty, is compatible with another of Green's observations. If a low level sinusoid of the same frequency and starting phase as the signal (a pedestal) is added to the noise on both signal-plus-noise and noise-alone trials, the performance of the human will improve dramatically. The slope of the human psychometric function for the pedestal condition is equal to that of the ideal. Further, the absolute level of performance is only 6 dB below that of the ideal. A common interpretation of this result is that because the pedestal has the same frequency and starting phase as the signal, it reduces the human observer's uncertainty about the parameters of the signal; that is, it reduces the effective value of M . The absolute difference in performance could again be explained by assuming that because of "internal" noise, the human observer is operating at a lower effective signal-to-noise ratio.

The ROC for the SKE observer will be a straight line of unit slope when plotted in normal-normal coordinates. Egan, Schulman and Greenberg (1959) found that human ROCs were well fit by straight lines in normal-normal coordinates. However, the slope of the best-fitting line was consistently less than one. This suggests that the variance of the signal-plus-noise distribution is greater than that of the noise-alone distribution, a result that is incompatible with a correlation observer.

Peterson, et al. were also able to show that for the case where the parameters of the signal are known except for starting phase (SKEP), optimal performance could be obtained using a narrowband filter with a bandwidth equal to the reciprocal of the signal duration, followed by a linear detector (envelope detector). Marill (1956) derived the psychometric function for the Envelope Detector. He found that if it is assumed that the absolute performance of the Envelope Detector is 11 to 15 dB worse than it actually is, a good fit between the psychometric function of the human and the psychometric function of the Envelope Detector is achieved. This fit is better than that achieved between the human psychometric function and a normal ogive. Green and Swets (1974) found, as Green (1960) had for the SKE observer, that the slope of the psychometric function is less for the Envelope Detector than it is for the human observer. Again, if the observer was assumed to be detecting one of M orthogonal signals, the slope could be made as steep as that of the human observer's psychometric function. As with the SKE observer, the performance of the human observer was always lower than that for the Envelope Detector.

Jeffress (1964) noted that the Envelope Detector generates distributions for which the variance of the signal-plus-noise distribution is greater than that of the noise-alone distribution.

Further, the noise-alone distribution is a Rayleigh distribution, whereas the signal-plus-noise distribution is a Rice distribution. Using these two distributions, Jeffress was able to generate ROCs that had the desired slope on normal-normal coordinates. Further, Jeffress obtained an excellent fit to the 36-point rating scale data of Watson, Rilling, and Bourbon (1964).

The Energy Detector (i.e., a device for which the output voltage is proportional to the energy in the input waveform, after filtering) has traditionally been of importance in radio electronics. It has also been found to be the ideal detector for the case when the signal is an increment in the intensity of the noise (Peterson et al., 1954). Pfafflin and Mathews (1962) found that the psychometric functions for the Energy Detector have slopes which were quite similar to those of the human psychometric functions even when it was assumed that M was equal to 1. However, if a "critical-band-like" bandwidth (200 Hz for a 1000-Hz signal) was assumed for the initial filtering stage, the absolute performance of the Energy Detector was 5 to 10 dB better than that of the human. If the initial filter was assumed to have a much wider bandwidth (in some cases, several thousand Hz), the performance of the Energy Detector could be degraded until it matched that of the human. After considering the evidence from critical band experiments, which suggested that the initial filtering in the human auditory system was probably relatively narrow, Pfafflin and Mathews decided that a more reasonable explanation of the discrepancy was to assume that the human detector was operating in the presence of "internal" noise, which reduced the effective signal-to-noise ratio.

Pfafflin and Mathews also used the concept of "internal" noise to explain the results from pedestal experiments. As mentioned above, when a

low level pedestal is added to the noise, the performance of a human observer is improved. In addition, the slope of the human psychometric function becomes shallower and approximates that of the SKE observer. The Energy Detector predicts these changes in the psychometric function without resorting to the uncertainty hypothesis. The correlation between the pedestal and the signal will determine the effect of the pedestal on the performance of both the human and the Energy Detector. When the signal is in phase with the pedestal (i.e., positively correlated), the increment in energy caused by adding the signal will be greater than the energy in the signal. As the amplitude of the pedestal increases to infinity, the performance of the Energy Detector approaches that of the SKE observer. Although human performance does improve in the presence of a low level pedestal, when the amplitude of the pedestal becomes very large, performance, rather than approaching that of the SKE observer, declines to a level below that obtained with no pedestal. Pfafflin and Mathews point out that this result can be explained by assuming that the human observer is operating in the presence of "internal" noise which is proportional to the level of the external stimulus. Hence, as the magnitude of the pedestal is increased, the effective signal-to-noise ratio will decrease, causing the reduction in performance.

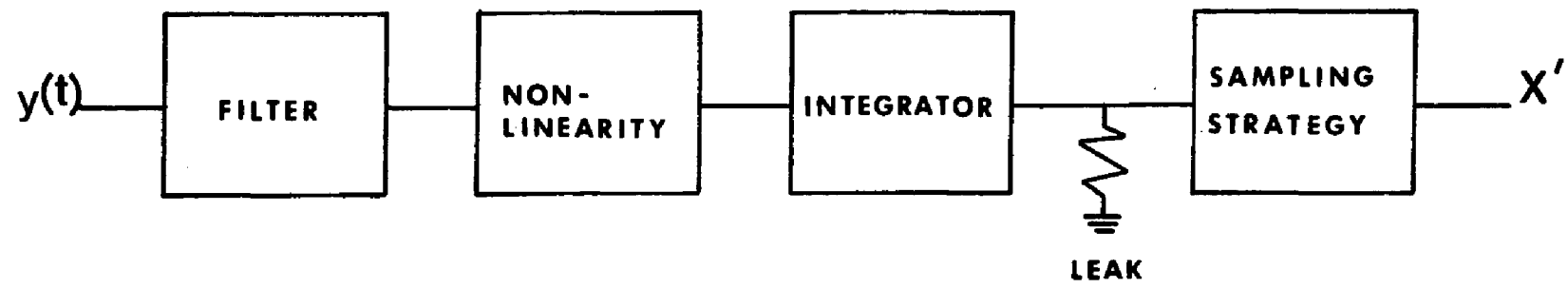
Green and Swets (1974) observed that the ROC for the Energy Detector is asymmetric, a result compatible with the human data. The outputs of the Energy Detector are distributed as chi-square on noise-alone trials and as non-central chi-square on signal-plus-noise trials. The degree of asymmetry is thus inversely related to the number of degrees of freedom, which will be equal to twice the product of the effective bandwidth of the stimulus (W) and the effective duration (T). Because the values of T and W are free parameters in the model, the exact form of the ROC is not specified for the general model.

Jeffress (1967,1968) introduced an electrical analog model of auditory processing. The model has a general structure (see Figure 1.2) that is capable of mimicking several other models. The input waveform, $y(t)$, is passed through a filter, which typically has a relatively narrow bandwidth. This stage of the model may correspond to the mechanical and neural filtering which occurs in the auditory periphery. The next stage is a non-linear transform which results in a waveform containing only positive values. This stage may represent rectification processes inherent in the hair cells and neural fibers. The next stage is an integrator, typically one with an appreciable decay ("leak"). This stage may correspond to temporal summation at some point in the auditory system. A sampling process is applied to the output of the integrator to obtain the value of the decision variable, X' .

By changing the parameters of the various stages of the model, its performance can be altered. Jeffress (1967) found that when a narrow (50-Hz) "critical-band" filter was used for the first stage of the model, followed by a halfwave rectifier and an integrator with a short decay constant (1 ms) the output of the model followed the envelope of the waveform at the output of the 50-Hz filter. By collecting several hundred independent samples of the output of the model, Jeffress was able to generate relative frequency distributions that agreed well with the distributions Peterson, et al. derived mathematically for the Envelope Detector.

Typically, the Energy Detector has been implemented as a bandpass filter followed by a square-law device (i.e., a device for which the output voltage is proportional to the square of the input voltage) and a true integrator (i.e., an integrator without a "leak"). Within Jeffress' model, the Energy Detector is achieved by employing a square-law device

Figure 1.2. The general structure of the model of Jeffress (1967).



as the nonlinear stage and using the integration stage and the sampling strategy to approximate true integration. (Two methods achieving true integration will be discussed in Chapter 4.)

Although Jeffress in his 1964 paper had found a remarkably close fit between the ROC generated by the Envelope Detector and the 36-category rating data from the human subject of Watson, et al. (1964), he later found, as he stated in his 1967 paper, that "...the ROC curve is not a sufficiently sensitive indicator to permit distinguishing definitely between the subtly different distribution shapes with which we are concerned" (Jeffress, 1967; p. 487). The subtly different distributions to which Jeffress referred ranged from the normal-normal distributions of the Cross-Correlator to the Rayleigh-Rice distributions of the Envelope Detector. In an attempt to find more sensitive indicators of the processes underlying human auditory detection, Jeffress investigated the effects of manipulating other stimulus parameters on the performance of his electrical model. Of particular concern for Jeffress was a fact that he had demonstrated empirically for the Envelope Detector configuration of his model, and that Peterson, et al. had shown mathematically for the SKEP observer: The best performance of both models occurred when the duration of the signal was equal to the reciprocal of the bandwidth of the model's filter. In sharp contrast, Green, Birdsall and Tanner (1957) found that human performance did not vary significantly over a wide range of signal durations (20 to 150 ms). Jeffress (1964), noting this fact, suggested that the human observers might adjust their bandwidth to the particular detection task. Jeffress (1967, 1968) was able to explain the duration data without resorting to the questionable hypothesis of an adjustable bandwidth. Although with a short decay constant the detectability index of the model showed a sharp peak when the duration of

the signal was equal to the reciprocal of the bandwidth of the filter, if the decay constant of the integrator was increased from 1 ms to 100 ms, the peak was flattened out and the model showed little variation over a range comparable to that shown by the human observer.

Jeffress also found that this specific configuration of the model, in addition to fitting the psychometric function, the ROC curves, and the changes in performance that are found when signal duration is varied, showed differences in performance for continuous and gated maskers that were qualitatively similar to those shown by the human observers of Tucker, Williams, and Jeffress (1968). That is, Jeffress' model predicts the improved detectability of signals in gated noise, relative to signals in continuous noise. Further, the model predicts the increased advantage for the gated noise condition when the signal duration is short.

In this section, several efforts to relate the molar performance of human subjects in auditory detection tasks to the outputs of various mathematically or electrically defined models have been discussed. In each case the outputs of the model, which are typically "voltage-like" or "power-like" quantities, are transformed into some performance variable as would be measured for a human subject in a psychophysical task. This transformation is accomplished in the following way. The expected distributions of outputs for the model is obtained either mathematically or empirically. Then, by assuming the structure of TSD, the expected hit and false-alarm rates can be obtained, and from these, the normalized distance between the means, d_z . Using these data, ROCs and psychometric functions for the model are derived.

This approach assumes that one can discriminate among a number of possible population distributions based on the experimental data. However, there are several results indicating that this may be quite

difficult: 1) The differences that exist among the population distributions which we have considered are small. 2) There is considerable variability in the experimental data which will tend to distort the distributions. That is, the analysis assumes that the subject's response reflects the distribution of the stimulus-dependent outputs of the model. If, however, the subject's response reflects not only the distribution of stimulus dependent outputs, but also "internal" noise, the shape of the combined distribution will in general be different from that of the model output, unless, for example, both the model output and the "internal" noise are normally distributed; 3) Although the psychometric function and the ROC are the tools most frequently used to discriminate among the models, neither is particularly sensitive to changes in distribution shape.

Even if these distributions could be distinguished using the tools that are available on the molar level, comparing distributions is not necessarily a good way to discriminate among models. Two different models may produce identical distributions in many situations. For example, the form of the distributions for several of the models we have discussed is dependent only on the number of degrees of freedom in the output. In general, the number of degrees of freedom is proportional to the product of the effective bandwidth of the system and the effective integration time. Hence, one cannot estimate the value of one of these parameters without assuming the value of the other (Jeffress, 1968).

One final difficulty with the molar approach is that many of the models yield only qualitative agreement with the human data, performing much better than the human, at least in some situations. Typically, the discrepancy between the model and the data is explained by assuming that the human is uncertain about the parameters of the signal or is operating

in the presence of "internal" noise. It is no doubt true that human performance is degraded by these factors, and any complete model of auditory processing will have to take uncertainty and "internal" noise into account. However, these constructs have, in the molar studies reviewed here, been added after the fact and used as free parameters. No attempt has been made to estimate their value outside of the model-fitting process.

Molecular psychophysics

The goal of "truly" molecular psychophysics, as stated by Green (1964), is to predict the responses of the subjects on a trial-by-trial basis. Sherwin, Kodman, Kovally, Prothe, and Melrose (1956) compared the trial-by-trial responses of subjects to the output of an electrical model that was quite similar to the electrical model of Jeffress (1967). It was composed of a 60-Hz single-tuned filter, followed by a square-law detector and then by an exponential integrator. The task of the subjects and the model was to detect a 1000-Hz signal presented at random intervals within a continuous noise. The signal-level was adjusted such that the human observers correctly reported the presence of the signal approximately 60 percent of the time. The threshold of the model was then adjusted to give a 60 percent hit rate at the same signal-level. The decisions of the subjects and the model for the same stimuli were recorded on a trial-by-trial basis. The highest correlations between the model and the subjects were achieved when the duration of the signal was 300 ms and the time constant of the integrator was 150 ms. However, for this case, even though the hit rates of the subject and the model were matched, the false-alarm rate of the model was twice that of the human. Further, the few false-alarms reported by the human subject were not well correlated with those reported by the model.

Although Watson (1962) did not try to predict the trial-by-trial responses of his subjects, he did perform a fine-grain analysis of the relationship between stimulus and response. He tape-recorded individual noise-alone and signal-plus-noise stimuli as they were presented to subjects during a single-interval task. He then passed the stimuli through a 100-Hz bandwidth filter and recorded the number of peaks in the filtered waveform that exceeded each of 11 predetermined voltage thresholds. The stimuli were then grouped for a given subject according to the four-category rating response they had received when presented to that subject. The average number of peaks which exceeded each of the 11 thresholds was computed for each group. Watson found that these average peak counts increased in an orderly fashion as a function of the confidence the subject had that the signal was present.

Williams and Jeffress (1967) used a model similar to that of Jeffress (1967) to predict the responses of three human observers on individual two-alternative forced-choice (2AFC) trials. The model was able to predict the responses of a subject better than the responses of each subject were able to predict the responses of the other subjects. The model was also a better predictor of the responses of the subjects than was the presence or absence of the signal. On trials where the three subjects made the same response, the model made the correct prediction 81 percent of the time.

Although Watson and Williams and Jeffress no doubt realized the importance of nonstimulus variables in predicting the psychophysical response, they did not specifically include them in their models. Sherwin, et al. assumed Gaussian variability on their model's threshold, in an attempt to explain some of the differences between the prediction of their fixed-threshold model and the human responses. However, no

attempt was made to predict where the threshold would be on any particular trial.

Green (1964) argued that there are two components to any psychophysical response. One component is determined by the stimulus, and the other is independent of the stimulus. In order to be successful in predicting the trial-by-trial responses of the subject, the molecular psychophysicist must understand the influences of both of these factors. The experiments Green presented were directed toward understanding the stimulus-independent aspects of the subject's response. In order to control the influences of the stimulus, several sequences of 2AFC trials were tape-recorded. Each tape-recorded sequence of trials was then presented to the same subjects several times. Responses were recorded on a trial-by-trial basis. This procedure allowed Green to measure the consistency of responses across trials that contained identical stimuli. Green hoped to find evidence for response biases that could be used to augment the predictions of stimulus-oriented models. Although he found evidence for such biases, the magnitude of these effects was small. He concluded that the largest share of the stimulus-independent component of the response continued to elude prediction. Green also estimated the magnitude of the contribution of the stimulus-dependent component (the "external" noise) relative to the contribution of the stimulus-independent component ("internal" noise), and found them to be about equal. Noting these facts, Green concluded that the future of a "truly" molecular psychophysics was in doubt. Other evidence (Swets, Shipley, McKee, and Green, 1959; Watson, 1962) also indicates that the contribution of the "internal" noise is surprisingly large. Indeed, the data from Gilkey, Hanna, and Robinson (1981) indicate that in many situations the contribution of stimulus-independent factors may exceed

the contribution of stimulus-dependent factors by as much as two to one. As a remedy, Green suggested the possibility of a quasi-molecular approach, in which by presenting the same stimulus on several trials one could measure the average response of the subject to that stimulus, and thereby minimize the effects of nonstimulus variables. It might then be possible to use the parameters of the stimulus to predict this average response.

The current study will use an approach that would be considered by Green as a quasi-molecular approach. The first study to use such an approach was that of Pfafflin and Mathews (1966). They investigated the detectability of a 312.5-Hz sinusoidal signal that was masked by each of 12 bursts of computer-generated noise. The stimuli were presented in pairs to form 2AFC trials. Each stimulus pair was presented 72 or more times and the average probability of choosing the first interval for each pair was recorded. For each stimulus, they computed the energy passed by a 100-Hz wide rectangular filter centered at the signal frequency and found that the probability of choosing the first interval was related to the difference in energy between the two intervals. However, this quantity did not explain all of the variance in their data.

An examination of responses to pairs which did not contain a signal in either interval and to pairs which contained the identical stimulus in both intervals revealed "biases" which were independent of the energy difference between the intervals. The relationship between the energy difference and performance was weak on non-signal trials. For several pairs, the interval with the least energy was more often chosen as containing the signal. Although this result indicated that stimulus factors other than the energy difference between the intervals were controlling the responses of subjects, Pfafflin and Mathews were unable

to determine what these other factors might be. For the pairs that contained the same stimuli in both intervals, biases were found to be sample-dependent. It appeared that subjects had biases toward different intervals in the case where both intervals would have been identified as noise-alone and in the case where both intervals would have been identified as signal-plus-noise.

Ahumada (1967) also used the quasi-molecular approach in an attempt to estimate the critical bandwidth of his subjects. He tape-recorded a series of 33 signal-plus-noise and 27 noise-alone single-interval trials. Bursts of thermal noise, 100 ms in duration and bandpass-filtered from 250 to 750 Hz, were used as maskers. The signal was a 100-ms pulse of a 500-Hz sinusoid. The taped sequence of trials was presented to the subjects five times. The number of positive responses was summed for each stimulus across the five presentations of the tape. The stimuli were sampled from the tape-recording into a digital computer for subsequent analysis. The energy in each stimulus was computed at the output of a single-tuned digital filter centered at 500 Hz. This quantity was computed for several filter bandwidths. Ahumada found that the performance of his subjects on signal-plus-noise trials was best correlated with the outputs of this simple Energy Detector when the bandwidth of the filter was 10 to 20 Hz. However, on noise-alone trials, considerably wider filters (100 to 200-Hz) were found to correlate best with subject performance. He explained this discrepancy by assuming that the subject monitors a 100 to 200-Hz wide bank of narrow (10 to 20-Hz) filters and that the value of the maximum filter output within the bank is used as a decision variable. On signal-plus-noise trials, the filter centered at 500 Hz would be the one most frequently selected, leading to relatively good correlations between the output of this filter and

performance on signal-plus-noise trials. However, on noise-alone trials, the selected filter would vary randomly from stimulus to stimulus, leading to a relatively poor correlation between the output of the filter centered at 500 Hz and performance, and also leading to an estimate of the critical bandwidth that corresponded more nearly to the width of the filter bank than to the width of an individual filter. Ahumada did not attempt to fit this model to his data, but merely offered it as a possible explanation of the results he had found.

The possibility that the auditory system performs a more broad-band analysis of the input waveform when attempting to detect a signal in noise was investigated by Ahumada and Lovell (1971). The results of two experiments were reported. In the first experiment, 25 signal-plus-noise and 25 noise-alone stimuli were investigated. The 100-ms noise waveforms were generated by a computer program and consisted of 32 sinusoidal components spaced at 10-Hz intervals over the range from 350 to 660 Hz. The signal was a 100-ms sample of a 500-Hz sinusoid. The 50 stimuli were converted to analog form and recorded on audio-tape in eight random sequences for later presentation to ten subjects. Each of the sequences was presented to the subjects four times, for a total of 32 responses per stimulus per subject. The four-category rating responses of the subjects were summed across the 32 presentations. The second experiment was essentially identical to the first, except that 200 stimuli were presented to seven subjects, 16 times each.

A Fourier spectrum was computed from the digital representation of each stimulus. A multiple regression was then performed, using the power in adjacent 50-Hz (30-Hz for Experiment 2) bands as predictor variables and the summed rating responses as the variable to be predicted. The functions that related the obtained weighting coefficients to component

frequency were found to be quite variable across subjects. Ahumada and Lovell described some of these weighting functions as peaked, some as flat, and others as showing a high-pass characteristic. Several of their functions showed negative weightings at frequencies other than the signal frequency, but others did not. Significantly, Ahumada and Lovell were able to reduce the number of predictor variables in the second experiment from nine to three with only a small decrease in predicted variance. They accomplished this by defining three weighting contours which they claimed corresponded to the auditory "features" of "pitch," "loudness," and "tone presence." Many of the seemingly random differences in weighting functions across subjects were explained by assuming that the subjects applied different weights only to these three features.

As Ahumada (1967) had found, there were differences between signal-plus-noise and noise-alone trials. The weighting functions obtained for signal-plus-noise and noise-alone trials were not identical. A filter-bank model like that proposed in Ahumada's earlier paper was used in an attempt to predict this difference. However, the results indicated that wide filters and wide banks predicted best on noise-alone trials, whereas narrow filters and narrow banks predicted best on signal-plus-noise trials.

The multiple regression approach was extended by Ahumada, Marken, and Sandusky (1975). In their analysis, they allowed for the possibility that the subject might differentially weight the stimulus in the time domain as well as in the frequency domain. A computer was used to generate 400 samples of noise. The noise samples were 500 ms in duration. A 500-Hz signal, 100 ms in duration and temporally centered with respect to the noise, was added to 200 of the noise bursts. The stimuli were then converted to analog form, bandpass-filtered from 20 to 4000 Hz, and

tape-recorded in eight random sequences for later presentation to subjects. Each sequence was presented to the subjects once, and their four-category rating responses were summed across the eight presentations of each stimulus. Fourier analyses were computed for successive nonoverlapping 100-ms intervals of each waveforms. The power in the Fourier components computed from each of these intervals was then summed across adjacent 50-Hz bands over the range from 425 to 625 Hz, yielding a total of 25 spectral-temporal components. These 25 components were then used as predictor variables in a multiple regression analysis similar to that used by Ahumada and Lovell (1971). The resulting weighting contours appeared to be more consistent than those of Ahumada and Lovell. All subjects showed maximum weighting at the 500-Hz component during the signal interval. In addition, most subjects showed negative weightings before the signal interval at the 500-Hz component, and also showed negative weightings at the 450-Hz component during the signal interval. Ahumada, et al. (1975) explained these negative weightings by assuming that the decision of the subject was based on a comparison of the on-frequency energy during the signal interval to both the on-frequency energy before the signal interval and the off-frequency energy during the signal interval.

In addition to the multiple regression analysis, Ahumada, et al. compared the output of a single-channel Energy Detector like that used by Ahumada (1967) to the responses of subjects. The output of a 40-Hz-wide single-tuned filter corresponded most closely to the performance of subjects across all trials. When signal-plus-noise and noise-alone trials were considered separately, a 20-Hz bandwidth was most appropriate on signal-plus-noise trials, whereas a 40-Hz bandwidth was most appropriate on noise-alone trials. Although three values of integration time were

considered, they were found to have only a negligible influence on the predictive value of the model. Although slight differences were found between signal-plus-noise and noise-alone trials, these results are encouraging in light of the results of Ahumada (1967), who found large differences in bandwidth estimates between noise-alone and signal-plus-noise trials. In addition, weighting contours derived separately for noise-alone and signal-plus-noise trials appeared to be more similar than those reported by Ahumada and Lovell (1971). However, while negative weightings were found for some components on signal-plus-noise trials, no significant negative weightings were found for any component on noise-alone trials.

All of these quasi-molecular studies have assumed that an Energy Detector, or a weighted combination of Energy Detectors, is an appropriate model of the human auditory system. Although Ahumada has, in some cases, been able to explain as much as 90% of the variability in the data of some of his subjects with a weighted combination of Energy Detector outputs, in other cases he has only been able to explain 8% of the variance. An examination of the relationship between the percentage of correct responses, $P(C)$, and the proportion of variance accounted for in the data presented by Ahumada and Lovell (1971) and by Ahumada et al. (1975) reveals that these two statistics are strongly correlated. Although this may only mean that subjects who perform well are more consistent in their strategies and are, therefore, more predictable, it may also indicate that a major factor determining the Energy Detector's success as a model, is its ability to predict the presence of the signal. A comparison of these results to other models might give a better view of how appropriate the Energy Detector is as a model of the auditory system.

Frank (1979) compared the performance of several models to his quasi-molecular data, including the Cross-Correlator, the Energy Detector, and one configuration of the model of Jeffress (1967). He investigated the detectability of a 500-Hz sinusoid that was masked by four samples of computer-generated Gaussian noise. The noise was band-pass filtered from 100 to 3000 Hz. Each of the four noise samples occurred on several randomly selected trials during each block of 100 trials. Half of the trials in each block contained random samples of noise in an attempt to keep the subjects from "learning" any of the four samples. Each noise sample occurred during both noise-alone and signal-plus-noise trials. The signal-level was manipulated for each sample individually such that the sample's psychometric function could be obtained. The value of $10 \log(E/No)$ required to yield 80% correct detection was estimated for each sample from its psychometric functions. Four values of signal starting phase (Alpha) over the range 0 to 90 degrees were investigated. Because the models do not make specific predictions of P(C) for specific noise samples (an assumption about the magnitude of the "internal" noise is required in order to arrive at a detectability index for a specific sample), the fit of the models was evaluated by comparing the relative changes in the outputs of the models as a function of Alpha to the relative changes in average performance of the subjects as a function of Alpha. Unfortunately, the results of Frank's model-fitting efforts were inconclusive. There was considerable variability in his data across subjects and across samples. None of the models fit the data for all samples and for all subjects well. Because a limited number of samples was investigated, it was difficult to determine the source of the discrepancies between the models and the data.

Bell and Schubert (1975), Bell and Becker (1975), and Dolan, Hirsh, and Yost (1981) used a 2AFC paradigm, and also found dramatic changes in detectability of a signal masked by individual samples of noise when the starting phase of the signal was varied. Bell and Becker were fairly well able to predict their narrow-band noise masking data using an envelope detector. Becker and Bell (1975) had minimal success at relating the wide-band masking data of Bell and Schubert to any of a variety of stimulus measures.

The present study will also investigate models other than the Energy Detector. This will be accomplished by estimating parameters of the general form of the model described by Jeffress (1967). As previously mentioned, given an appropriate choice of parameters, this model will simulate an Envelope-Detector, an Energy-Detector, and a Leaky Integrator. The data will be collected using a single-interval procedure to avoid the problem of how the subjects combine the decision variables computed during the two intervals of a 2AFC trial. Twenty-five noise samples will be investigated. Each sample will be used on both noise-alone trials and signal-plus-noise trials. In addition, four values of Alpha will be investigated: 0, 90, 180, and 270 degrees. No attempt will be made to obtain thresholds for individual samples. Instead, hit and false-alarm rates for each sample obtained at two fixed signal-levels will be related to the predictions of the models. The models predict that the probability of a "Yes" response will increase monotonically with the output of the model. However, as mentioned previously, they do not make specific predictions regarding the detectability of signals masked by individual samples of noise.

Footnote

1.

$$dz = (M_n - M_{sn}) / \sqrt{V_n + V_{sn}}$$

where M_n is the mean of the noise-alone distribution, M_{sn} is the mean of the signal-plus-noise distribution, V_n is the variance of the noise-alone distribution and V_{sn} is the variance of the signal-plus-noise distribution. If the noise-alone and signal-plus-noise distributions are assumed to have equal variance and be normal in form, $d' = dz$. The term d' will here be reserved for this case.

Chapter 2

METHODS

Subjects

The subjects were four undergraduate work-study students (2 males, 2 females) who were paid for their participation in the experiment. Their ages ranged from 19 years to 25 years. All four subjects were experienced auditory observers with audiometrically normal hearing. Each subject had participated in similar auditory experiments for a period of at least three months before beginning the experiments reported here. In addition, each subject received several thousand practice trials under the present experimental procedure before any of the data reported here were collected.

Apparatus

Signal and noise stimuli were generated on a Digital Equipment Corporation PDP-11/34A computer. They were output through separate Analogic Corporation 14-bit digital-to-analog converters (DACs) at a sampling rate of 20,000 samples per second. The waveform in each channel was then smoothed by a 6.3-kHz low-pass filter with an 80-dB per octave roll-off to prevent aliasing. The noise channel was additionally band-pass filtered from 100 to 3000 Hz. The signal was passed through a programmable attenuator to control the presentation level. The signal and the noise were then mixed analogically, passed through a final attenuator, and presented to the subjects through TDH-49 headphones. The four subjects were seated in a Suttle Equipment Corporation double-walled soundproof room during the experiment.

Procedure

The signal was a 100-ms sample of a 500-Hz sinusoid. The sinusoid was generated using the sine function provided with the RT-11 FORTRAN library. The onsets and offsets were shaped by 8-ms linear ramps. The signal-level was controlled by a programmable attenuator. Signals with four different starting phase angles (Alphas) were investigated over the course of the experiment: 0, 90, 180, and 270 degrees.

The noise waveforms were generated by a 33-bit software shift-register (Gilkey and Frank, 1981). Within the 100 to 3000-Hz passband, the long term power spectrum of the noise is white, and to a very good approximation the distribution of instantaneous pressures is Gaussian. Each time the shift-register is initialized to the same starting value, the identical noise sample is produced. In the experiments reported here, 25 nonoverlapping 148-ms samples of noise were selected for investigation. Each day the same noise sample (not one of the 25 studied) was used to calibrate the noise channel of the circuit. This sample was output repeatedly (with no temporal gap between the offset and the onset) and its level was adjusted to be equivalent to that of a thermal noise with a spectrum level of 50 dB SPL. The average spectrum level of the 25 samples was then assumed to be approximately 50 dB SPL.

Two signal-levels were used under each condition of the experiment. Within each set of four blocks, the signal-level on the first and third blocks resulted in a $10 \text{ Log}(E_s/N_o)$ of 11.5 dB. The signal-level on the second and fourth blocks resulted in a $10 \text{ Log}(E_s/N_o)$ of 8.5 dB. Each set of four blocks was preceded by a practice block during which the signal-level resulted in a $10 \text{ Log}(E_s/N_o)$ of 14.5 dB.

All of the data reported here were collected using a single-interval (Yes-No) procedure. Each trial began with a 198-ms warning light, followed by a 100-ms pause, a 198-ms observation interval marked by a light, a 1500-ms response interval, and a 198-ms feedback interval. During the observation interval, the noise burst began 25 ms after the onset of the light and was centered temporally with respect to the light. The signal, if present, began 20 ms after the onset of the noise and was centered temporally with respect to both the light and the noise. The subjects' task was to press one of two buttons on the response panel in front of them during each response interval, to indicate whether or not they believed a signal had been presented on that trial. Feedback was used only during training and practice blocks. During the feedback interval, a light indicated whether or not the signal had been presented. Because the 25 noise samples under investigation were never presented during training or practice blocks, subjects never received feedback about their trial-by-trial performance for these twenty-five samples. However, at the end of each set of four blocks subjects were given feedback on their average performance on each block.

During each two-hour experimental session four sets of four blocks of trials were presented. Each set of four blocks was preceded by a practice block. Practice blocks contained twenty trials; all other blocks contained 100 trials.

Within each block of 100 trials, each of the 25 noise samples was presented four times. On two of those four trials a signal was added to the noise. On the other two trials only the noise was presented. Over the course of the experiment each noise sample was presented between 156 and 396 times for each combination of signal-level and Alpha. Again, on half of these trials (about 100 trials for each combination of signal-level

and phase), a signal was added to the noise sample. On the other half of the trials, the noise sample was presented alone. The actual number of presentations of each sample to each subject under each condition is shown in Table A1.1 of Appendix A1.

Stimulus Analyses

All noise-alone and signal-plus-noise waveforms were output through the DAC, mixed analogically, and presented through headphones as they would be on a normal trial. The mixed waveform was simultaneously sampled into the PDP 11/34 through an analog-to-digital converter at a point in the circuit immediately before the final attenuator. The sampling rate was 20,000 samples per second. The digitized waveforms were then transferred to the DEC-10 computer system on the campus of Indiana University-Purdue University at Indianapolis. Fast Fourier transforms (FFTs) were computed on the waveforms and stored for subsequent analysis (the mixed-radix fast Fourier transform algorithm of Singleton (1969) was used to compute all FFTs and inverse FFTs).

A model like that of Jeffress (1967) was implemented on the computer. To mimic the first stage of his model, a subroutine was written to compute the amplitude and phase characteristics of a single-tuned (RLC) filter. The amplitude and phase characteristics defined by the subroutine were then applied to the stored amplitude and phase spectra of each stimulus. The filtered spectra were transformed into the time domain by an inverse FFT. Seven filter bandwidths (10, 25, 50, 75, 100, 302, and 538 Hz) were used with the filter centered at 500 Hz. In addition, seven filters, each with a bandwidth of 50 Hz, but different center frequencies (350, 400, 450, 500, 550, 600, and 650 Hz) were employed in later analyses.

The nonlinearity in Jeffress' model was approximated in two ways. Half-wave rectification was achieved by replacing the negative values in each filtered waveform with zeros. The square-law device was simulated by squaring each element in each filtered waveform.

Each element in the output of the integration stage was defined as the sum of the corresponding input element and all previous input elements weighted by an exponential decay. The value of the exponential decay function was replaced with a value of zero if the computed weighting was less than .01. Six values were used for the decay constant of the exponential (.01, 1, 10, 50, 100, and 200 ms). The .01-msms decay constant was sufficiently short that the digitized waveforms were passed through the integration stage unaltered.

The output of the integration stage is a waveform, containing 3000 digital values. Exactly what sampling strategy should be applied to these 3000 values in order to obtain a single value as a decision variable (X') is not obvious a priori. The five sampling strategies considered here were thus chosen rather arbitrarily. The resultant value of X' was equal to:

1. the average output of the integration stage during the stimulus interval (Strategy 1)
2. the average output of the integration stage during the signal interval (Strategy 2)
3. the average output of the integration stage during an 8-ms interval that began simultaneously with the signal offset (Strategy 3)
4. the average output of the integration stage during an 8-ms interval that began 16 ms after the signal offset (Strategy 4)
5. the maximum value of the integrator output during the stimulus interval (Strategy 5)

"Stimulus interval" refers to an interval that starts at the onset of the noise and ends approximately 2 ms after its offset, and "Signal interval" refers to an interval that begins 20 ms after the onset of the noise and ends 28 ms before its offset ("Signal interval" refers to the same interval on both signal-plus-noise and noise-alone trials.)

Chapter 3

RESULTS

As was mentioned in the introduction, Green (1964) distinguished between two methods of psychophysical analysis. The method which has traditionally been applied in psychoacoustics he referred to as molar psychophysics. The techniques applied in the experiments described here are closer to the approach Green referred to as molecular psychophysics (Note 2). In this chapter the data from the present experiments will be described on both of these levels. As will be seen, the results of these two forms of analysis are quite distinct. Some of the implications of these differences will be considered.

Molar Level

The psychometric function has frequently been used to describe the results from simple detection experiments such as the one reported here. Figures 3.1 through 3.4 show two-point psychometric functions for each of the four subjects. The four points shown at each signal-level are the maximum probability of a correct response, $P(C)_{max}$, for each Alpha. $P(C)_{max}$ was obtained from d' by assuming an optimal criterion and calculating the expected value of $\{P(Y/SN)+[1-P(Y/N)]\}/2$. The curves were generated by finding the least-squares fit to the logarithmic transform of the function $d'=m(E/No)^k$ using the logistic approximation to the cumulative normal. The slopes (k 's) and intercepts (m 's) are well within the bounds typically found for a tone-in-noise detection task (Egan, Lindner and McFadden, 1969). The average performance of the subjects is well fit by a psychometric function with a slope of 5% per dB over the approximately linear portion ($k=1.00$), and an intercept such that a 10

Figure 3.1. Psychometric function for subject SG. Points plotted show $P(C)_{max}$ obtained under each condition. Square symbols are with Alpha equal to 0. Circular symbols are with Alpha equal to 90. Diamond symbols are with Alpha equal to 180. Triangular symbols are with Alpha equal to 270.

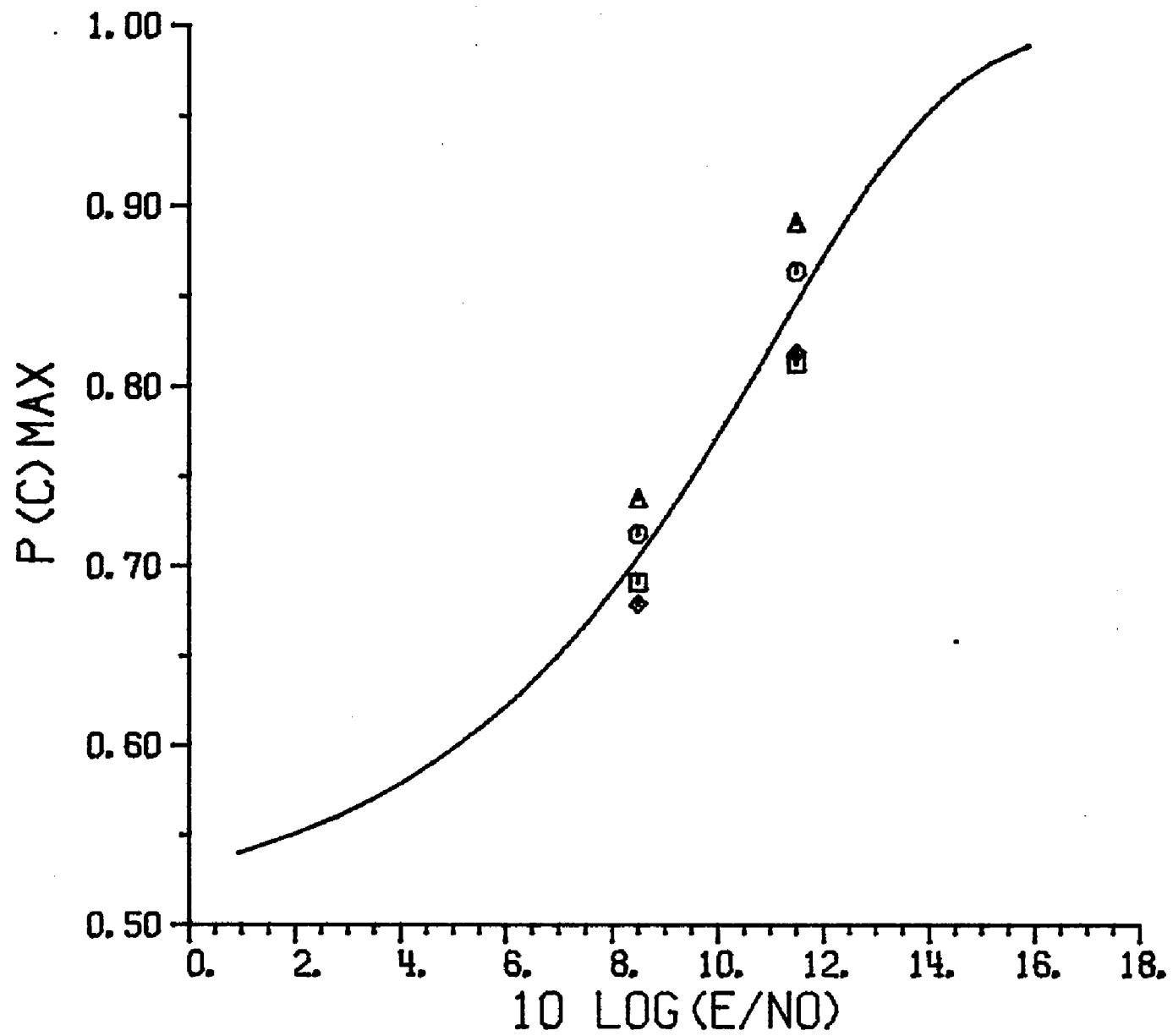


Figure 3.2. Psychometric function for subject CV. Points plotted show $P(C)_{max}$ obtained under each condition. Square symbols are with Alpha equal to 0. Circular symbols are with Alpha equal to 90. Diamond symbols are with Alpha equal to 180. Triangular symbols are with Alpha equal to 270.

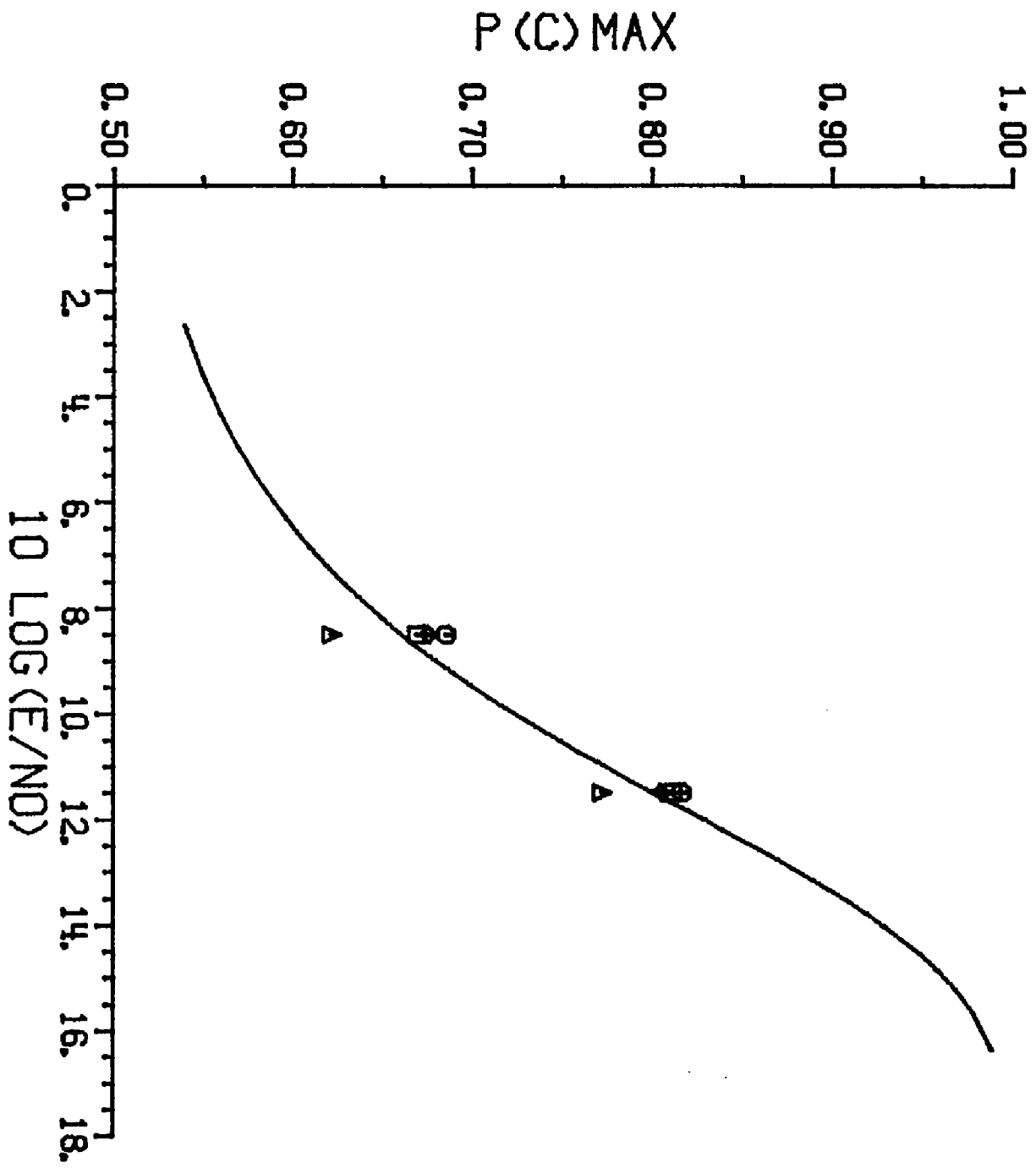


Figure 3.3. Psychometric function for subject TW. Points plotted show $P(C)_{max}$ obtained under each condition. Square symbols are with Alpha equal to 0. Circular symbols are with Alpha equal to 90. Diamond symbols are with Alpha equal to 180. Triangular symbols are with Alpha equal to 270.

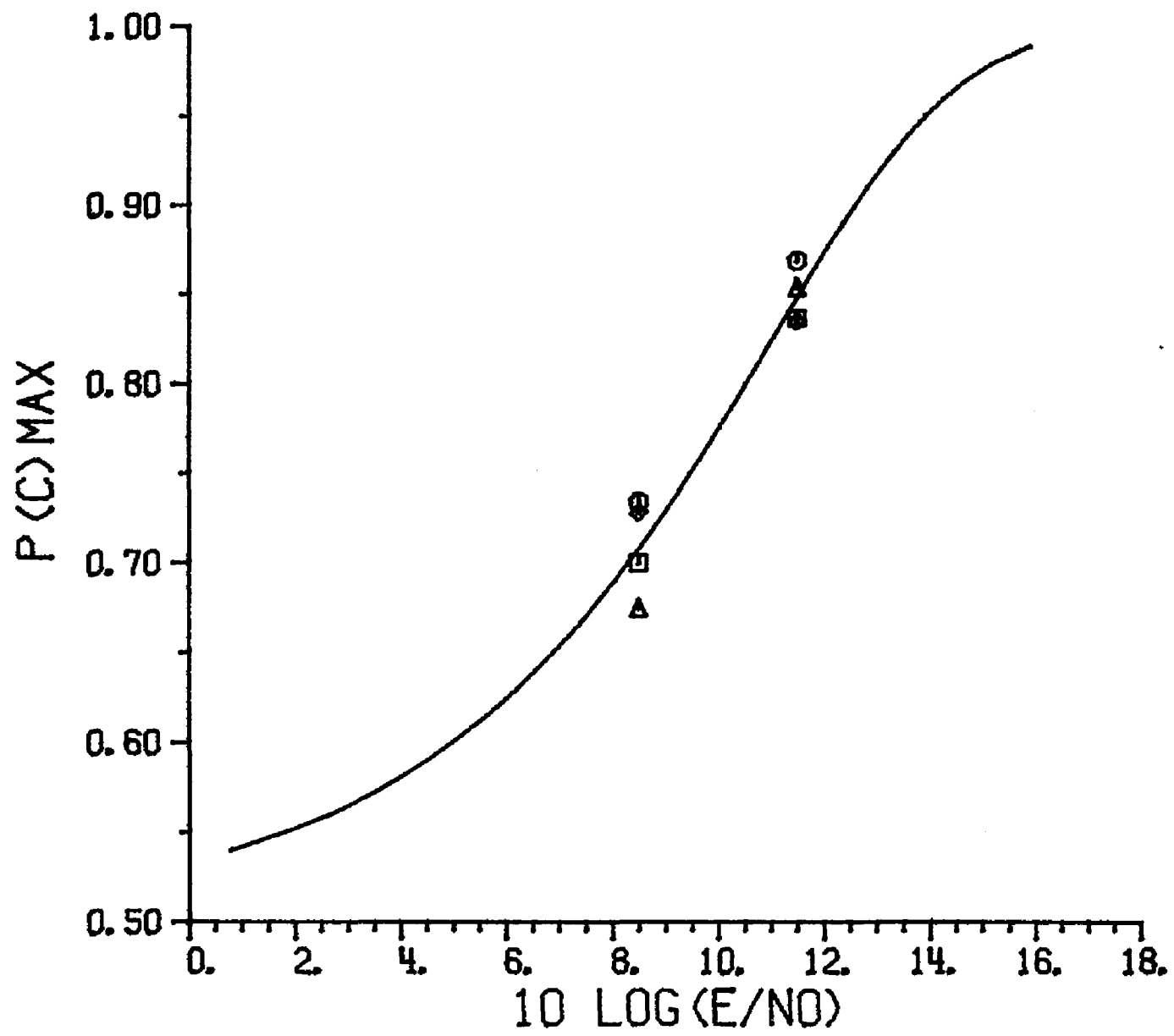
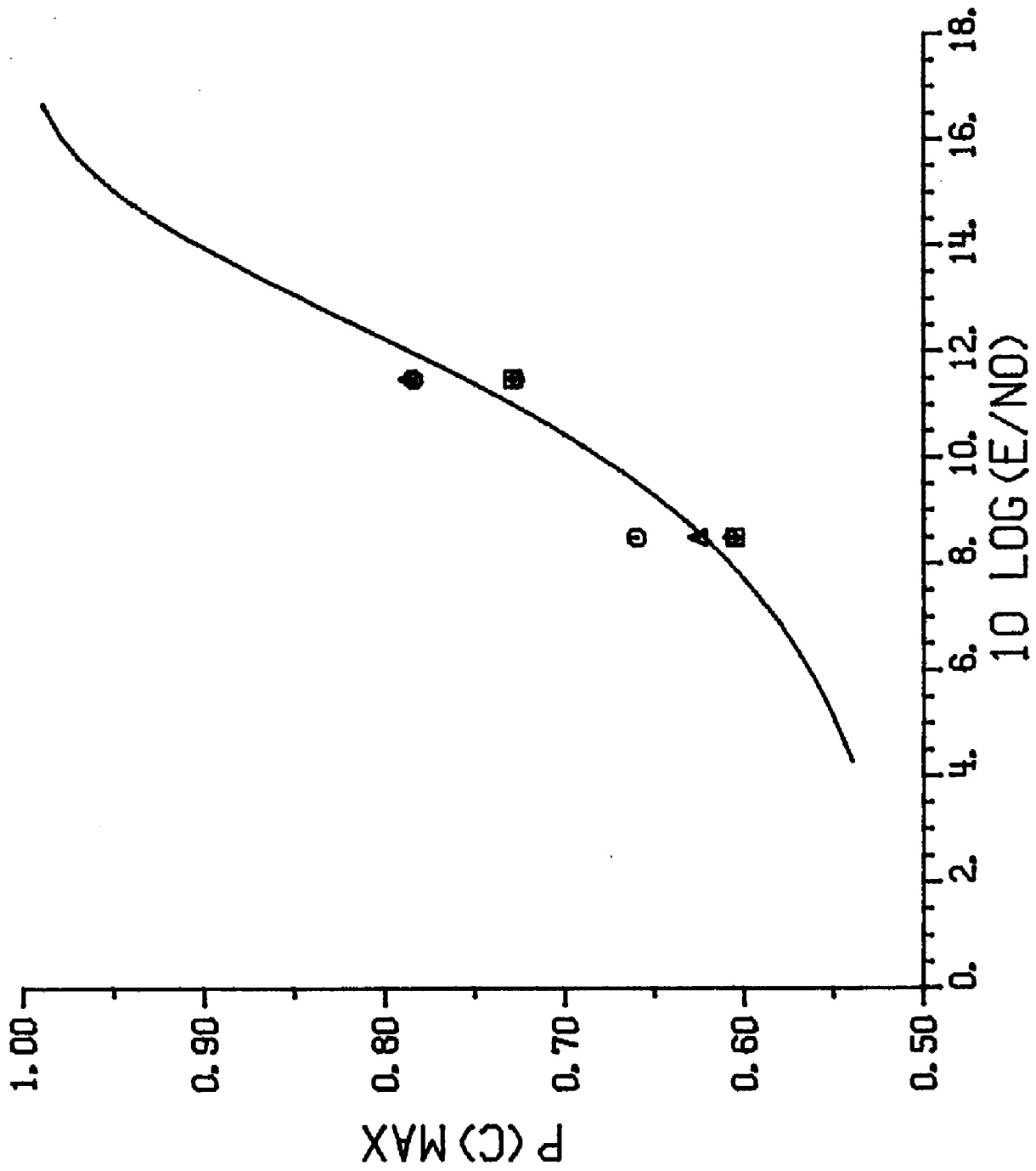


Figure 3.4. Psychometric function for subject JM. Points plotted show $P(C)_{max}$ obtained under each condition. Square symbols are with Alpha equal to 0. Circular symbols are with Alpha equal to 90. Diamond symbols are with Alpha equal to 180. Triangular symbols are with Alpha equal to 270.



Log(E/No) of 10 leads to a d' of one ($m=-10.51$). Tables 3.1 and 3.2 show the values of P(C)max and Beta obtained for each subject under each experimental condition. Unfortunately, data for the four values of Alpha were not collected simultaneously, but during successive 8 to 16 day periods. Presumably, the small differences that occur across different Alphas were more strongly influenced by the fact that the conditions were run during different periods of time than by any small changes in the average stimulus that might have occurred as a result of the change in Alpha.

Molecular Level

When examining the data on the molecular level, the number of data points to be considered increases dramatically. In an attempt to return the amount of data to manageable size, the remainder of the figures presented in this chapter will only show data that have been averaged across subjects. This procedure is, however, in conflict with a truly molecular philosophy, and does obscure some real and, no doubt, important individual differences which exist between subjects. Figures for individual subjects have, therefore, been included in Appendix A2. To reduce further the amount of data to be presented, the remainder of the figures in this chapter will only show data collected when $10 \text{ Log}(E/No)$ was equal to 8.5 dB.

One way to obtain an initial perspective on the data is to plot the results for individual samples in Receiver Operating Characteristic (ROC) space. Figures 3.5 through 3.8 show data that have been averaged across subjects plotted in ROC space for each of four values of Alpha. Each number is plotted at the hit and false-alarm rates obtained for the sample associated with that number. It is important to realize that these

TABLE 3.1
P(C)max at each Alpha by Subject

10 Log(E/No)=11.5 dB

	SG	CV	TW	JM
Alpha=0	.813	.812	.836	.729
Alpha=90	.864	.817	.869	.784
Alpha=180	.819	.806	.835	.726
Alpha=270	.891	.773	.855	.787

10 Log(E/No)=8.5 dB

	SG	CV	TW	JM
Alpha=0	.691	.670	.700	.606
Alpha=90	.718	.686	.734	.660
Alpha=180	.679	.676	.728	.607
Alpha=270	.738	.622	.675	.626

TABLE 3.2

Beta at each Alpha by Subject

	10 Log(E/No)=11.5 dB			
	SG	CV	TW	JM
Alpha=0	1.17	.88	.80	.91
Alpha=90	1.32	.76	.93	.69
Alpha=180	1.21	.70	1.07	.72
Alpha=270	2.09	.87	.57	1.03

	10 Log(E/No)=8.5 dB			
	SG	CV	TW	JM
Alpha=0	1.00	1.04	.95	.95
Alpha=90	1.13	1.02	1.12	.94
Alpha=180	.96	.94	1.12	.87
Alpha=270	1.42	1.01	.91	1.00

Figure 3.5. Hit and false-alarm rates obtained for individual samples are shown in ROC space. Each number plotted shows the data for the sample associated with that number. The square symbol shows the average hit rate and false-alarm rate across all samples. The data shown have been averaged across subjects and were collected with Alpha equal to 0.

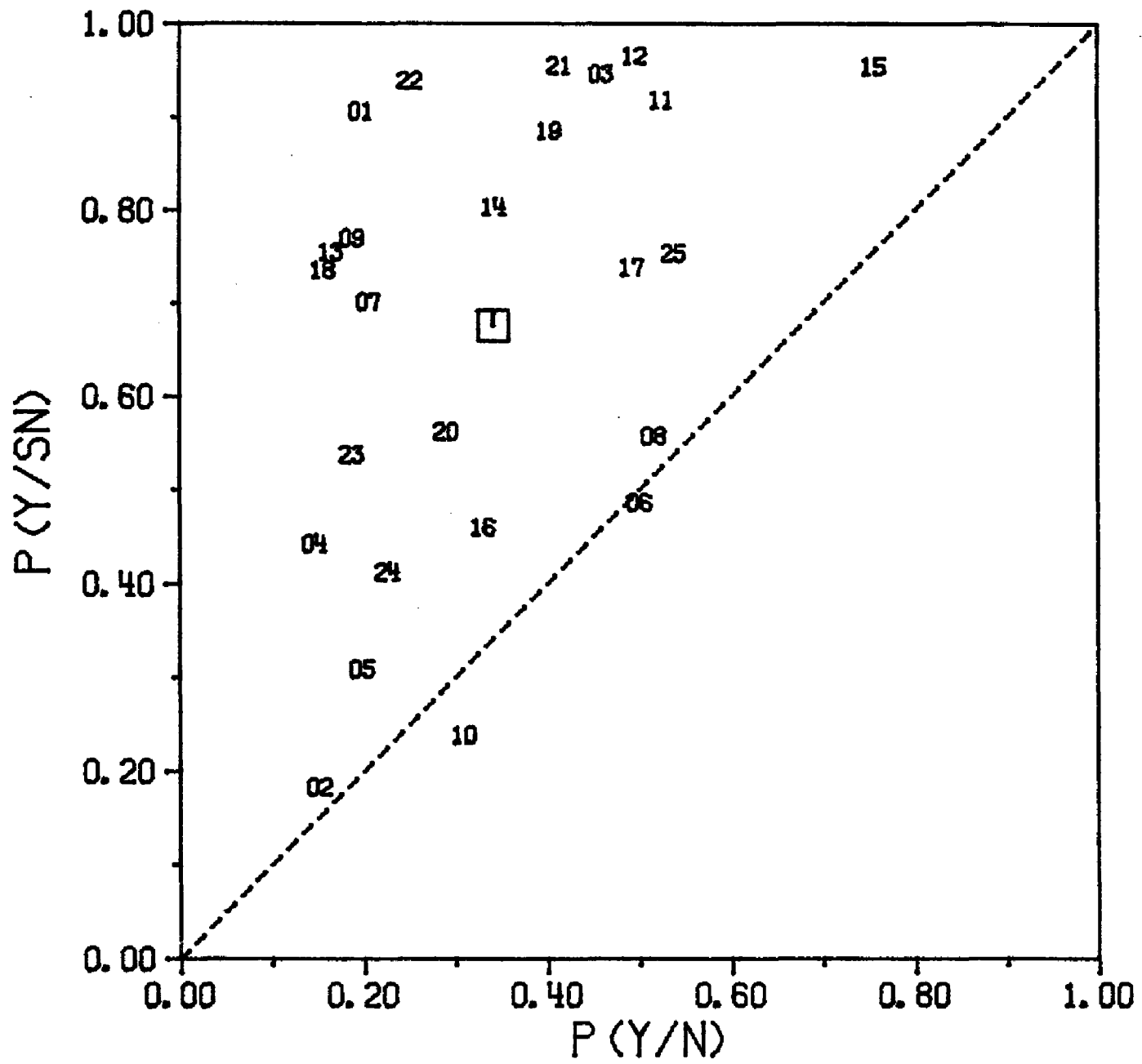


Figure 3.6. Hit and false-alarm rates obtained for individual samples are shown in ROC space. Each number plotted shows the data for the sample associated with that number. The square symbol shows the average hit rate and false-alarm rate across all samples. The data shown have been averaged across subjects and were collected with Alpha equal to 90.

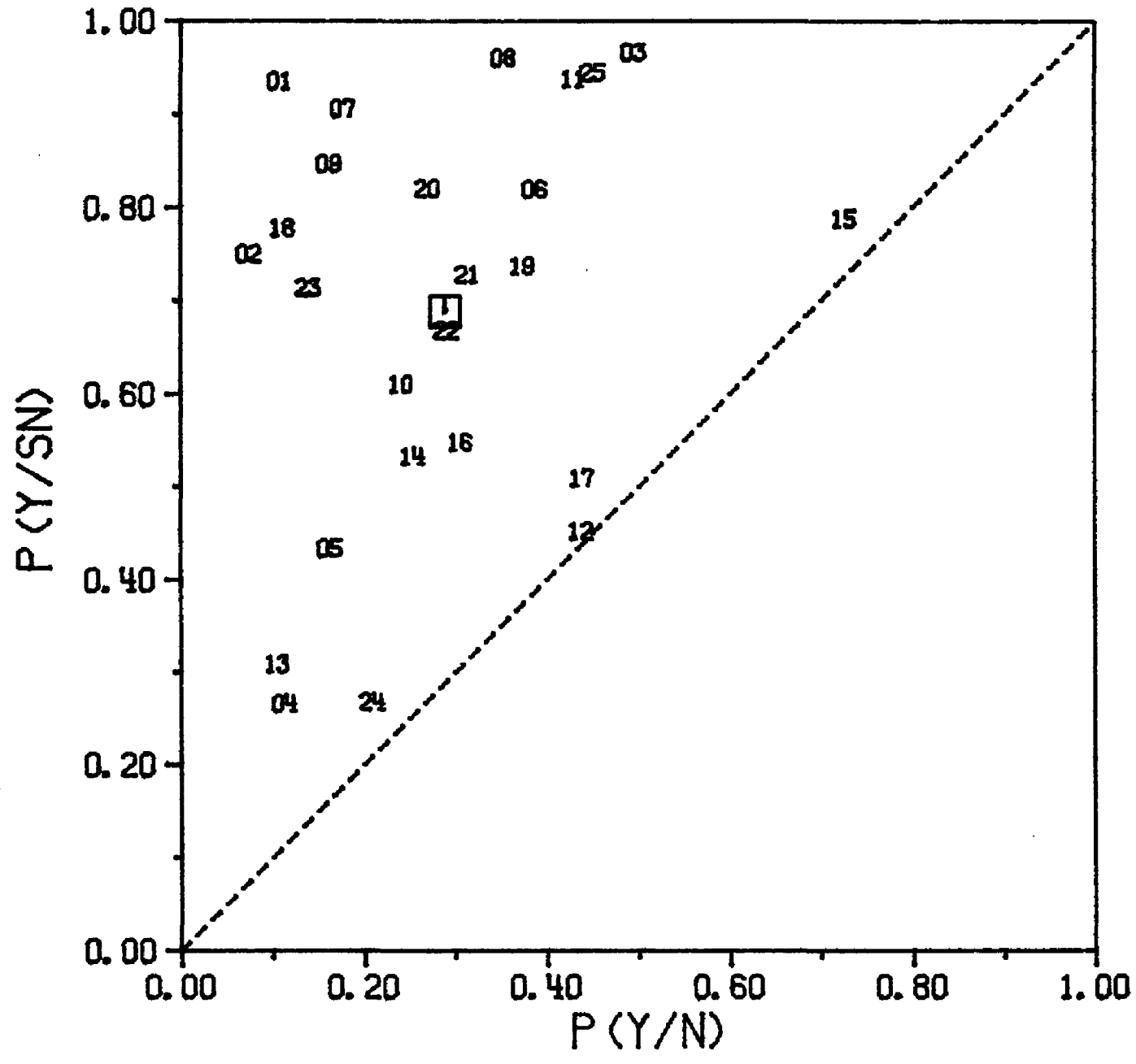


Figure 3.7. Hit and false-alarm rates obtained for individual samples are shown in ROC space. Each number plotted shows the data for the sample associated with that number. The square symbol shows the average hit rate and false-alarm rate across all samples. The data shown have been averaged across subjects and were collected with Alpha equal to 180.

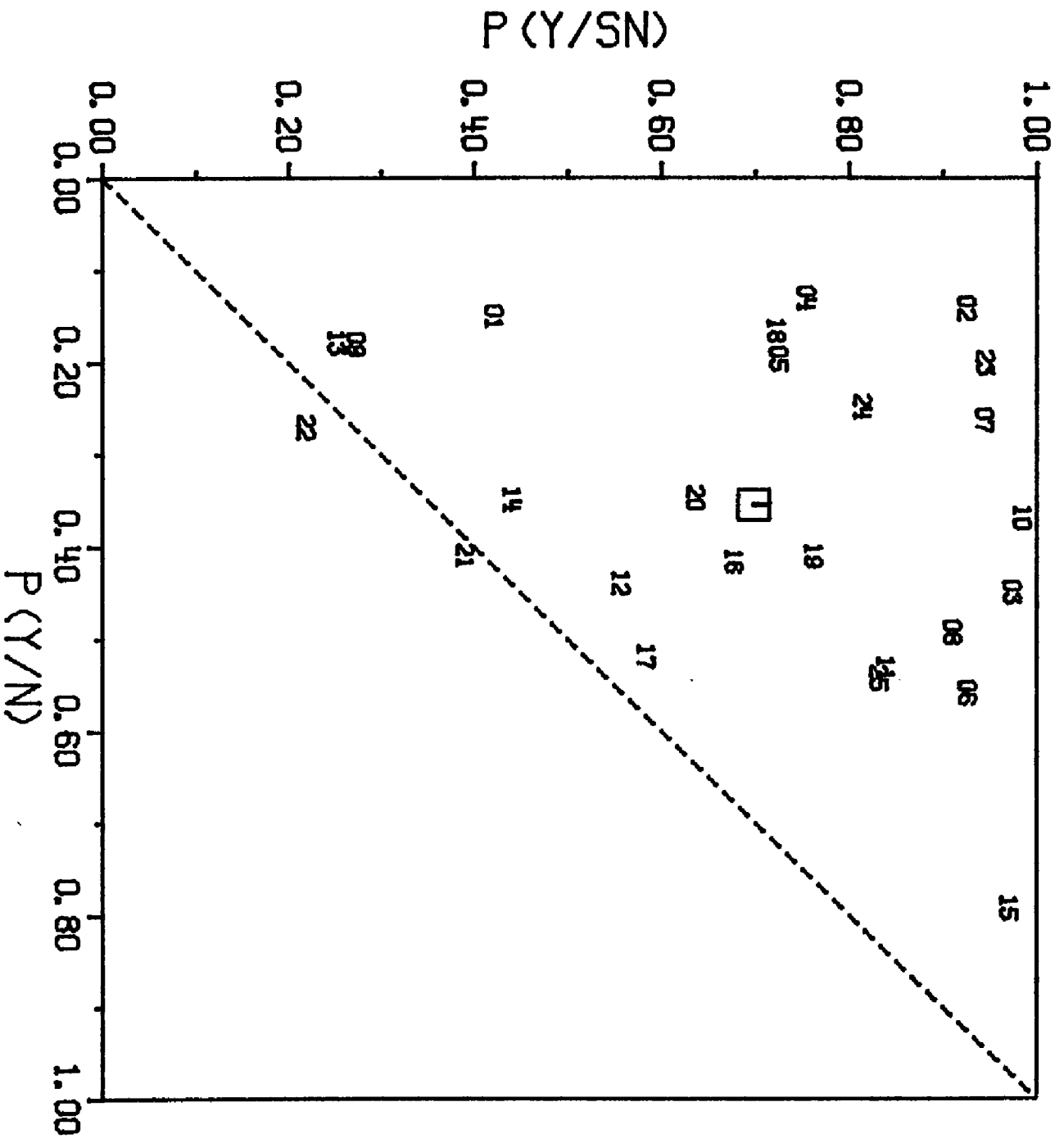
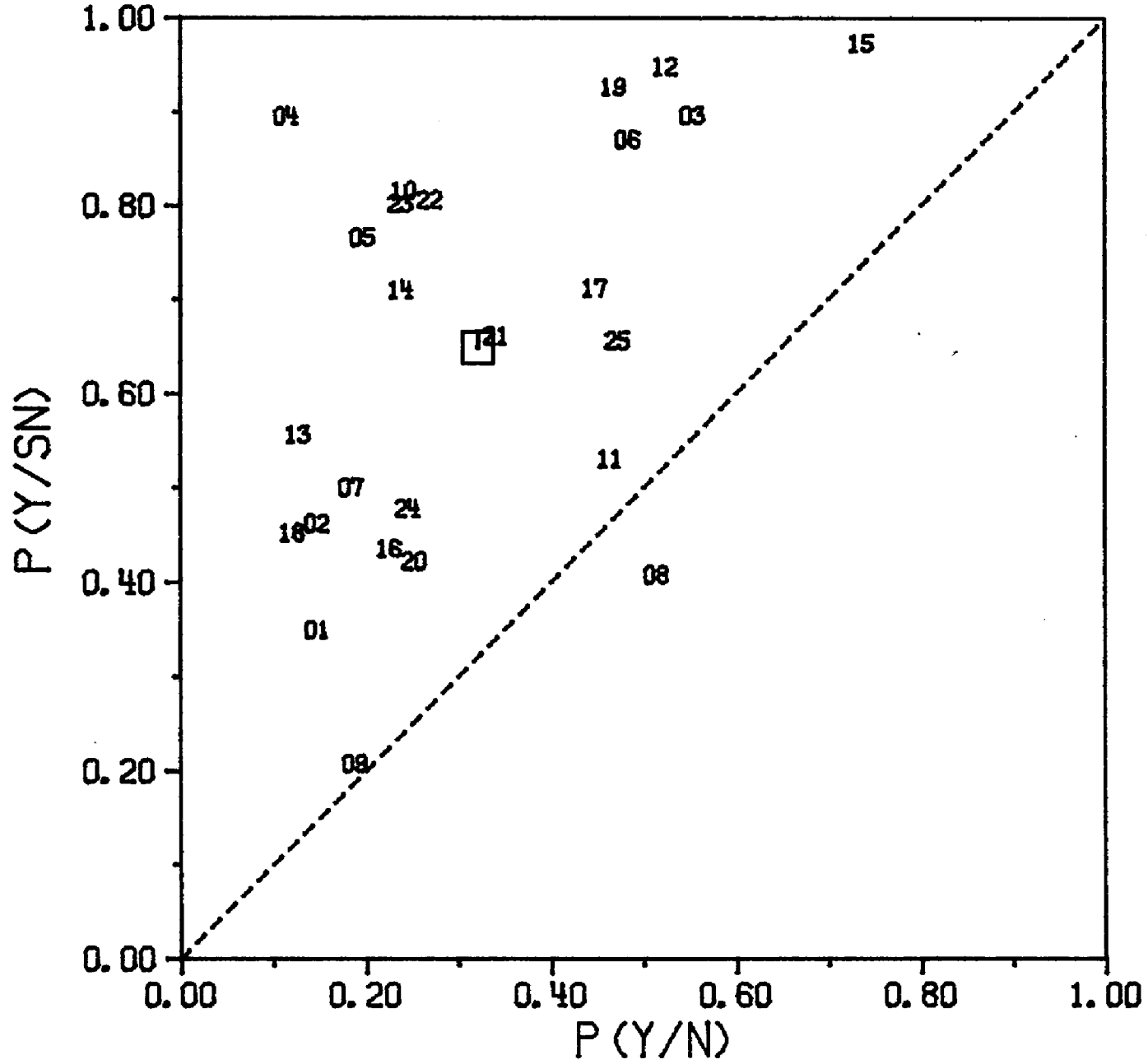


Figure 3.8. Hit and false-alarm rates obtained for individual samples are shown in ROC space. Each number plotted shows the data for the sample associated with that number. The square symbol shows the average hit rate and false-alarm rate across all samples. The data shown have been averaged across subjects and were collected with Alpha equal to 270.



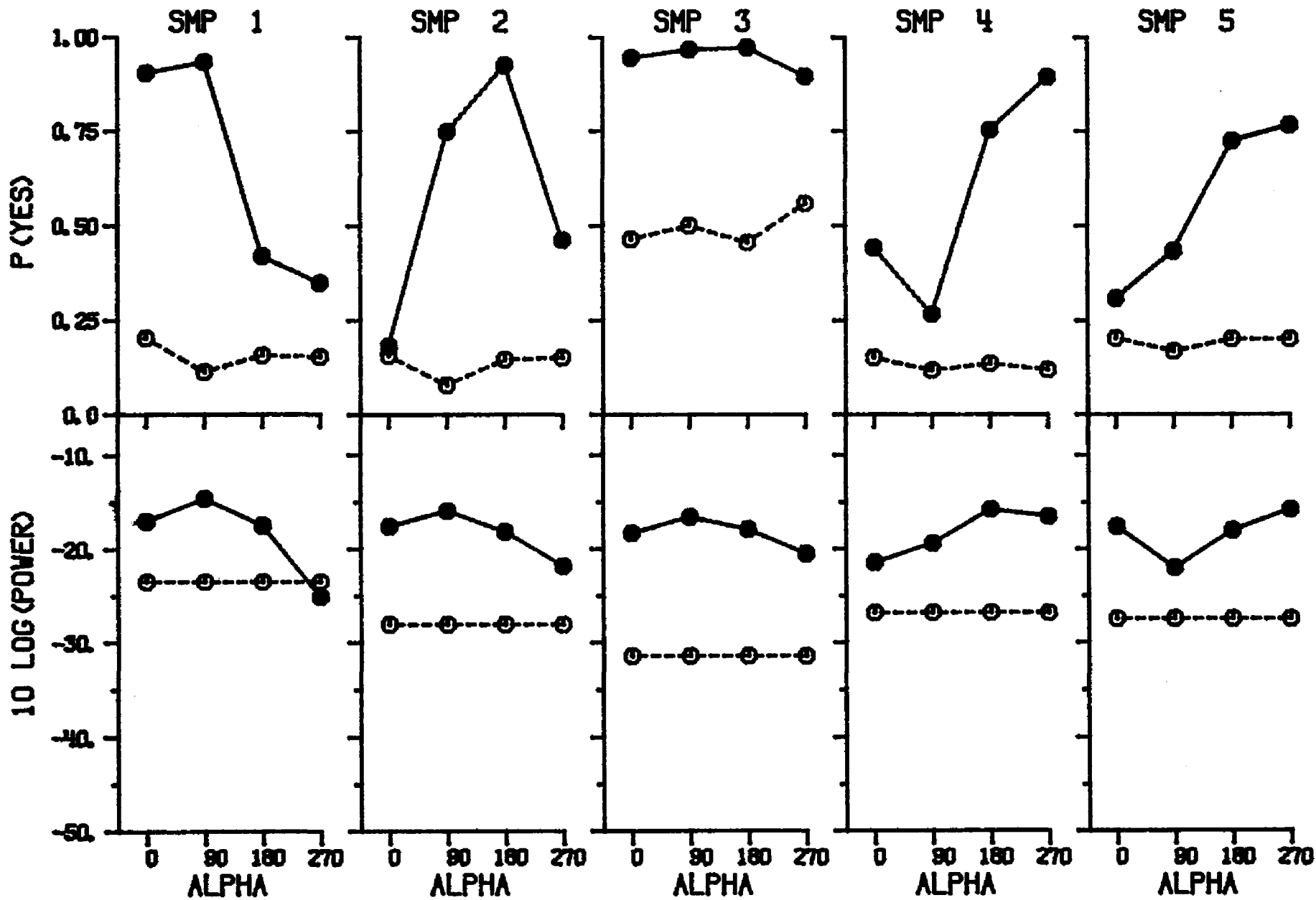
points do not represent an ROC curve. Presumably the subject has established only one criterion. The individual points in ROC space do not, therefore, represent changes in the subject's criterion across samples, but rather the position of each noise-alone and signal-plus-noise sample relative to the subject's single criterion. On the molar level, all of these data would be summarized by a single point. This point is shown as the open square in each figure. As can be seen, the average may not provide an adequate summary of the data. The data for individual samples are distributed rather broadly throughout ROC space. An examination of the data in these figures will show that false-alarm rates for individual samples range from .08 to .80. Hit rates span an even broader range, from .18 to .98. When one considers the data for individual subjects, even greater ranges can be found for some subjects. False-alarm rates for subject TW range from .00 to .96. His hit rates range from .03 to 1.00. These ranges give a rough estimate of the degree to which the subject is stimulus-bound. If a subject's responses were totally determined by the stimulus (i.e., if the subject had no "internal" noise), when the identical stimulus was presented, the subject would make the same response. The data, when plotted in ROC space, would appear only in the four corners of each figure. On the other hand, if the subject's responses were totally independent of the external stimulus (i.e., if the responses of the subject were determined by the "internal" noise), the data would all lie within binomial variance of the average point. TW is by this, and by other measures (Gilkey, et al., 1981), a subject with a high degree of internal consistency, as if he were operating in the presence of relatively little "internal" noise. It is of interest that although subject SG is, by this and other measures, operating in the presence of considerably more "internal" noise, his

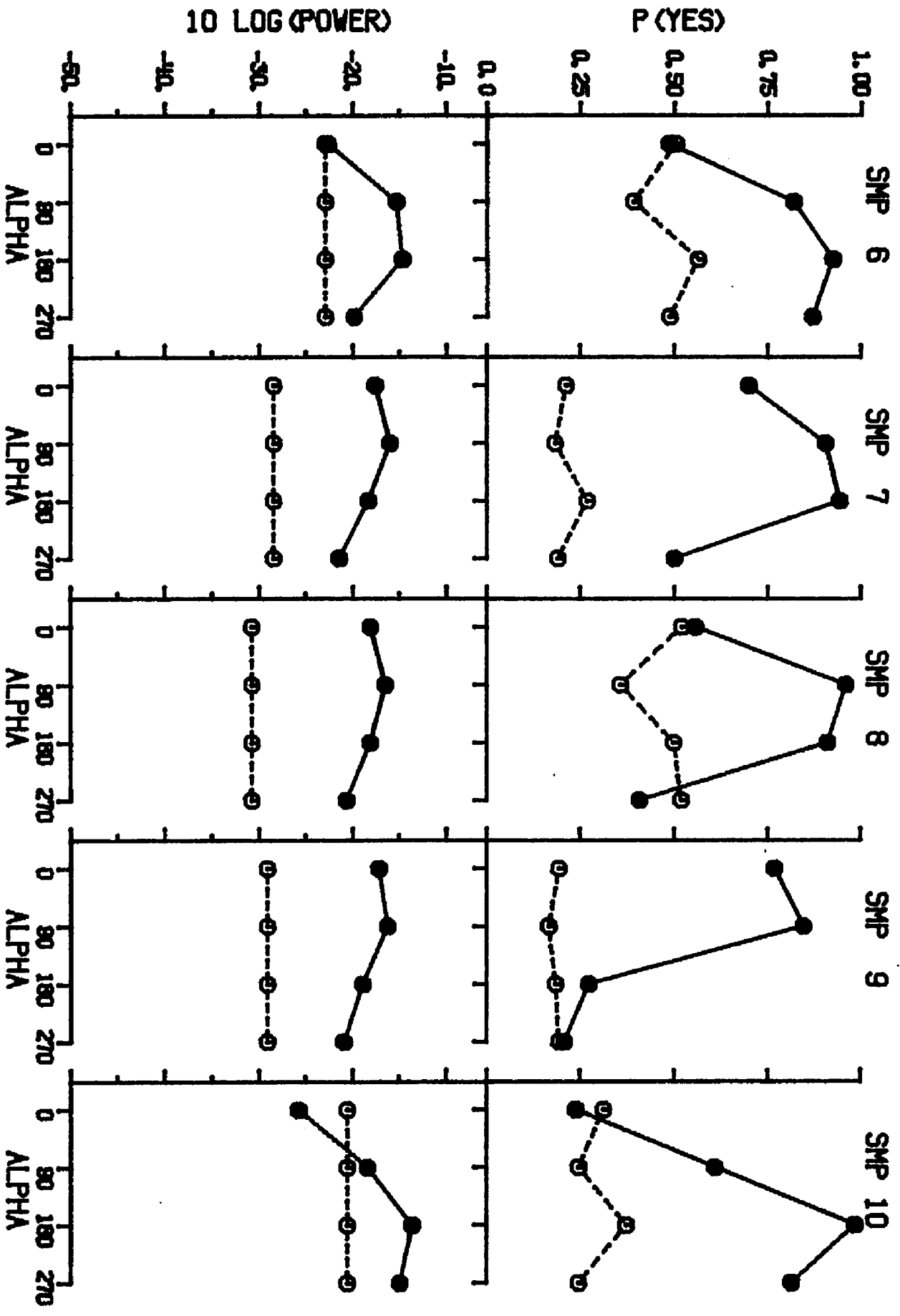
molar performance is almost identical to that of TW. This result is difficult to reconcile with the assumption of many of the models discussed in the introduction that the effect of "internal" noise is simply to reduce the effective signal-to-noise ratio.

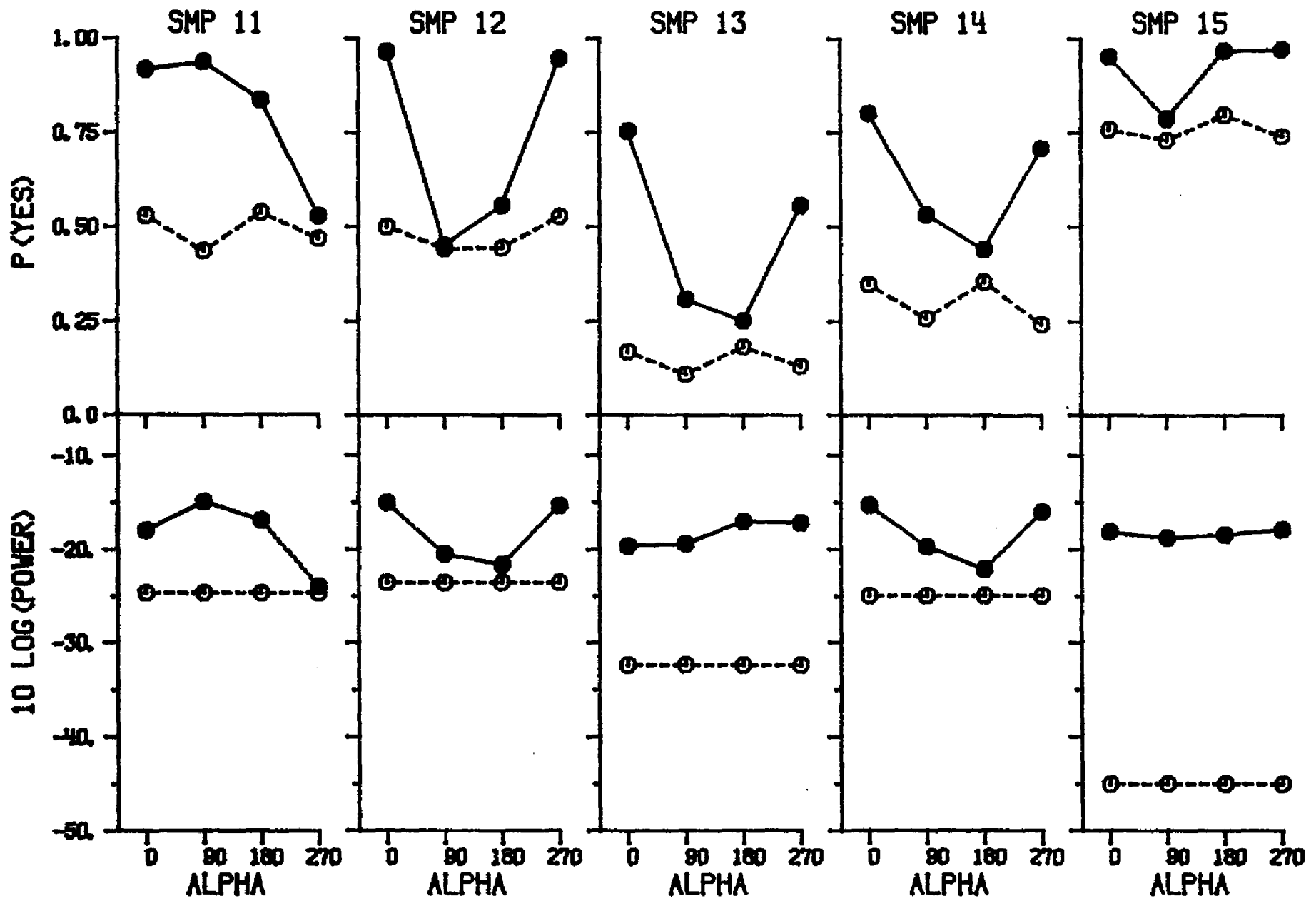
It should be noted from these figures that the points for particular samples under certain conditions consistently fall below the chance line. For example, the average subject had a false-alarm rate of .31 for Sample 10 when Alpha was set to zero, yet attained a hit rate of only .24. An examination of the data for individual subjects reveals that Sample 10 fell below the chance line for all subjects. This implies that Sample 10 sounds more like signal-plus-noise when it is presented alone than when a signal at this Alpha is added to it.

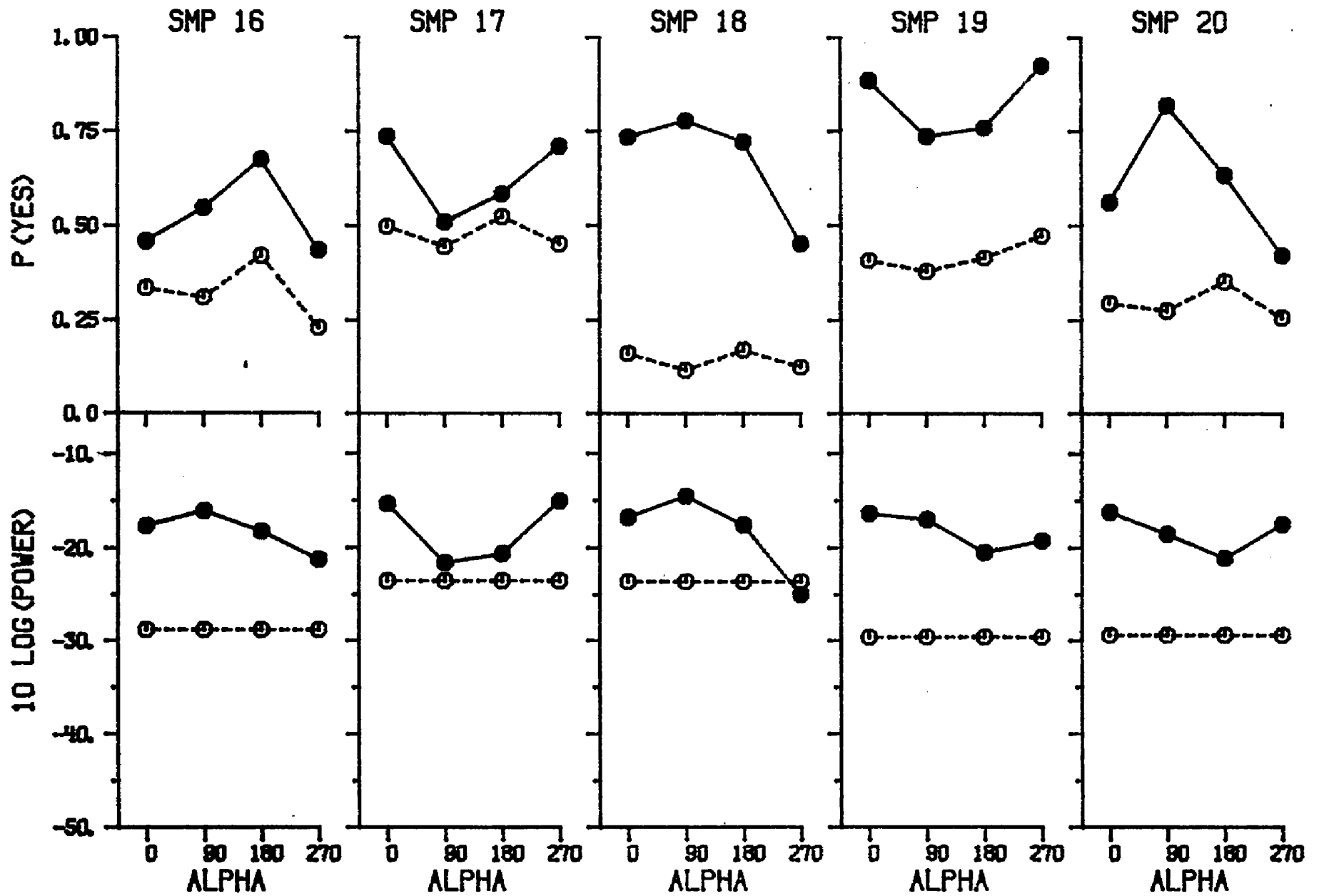
The position of the samples within ROC space changes when Alpha is varied. Although the false-alarm rates tend to stay relatively constant, the hit rates, in many cases, change appreciably. For example Sample 10 is found below the chance line in Figure 3.5, where Alpha is equal to zero; but in Figure 3.7, where Alpha is equal to 180, it has moved to the top of ROC space, with a hit rate of .98 and a false-alarm rate of .37. These effects of Alpha can be seen more clearly by examining Figure 3.9. Each panel of this figure describes data for an individual noise sample. The top half of each panel shows the hit rate (filled circles) and the false-alarm rate (open circles) obtained by the average subject for that particular sample as a function of Alpha. The lower panel shows the power at the 500-Hz component of the Fourier spectrum on signal-plus-noise (filled symbols) and noise-alone (open symbols) trials for that same sample. There are, in many cases, dramatic changes in hit rate which are associated with changes in Alpha. As shown above for Sample 10, the hit rate of the average subject for an individual sample may change by as

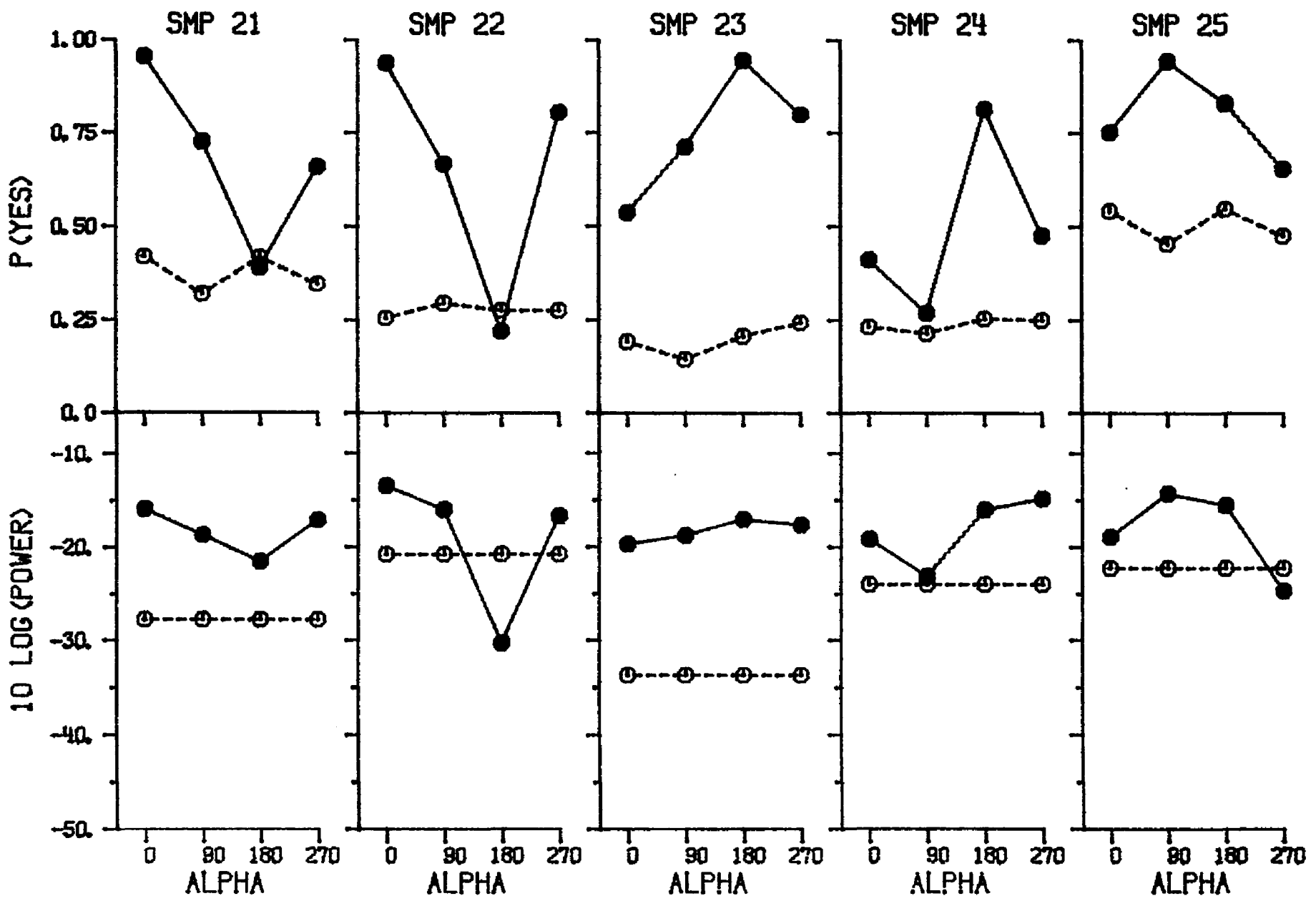
Figure 3.9. Performance and stimulus measures as a function of Alpha. Each panel shows the results for a particular sample. The upper half of each panel shows the obtained proportion of "Yes" responses. The lower half of each panel shows the power at the 500-Hz component of the Fourier spectrum of the stimulus. Filled symbols are for signal-plus-noise trials. Open symbols are for noise-alone trials. Performance data have been averaged across subjects, and were collected at $10 \text{ Log}(E/No)$ equal to 8.5 dB. (The figure extends through five pages.)











much as .70 with a 180 degree change in Alpha. The data for individual subjects indicate that the hit rate may change from near zero to near one with as little as a 90 degree change in Alpha. These changes are, to a first approximation, associated with changes in the power at the 500-Hz component of the Fourier spectrum. A fairly good correspondence, for example, is seen between the hit rate of the average subject and the power of the 500-Hz component of Sample 10. In some cases, however, there is a relatively poor correspondence between the 500-Hz component and the obtained hit rate. This correspondence is weak, at best, for a sample like Sample 13. The relationship between performance and the power at the 500-Hz component appears to be weaker when both signal-plus-noise and noise-alone trials are considered. The below-chance performance, which is found for Sample 10 when Alpha is equal to zero, corresponds to a negative difference between the power of the 500-Hz component on signal-plus-noise trials, and the power of the 500-Hz component on noise-alone trials. However, such a negative difference in power exists for Sample 1 when Alpha is equal to 270, but does not lead to below chance performance. Further, the average performance for Sample 8 when Alpha is equal to 270 is below chance, but the difference between the power in the 500-Hz component on signal-plus-noise trials and noise-alone trials is positive and greater than 10 dB.

Comparing false-alarm rates across samples also reveals some striking discrepancies. For example, there is less power at the 500-Hz component for Sample 15 than there is for any other noise-alone sample. In fact, there is more than 11 dB less power. Yet Sample 15 received the highest number of false-alarms of any sample.

In summary, the data, when analyzed on the molar level, indicate that the performance of all subjects is well within the bounds normally

expected for a tone-in-noise detection task. There were, at most, small effects of manipulating Alpha when examined on this level. In sharp contrast, when the data were considered on the molecular level, large changes in performance were found with relatively small changes in Alpha. A wide range of variations in performance was found across samples. For individual samples, a correspondence was found between the observed changes in hit rate as a function of Alpha and the concurrent changes in the power at the 500-Hz component of the Fourier spectrum. This relationship seemed to be considerably weaker when noise-alone trials were also considered, or when performance was compared across samples.

Footnote

2. The experiment reported here would be classified by Green (1964) as quasi-molecular. However, no distinction between molecular and quasi-molecular will be made in the remainder of this thesis.

Chapter 4

DISCUSSION: MODELS

As described in Chapter 2, a model with a structure similar to the model of Jeffress (1967) was implemented on the computer. During the initial analysis, a half-wave rectifier was used as the non-linear stage of the model. With a $10 \text{ Log}(E/N_0)$ of 8.5 dB, the output of the model was computed in response to each of the 125 stimuli (25 noise-alone stimuli and 100 signal-plus-noise stimuli) for all combinations of the seven bandwidths (10, 25, 50, 75, 100, 300 and 500 Hz) and six time constants (.01, 1, 10, 50, 100 and 200 ms). Each of the five sampling strategies described in Chapter 2 was applied to the output of the integration stage to obtain a value of the model's "decision variable" (X'). In order to compare the value of the decision variable of the model to the responses of the subjects, the logarithm of X' for each sample was transformed into a predicted proportion of "Yes" responses, $P'(Y)$, using the logistic approximation to the cumulative normal, $P(Y)=1/\{1+\exp[-(X'-a)/b]\}$. The parameters of the logistic were chosen to minimize the squared deviation between the obtained proportions of "Yes" responses, $P(Y)$ s, and the $P'(Y)$ s (Note 3). This least-squares fit was obtained using a function minimization routine called STEPIT (Chandler, 1970).

The results of this analysis are summarized in Figures 4.1 through 4.4. The points plotted were selected to summarize the effects of the model's major parameters (filter bandwidth and integrator decay constant) in the regions of the parameter space where the model is able to predict the data relatively well. The upper panel in each figure shows the effect of bandwidth on the value of R^2 , where R^2 is defined as the sum of the squared deviations between the $P'(Y)$ s and the mean of the $P(Y)$ s divided

Figure 4.1. R^2 as a function of the bandwidth of the filter and the decay constant of the integrator. Square symbols are for a $10 \text{ Log}(E/N_0)$ of 8.5 dB. Circular symbols are for a $10 \text{ Log}(E/N_0)$ of 11.5 dB. Filled symbols are for Strategy 2. Open symbols are for Strategy 5. In the upper panel, the decay constant of the integrator has been fixed at .01 ms for the filled symbols, and 200 ms for the open symbols. In the bottom panel, the bandwidth of the filter has been fixed at 50 Hz for both filled and open symbols. The results shown are for subject SG.

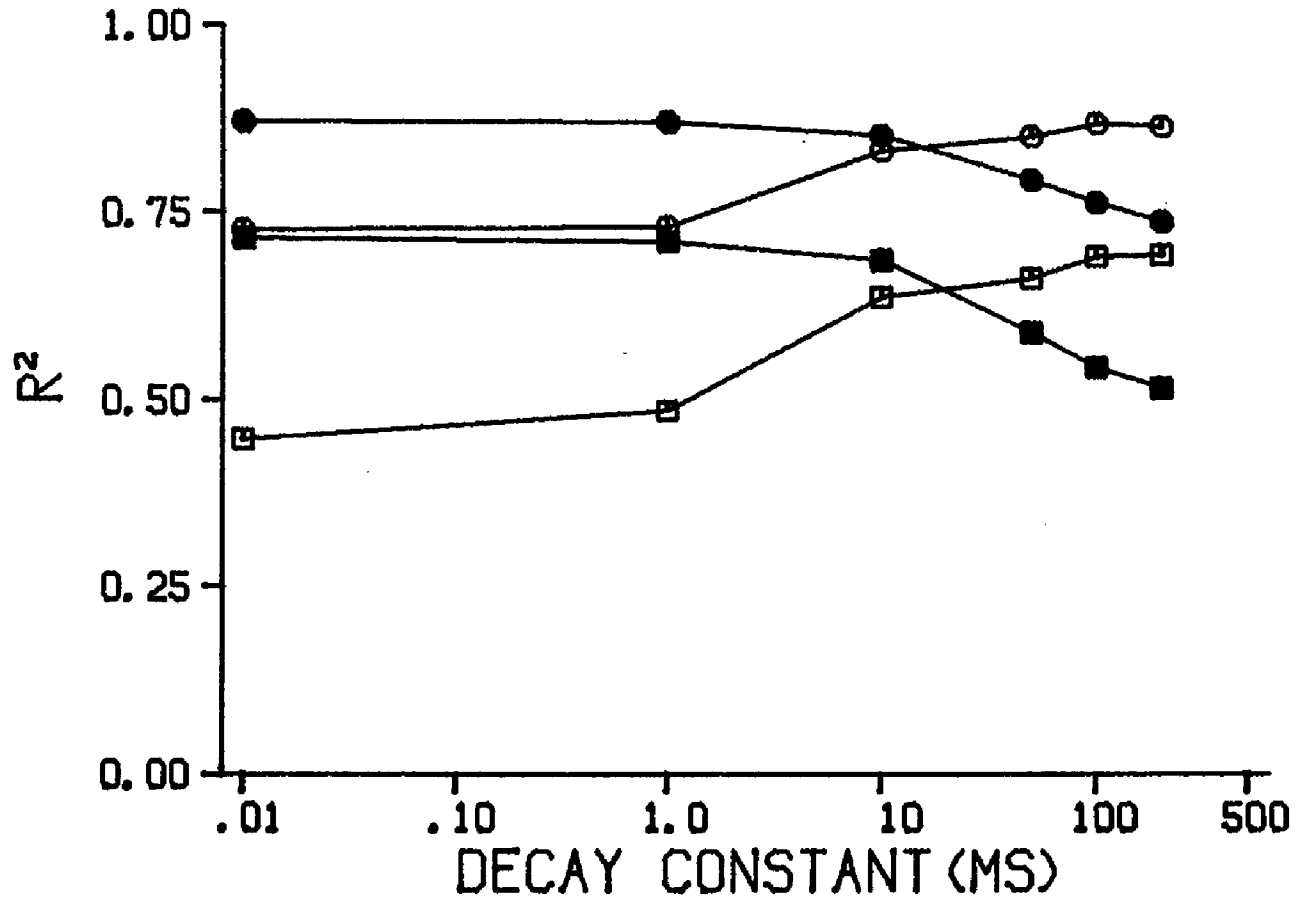
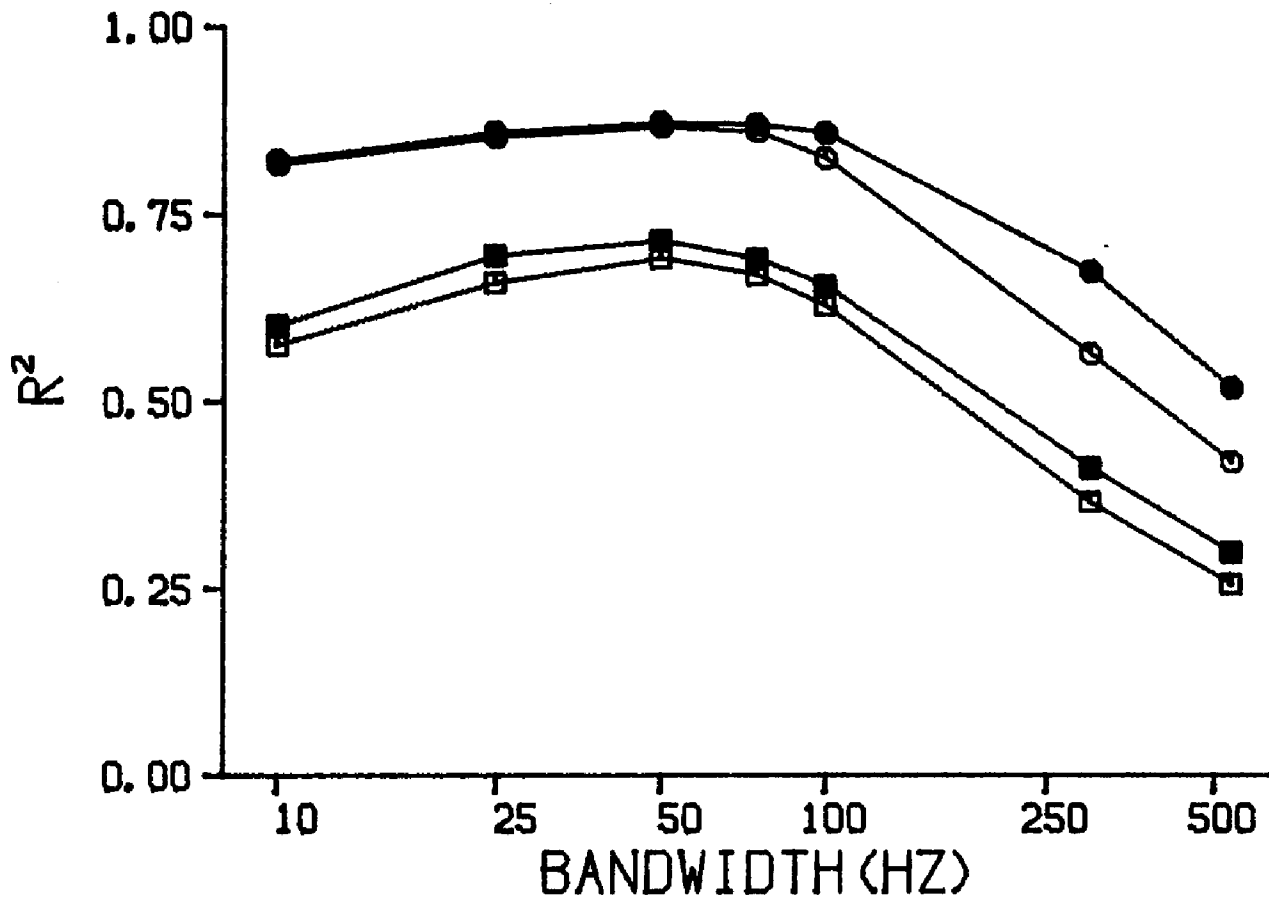


Figure 4.2. R^2 as a function of the bandwidth of the filter and the decay constant of the integrator. Square symbols are for a $10 \text{ Log}(E/N_0)$ of 8.5 dB. Circular symbols are for a $10 \text{ Log}(E/N_0)$ of 11.5 dB. Filled symbols are for Strategy 2. Open symbols are for Strategy 5. In the upper panel, the decay constant of the integrator has been fixed at .01 ms for the filled symbols, and 200 ms for the open symbols. In the bottom panel, the bandwidth of the filter has been fixed at 50 Hz for both filled and open symbols. The results shown are for subject CV.

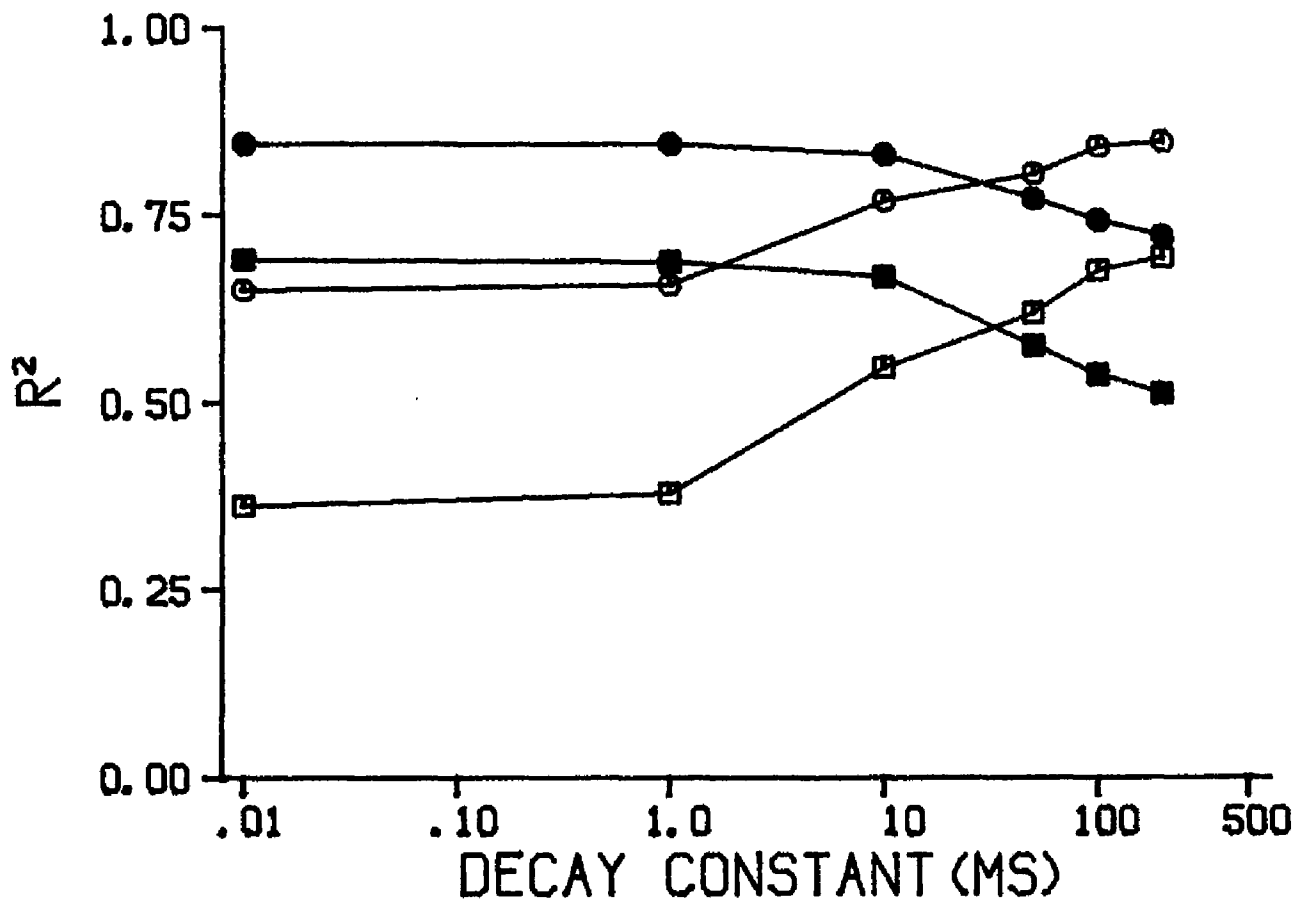
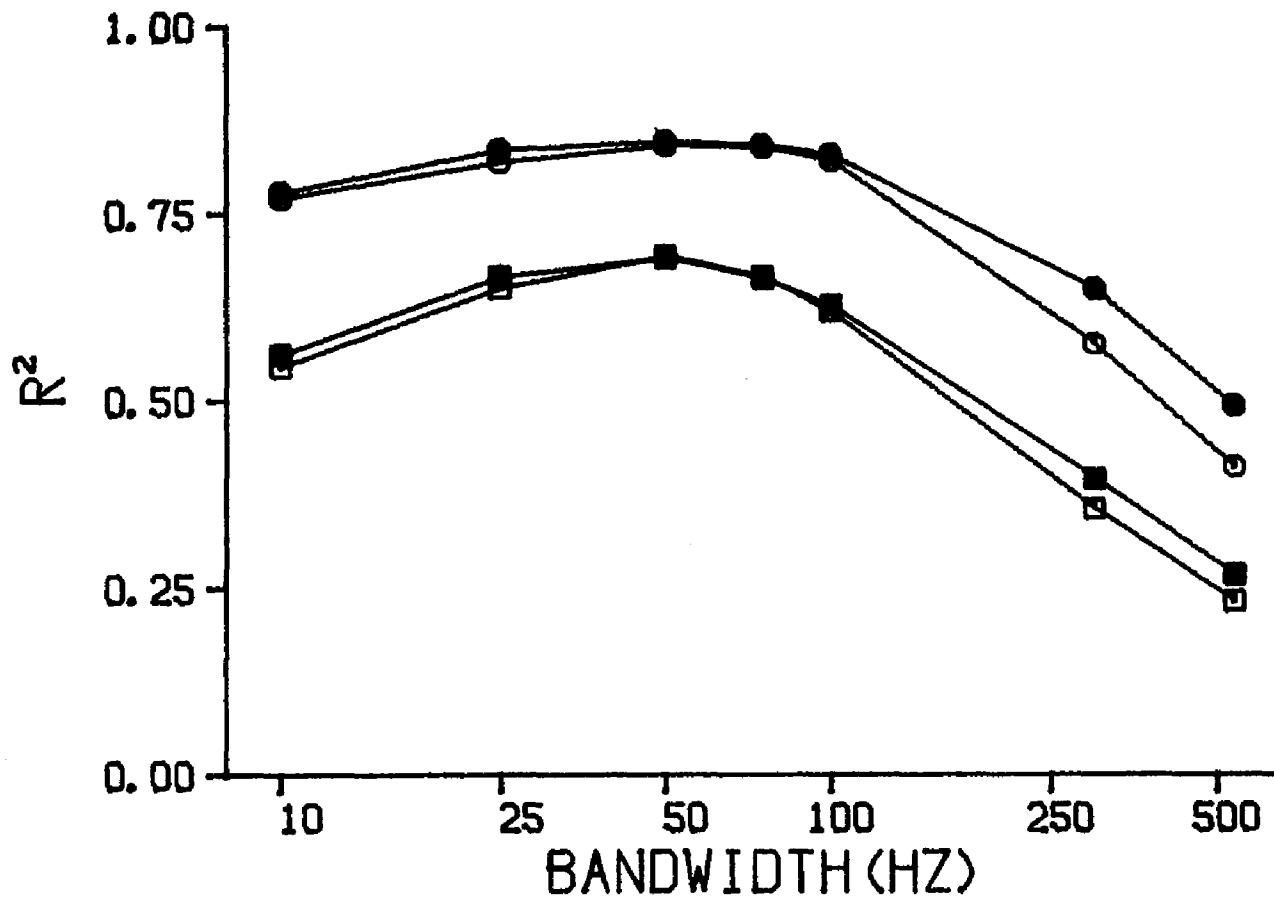


Figure 4.3. R^2 as a function of the bandwidth of the filter and the decay constant of the integrator. Square symbols are for a $10 \text{ Log}(E/N_0)$ of 8.5 dB. Circular symbols are for a $10 \text{ Log}(E/N_0)$ of 11.5 dB. Filled symbols are for Strategy 2. Open symbols are for Strategy 5. In the upper panel, the decay constant of the integrator has been fixed at .01 ms for the filled symbols, and 200 ms for the open symbols. In the bottom panel, the bandwidth of the filter has been fixed at 50 Hz for both filled and open symbols. The results shown are for subject TW.

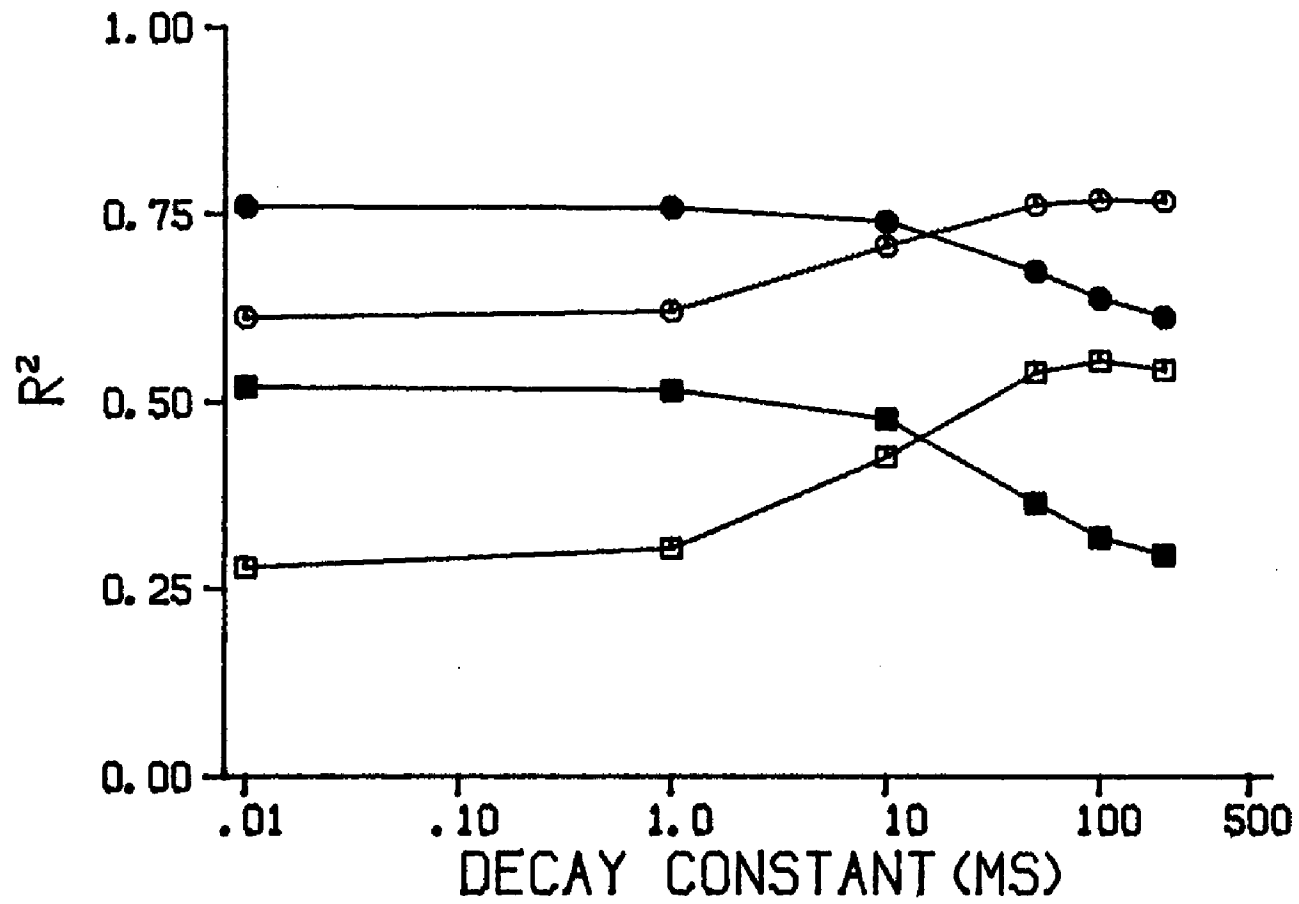
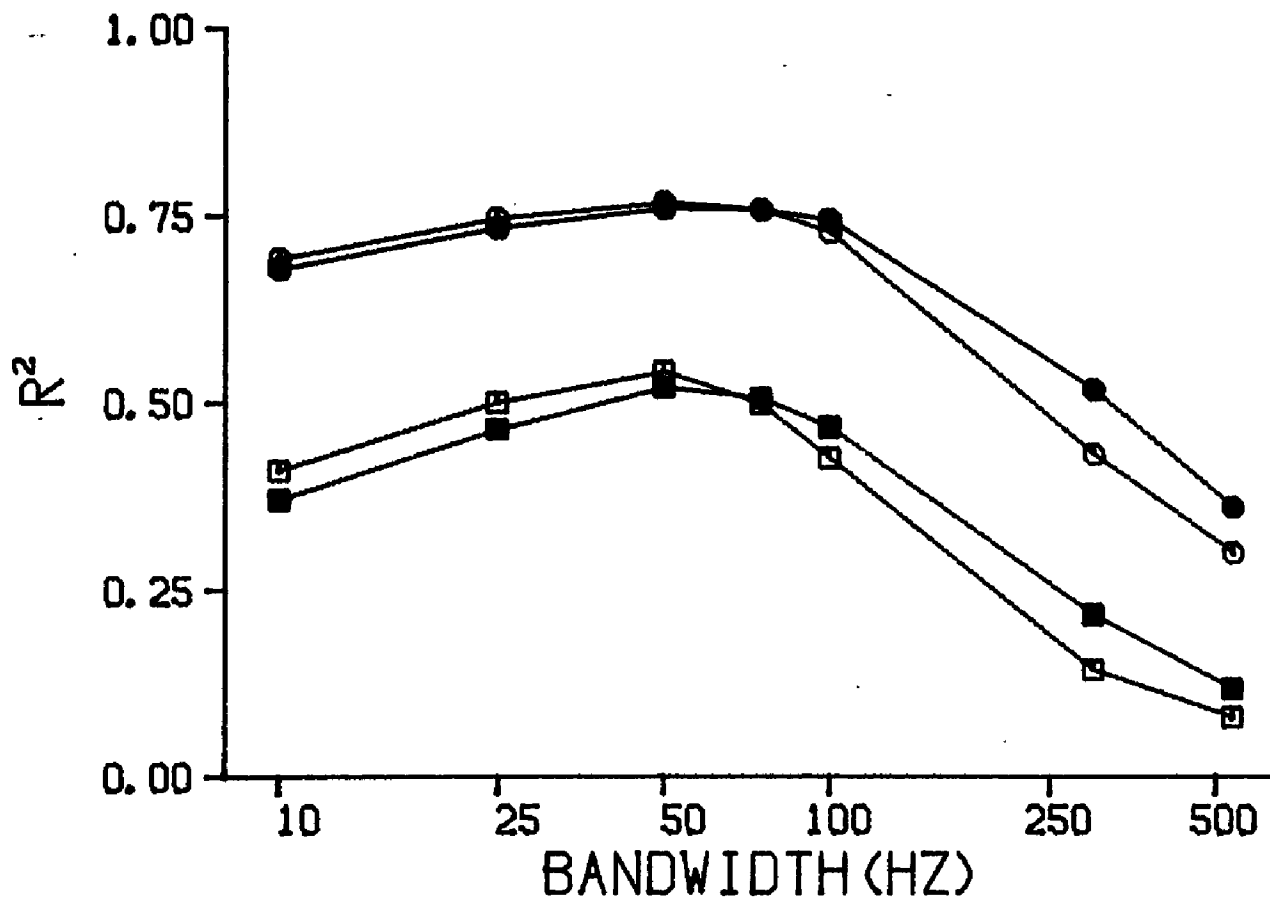
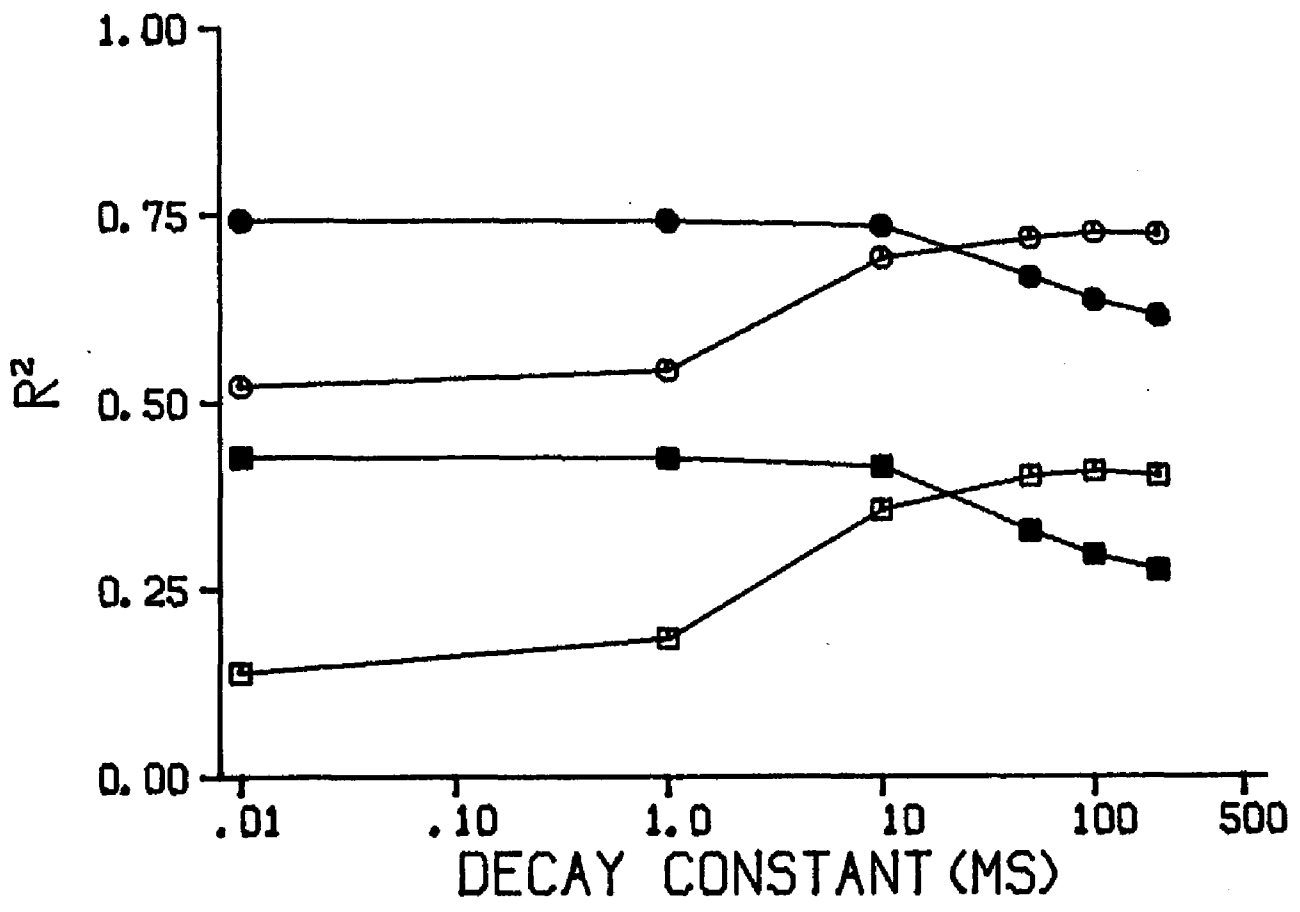
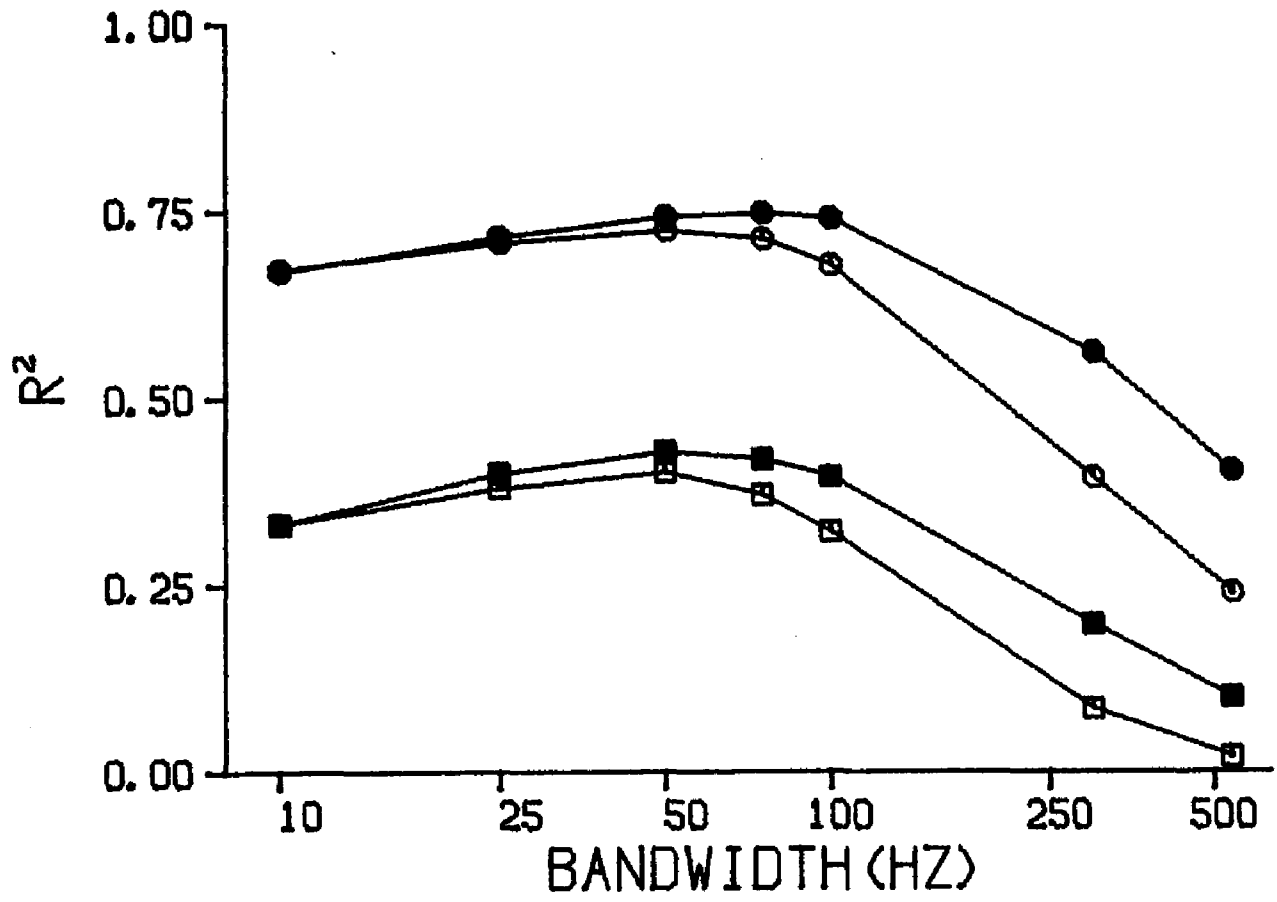


Figure 4.4. R^2 as a function of the bandwidth of the filter and the decay constant of the integrator. Square symbols are for a $10 \text{ Log}(E/N_0)$ of 8.5 dB. Circular symbols are for a $10 \text{ Log}(E/N_0)$ of 11.5 dB. Filled symbols are for Strategy 2. Open symbols are for Strategy 5. In the upper panel, the decay constant of the integrator has been fixed at .01 ms for the filled symbols, and 200 ms for the open symbols. In the bottom panel, the bandwidth of the filter has been fixed at 50 Hz for both filled and open symbols. The results shown are for subject JM.



by the sum of the squared deviations between the $P(Y)$ s and their mean. The square symbols show these initial results obtained at a $10 \text{ Log}(E/N_0)$ of 8.5 dB. The curves for two different sampling strategies are shown. The filled symbols show the results when the decision variable of the model, X' , is the average value of the output of the integration stage during the signal interval (Strategy 2). The open symbols show the results when X' is equal to the maximum value of the output of the integration stage during the stimulus interval (Strategy 5). Strategy 2 is most effective when the decay constant of the integrator is relatively short. The results when the decay constant of the integration stage is .01 ms are shown. Strategy 5 is most effective when the decay constant of the integration stage is relatively long. The results when the decay constant is 200 ms are shown. The peak for both curves is obtained when the bandwidth of the filter is 50 Hz. However, filter bandwidths between 25 Hz and 100 Hz predict the data relatively well. The differences between the two curves are small, particularly near the 50-Hz peak. The similarity of these two curves is to be expected from a consideration of the value of X' in these two cases. For the first case, the .01-ms decay constant is short relative to the 20 KHz sampling rate at which the stimuli were digitized. As a result, the integration stage is functionally removed from the model. That is, the output of the integration stage is identical to the input. However, the sampling strategy averages over the signal interval, and is therefore proportional to true integration (i.e., integration without a "leak"). X' for this case is proportional to the integral of the half-wave rectified filter output over the signal interval. In the second case, the 200-ms decay constant of the integration stage is long relative to the duration of the stimulus. Thus, at the end of the stimulus interval the inputs from the

beginning of the stimulus have not decayed completely and retain approximately half of their original value. That is, because the decay constant is long and the stimulus duration relatively short, the output of the integration stage will, to a rough approximation, be equal to the true integral of the input. Further, when the decay constant of the integrator is relatively long, the output of the integration stage tends to grow throughout the stimulus interval, reaching a maximum near the end of the interval. As a result, X' will be approximately equal to the true integral of the half-wave rectified output of the filter over the stimulus interval. Thus, the values of X' used to compute the two curves are very similar. The circular symbols show the results for $10 \text{ Log}(E/N_0)$ equal to 11.5 dB. As at the lower signal-level, the nonlinear stage of the model is always a half-wave rectifier. At this signal-level the output of the model has been computed only for combinations of filter bandwidth and integrator decay constant which led to relatively high values of R^2 with $10 \text{ Log}(E/N_0)$ equal to 8.5 dB. As can be seen, the shape of the curves is similar to that found at the lower signal-level. The curves are somewhat flatter than those obtained at the lower signal-level, but still peak near 50 Hz. (One of the curves for subject JM reaches a slightly higher value at 75 Hz than at 50 Hz.) The open and closed symbols show the results for the two combinations of integrator decay constant and sampling strategy shown at the lower signal-level. Again, only small differences are found between the two curves.

The lower panel of Figures 4.1 through 4.4 shows the effect of the decay constant of the integrator. The bandwidth of the initial filter has been fixed at 50 Hz. As in the upper panel, the square symbols show the results for $10 \text{ Log}(E/N_0)$ equal to 8.5 dB and the circular symbols show the results for the $10 \text{ Log}(E/N_0)$ equal to 11.5 dB. Except for an overall

increase in R^2 , the results are quite similar at the two signal-levels. The filled symbols show the results when the value of the decision variable, X' , is equal to the average output over the signal interval (Strategy 2), while the unfilled symbols show the results when X' is the maximum output during the stimulus interval (Strategy 5). As can be seen, Strategy 2, the average, is most effective with relatively short decay constants, while Strategy 5, the maximum, is most effective with relatively long decay constants.

Jeffress (1967) reported that for the case when the bandwidth of the initial filter is 50 Hz, the non-linearity is a half-wave rectifier, and the decay constant of the integrator is 1 ms, the model is roughly equivalent to an Envelope Detector. To obtain a value of the decision variable, Jeffress sampled the output of the model at the end of the signal interval (Strategy 3). The results of this form of the Envelope Detector are shown in the first line of Tables 4.1 through 4.4. As can be seen, the model with this strategy is not particularly effective at predicting the data of any of the subjects. However, Strategy 1, averaging the output of the integration stage over the signal interval, proved to be effective. The results for this form of the model are shown in the second line of each table. Jeffress (1967, 1968) found that when the decay constant of the integrator is increased to 50 or 100 ms, the model is better able to fit some of the data. The results for several forms of this Leaky Integrator model can be seen in the tables. When a 50-Hz bandwidth for the filter and a 50-ms decay constant for the integrator are employed, sampling the output of the model near the end of the signal interval (Strategy 3) is relatively effective. However, as can be seen, using the maximum value of the output of the integrator during the stimulus interval (Strategy 5) proved to be even more effective. The

TABLE 4.1

Parameters of various models and R^2 obtained
between the data of subject SG and each model
 $10 \text{ Log}(E/N_0)=8.5 \text{ dB}$

MODEL	BAND- WIDTH	NON- LINEARITY	DECAY CONSTANT	SAMPLING STRATEGY	R^2
Envelope	50 Hz	Half-wave	1 ms	3	.132
Envelope	50 Hz	Half-wave	1 ms	2	.709
Leaky Integrator	50 Hz	Half-wave	50 ms	3	.652
Leaky Integrator	50 Hz	Half-wave	50 ms	5	.661
Leaky Integrator	50 Hz	Half-wave	100 ms	5	.689
Leaky Integrator	75 Hz	Half-wave	50 ms	5	.653
Leaky Integrator	75 Hz	Half-wave	100 ms	5	.674
Energy	25 Hz	Square-law	.01 ms	1	.681
Energy	25 Hz	Square-law	.01 ms	2	.701
*Model 1	50 Hz	Half-wave	.01 ms	2	.716
Model 2	50 Hz	Half-wave	200 ms	5	.692
Frequency Weight					.780
Temporal Weight					.718

(* -- Best fitting model)

TABLE 4.2

Parameters of various models and R^2 obtained
between the data of subject CV and each model
10 Log(E/No)=8.5 dB

MODEL	BAND- WIDTH	NON- LINEARITY	DECAY CONSTANT	SAMPLING STRATEGY	R^2
Envelope	50 Hz	Half-wave	1 ms	3	.115
Envelope	50 Hz	Half-wave	1 ms	2	.687
Leaky Integrator	50 Hz	Half-wave	50 ms	3	.612
Leaky Integrator	50 Hz	Half-wave	50 ms	5	.619
Leaky Integrator	50 Hz	Half-wave	100 ms	5	.676
Leaky Integrator	75 Hz	Half-wave	50 ms	5	.613
Leaky Integrator	75 Hz	Half-wave	100 ms	5	.663
Energy	50 Hz	Square-law	.01 ms	1	.661
Energy	25 Hz	Square-law	.01 ms	2	.661
Model 1	50 Hz	Half-wave	.01 ms	2	.690
*Model 2	50 Hz	Half-wave	200 ms	5	.693
Frequency Weight					.745
Temporal Weight					.733

(* -- best fitting model)

TABLE 4.3

Parameters of various models and R^2 obtained
between the data of subject TW and each model
 $10 \text{ Log}(E/N_0)=8.5$

MODEL	BAND- WIDTH	NON- LINEARITY	DECAY CONSTANT	SAMPLING STRATEGY	R^2
Envelope	50 Hz	Half-wave	1 ms	3	.104
Envelope	50 Hz	Half-wave	1 ms	2	.515
Leaky Integrator	50 Hz	Half-wave	50 ms	3	.502
Leaky Integrator	50 Hz	Half-wave	50 ms	5	.540
*Leaky Integrator	50 Hz	Half-wave	100 ms	5	.555
Leaky Integrator	75 Hz	Half-wave	50 ms	5	.525
Leaky Integrator	75 Hz	Half-wave	100 ms	5	.522
Energy	50 Hz	Square-law	.01 ms	1	.495
Energy	50 Hz	Square-law	.01 ms	2	.505
Model 1	50 Hz	Half-wave	.01 ms	2	.521
Model 2	50 Hz	Half-wave	200 ms	5	.542
Frequency Weight					.587
Temporal Weight					.618

(* -- best fitting model)

TABLE 4.4

Parameters of various models and R^2 obtained
between the data of subject JM and each model
10 Log(E/No)=8.5 dB

MODEL	BAND- WIDTH	NON- LINEARITY	DECAY CONSTANT	SAMPLING STRATEGY	R^2
Envelope	50 Hz	Half-wave	1 ms	3	.033
Envelope	50 Hz	Half-wave	1 ms	2	.425
Leaky Integrator	50 Hz	Half-wave	50 ms	3	.376
Leaky Integrator	50 Hz	Half-wave	50 ms	5	.401
Leaky Integrator	50 Hz	Half-wave	100 ms	5	.407
Leaky Integrator	75 Hz	Half-wave	50 ms	5	.399
Leaky Integrator	75 Hz	Half-wave	100 ms	5	.380
Energy	25 Hz	Square-law	.01 ms	1	.386
Energy	25 Hz	Square-law	.01 ms	2	.408
*Model 1	50 Hz	Half-wave	.01 ms	2	.428
Model 2	50 Hz	Half-wave	200 ms	5	.401
Frequency Weight					.577
Temporal Weight					.482

(* -- best fitting model)

following three lines of the tables show values of R^2 for the Leaky Integrator with other combinations of bandwidth and decay constant which have previously been considered by Jeffress (Strategy 5 is employed in all cases). For each subject, the combination of a 50-Hz bandwidth and a 100-ms decay constant proved to be the most effective form of the Leaky Integrator. It should be noted that although the bandwidths employed here are similar to those used by Jeffress (1967, 1968), the actual shapes of the filters are quite different. Here, a single-tuned filter has been used for both the 50-Hz and 75-Hz bandwidths. Jeffress employed a "steep-sided" 50-Hz bandpass filter and an asymmetric 78-Hz wide filter, which was formed by subtracting the output of a steep 525-Hz low-pass filter and a steep 500-Hz low-pass filter. Although different filter shapes have not been studied in the work reported here, it seems reasonable to assume that changes in the shape of the initial filter would have some influence on the values of R^2 .

All of the results shown in Figures 4.1 through 4.4 were obtained using a half-wave rectifier as the nonlinear stage of the model. As stated in the Introduction, the nonlinear stage of an Energy Detector is a square-law device. The results for this case are shown in Figures 4.5 through 4.8. The values of R^2 are for a $10 \text{ Log}(E/N_0)$ equal to 8.5 dB. The open symbols show the results for the square-law device with the decision variable, X' , equal to the average output of the integration stage over the signal interval (Strategy 2). For comparison, the filled symbols show the results for the half-wave rectifier and Strategy 2, shown previously in Figures 4.1 through 4.4. As can be seen, the curves for these two cases are quite similar. The curves for the square-law device tend to peak at lower bandwidth than those obtained with the half-wave rectifier. For three out of four subjects, slightly higher values of R^2 are found at

Figure 4.5. R^2 as a function of the bandwidth of the filter and the decay constant of the integrator. The filled symbols are for a half-wave rectifier. The open symbols are for a square-law device. In the upper panel, the decay constant of the integrator was .01 ms. In the lower panel, the bandwidth of the filter was 50 Hz. All values are for a $10 \text{ Log}(E/N_0)$ of 8.5 dB and Strategy 2. The results shown are for subject SG.

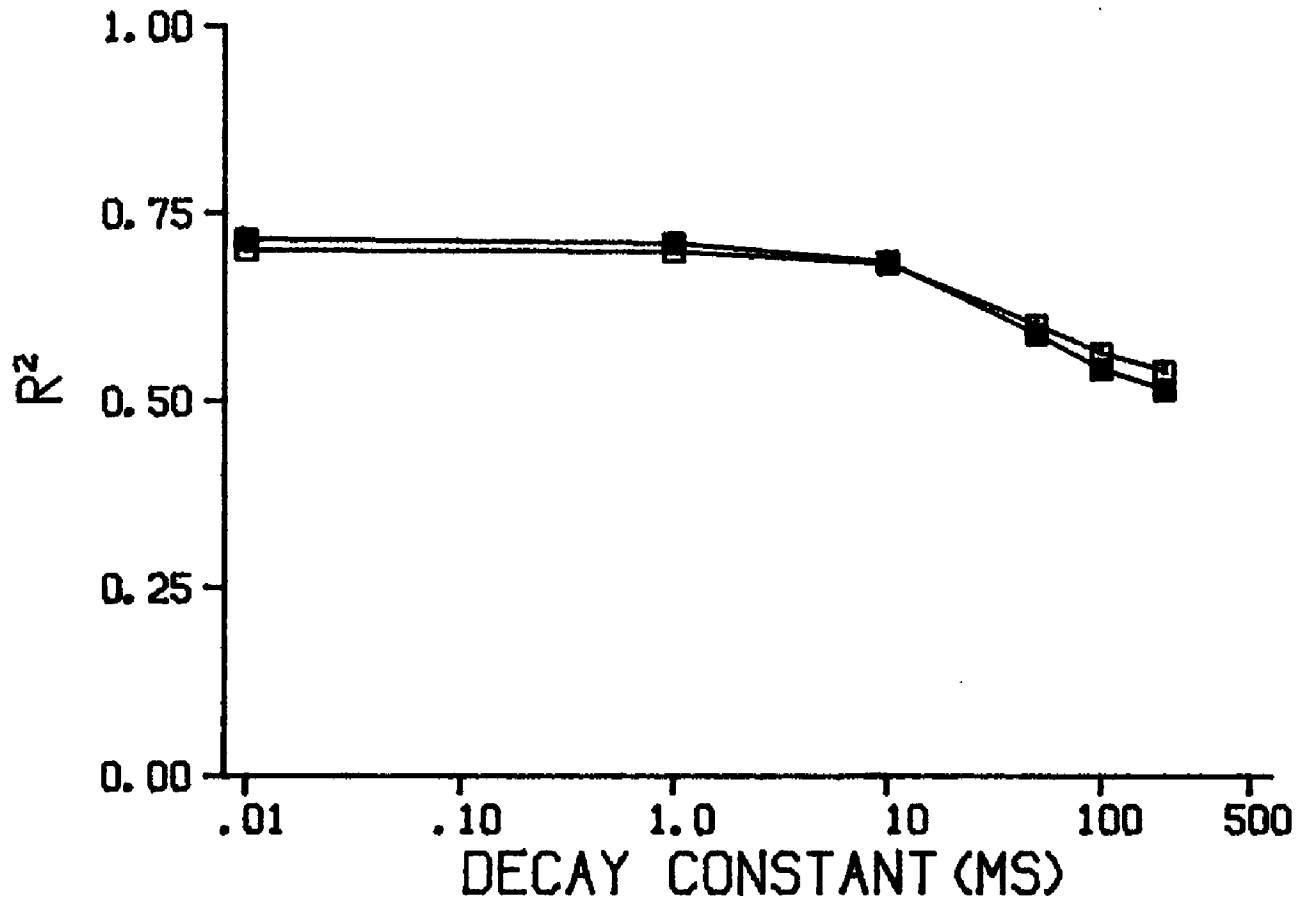
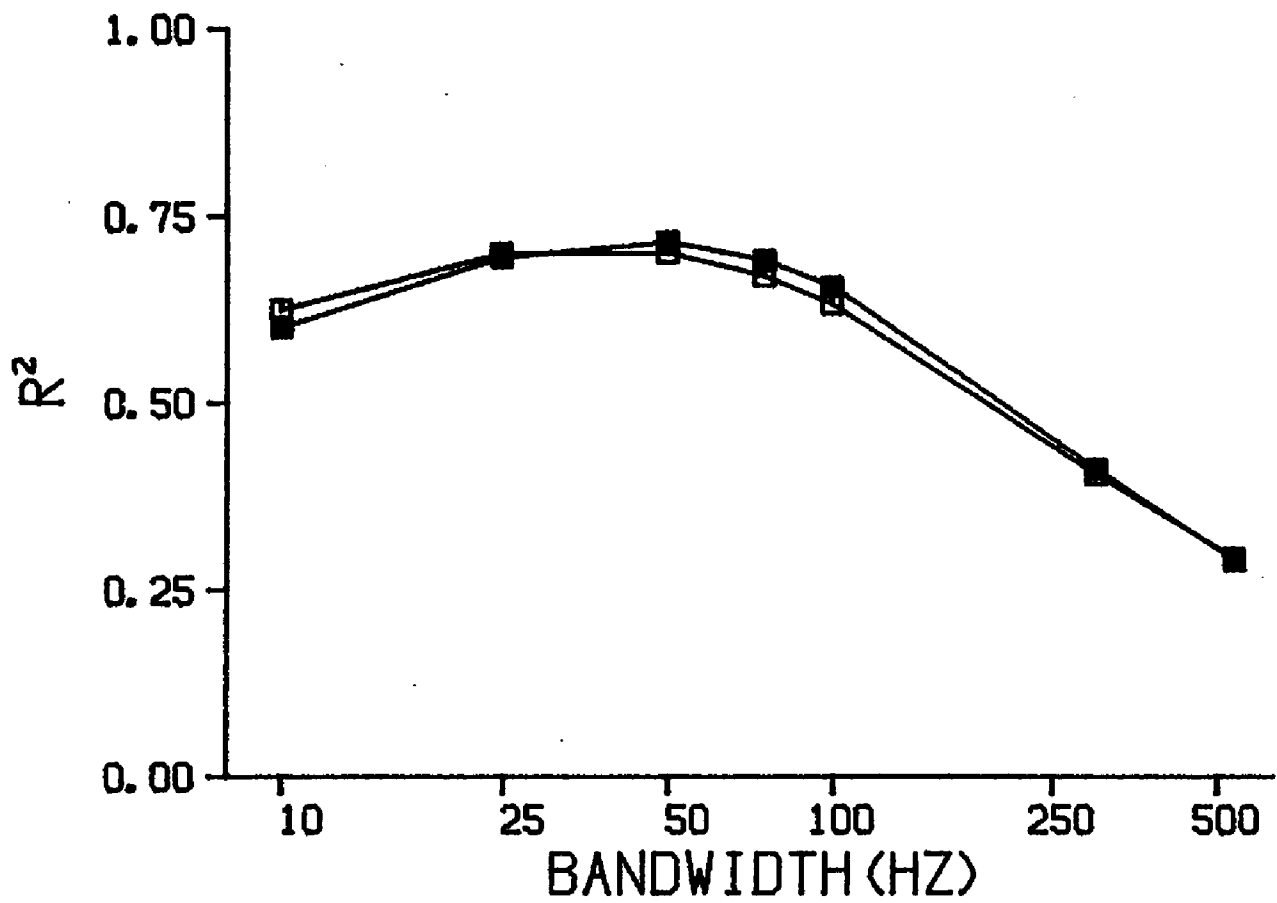


Figure 4.6. R^2 as a function of the bandwidth of the filter and the decay constant of the integrator. The filled symbols are for a half-wave rectifier. The open symbols are for a square-law device. In the upper panel, the decay constant of the integrator was .01 ms. In the lower panel, the bandwidth of the filter was 50 Hz. All values are for a $10 \text{ Log}(E/N_0)$ of 8.5 dB and Strategy 2. The results shown are for subject CV.

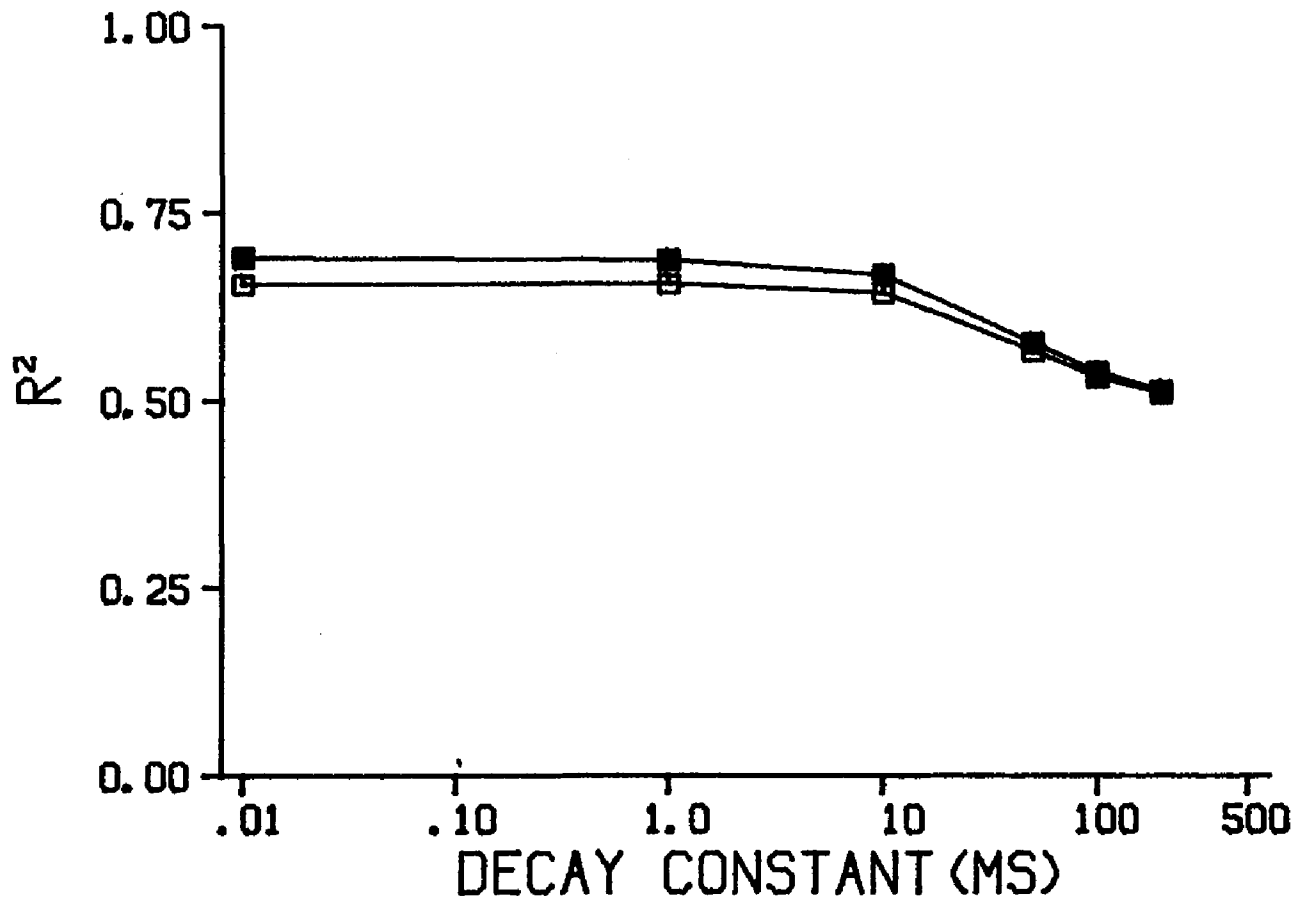
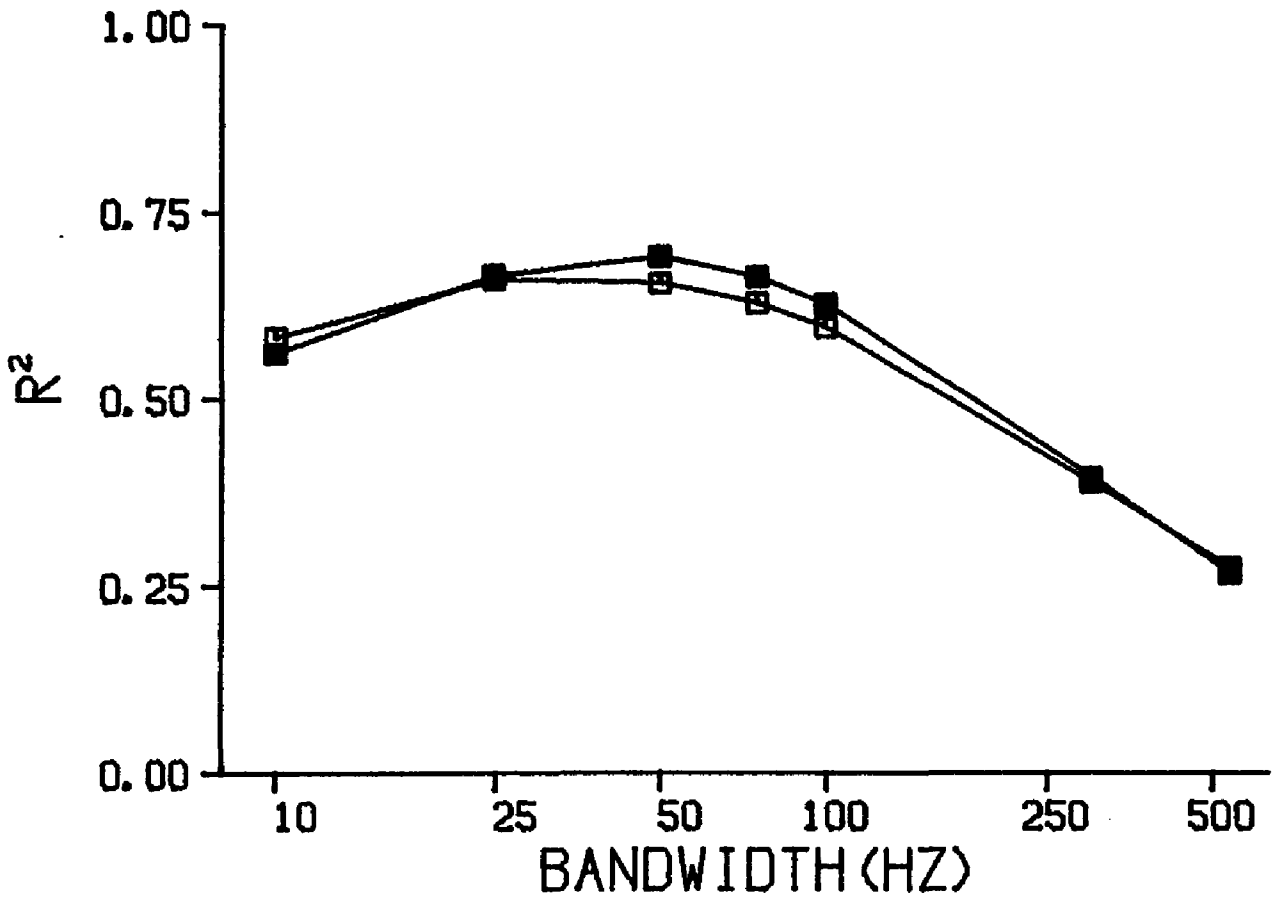


Figure 4.7. R^2 as a function of the bandwidth of the filter and the decay constant of the integrator. The filled symbols are for a half-wave rectifier. The open symbols are for a square-law device. In the upper panel, the decay constant of the integrator was .01 ms. In the lower panel, the bandwidth of the filter was 50 Hz. All values are for a 10 Log(E/No) of 8.5 dB and Strategy 2. The results shown are for subject TW.

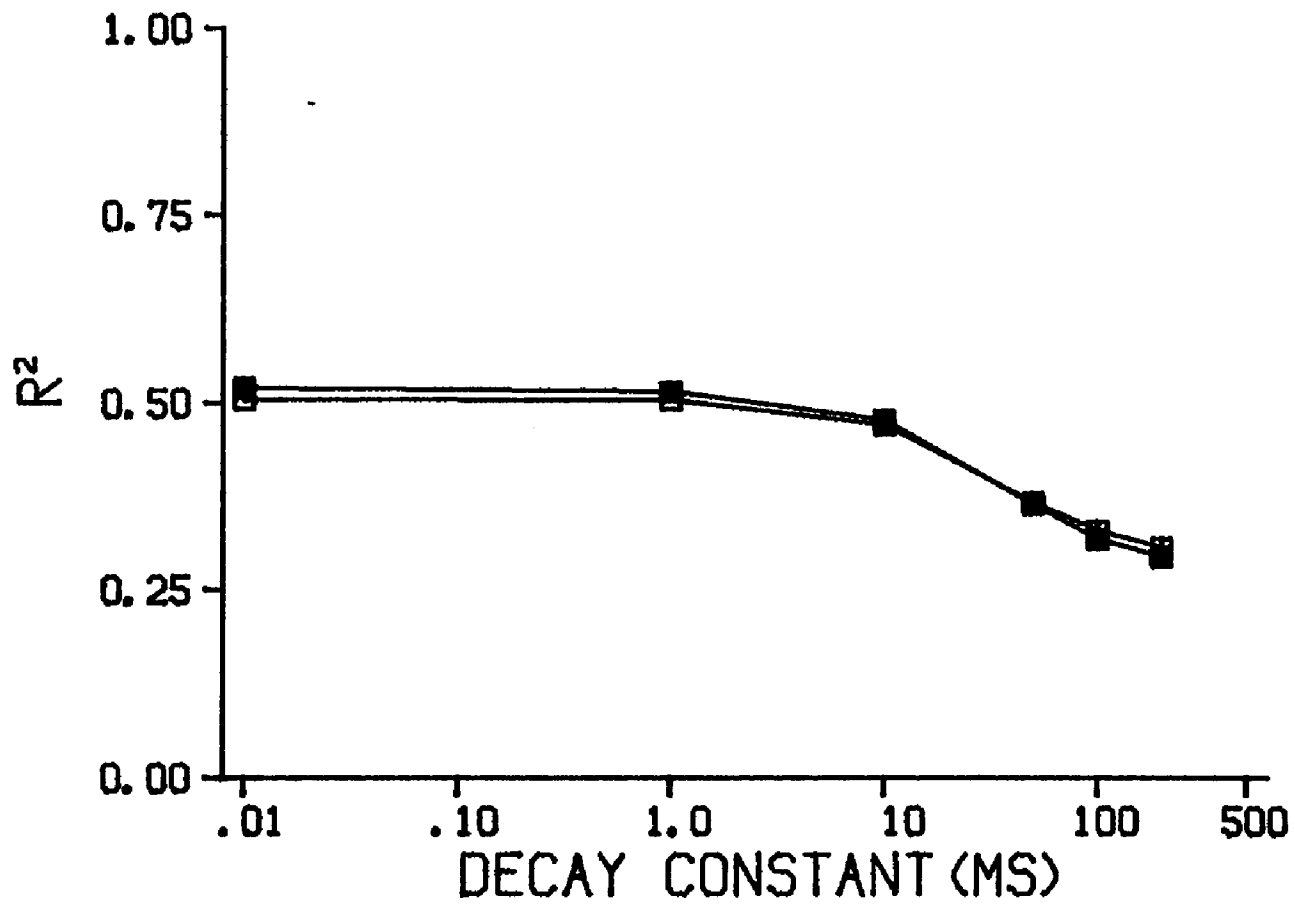
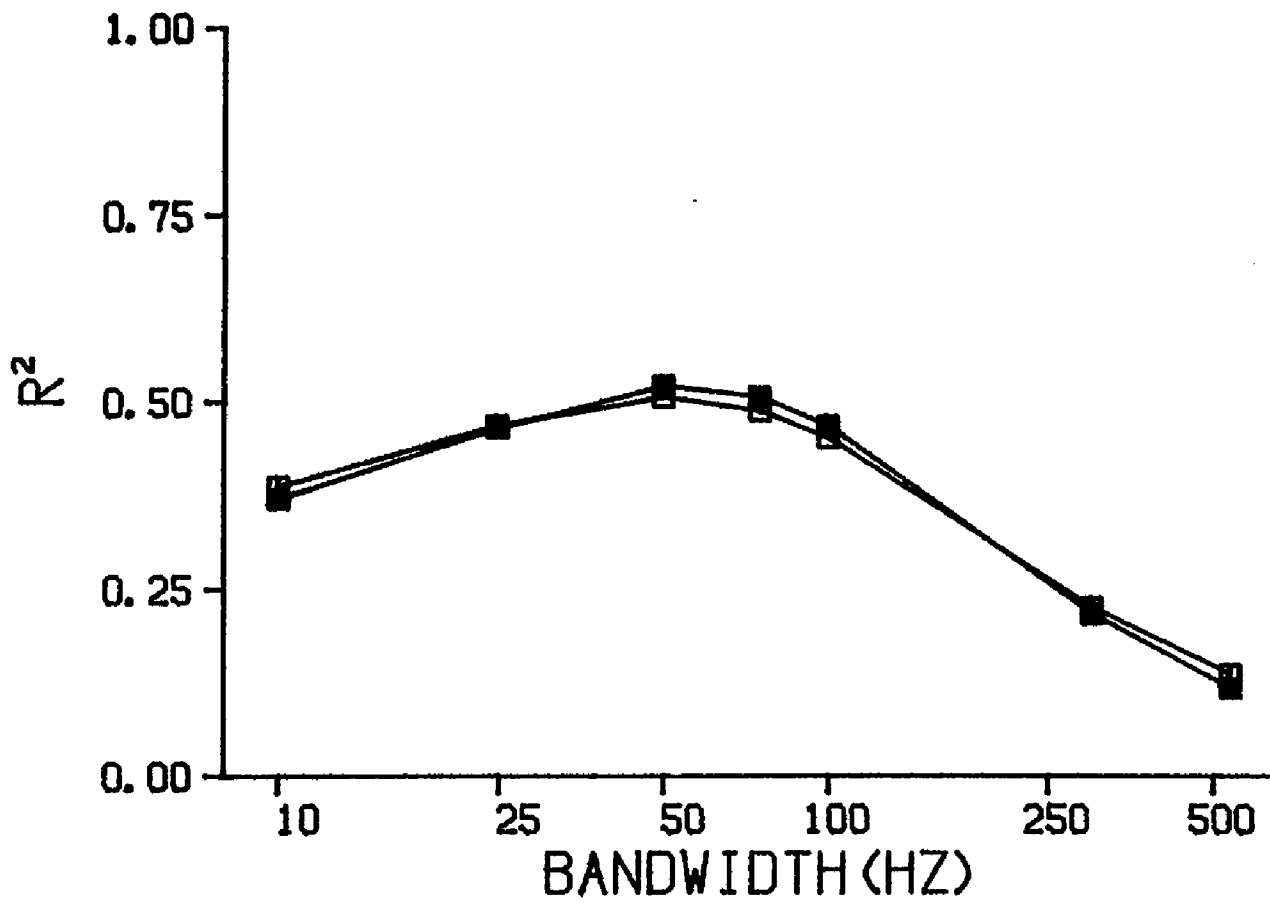
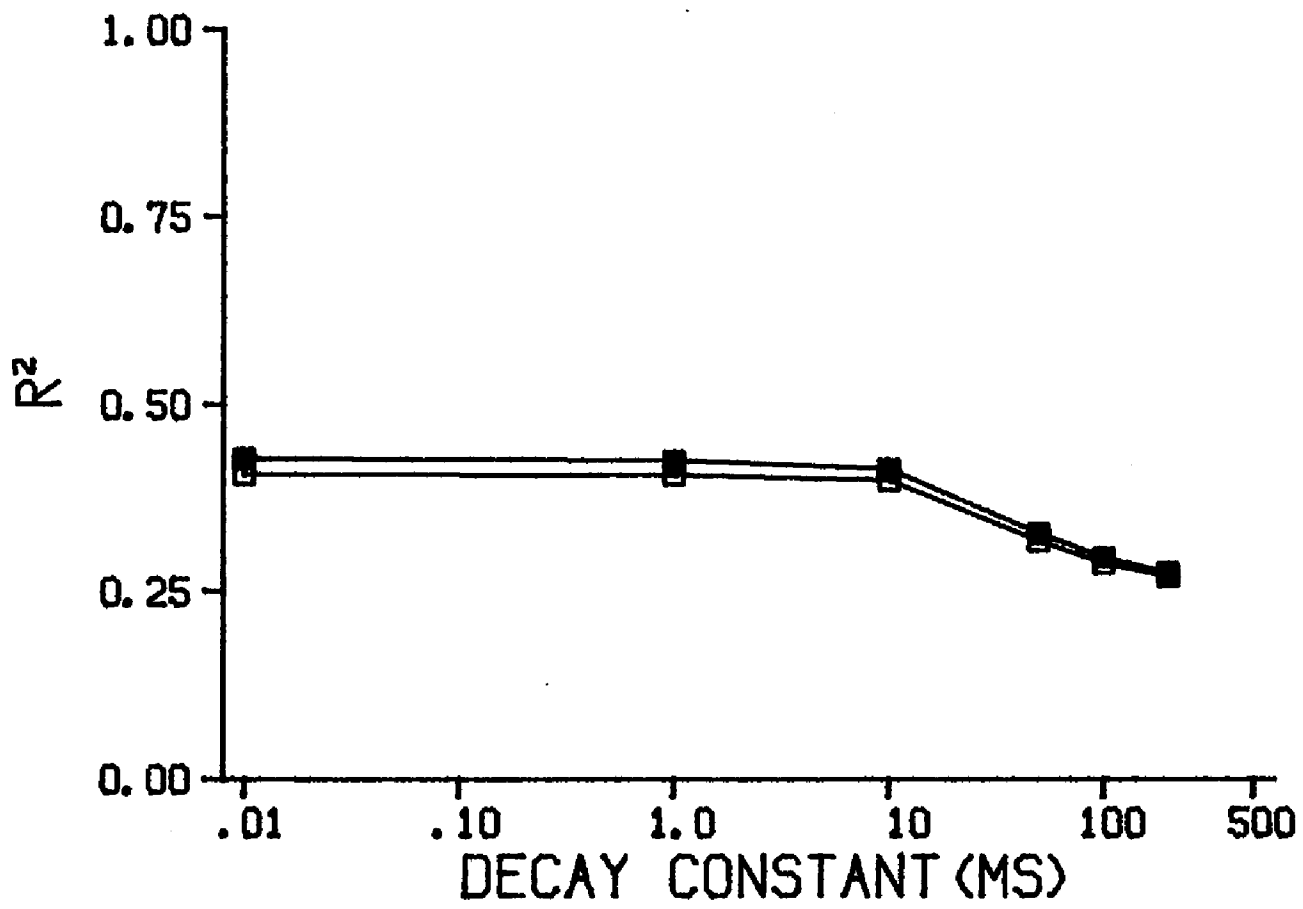
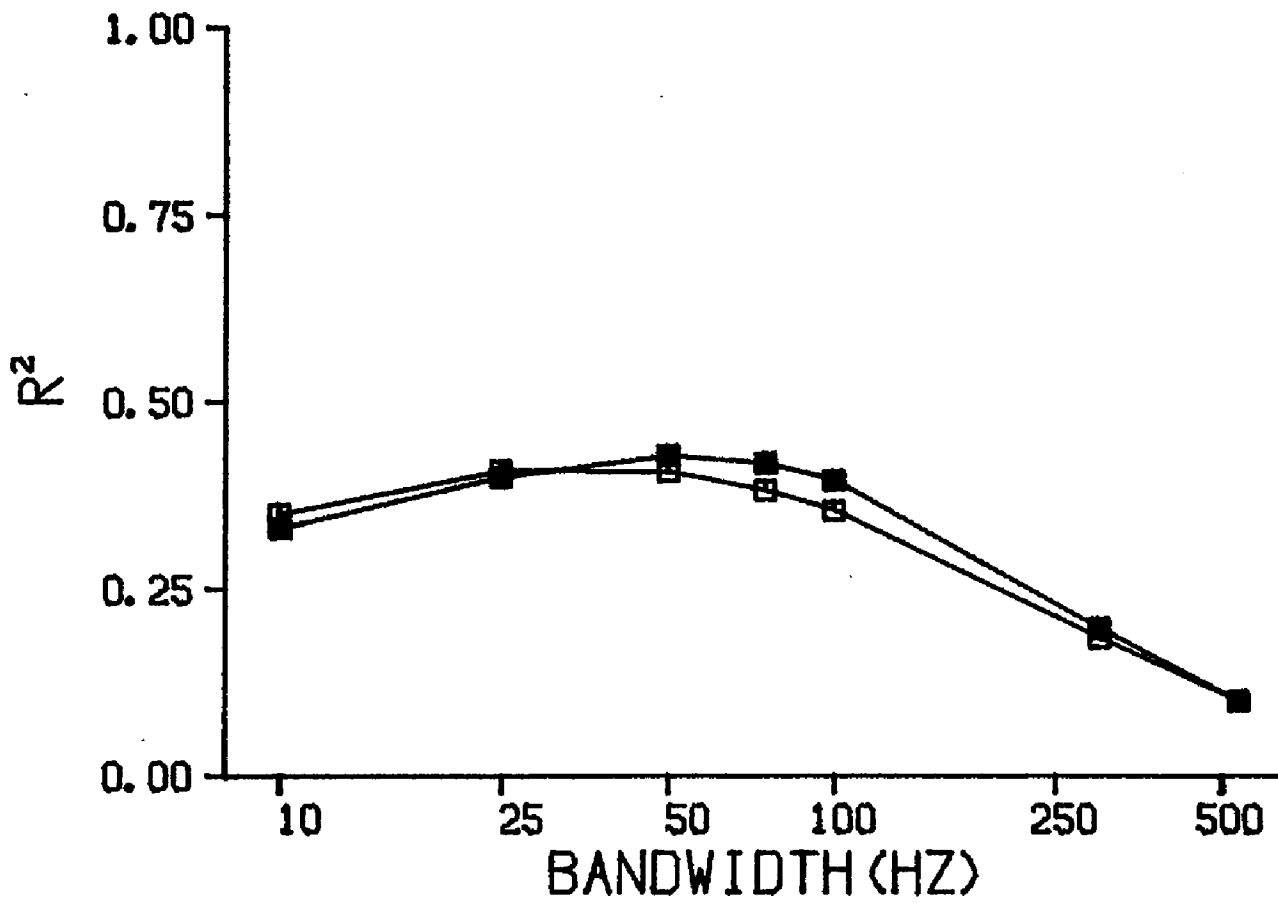


Figure 4.8. R^2 as a function of the bandwidth of the filter and the decay constant of the integrator. The filled symbols are for a half-wave rectifier. The open symbols are for a square-law device. In the upper panel, the decay constant of the integrator was .01 ms. In the lower panel, the bandwidth of the filter was 50 Hz. All values are for a 10 Log(E/No) of 8.5 dB and Strategy 2. The results shown are for subject JM.



25 Hz than at 50 Hz. The highest value of R^2 obtained by the square-law device is almost as high as that obtained by the half-wave rectifier. However, for all subjects the half-wave rectifier proved to be more effective at predicting their responses. For the typical configuration of the Energy Detector, the integration stage of the model is assumed to be a true integrator. As mentioned previously, true integration can be accomplished within the current model by providing the integration stage with a very short decay constant (effectively removing this stage from the model) and allowing the integration to be performed by the sampling strategy. Either Strategy 1, averaging over the stimulus interval, or Strategy 2, averaging over the signal interval, is appropriate. The results for both of these cases are shown in Tables 4.1 through 4.4. In both cases, the bandwidth shown is the one which leads to the maximum value of R^2 .

The Envelope Detector, the Leaky Integrator and the Energy Detector all predict the data relatively well. The differences in R^2 between the models are, in general, fairly small. For three out of four subjects, the combination of an Envelope Detector and Strategy 2, averaging over the signal interval, yielded the highest value of R^2 for any of the models thus far considered. For subject TW, the Leaky Integrator with the 50-Hz bandwidth and 100-ms decay constant proved to be the most effective model. For each subject, the value of R^2 could be increased, relative to that obtained by the combination of an Envelope Detector and Strategy 2, by shortening the decay constant of the integrator to .01 ms (i.e., removing the integration stage from the model). This particular configuration: 50-Hz wide single-tuned filter, half-wave rectifier, integrator with a .01-ms decay constant and Strategy 2; will be referred to as Model 1. For two subjects, this model proved to be the most

effective configuration of the general model of Jeffress (1967). For two subjects, a closely related configuration: 50-Hz wide single-tuned filter, half-wave rectifier, integrator with a 200-ms decay constant and Strategy 5; yielded somewhat larger values of R^2 . This configuration will be referred to as Model 2. Although Model 1 is able to predict the data of subject CV nearly as well, Model 2 is best able to predict her data. The results for both Model 1 and Model 2 can be seen in Tables 4.1 through 4.4. As mentioned previously, for subject TW the best-fitting form of the model is the Leaky Integrator with a bandwidth of 50 Hz and a decay constant of 100 ms.

All of the models shown in Tables 4.1 through 4.4 correlate about equally well with the data. That is, the changes in parameters suggested by these models have relatively minor influences on the value of R^2 . This can also be seen from an inspection of Figures 4.1 through 4.8. Although the curves relating R^2 to the bandwidth of the filter tend to peak at 50 Hz, bandwidths between 25 Hz and 100 Hz all predict the data relatively well. Further, changes in the decay constant, which range over several orders of magnitude, make only minor changes in the value of R^2 . There are several possible explanations for the insensitivity of the model-fitting procedures to changes in the parameters of the general model. If, for example, the bandwidth used by the subject varied from trial to trial, we might expect that the average bandwidth would predict the data most accurately. However, other bandwidths within the range used by the subject might predict the data almost as well. As a result, flat curves like those seen in Figures 4.1 through 4.4 would be expected. A second explanation, which is also compatible with the fact that the values of R^2 obtained are relatively low, is that the "true" model of auditory detection is quite different from any of the models we have

investigated, and therefore the models tested fit the data about equally poorly. On the other hand, the fact that so many models can be incorporated within the single structure suggested by Jeffress (1967) indicates that these models are relatively similar. If the outputs of the models are highly correlated, then the correlations between each of the models and the subject will be similar. Thus, there are at least three possible explanations of the general model's apparent insensitivity to parametric manipulations. First, there may be a problem in the data which are being modeled (i.e., they may be influenced by some form of internal variability). Second, there may be a problem in the models which are being applied to the data (i.e., their structure may not be adequate to the task of modeling the auditory system). Third, the techniques used to determine the best-fitting model may themselves be relatively insensitive (i.e., large changes in R^2 may not be expected when manipulating parameters over a moderate range). It is difficult to establish a priori if these factors are influencing the results reported here, or even to determine exactly what the effects of these factors would be if they were present.

One way to obtain a better understanding of these issues is to attempt to model a known system rather than a human subject. Thus far the system to be investigated has been the human subject. We can, however, replace the human with Model 1, as the system to be investigated, and then generate curves for Model 1 like those which were shown for the human subjects in Figures 4.1 through 4.4. Remember, Model 1 is a fixed parameter model composed of: a 50-Hz filter, a half-wave rectifier, an integration stage which has functionally been removed from the circuit, and a sampling strategy which averages over the signal interval (Strategy 2). If the curves relating bandwidth to R^2 with Model 1 as the

system to be investigated are flat like those found for human subjects, then the possibility that the bandwidth used by the subject varies from trial to trial need not be introduced; the bandwidth of Model 1 is fixed. Further, the structure of the models considered here are certainly adequate to the task of modeling Model 1. Indeed, one combination of parameters will fit Model 1 perfectly. Similarly, the output of Model 1 can be related to the outputs of each of the models reported in Tables 4.1 through 4.4, thereby generating such a table for Model 1. Again, if we find that all the models are reasonably well able to predict the data of Model 1, then the similar ability of these models to predict the data of the human subjects would not be surprising.

Figures 4.9 and 4.10 show curves like those in Figures 4.1 through 4.4 except they are computed with Model 1 as the system to be investigated. The results in Figure 4.9 are for $10 \text{ Log}(E/N_0)$ equal to 8.5 dB, while the results in Figure 4.10 are for $10 \text{ Log}(E/N_0)$ equal to 11.5 dB. As in the figures for individual subjects, the filled symbols are for the case where X' is equal to the average value of the output of the integration stage over the signal interval (Strategy 2). The open symbols are for the case where X' is equal to the maximum value of the integration stage during the stimulus interval (Strategy 5). In the upper panel, the filled symbols are with the decay constant of the integration stage equal to .01 ms (i.e., the waveform passes through the integration stage unaltered). The unfilled symbols are with the decay constant of the integration stage equal to 200 ms. In the lower panel, the bandwidth of the initial filter is fixed at 50 Hz for both curves. Like those for the human subjects, these curves show a rather flat response as a function of the bandwidth of the initial filter. Again, both curves peak at a 50-Hz bandwidth, but bandwidths between 25 Hz and 100 Hz all predict the output

Figure 4.9. R^2 as a function of the bandwidth of the filter and the decay constant of the integrator. Filled symbols are for Strategy 2. Open symbols are for Strategy 5. In the upper panel, the decay constant of the integrator has been fixed at .01 ms for the filled symbols, and 200 ms for the open symbols. In the bottom panel, the bandwidth of the filter has been fixed at 50 Hz for both filled and open symbols. All points were obtained with $10 \text{ Log}(E/N_0)$ equal to 8.5 dB. The results shown are for Model 1 as the system to be investigated.

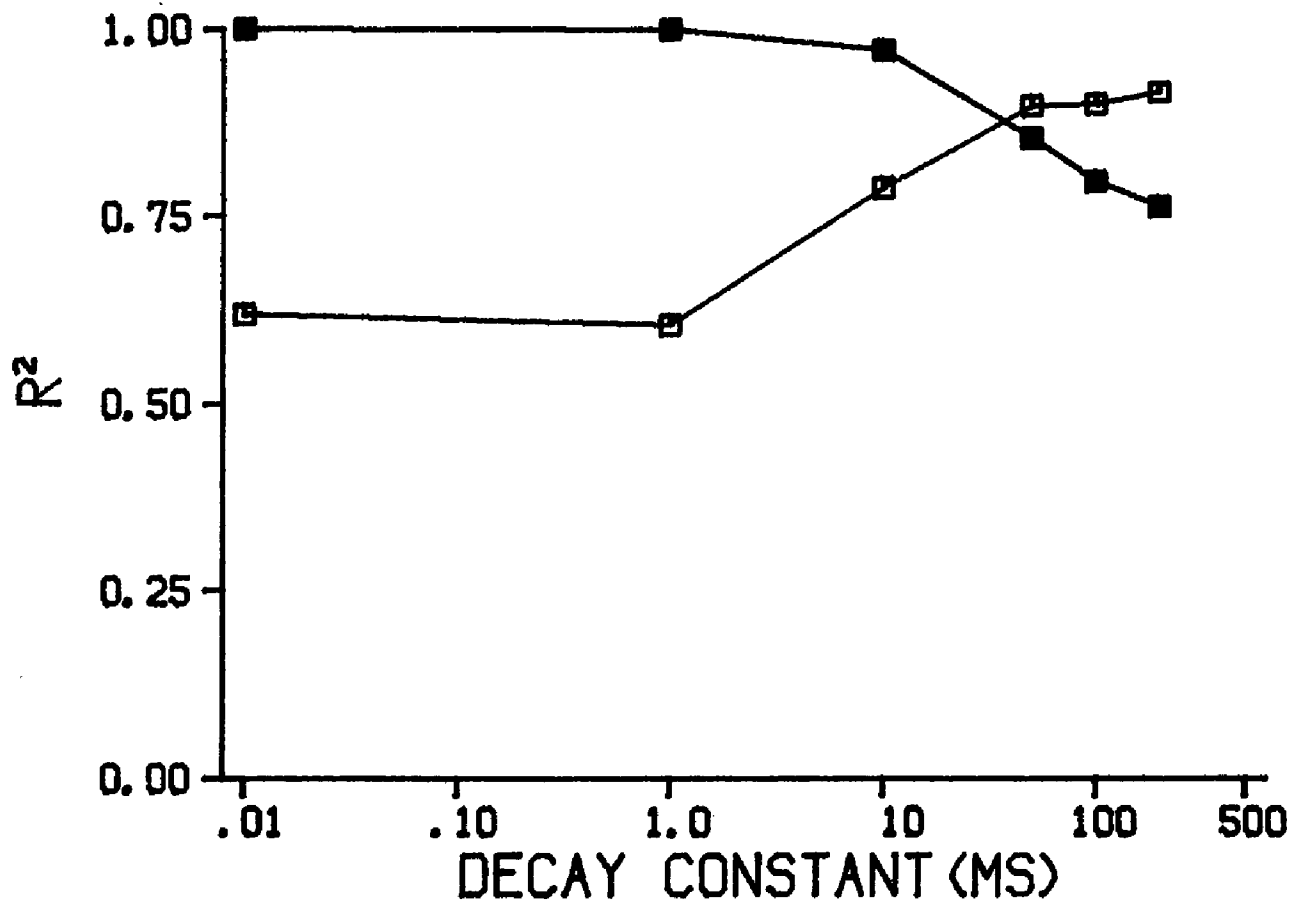
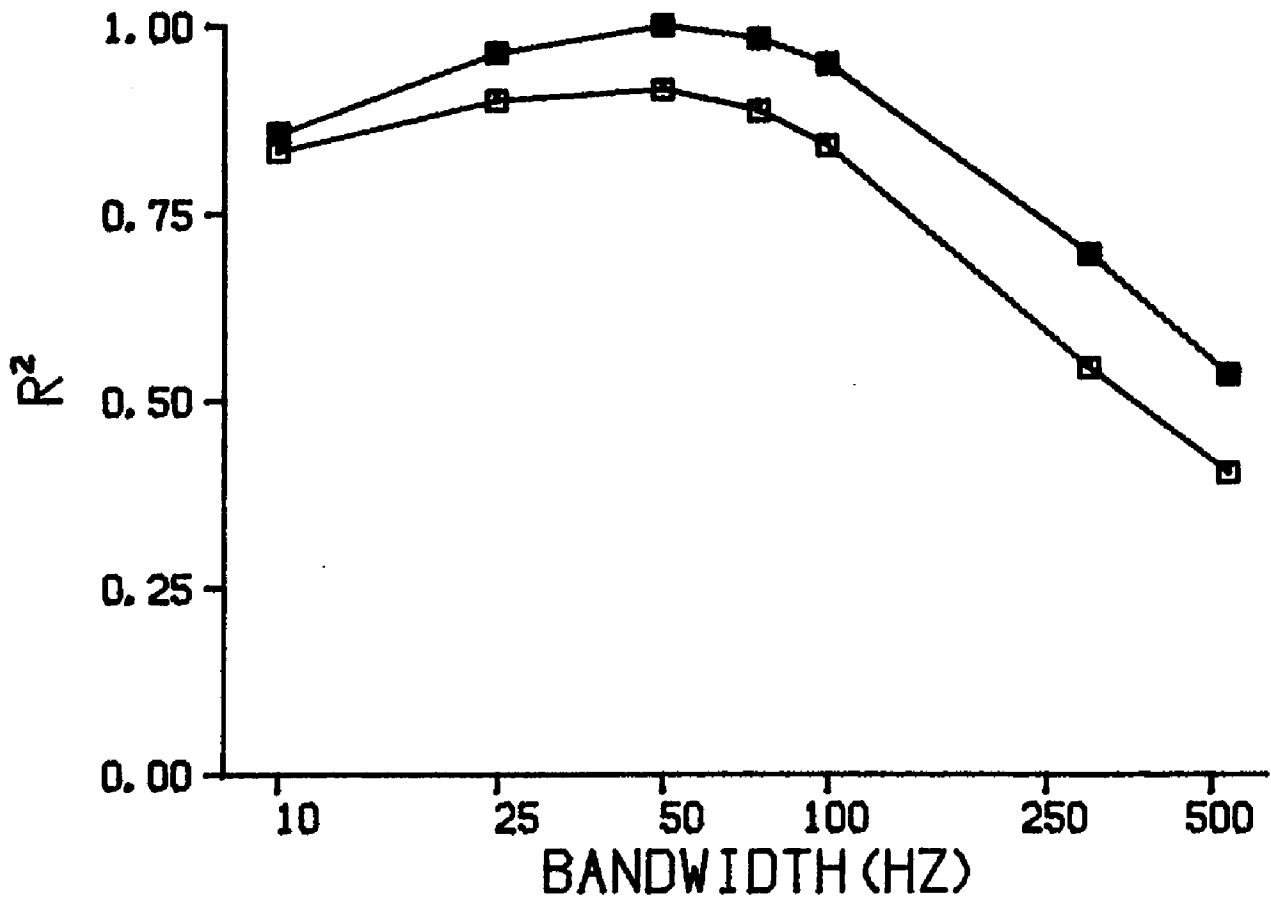
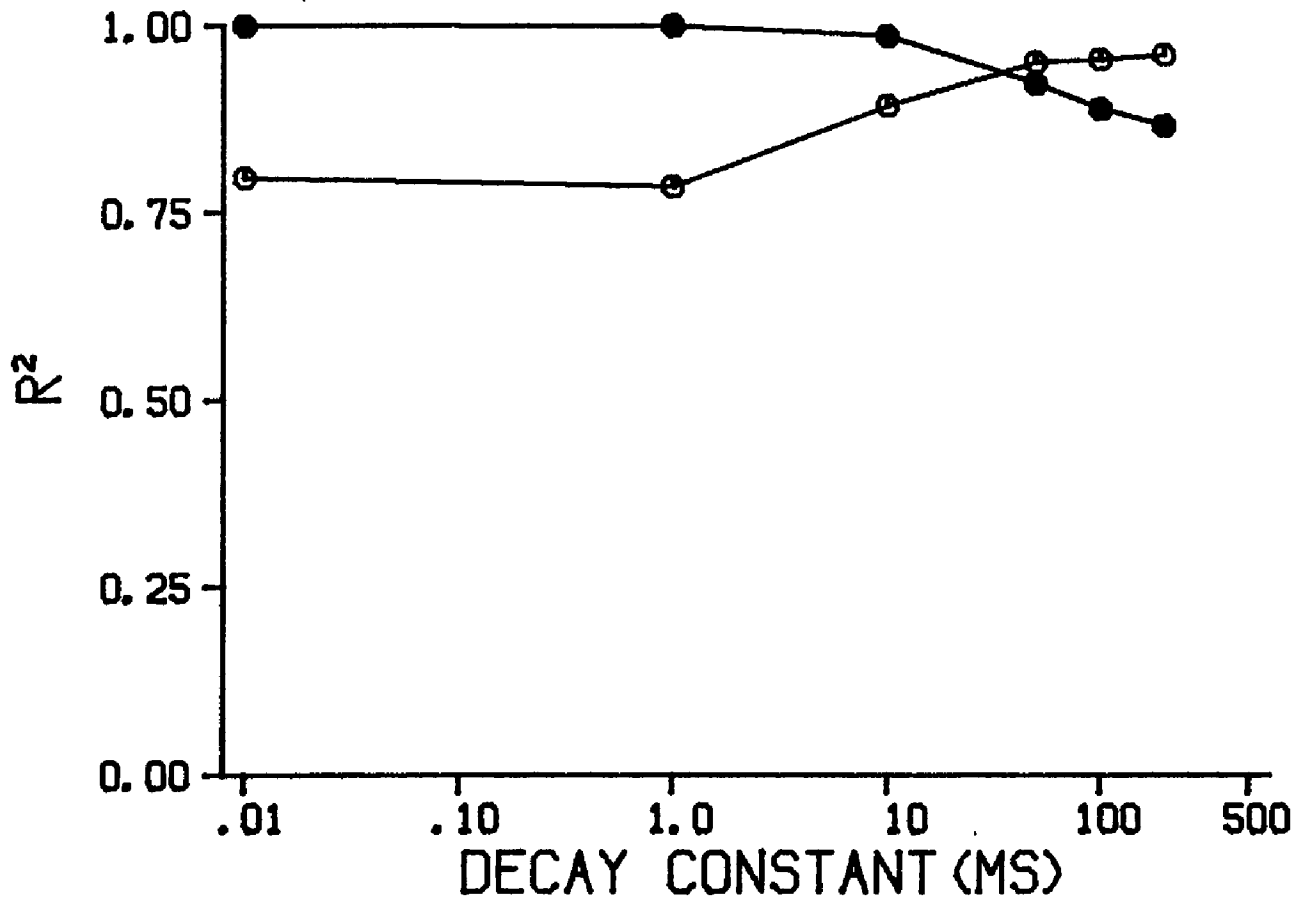
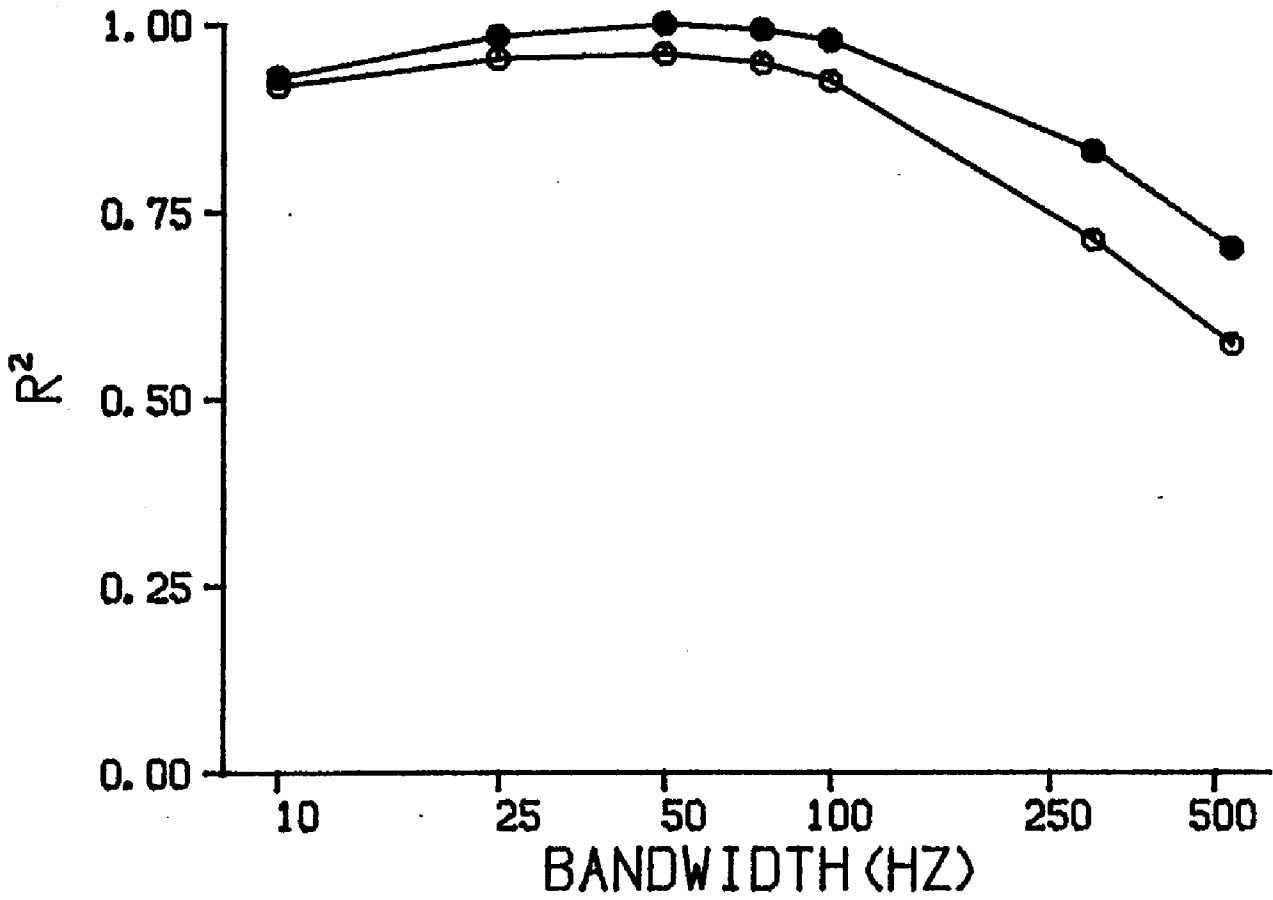


Figure 4.10. R^2 as a function of the bandwidth of the filter and the decay constant of the integrator. Filled symbols are for Strategy 2. Open symbols are for Strategy 5. In the upper panel, the decay constant of the integrator has been fixed at .01 ms for the filled symbols, and 200 ms for the open symbols. In the bottom panel, the bandwidth of the filter has been fixed at 50 Hz for both filled and open symbols. All points were obtained with $10 \text{ Log}(E/N_0)$ equal to 11.5 dB. The results shown are for Model 1 as the system to be investigated.



of Model 1 relatively well. The curves obtained at a $10 \text{ Log}(E/N_0)$ of 11.5 dB are even flatter than those obtained at a $10 \text{ Log}(E/N_0)$ of 8.5 dB. These results indicate that the value of R^2 is not dramatically affected by small changes in the bandwidth of the initial filter even when the system under investigation has a fixed bandwidth. Therefore, it is not necessary to assume a variable bandwidth to explain the bandwidth curves for human subjects shown in Figures 4.1 through 4.4. Similarly, the flat curves obtained for Model 1 cannot be explained by assuming that no combination of parameters is adequately predicting the output of Model 1. One combination is predicting perfectly. Considering the data in the lower panels of Figures 4.9 and 4.10, it can be seen that changes in the value of the decay constant over several orders of magnitude may have a minimal effect on the value of R^2 . Those regions of the curves where relatively large changes in R^2 are observed are the same regions where relatively large changes were observed for human subjects. The ability of the various models to predict the data for Model 1 is shown by the values of R^2 in Table 4.5. Most of the models are able to predict the outputs of Model 1 relatively well. Further, the values of R^2 for most of the models are reasonably similar.

The results from Figures 4.9 and 4.10 and from Table 4.5 demonstrate that even for the case of a fixed parameter ("noiseless") subject, like Model 1, many different models predict the data well. The techniques employed are not particularly sensitive to changes in the parameters under investigation, and the outputs of the models are highly correlated. Additional insights into the data of the human subjects can be gained by a more thorough investigation of Model 1 as a system to be modeled. Ahumada and his associates (Ahumada, 1967; Ahumada and Lovell, 1971; and Ahumada, Marken and Sandusky, 1975) have consistently found differences

TABLE 4.5

Parameters of various models and R^2 obtained
between the output of Model 1 and each model
 $10 \text{ Log}(E/N_0)=8.5 \text{ dB}$

MODEL	BAND- WIDTH	NON- LINEARITY	DECAY CONSTANT	SAMPLING STRATEGY	R^2
Envelope	50 Hz	Half-wave	1 ms	3	.112
Envelope	50 Hz	Half-wave	1 ms	2	.998
Leaky Integrator	50 Hz	Half-wave	50 ms	3	.894
Leaky Integrator	50 Hz	Half-wave	50 ms	5	.897
Leaky Integrator	50 Hz	Half-wave	100 ms	5	.899
Leaky Integrator	75 Hz	Half-wave	50 ms	5	.883
Leaky Integrator	75 Hz	Half-wave	100 ms	5	.874
Energy	25 Hz	Square-law	.01 ms	1	.930
Energy	50 Hz	Square-law	.01 ms	2	.985
Model 1	50 Hz	Half-wave	.01 ms	2	1.00
Model 2	50 Hz	Half-wave	200 ms	5	.915

between signal-plus-noise trials and noise-alone trials. First, their ability to predict responses on noise-alone trials is almost always less than their ability to predict responses on signal-plus-noise trials. Second, bandwidth estimates obtained for noise-alone trials tend to be wider than those obtained for signal-plus-noise trials. The models considered here have also been less able to predict responses on noise-alone trials. However, bandwidth estimates are at most slightly wider on noise-alone trials than on signal-plus-noise trials. Ahumada has argued that a model composed of a bank of several relatively narrow filters should be able to predict the data. The decision variable for this "filter-bank" model is functionally related to the magnitude of the largest output of any filter within the bank. Ahumada and his associates have found relatively little support for such a model within their data.

Can either of these discrepancies between noise-alone and signal-plus-noise trials be captured by a single-filter model like Model 1? The answer appears to be yes. Figures 4.11 and 4.12 show curves similar to those shown in Figure 4.9. Again, the outputs of Model 1 have replaced the subject's data in the model-fitting process. Here, however, the square symbols show the results when only signal-plus-noise trials are considered, while the triangular symbols show the results when only noise-alone trials are considered. Strategy 2, averaging over the signal interval, has been used to compute the decision variable, X' , for all of the curves in Figure 4.11. In the upper panel, the decay constant of the integration stage has been fixed at .01 ms; in the lower panel, the bandwidth of the filter has been fixed at 50 Hz. In Figure 4.12, X' is equal to the maximum output of the integration stage (Strategy 5). In the upper panel, the decay constant has been fixed at 200 ms; in the lower panel, the bandwidth of the filter has been fixed at 50 Hz. In the upper

Figure 4.11. R^2 as a function of the bandwidth of the filter and the decay constant of the integrator. Square symbols are for signal-plus-noise trials. Triangular symbols are for noise-alone trials. All results are for $10 \text{ Log}(E/N_0)$ equal to 8.5 dB and Strategy 2. In the upper panel, the decay constant of the integrator has been fixed at .01 ms. In the bottom panel, the bandwidth of the filter has been fixed at 50 Hz for both filled and open symbols. The results shown are for Model 1 as the system to be investigated.

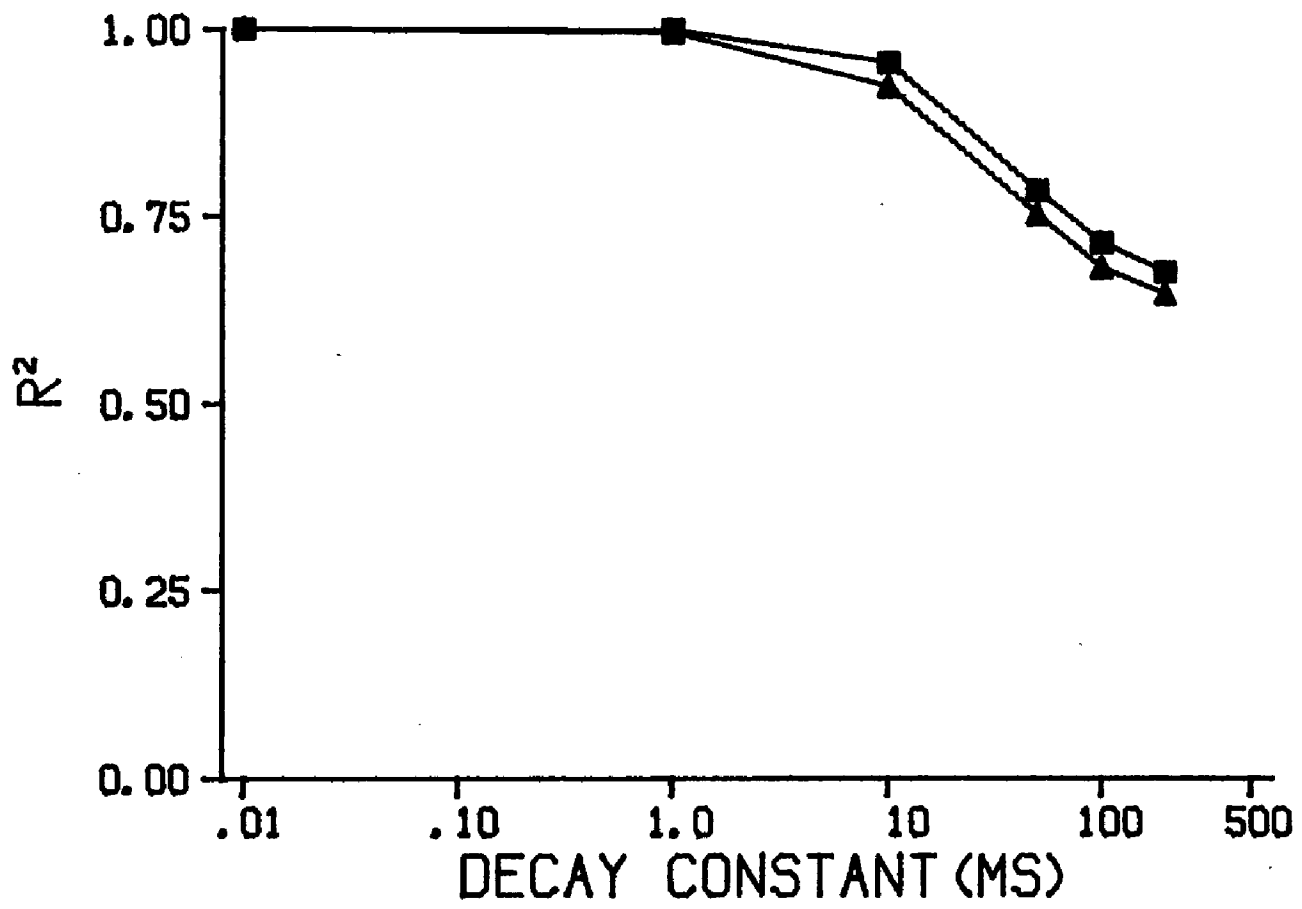
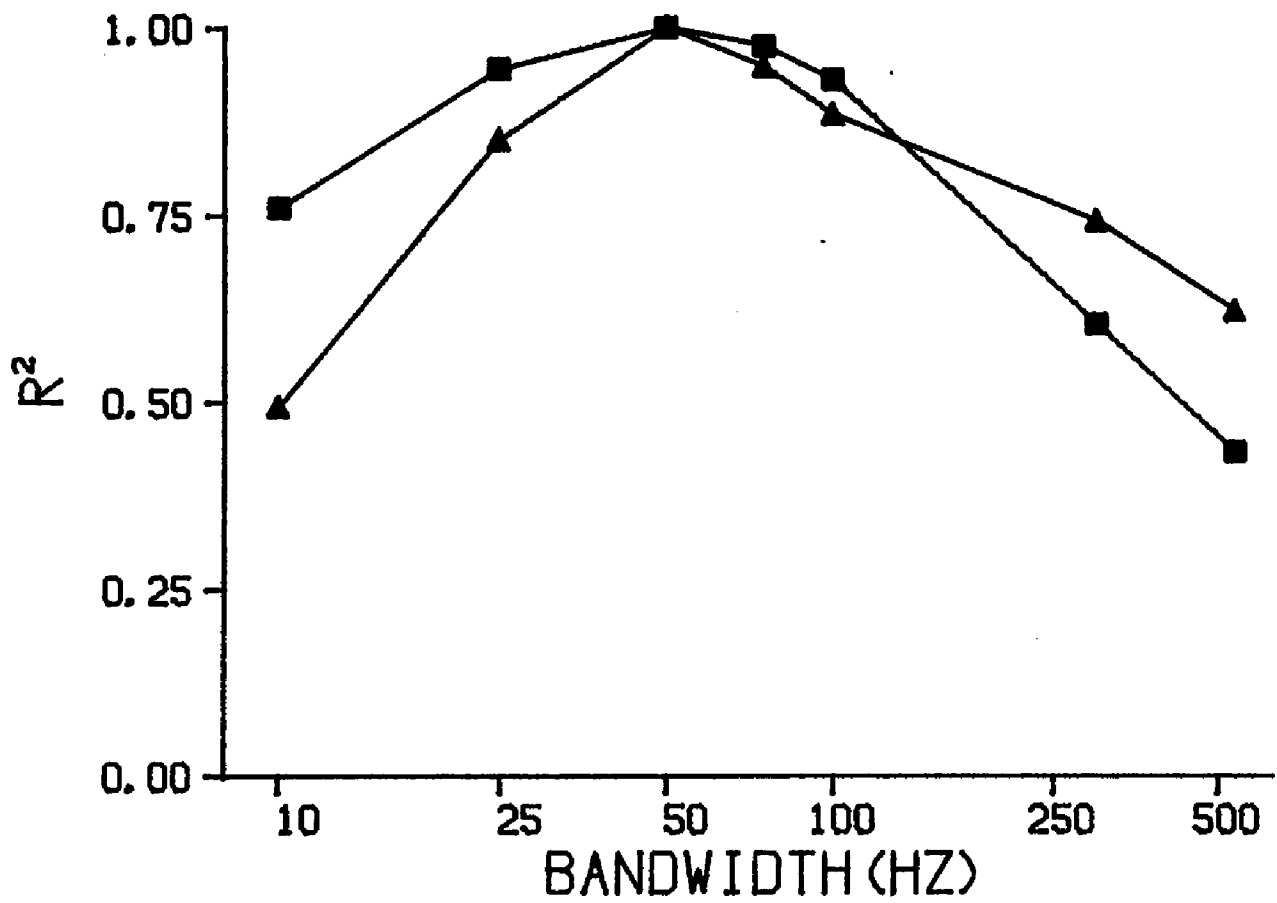
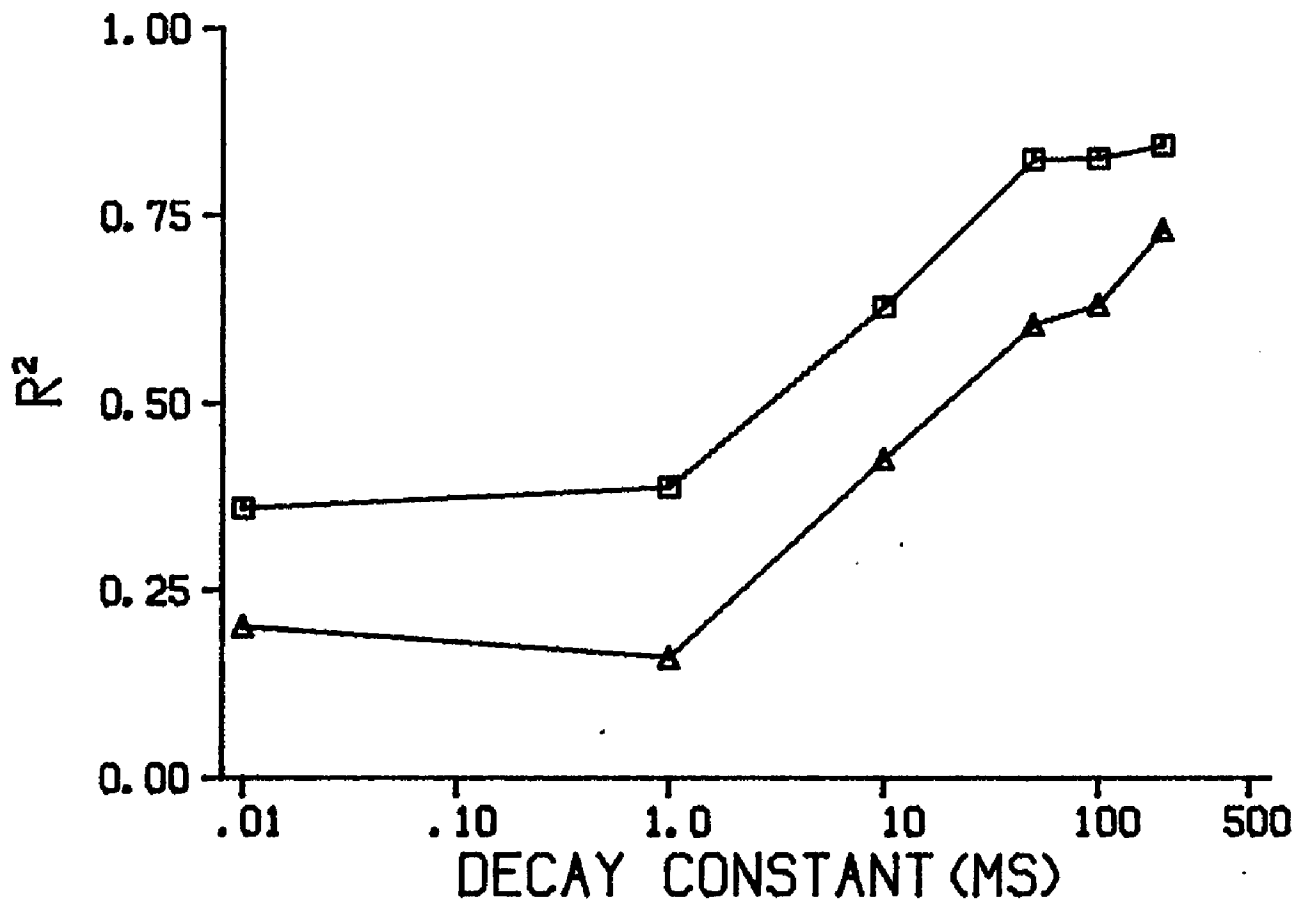
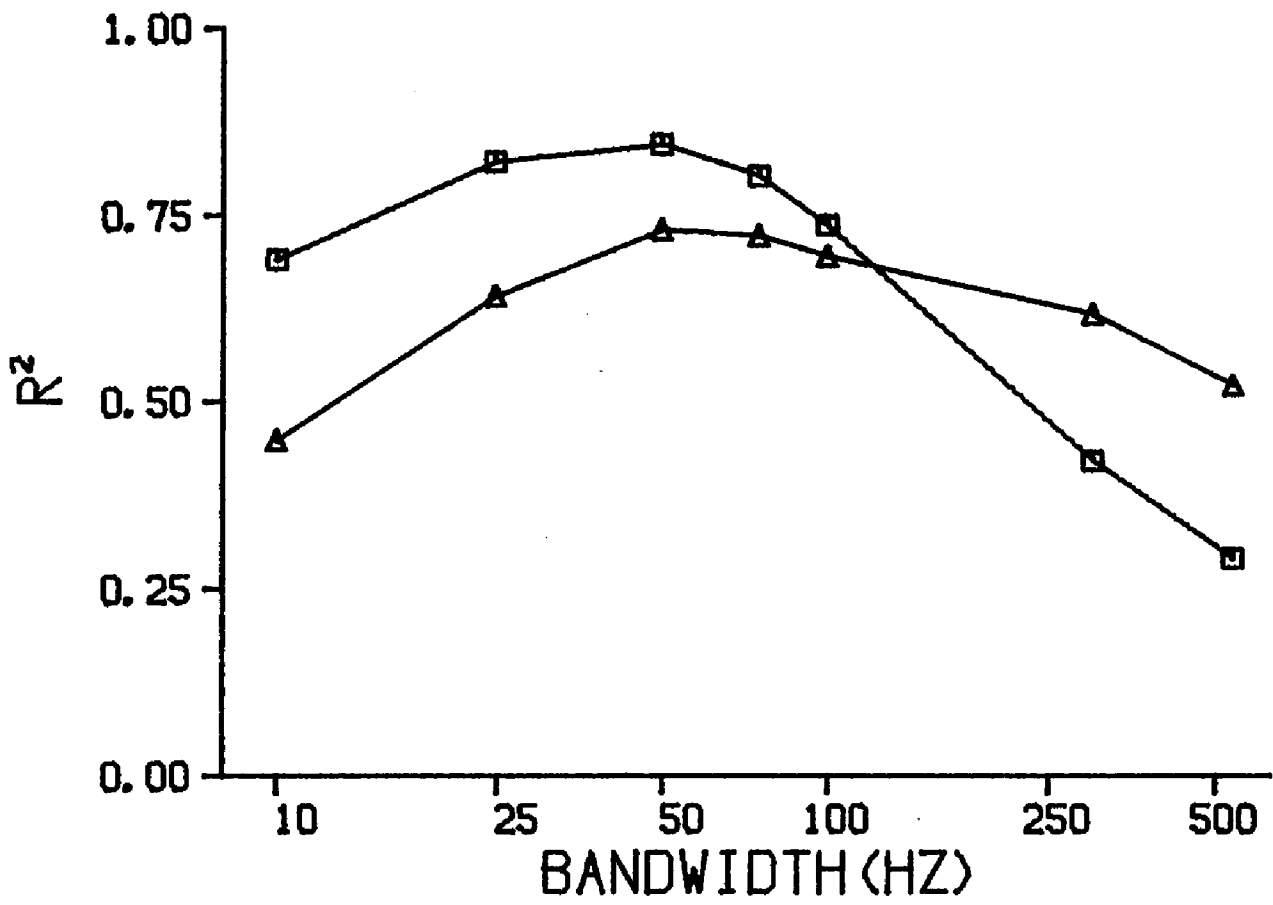


Figure 4.12. R^2 as a function of the bandwidth of the filter and the decay constant of the integrator. Square symbols are for signal-plus-noise trials. Triangular symbols are for noise-alone trials. All results are for $10 \text{ Log}(E/N_0)$ equal to 8.5 dB and Strategy 5. In the upper panel, the decay constant of the integrator has been fixed at 200 ms. In the bottom panel, the bandwidth of the filter has been fixed at 50 Hz for both filled and open symbols. The results shown are for Model 1 as the system to be investigated.



panel of Figure 4.11, the two curves are constrained to reach a value of unity when the bandwidth is equal to 50 Hz. At 50 Hz the model being fit to the system is the same as the system to be modeled (Model 1). However, it can be seen that while small changes in bandwidth have relatively little effect on the value of R^2 obtained on signal-plus-noise trials, R^2 drops relatively rapidly when the bandwidth is varied from 50 Hz. The results shown in the lower panel depict a similar result when the decay constant is varied from .01 ms. Again, both curves are constrained to reach a value of unity when the decay constant is .01 ms. As the decay constant is varied away from .01 ms, the values of R^2 are slightly, but consistently, smaller for noise-alone trials than for signal-plus-noise trials. The results shown in Figure 4.12 show similar discrepancies between the accuracy of predictions on signal-plus-noise and noise-alone trials. Notice the large discrepancy between the values of R^2 even at the 50-Hz bandwidth. Here the values of R^2 have been computed between Model 1 and Model 2. Remember the decision variable for Model 1, the system under investigation, is equal to the "true" integral of the filtered and half-wave rectified waveform over the signal interval, while the decision variable for Model 2, the model being fit to the data of the system under investigation, is approximately equal to the "true" integral of the filtered and half-wave rectified waveform over the stimulus interval. As was shown in Table 4.5, these models are very similar, yielding a value of R^2 of .915 across all trials. However, on signal-plus-noise trials, the value of R^2 is .843, and on noise-alone trials, the value is only .729. These results indicate that unless the model fits the data perfectly, discrepancies between the values of R^2 obtained on signal-plus-noise and noise-alone trials would be the typical result. Further, these discrepancies occur even when the data are generated by a relatively simple, single-channel model like Model 1.

The results shown in Figures 4.11 and 4.12 do not lead to different estimates of the bandwidth on signal-plus-noise and noise-alone trials. However, notice that the shapes of both curves are asymmetric. Further, the curve for signal-plus-noise trials tends to reach somewhat higher values at narrow bandwidths, while the curve for noise-alone trials tends to reach higher values at wider bandwidths. Hence, although both curves peak at 50 Hz, if there were any error in the bandwidth estimate, we would expect the erroneous estimates on signal-plus-noise trials to tend towards narrower bandwidths, while the erroneous estimates on noise-alone trials would tend towards wider bandwidths. The resultant discrepancy would be in agreement with the bandwidth estimates of Ahumada and his associates.

Although the pattern of results obtained with Model 1 as the system to be investigated is fairly similar to the results observed for human subjects, the absolute ability of the models to predict the data for the human subjects is much less. Even the "best-fitting" model for each subject is able to explain only a relatively small proportion of the variability in the responses of subjects. Do these small values of R^2 indicate that the model is not fitting the data very well and that, potentially, a better one could be found? Or do they indicate that the model is fitting the data relatively poorly because there is a large error component in the data, and that the predictable component of the data is therefore relatively small? In order to obtain an estimate of how much predictable variance is present in the subjects data, split-half correlations were computed between data obtained from alternate blocks at the same signal-level. The values of r^2 and r for each subject at $10 \text{ Log}(E/No)$ equal to 8.5 dB are shown in Table 4.6. As can be seen, these values are large when compared to the the values of R^2 obtained

TABLE 4.6

Split-half correlations, r^2 and (r) , between
 data collected on alternate blocks of trials
 $10 \text{ Log}(E/N_0)=8.5 \text{ dB}$

SG	CV	TW	JM
.931 (.965)	.882 (.939)	.964 (.982)	.891 (.944)

between the subjects and the models. Further, subject TW, whose data were quite difficult to predict ($R^2=.555$), has the largest split-half correlation, while subject CV, whose data were relatively easy to predict ($R^2=.693$), has the smallest split-half correlation.

These split-half correlations would suggest that a considerable portion of the variance in the subjects' data is potentially predictable. In an attempt to explain this residual variance, a multiple component model similar to that employed by Ahumada and Lovell (1971) and Ahumada, et al. (1975) was applied to the data. The decision variable of the present multiple component model was based on the output of seven 50-Hz wide single-tuned filters. The filters differed only in center frequency. The seven center frequencies were 350 Hz, 400 Hz, 450 Hz, 500 Hz, 550 Hz, 600 Hz, and 650 Hz. Each filter was followed by a half-wave rectifier. The output of each rectifier was averaged over the signal interval. The logarithm of a linear combination of these seven values was converted to a $P'(Y)$ using the logistic function. The weighting coefficients of the linear combination and the parameters of the logistic function were chosen to minimize the squared differences between the $P(Y)$ s and the $P'(Y)$ s. As before, STEPIT was used to obtain this least-squares fit. The resultant weightings for each subject are shown in the upper panels of Figures 4.13 through 4.16. As Ahumada, Marken and Sandusky (1975) found for their subjects, and Ahumada and Lovell (1971) found for some of their subjects, negative weightings were found at some frequencies for all subjects. This would suggest that subjects might be making a comparison between the information at the signal frequency and the information present at other frequencies.

A second multiple component model was also fit to the data. In this case, the output of a single filter followed by a half-wave rectifier was

Figure 4.13. Best-fitting weights for the multiple-component models described in the text. The square symbols are for a $10 \text{ Log}(E/N_0)$ of 8.5 dB. The circular symbols are for a $10 \text{ Log}(E/N_0)$ of 11.5 dB. In the lower panel, the two arrows indicate the time of the onset and the offset of the signal. The results shown are for subject SG.

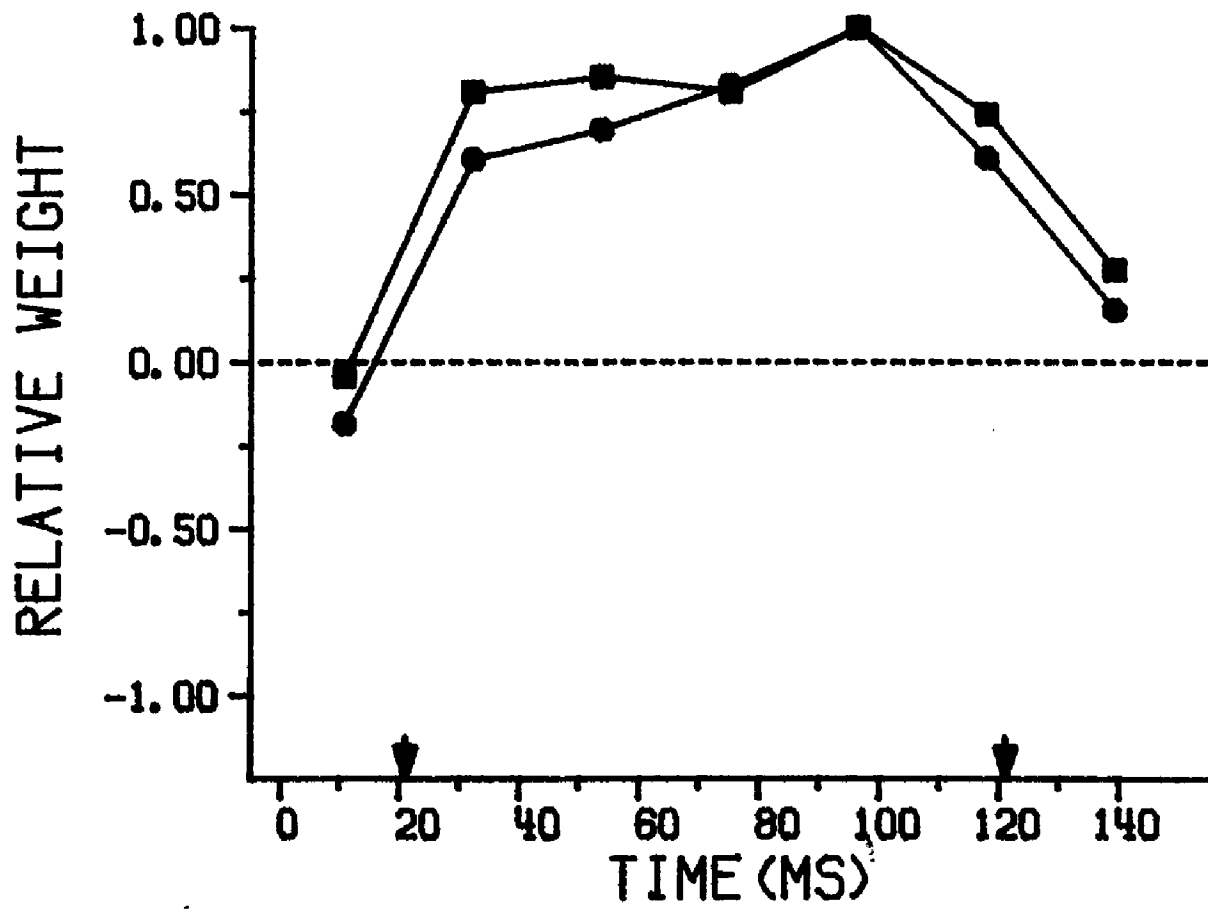
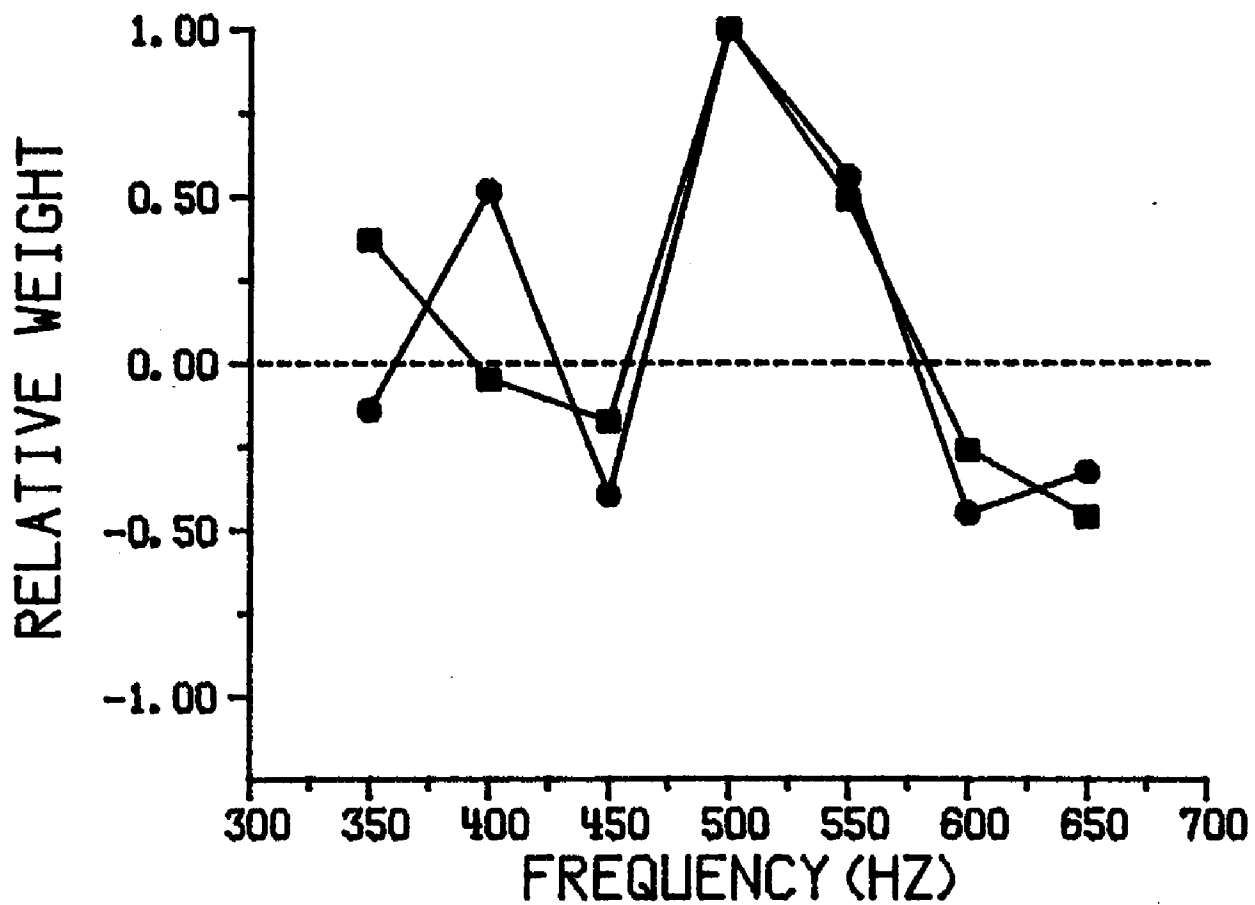


Figure 4.14. Best-fitting weights for the multiple-component models described in the text. The square symbols are for a $10 \text{ Log}(E/N_0)$ of 8.5 dB. The circular symbols are for a $10 \text{ Log}(E/N_0)$ of 11.5 dB. In the lower panel, the two arrows indicate the time of the onset and the offset of the signal. The results shown are for subject CV.

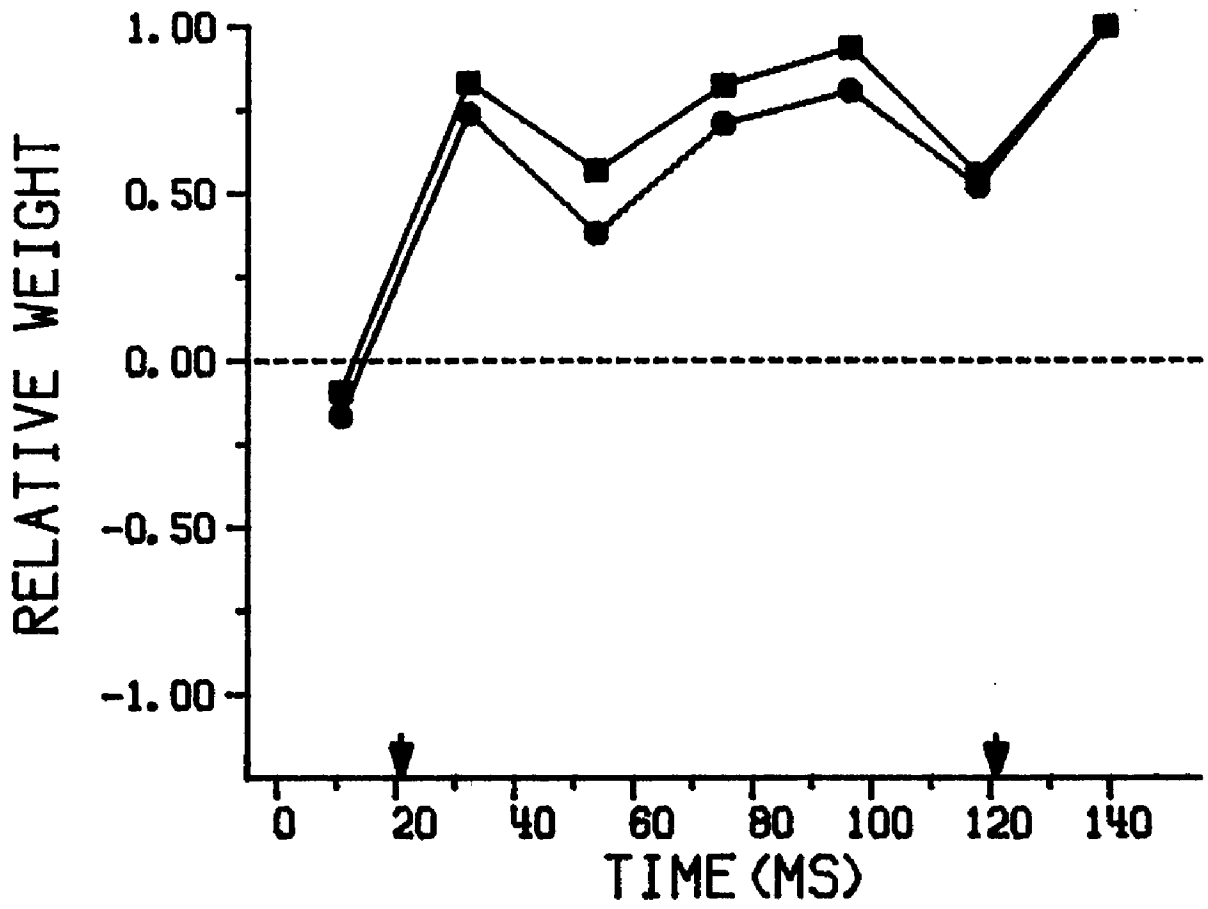
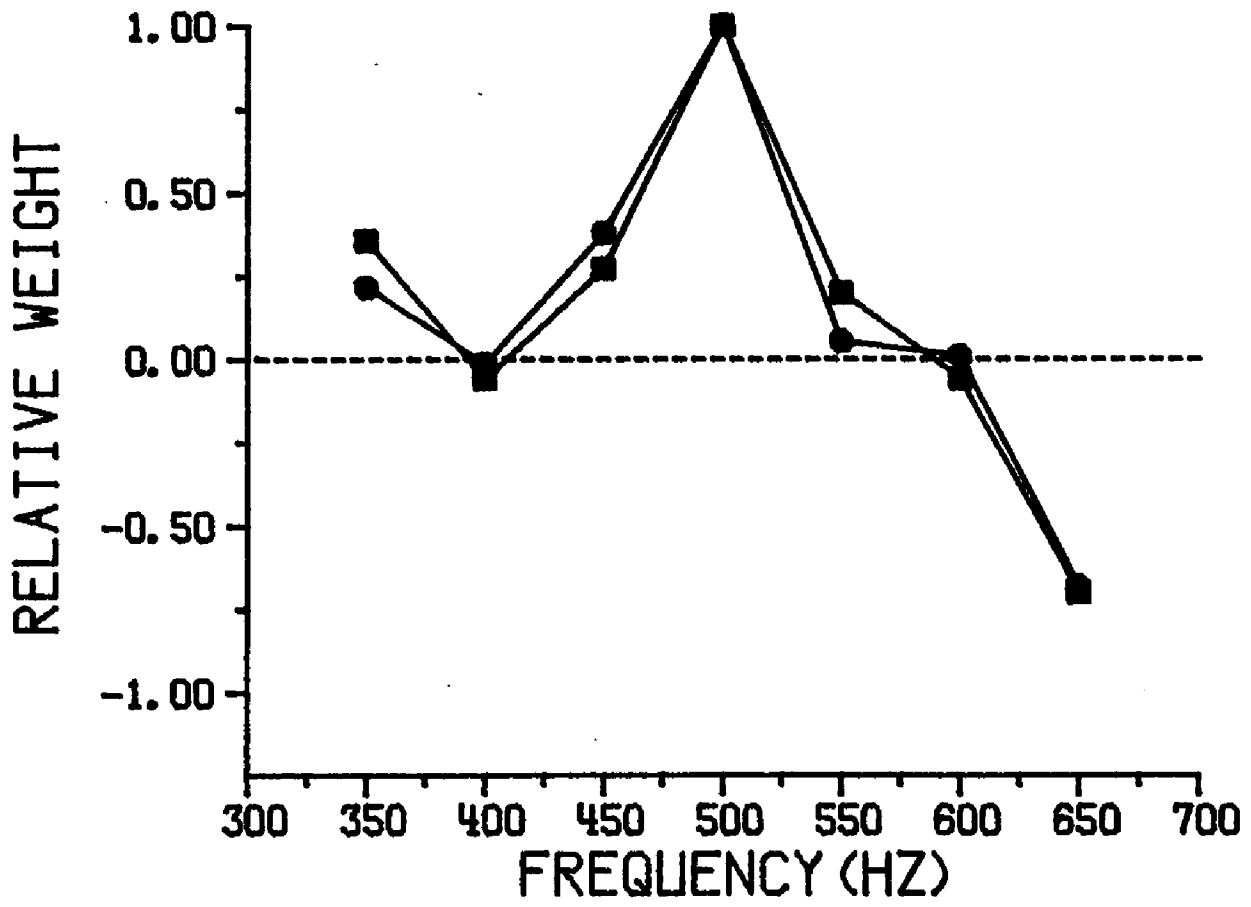


Figure 4.15. Best-fitting weights for the multiple-component models described in the text. The square symbols are for a $10 \text{ Log}(E/N_0)$ of 8.5 dB. The circular symbols are for a $10 \text{ Log}(E/N_0)$ of 11.5 dB. In the lower panel, the two arrows indicate the time of the onset and the offset of the signal. The results shown are for subject TW.

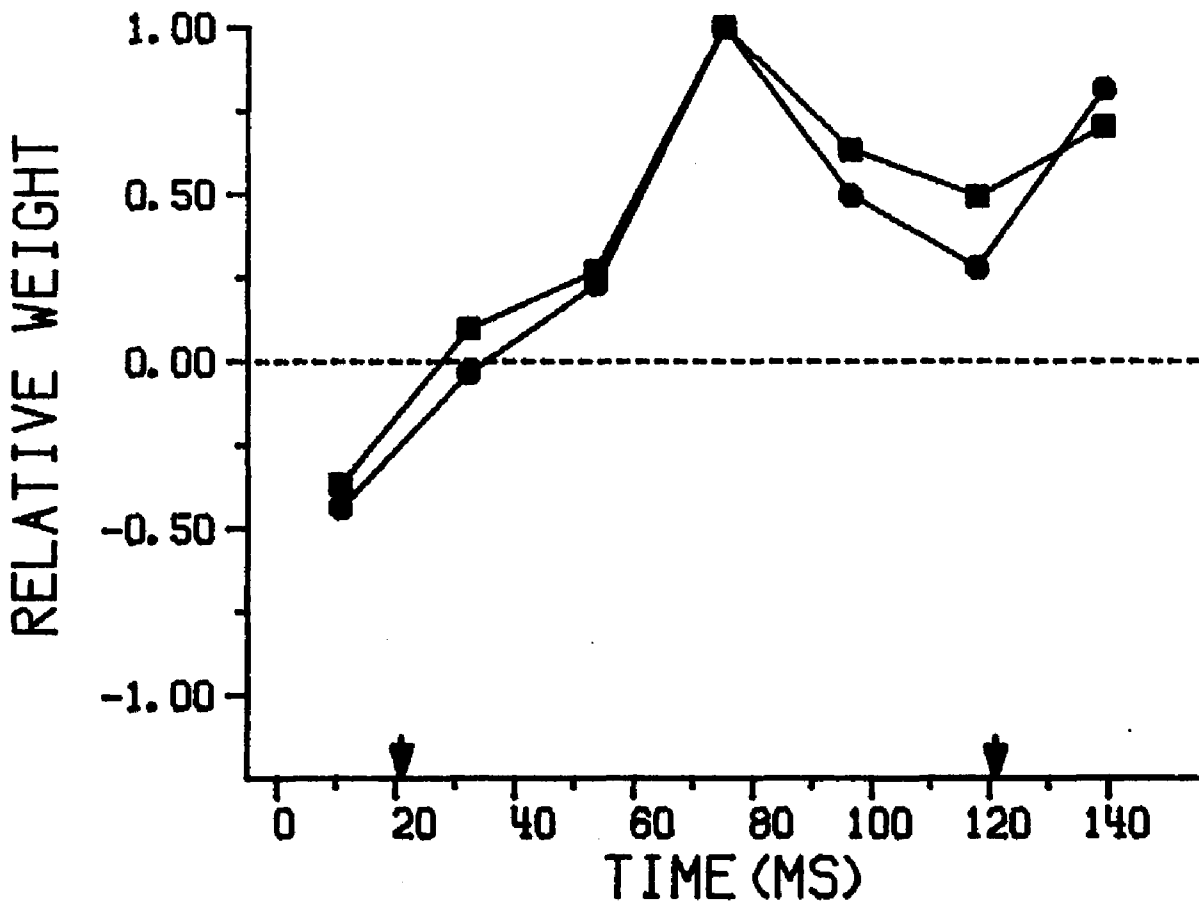
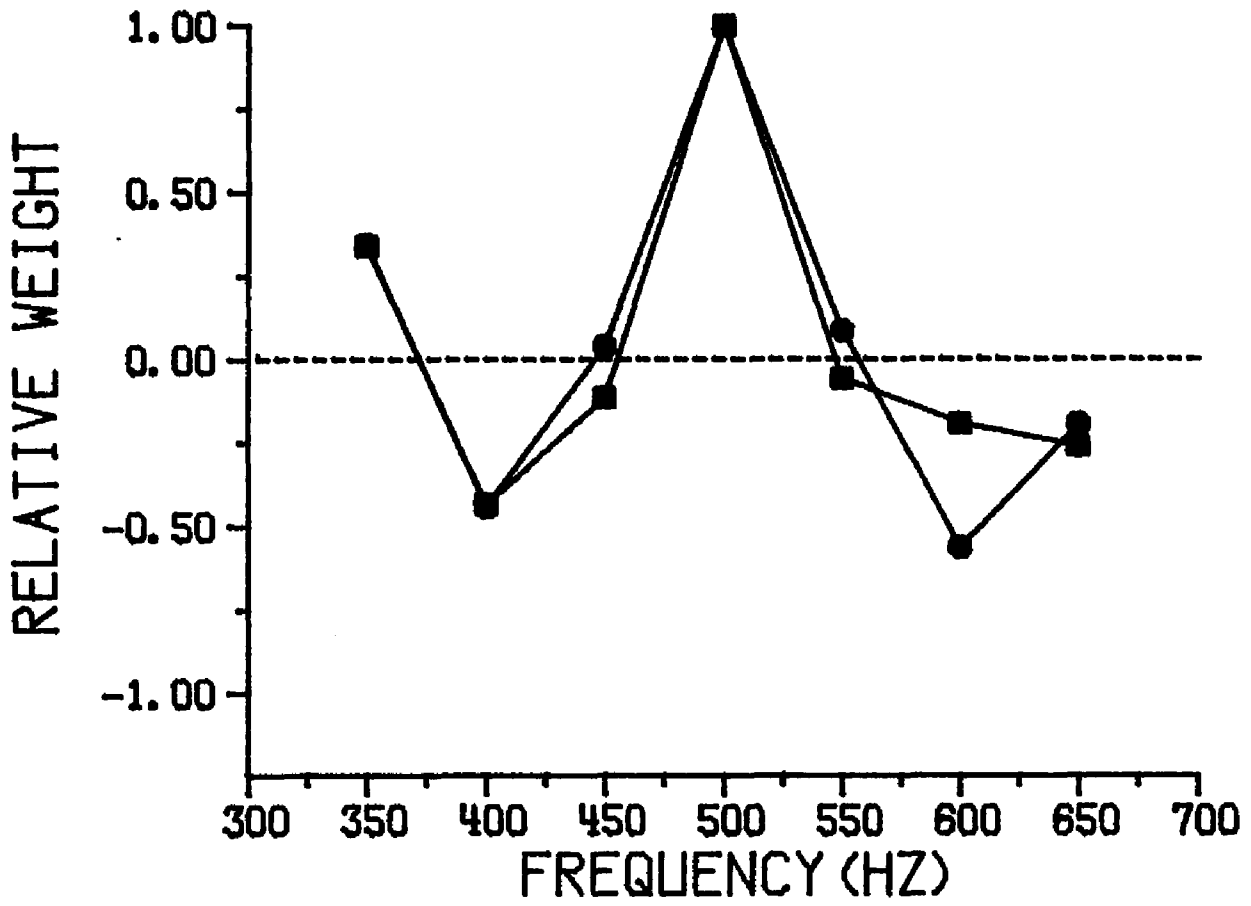
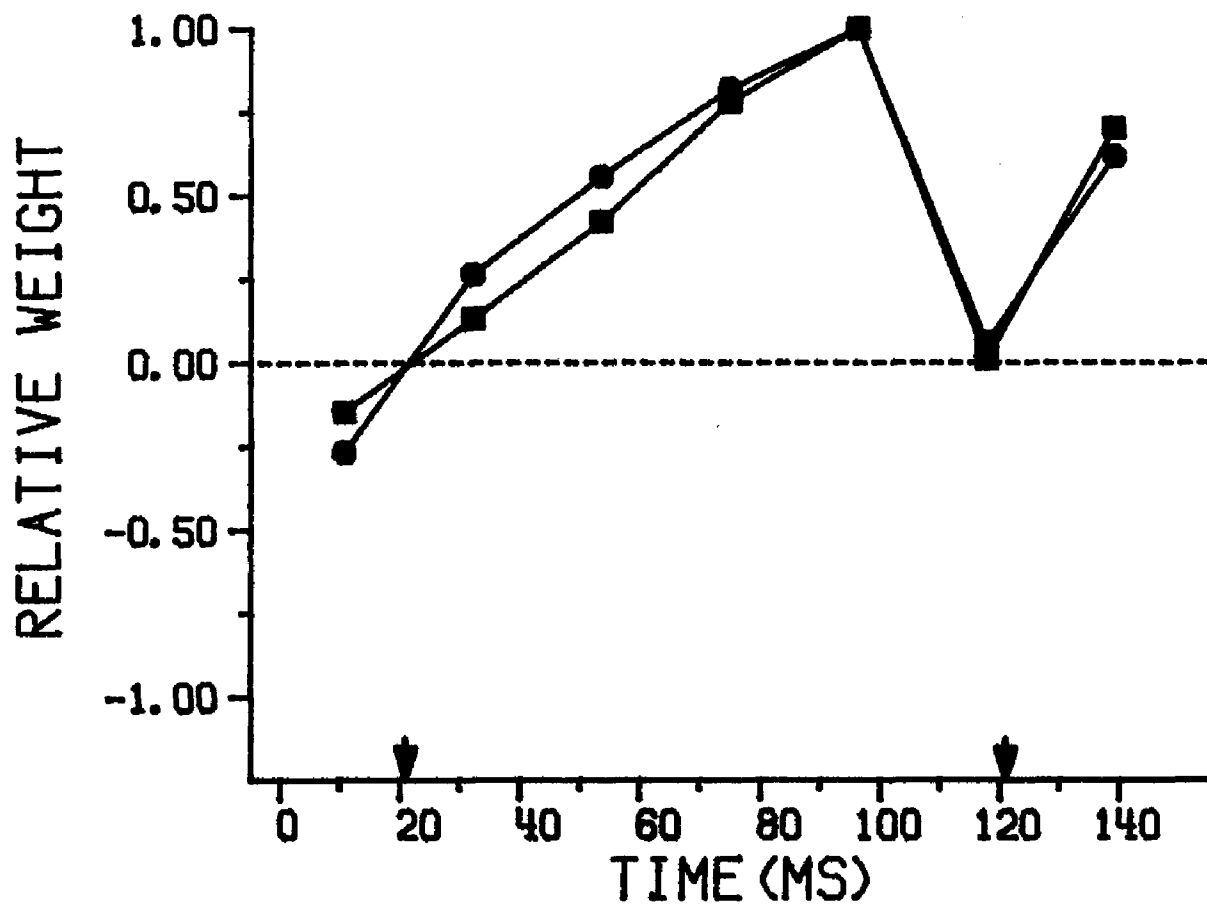
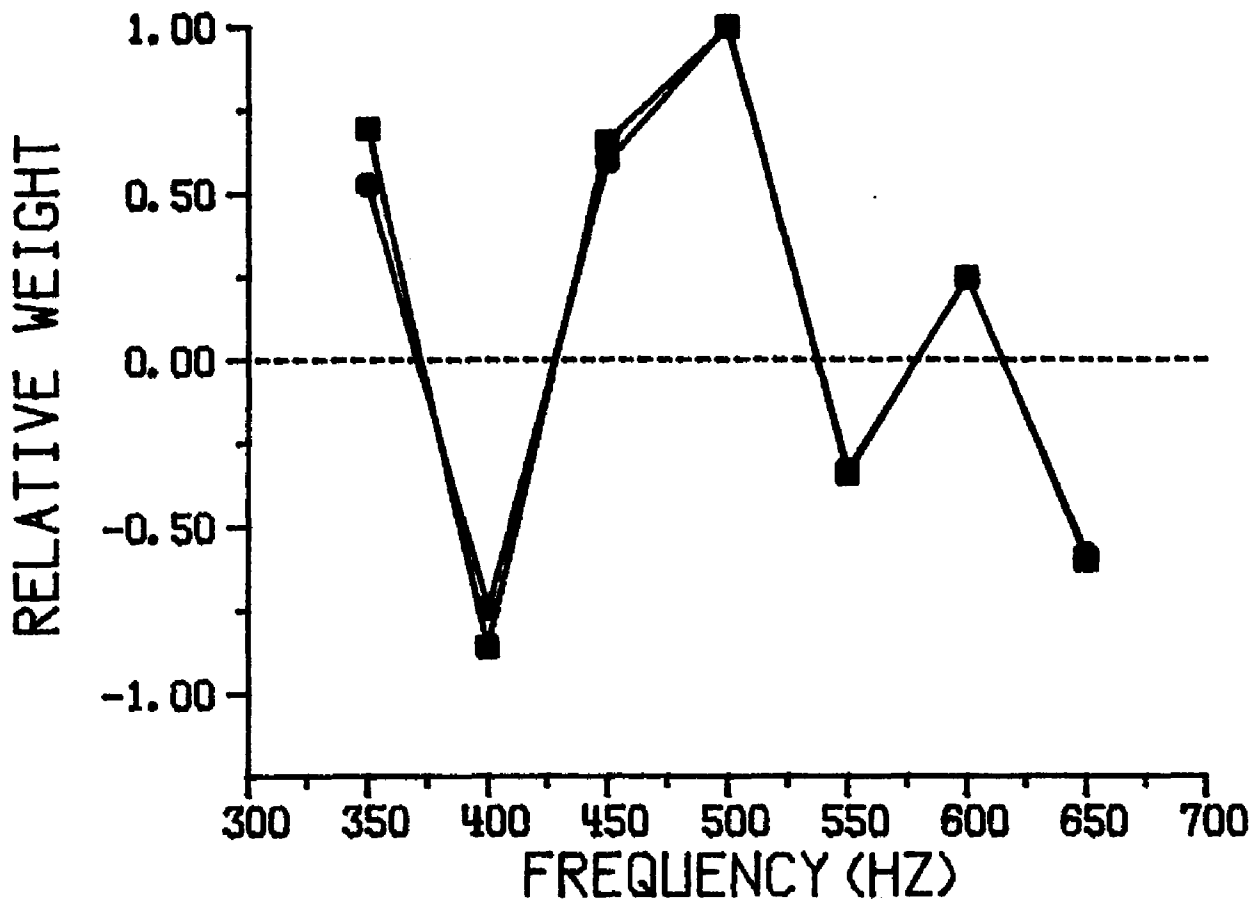


Figure 4.16. Best-fitting weights for the multiple-component models described in the text. The square symbols are for a $10 \text{ Log}(E/N_0)$ of 8.5 dB. The circular symbols are for a $10 \text{ Log}(E/N_0)$ of 11.5 dB. In the lower panel, the two arrows indicate the time of the onset and the offset of the signal. The results shown are for subject JM.



used to predict the data. However, the output was averaged over seven sub-intervals of the stimulus interval. The logarithm of a linear combination of these seven values was converted to a $P'(Y)$ using the logistic function. As before, STEPIT was used to obtain a least-squares fit to the data of each subject. The resultant weights are shown in the lower panels of Figures 4.13 through 4.16. The small arrows indicate the approximate time of the onset and offset of the signal. As Ahumada, Marken and Sandusky (1975) found for their subjects, the subjects tend to give negative weights to information which occurs immediately before the signal interval. Ahumada, et al. had used a 500-ms burst of noise and found that negative weights were given to the 100-ms interval of noise immediately before the onset of the signal. The present result is somewhat surprising given that the total duration of the noise burst in the present experiment was 148 ms and the portion of this noise which occurred before the signal onset was only 20 ms in duration. These result would suggest that the subject may be using the non-signal-carrying temporal fringe of the waveform to compare to the signal interval even with relatively short bursts of noise.

Some caution should be taken in interpreting these results. First, the weighting functions are not totally consistent across subjects. The frequency weightings, for example, show maximum positive peak at 500 Hz and consistent negative weightings at 650 Hz, but vary across subjects at the other frequencies. The temporal weighting functions show negative weightings before the signal interval and rise throughout most of the first half of the signal interval, but yield inconsistent weightings across subjects during the second half of the waveform. Adding these weighting functions to the model does produce an increase in explained variance. For subject JM, the increase in R^2 is fairly large, about .15.

For the other subjects, the increase is smaller, approximately .06 (see Tables 4.1-4.4).

Footnote

3. Because the number of responses to each sample was not always the same across conditions, each squared deviation was weighted by the average number of responses obtained from the particular subject under the particular condition. These values can be seen in Table A1.1 of Appendix A1.

Chapter 5

Summary and Conclusions

Before reviewing the results and conclusions from the previous chapters, it is important to consider the relationship between the molecular data presented here and more traditional views of masking. In the classical literature, masking phenomena have been described under the assumption that the signal and the masker are separable entities. Fletcher (1953, p. 153) argued that when a set of neural fibers was busy carrying information about the masker, that "such nerve fibers then can no longer be used to carry any other message to the brain...". Geldard (1972, p. 215), on the other hand, spoke of the "suppressive influence" of the masker upon the signal. Licklider (1951, p. 1005) pointed out that masking is the "opposite of analysis; it represents the inability of the auditory mechanism to separate the tonal stimulation into components and to discriminate between the presence and the absence of one of them" (Note 4). In these views, the differences among maskers are characterized by their ability to interfere with the signal. Differences among signals are similarly characterized by their ability to elude the influence of the masker.

The present data are best interpreted with a somewhat different view of masking. An examination of Figures 3.5 through 3.8 reveals that the probability that the subject will identify a particular sample of noise (a particular masker) as containing a signal varies widely depending on which masker has been selected. This variability exists not only for the case where the signal is present, but also on trials during which only the noise is present. With the classic view of masking, it is difficult to determine the amount of masking that has

occurred. Can one, for example, explain the wide variation in false-alarm rates as resulting from differences in the amount of masking of a non-existent signal? Even on signal-plus-noise trials, identifying the effects of masking may be difficult. Consider, for example, Sample 6 in Figure 3.5. Is Sample 6 an ineffective masker? The hit rate for Sample 6 is fairly high, nearly .5. On the other hand, its false-alarm rate is even higher. That is, more than 50 percent of the responses made to sample 6 are incorrect. A further complication for this classic view of masking can be seen by examining Figure 3.9. If, as indicated by Fletcher (1953), the role of the masker is to block the signal on the transmission lines to the brain, then it is difficult to postulate a mechanism for the phase effects reported here. Or if, as stated by Geldard (1972), the masker has a "suppressive influence" on the signal, by what mechanism does it differentially suppress signals with different starting phases? It is clear, from a consideration of the physics involved, that the waveform that is presented to the subject on signal-plus-noise trials is not two stimuli, but one. Similarly, we would not think of the power in the waveform as being the sum of the signal power and the masker power. Since the duration of the signal is reasonably long, the total power will be determined, to a good approximation, by the power in the vector sum of the amplitude of the 500-Hz component in the signal and the amplitude of the 500-Hz component in the noise (Note 5). Hence, rather than the flat functions predicted by a power sum, the power in the resultant waveform changes cyclically as a function of Alpha. These cyclic changes can be seen both in the stimulus measurements (the lower panels of Figure 3.9) and the human performance (the upper panels of Figure 3.9).

Thus, using the molecular data it has been difficult to specify the amount of masking. It is more reasonable to quantify the amount of masking on a molar level as the change in signal-level necessary to maintain a constant $P(C)_{max}$ when the masker is added. Although this is an adequate quantification of masking, it is a completely inadequate definition of masking. As Tanner (1958) pointed out, there are a variety of cases where the addition of a stimulus alters the detectability of another stimulus in a manner we would not typically refer to as masking. As was mentioned in the introduction, presenting a weak pedestal at the same frequency as the signal may actually increase the detectability of a tone in a background of noise. Typically, we would not consider this effect as masking.

The signals presented here have been masked by the noise. If the mechanism of masking cannot be seen on the molar level, perhaps it will be revealed by a deeper evaluation of the molecular data. Again, consider the data in Figures 3.5 through 3.8. As has been discussed, a broad range of both hit and false-alarm rates was obtained. Many of the noise-alone samples have the property of "sounding" like signal-plus-noise, while at the same time, many of the signal-plus-noise stimuli "sound" like noise alone. As has been pointed out before, within the Theory of Signal Detectability, the detector is thus forced to adopt a strategy such that either some noise-alone samples will be identified as containing signals, or some signal-plus-noise samples will be identified as noise-alone. Thus, masking occurs. When the noise level is decreased, the overlap between the signal-plus-noise and noise-alone samples decreases and the amount of masking decreases. As the level of the noise is increased, the amount of overlap increases, as does the amount of masking. The data

from the lower panel of Figure 3.9 indicate that this problem is more than a simple failure of analysis, as normally defined. Even if the observer considered only the power in the 500-Hz component, that is, if he were able to perform a complete analysis in the frequency domain, it would not be possible to discriminate perfectly between noise-alone and signal-plus-noise trials.

The models under consideration here do not assume that the noise interferes with the signal. They do, however, predict the overlap between noise-alone and signal-plus-noise samples. That is, the output decision variable, X' , for the models is sometimes greater on noise-alone trials than on signal-plus-noise trials. The models were in many cases able to predict below-chance performance for particular samples. Further, as would be expected, given that all of the models considered give maximum weight to the 500-Hz component, the models are able to capture the cyclic changes in performance as a function of Alpha.

The best-fitting model did not simply consider the 500-Hz component. It was found that models with approximately a 50-Hz bandwidth were best able to predict performance. However, bandwidths between 25 and 100 Hz were able to predict the data relatively well. Small changes in the estimated bandwidths were associated with changes in other model parameters, most particularly the form of the nonlinear stage.

The models were best able to predict the performance of subjects when the nonlinear stage was a half-wave rectifier. However, changing the nonlinearity to a square-law device (the only other nonlinearity considered), caused only a minimal decrement in the value of R^2 .

Within the current approach, the decay constant of the integrator interacted with the sampling strategy applied to the integrator output. Because many of the sampling strategies considered computed the average value of the integrator output over particular intervals of the stimulus waveform, the resultant value of X' is roughly proportional to the double integral of the input to the integration stage. Configurations that were best able to predict the data produced values of X' that were more nearly proportional to the single integral of the input to the integrator. These configurations either minimized or eliminated the integration performed by the integration stage (i.e., reduced its decay constant to near zero) or else employed sampling strategies that performed little or no averaging. Because of these interactions, it is difficult to specify the exact integration time of the system. However, a value of 100 to 200 ms seems appropriate. Similarly, it is difficult to determine the best approximation to the sampling strategy by which the system transforms the stream of acoustic information into a decision variable.

In many cases, the effectiveness of the models was not strongly influenced by changes in the parameters. Evaluation of the effectiveness of the model in predicting the output of a known model revealed that this insensitivity to parametric manipulations was not necessarily caused by noise in the data to be fitted, nor did it necessarily imply that the structure of the model was incompatible with the system to be modeled.

A few methodological points should be noted. Ahumada (1967) used techniques fairly similar to those employed here to estimate the critical bandwidth of the system. The estimates derived here are quite similar to other estimates of the critical bandwidth at 500 Hz.

Nevertheless, the flat curves relating R^2 to bandwidth indicate that the bandwidth estimates derived by this technique may not be particularly precise. The effects of manipulating the parameters of the model are even less distinct when $10 \text{ Log}(E/N_0)$ is increased from 8.5 dB to 11.5 dB. Thus, parametric investigations should be conducted using signal-to-noise ratios that are towards the low side of the practical limits.

Estimating parameters on the molecular level does have one distinct advantage over certain molar techniques. The distributions of outputs for several models are dependent only on the product of the effective bandwidth (W) and the effective duration (T). Therefore, in order to estimate either of these parameters on the molar level, it is necessary to assume a value of the other. Such an assumption is not required on a molecular level. These parameters are fairly independent. A 50-Hz value of W is most effective in almost all situations. Similarly, a value of 100 to 200 ms seems most appropriate for T.

The distinctions which Ahumada (1967), Ahumada and Lovell (1971), and Ahumada, et al. (1975) have made between predictions on signal-plus-noise trials and noise-alone trials can be explained without recourse to a "filter-bank" model. When fitting the other models to the outputs of Model 1, it was found that unless the fit was exact, the models tend to have differential success at predicting signal-plus-noise and noise-alone trials. Further, although the models made correct estimates of the bandwidth on both signal-plus-noise and noise-alone trials, it was argued that if there were any error in the bandwidth estimates, the estimates on noise-alone trials would be likely to tend toward wider bandwidths, whereas those on signal-plus-noise trials would tend toward narrower bandwidths.

Using a decision variable that was determined by the outputs of seven filters that differed in center frequency gave some improvement over the single filter case. Negative weightings were found at some frequencies. Similarly, combining the output of a single filter over seven 21.4-ms sub-intervals of the stimulus interval improved the predictions of the model. In this case, negative weightings were given to the sub-interval that immediately preceded the signal onset. The fact that negative weightings were found gives some support to the suggestion of Ahumada and Lovell (1971) and Ahumada et al. (1975) that the subject might compare information in the signal-carrying part of the waveform to information in the part of the waveform not carrying the signal.

In summary, a molecular experiment was conducted that investigated the detectability of a 500-Hz sinusoid in the presence of each of 25 different samples of white, approximately Gaussian, noise. Signals at each of four starting phase angles and at two levels were investigated. The estimated probability of a "Yes" response to individual noise samples was found to vary widely as a function of the noise sample selected. This was true on both signal-plus-noise and noise-alone trials. Manipulating the starting phase of the signal was also found to have large effects on the probability of a "Yes" response. The general form of the model of Jeffress (1967) was implemented as a series of computer subroutines and fit to the data. The combination of a 50-Hz wide single-tuned filter, followed by a half-wave rectifier and an integrator with an integration time of 100 to 200 ms was found to fit the data relatively well for all subjects. Slight variations in parameters of the best-fitting model were found across subjects. The proportion of variance explained by the model varied considerably

across subjects, over a range from .43 to .72. Combining the outputs of several models that differed in center frequency or integration interval increased the proportion of predicted variance. Negative weightings were found at some frequencies and for some time intervals, suggesting that the subject's decision might be based on a comparison between information in different parts of the stimulus.

Footnotes

4. It is not completely clear what Licklider (1953) meant by "analysis." Here Fourier analysis is assumed, although this may not be an adequate representation of Licklider's views.
5. Because the duration of the signal is finite, its bandwidth is not zero. Hence, vector sums described only at the 500-Hz component will not be a completely adequate description of the change in power when the signal is added to the noise.

References

- Ahumada, A. (1967) Detection of tones masked by noise: A comparison of human observers with digital-computer-simulated energy detectors of varying bandwidth. Department of Psychology, University of California at Los Angeles, Tech Report 29.
- Ahumada, A., & Lovell, J. (1971) Stimulus features in signal detection. Journal of the Acoustical Society of America, 53, 1751-1756.
- Ahumada, A., Marken, R., & Sandusky, A. (1975) Time and frequency analyses of auditory signal detection. Journal of the Acoustical Society of America, 57, 385-390.
- Becker, R. W., & Bell, D. W. (1975) Prediction of detection of sinusoids of different phases when masked by repeated waveforms of wide-band noise. Journal of the Acoustical Society of America, 57, s37 (A).
- Bell, D. W., & Becker, R. W. (1975) Comparison of phase effects in masking obtained from broad-band and narrow-band frozen noise waveforms. Journal of the Acoustical Society of America, 58, s35(A).
- Bell, D. W., & Schubert, E. D. (1975) Detectability of sinusoid signal as phase between sinusoid and noise microstructure is manipulated. Journal of the Acoustical Society of America, 57, s37 (A).
- Chandler J. P. (1970) STEPIT (QCPE, Program No. 66). Bloomington, Indiana: Indiana University, Chemistry Department, Quantum Chemistry Program Exchange.
- Dolan, T. R., Hirsh, I. R., & Yost, W. A. (1981) Detection of binaural signals partially masked by a reproducible noise masker: the influence of phase angle alpha. Journal of the Acoustical Society of America, 70, 886-887.
- Egan, J. P., Lindner, W. A., & McFadden, D. (1969) Masking-level differences and the form of the psychometric function. Perception and Psychophysics, 6, 209-215.
- Egan, J. P., Schulman, A. I., & Greenberg, G. Z. (1959) Operating characteristics determined by binary decisions and by ratings. Journal of the Acoustical Society of America, 31, 768-773.
- Fletcher, H. (1953) Speech and hearing in communication. New York: Van Nostrand.
- Frank, A. S. (1979) Detection of diotic and dichotic tones masked by repeatable samples of noise. Unpublished doctoral dissertation, Indiana University.
- Geldard, F. A. (1972) The human senses. New York: Wiley.
- Gilkey, R. H., & Frank, A. S. (1981) A software pseudo-random noise generator. Technical note, in preparation.

- Gilkey, R. H., Hanna, T. E., & Robinson, D. E. (1981) Estimates of the ratio of external to internal noise obtained using repeatable samples of noise. Journal of the Acoustical Society of America, 69, s22(A).
- Green, D. M. (1960) Psychoacoustics and detection theory. Journal of the Acoustical Society of America, 32, 1189-1203.
- Green, D. M. (1964) Consistency of auditory detection judgments. Psychological Review, 71, 392-407.
- Green, D. M., Birdsall, T. G., & Tanner, W. P., Jr. (1957) Signal detection as a function of signal intensity and duration. Journal of the Acoustical Society of America, 29, 523-531.
- Green, D. M., & Swets, J. A. (1974) Signal detection theory and psychophysics. Huntington, NY: Krieger.
- Jeffress, L. A. (1964) Stimulus-oriented approach to detection. Journal of the Acoustical Society of America, 36, 766-774.
- Jeffress, L. A. (1967) Stimulus-oriented approach to detection reexamined. Journal of the Acoustical Society of America, 41, 480-488.
- Jeffress, L. A. (1968) Mathematical and electrical models of auditory detection. Journal of the Acoustical Society of America, 44, 187-203.
- Licklider, J. C. R. (1951) Basic correlates of the auditory stimulus. In S. S. Stevens (Ed.), Handbook of experimental psychology. New York: Wiley.
- Marill, T. (1956) Detection theory and psychophysics. Massachusetts Institute of Technology Research Laboratory of Electronics Report No. 319.
- Peterson, W. W., Birdsall, T. G., & Fox, W. C. (1954) The theory of signal detectability. IRE Transactions on Information Theory, 4, 171-212.
- Pfafflin, S. M., & Mathews, M. V. (1962) Energy-detection model for monaural auditory detection. Journal of the Acoustical Society of America, 34, 1842-1853.
- Pfafflin, S. M., & Mathews, M. V. (1966) Detection of auditory signals in reproducible noise. Journal of the Acoustical Society of America, 39, 340-345.
- Sherwin, C. W., Kodman, F., Jr., Kovaly, J. J., Prothe, W. C., & Melrod, J. (1956) Detection of signals in noise: A comparison between the human detector and an electronic detector. Journal of the Acoustical Society of America, 28, 617-622.
- Singleton, R. C. (1969) An algorithm for computing the mixed radix fast Fourier transform. IEEE Transactions on Audiovisual Electroacoustics, AU-17, 93-103.

- Swets, J. A., Shipley, E. F., McKey, M. J., & Green, D. M. (1959) Multiple observations of signals in noise. Journal of the Acoustical Society of America, 31, 514-521.
- Tanner, W. P. (1958) What is masking? Journal of the Acoustical Society of America, 30, 919-921.
- Tanner, W. P., & Birdsall, T. G. (1958) Definitions of d' and η as psychophysical measures. Journal of the Acoustical Society of America, 30, 922-928.
- Tanner, W. P., & Swets, J. A. (1954) A decision-making theory of visual detection. Psychological Review, 61, 401-409.
- Tucker, A., Williams, P. I., & Jeffress, L. A. (1968) Effect of signal duration on detection for gated and for continuous noise. Journal of the Acoustical Society of America, 44, 813-816.
- Watson, C. S. (1962) Signal detection and certain physical characteristics of the stimulus during the observation interval. Unpublished doctoral dissertation, Indiana University.
- Watson, C. S., Rilling, M. E., & Bourbon, W. T. (1964) Receiver-operating characteristics determined by a mechanical analog to the rating scale. Journal of the Acoustical Society of America, 36, 283-289.
- Williams, P. I., & Jeffress, L. A. (1967) Agreement in detection: Observers and electrical model. Journal of the Acoustical Society of America, 42, 1194(A).

Appendix 1

TABLE A1.1

The number of presentations (P) of each sample to each subject under each condition and the average number of responses to each sample from each subject under each condition for signal-plus-noise trials (S) and for noise-alone trials (N)

10 Log(E/No)=11.5 dB					
		SG	CV	TW	JM
Alpha=0	P	130	136	136	198
	S	130	134	136	198
	N	130	135	136	198
Alpha=90	P	78	80	80	80
	S	78	79	80	80
	N	78	79	80	79
Alpha=180	P	88	128	128	178
	S	88	127	127	178
	N	88	127	128	178
Alpha=270	P	82	82	82	82
	S	82	82	82	82
	N	82	82	82	81
10 Log(E/No)=8.5 dB					
		SG	CV	TW	JM
Alpha=0	P	130	136	136	198
	S	130	134	136	197
	N	130	135	136	198
Alpha=90	P	80	80	80	80
	S	80	79	80	80
	N	80	79	80	78
Alpha=180	P	90	128	128	178
	S	90	127	127	178
	N	90	127	128	178
Alpha=270	P	80	82	80	80
	S	80	82	80	80
	N	80	81	80	80

Appendix 2

Figure A2.1. Hit and false-alarm rates obtained for individual samples are shown in ROC space. Each number plotted shows the data for the sample associated with that number. The square symbol shows the average hit rate and false alarm rate across all samples. The data shown are for subject SG and were collected with Alpha equal to 0.

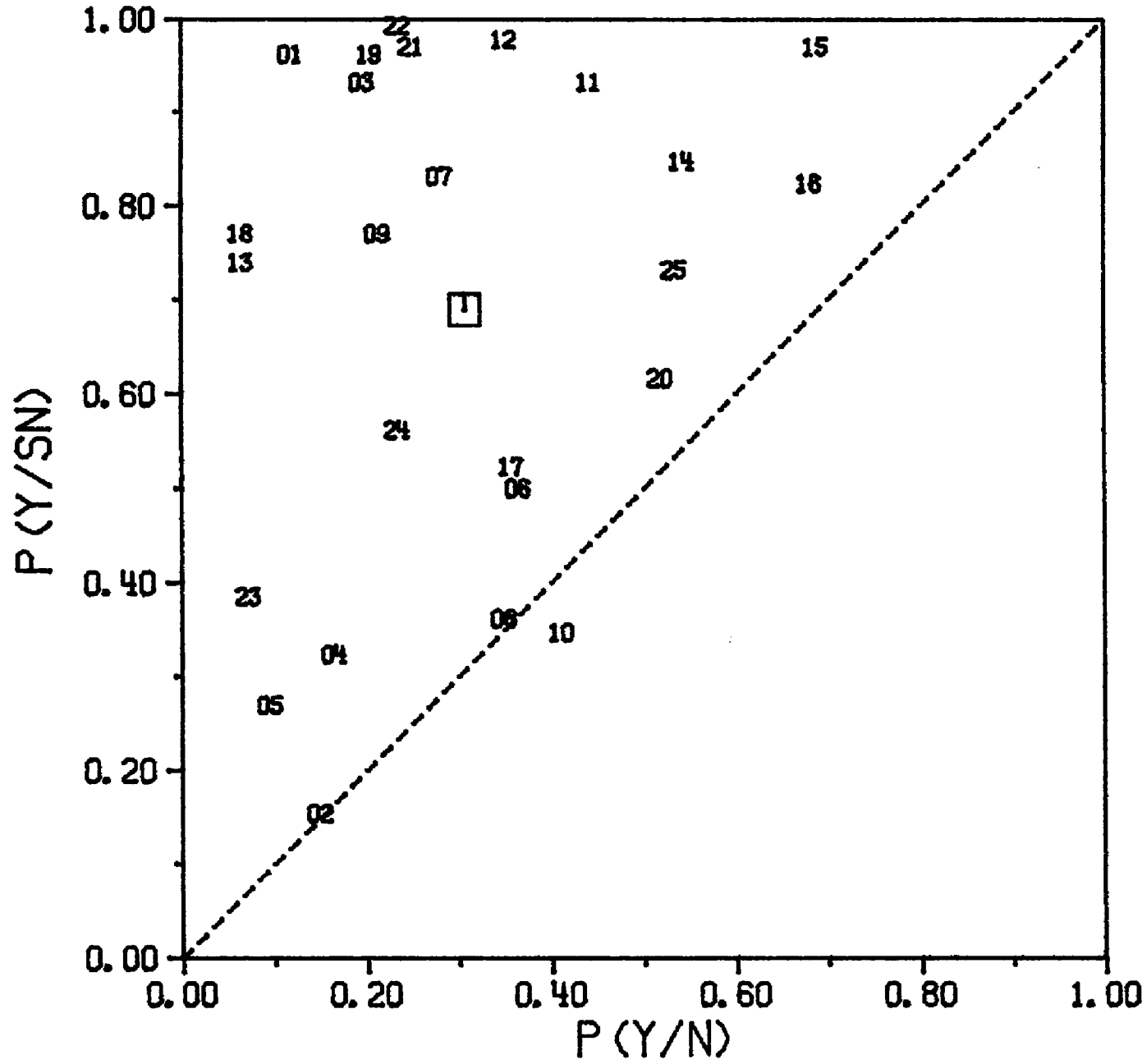


Figure A2.2. Hit and false-alarm rates obtained for individual samples are shown in ROC space. Each number plotted shows the data for the sample associated with that number. The square symbol shows the average hit rate and false alarm rate across all samples. The data shown are for subject SG and were collected with Alpha equal to 90.

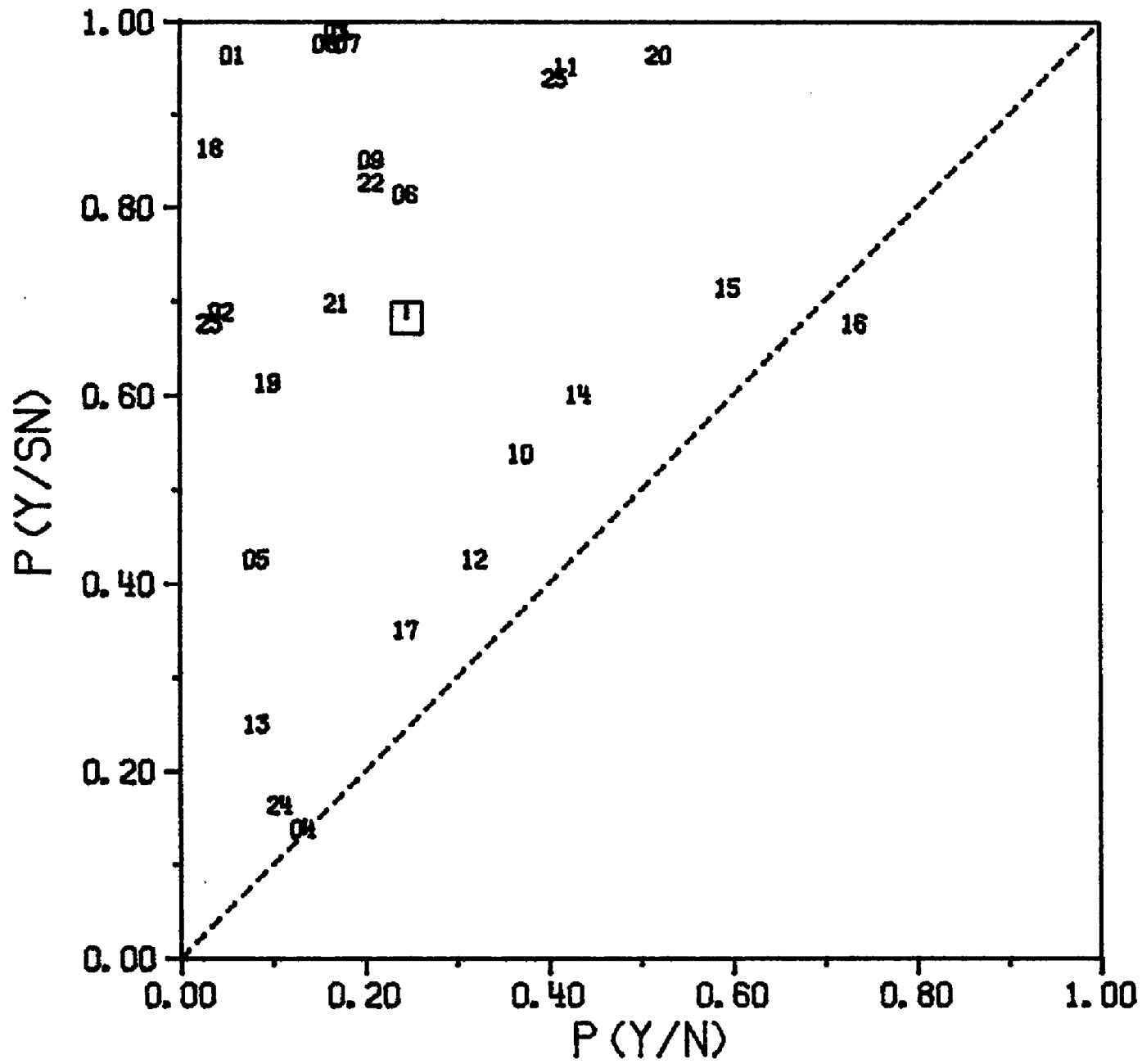


Figure A2.3. Hit and false-alarm rates obtained for individual samples are shown in ROC space. Each number plotted shows the data for the sample associated with that number. The square symbol shows the average hit rate and false alarm rate across all samples. The data shown are for subject SG and were collected with Alpha equal to 180.

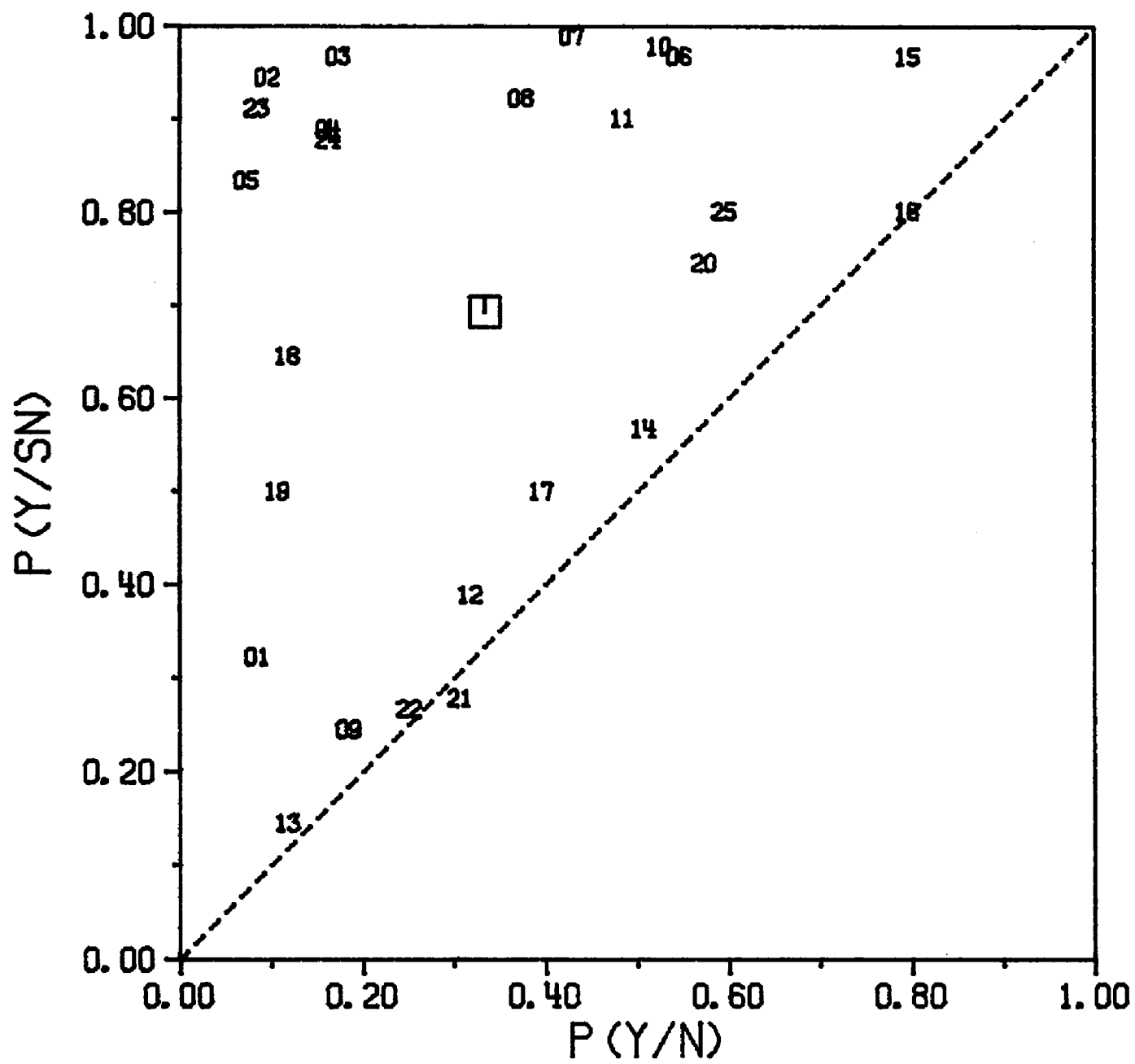


Figure A2.4. Hit and false-alarm rates obtained for individual samples are shown in ROC space. Each number plotted shows the data for the sample associated with that number. The square symbol shows the average hit rate and false alarm rate across all samples. The data shown are for subject SG and were collected with Alpha equal to 270.

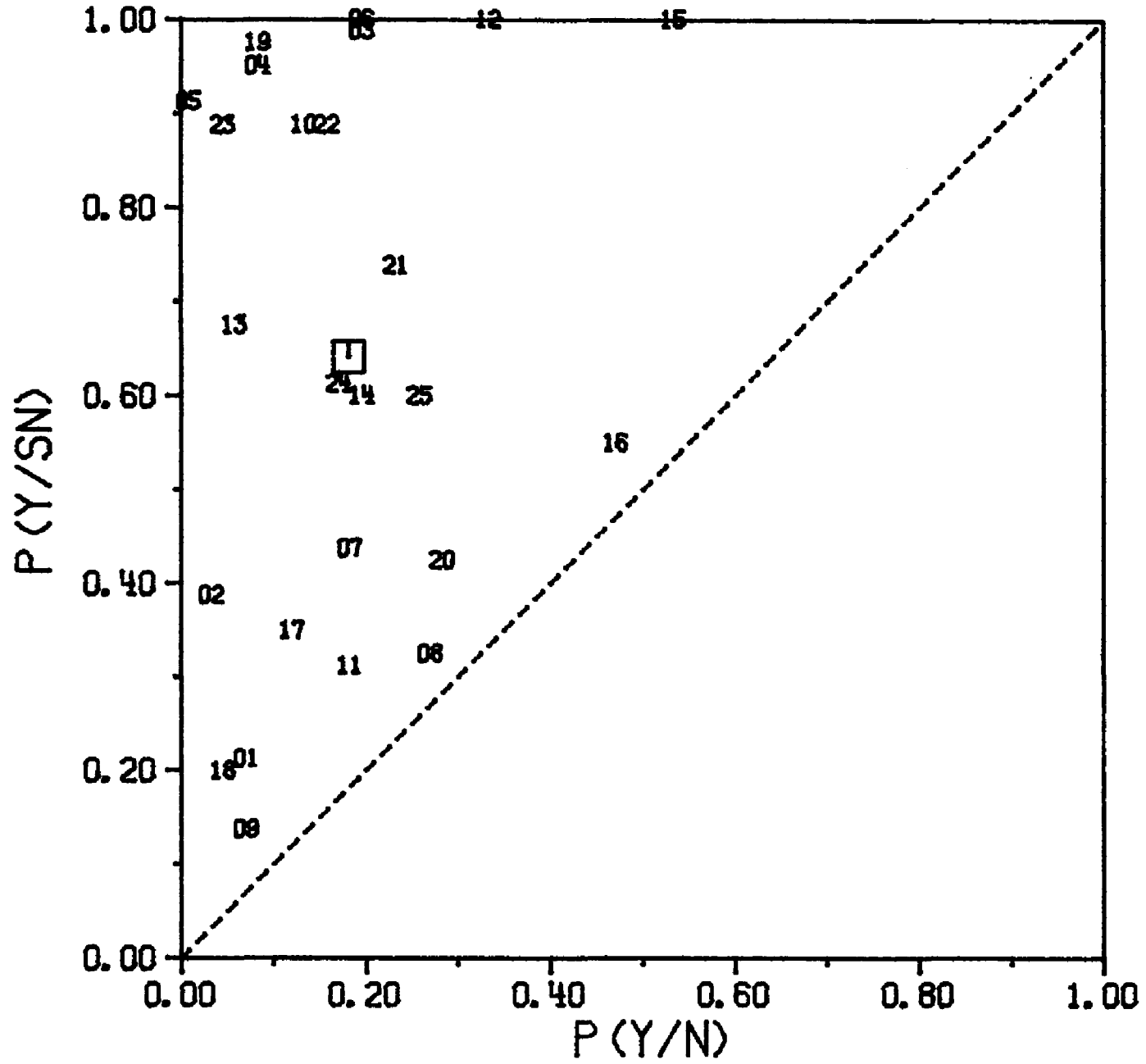


Figure A2.5. Hit and false-alarm rates obtained for individual samples are shown in ROC space. Each number plotted shows the data for the sample associated with that number. The square symbol shows the average hit rate and false alarm rate across all samples. The data shown are for subject CV and were collected with Alpha equal to 0.

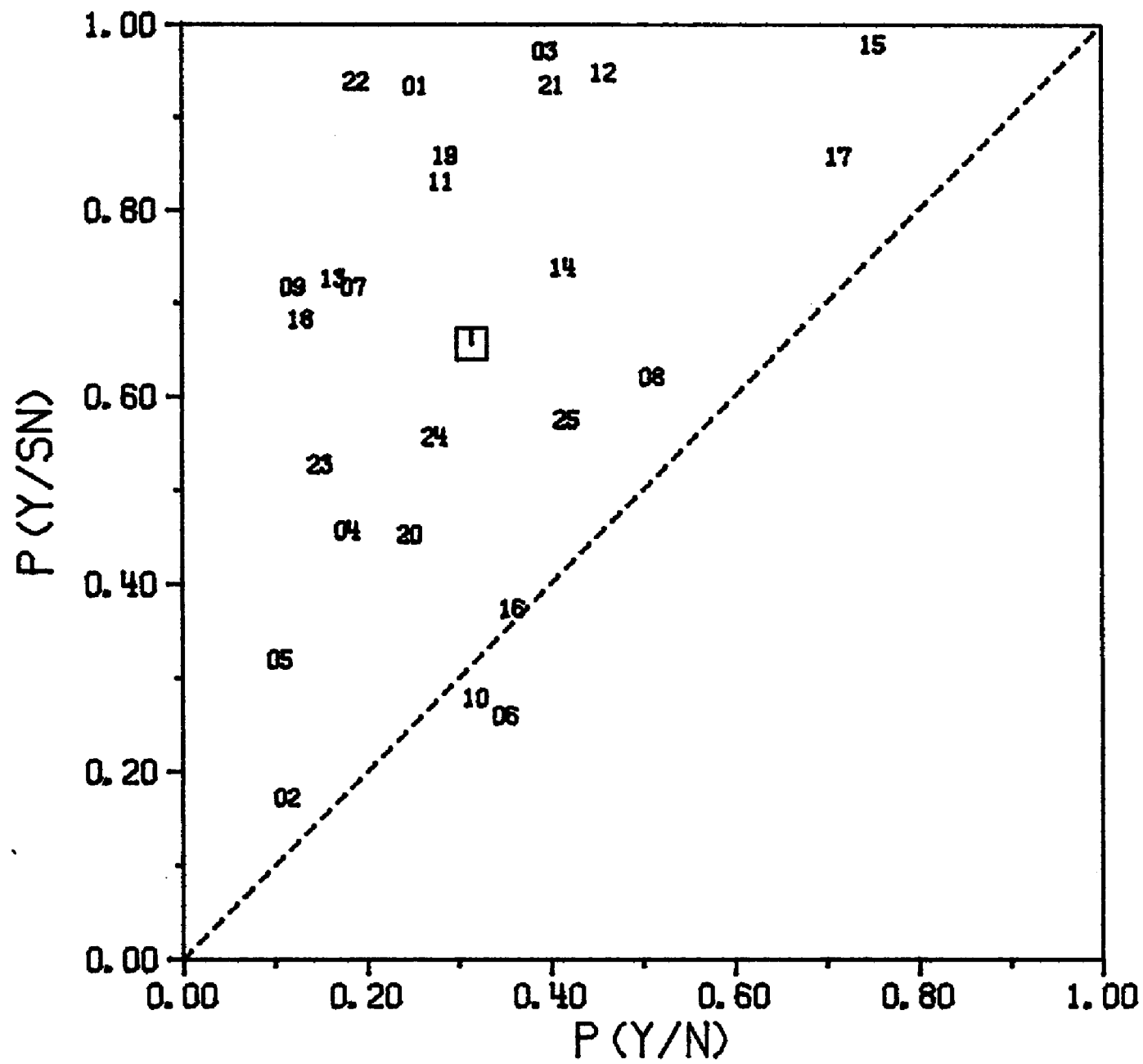


Figure A2.6. Hit and false-alarm rates obtained for individual samples are shown in ROC space. Each number plotted shows the data for the sample associated with that number. The square symbol shows the average hit rate and false alarm rate across all samples. The data shown are for subject CV and were collected with Alpha equal to 90.

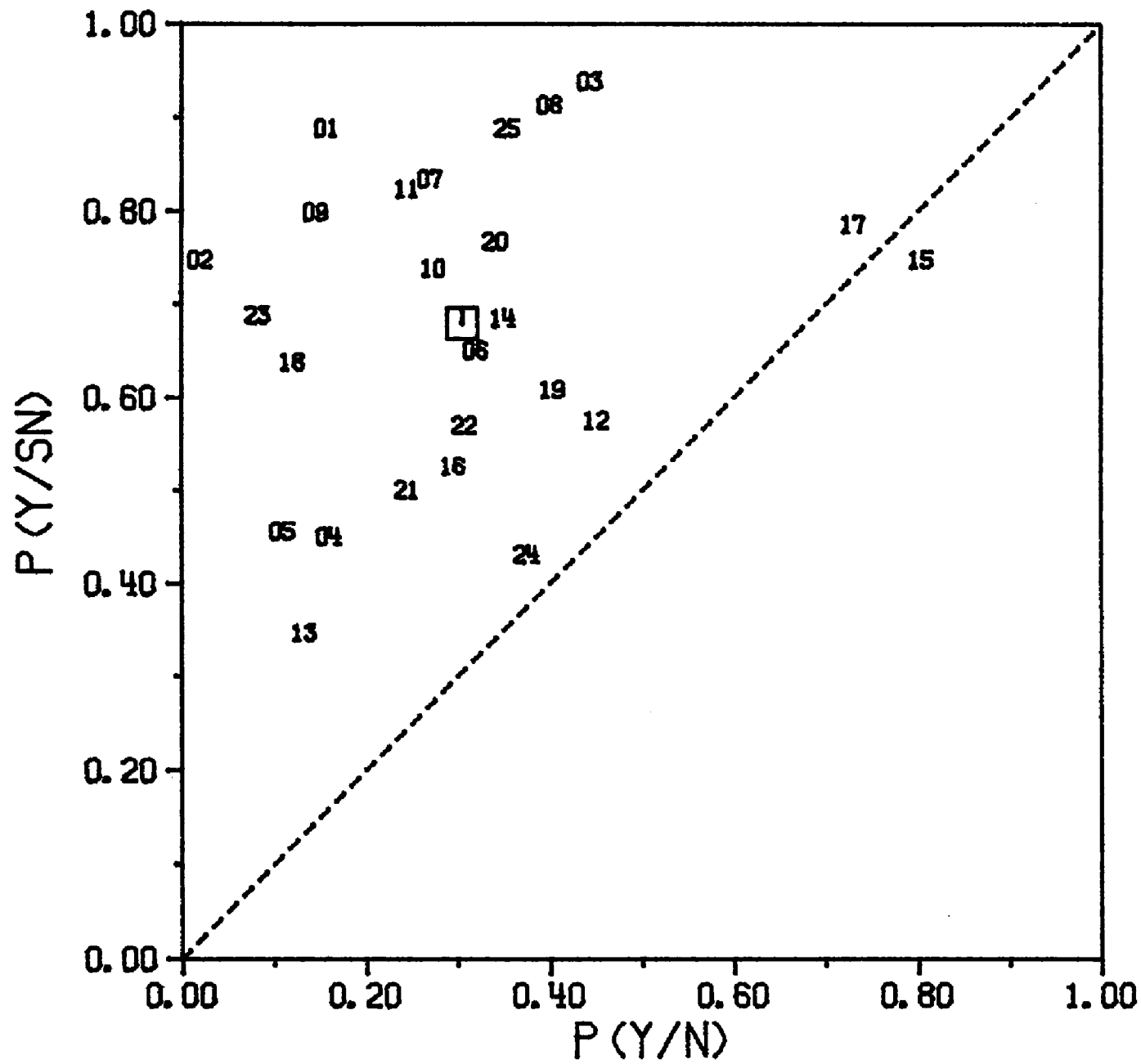


Figure A2.7. Hit and false-alarm rates obtained for individual samples are shown in ROC space. Each number plotted shows the data for the sample associated with that number. The square symbol shows the average hit rate and false alarm rate across all samples. The data shown are for subject CV and were collected with Alpha equal to 180.

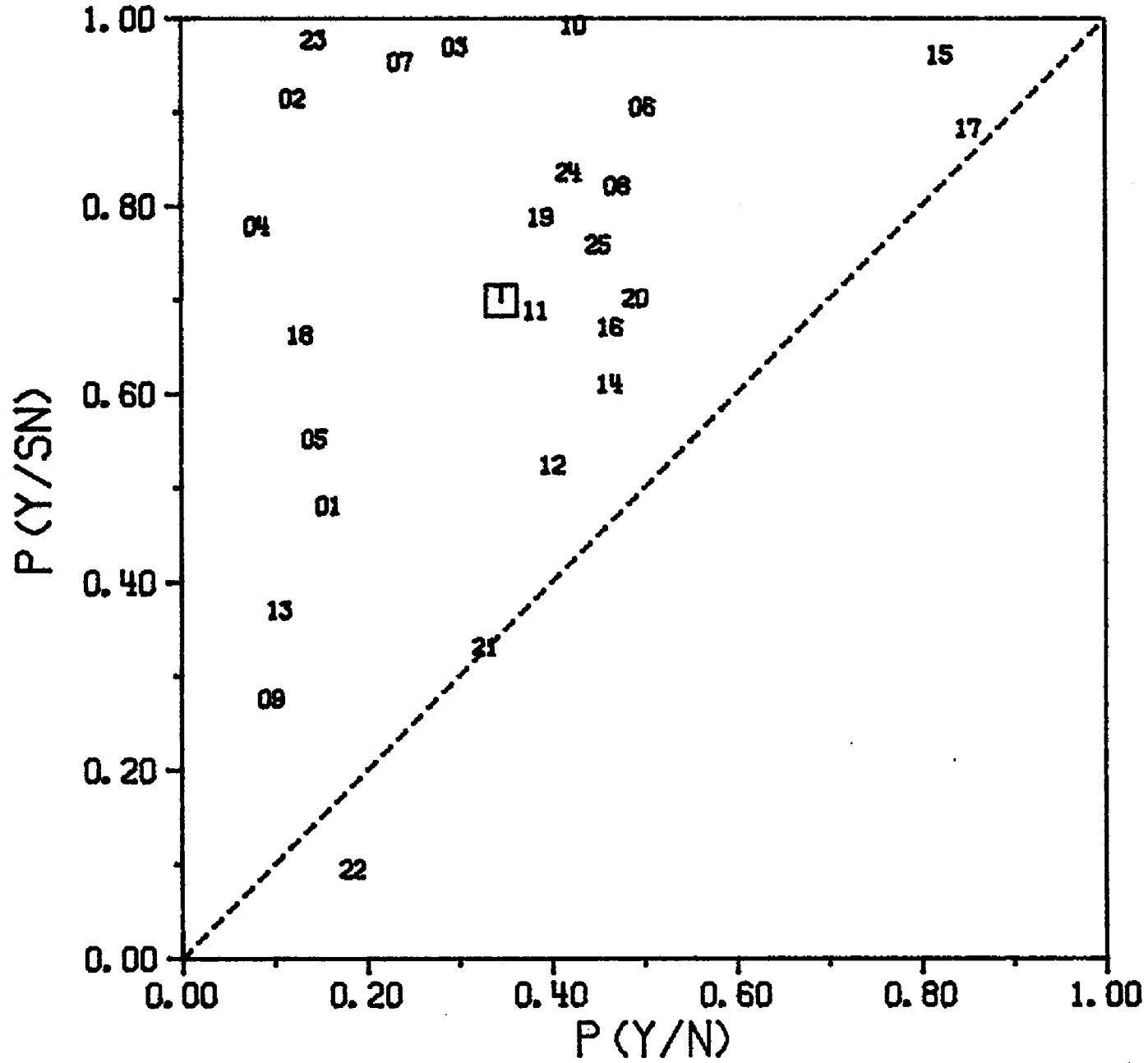


Figure A2.8. Hit and false-alarm rates obtained for individual samples are shown in ROC space. Each number plotted shows the data for the sample associated with that number. The square symbol shows the average hit rate and false alarm rate across all samples. The data shown are for subject CV and were collected with Alpha equal to 270.

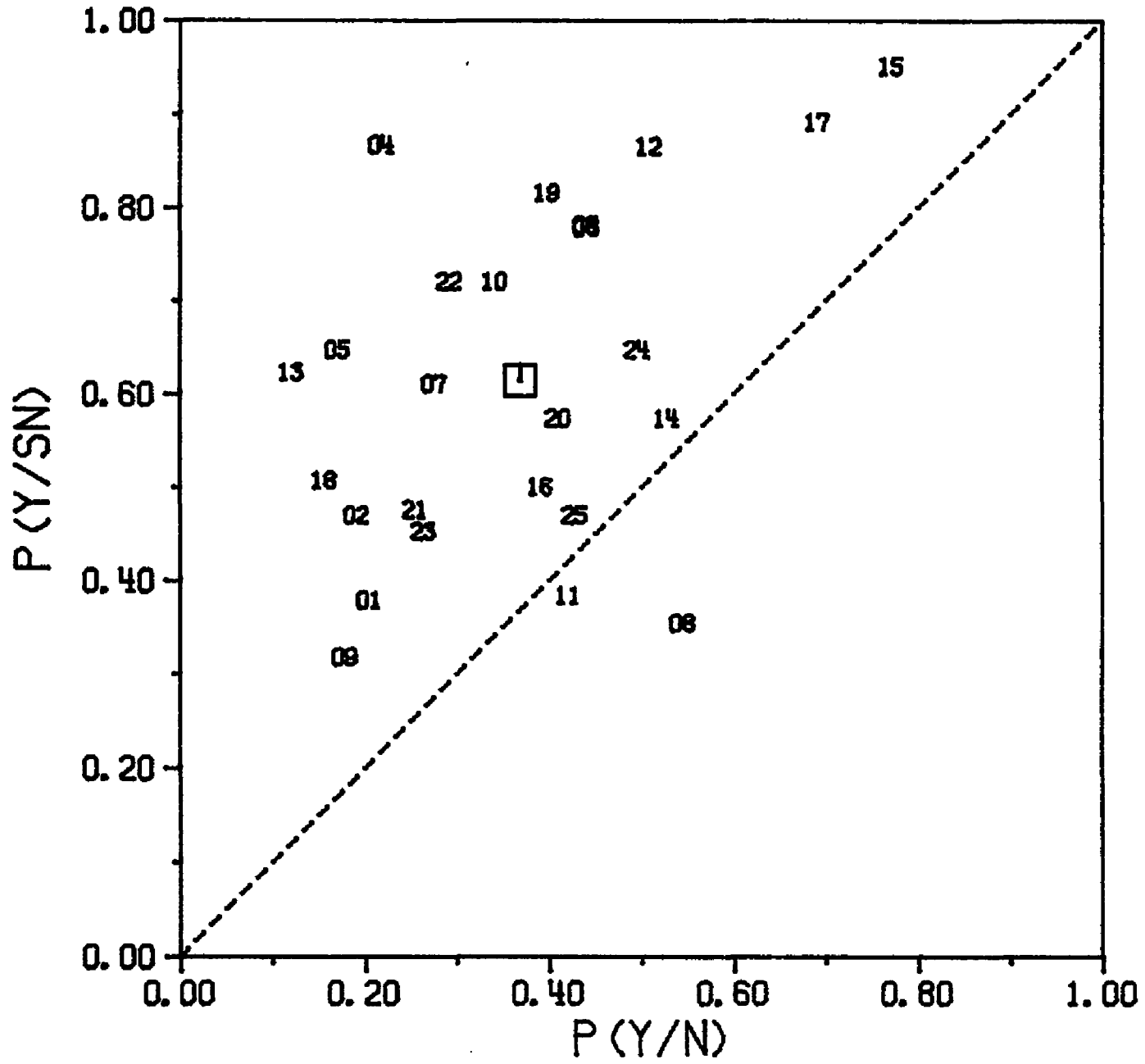


Figure A2.9. Hit and false-alarm rates obtained for individual samples are shown in ROC space. Each number plotted shows the data for the sample associated with that number. The square symbol shows the average hit rate and false alarm rate across all samples. The data shown are for subject TW and were collected with Alpha equal to 0.

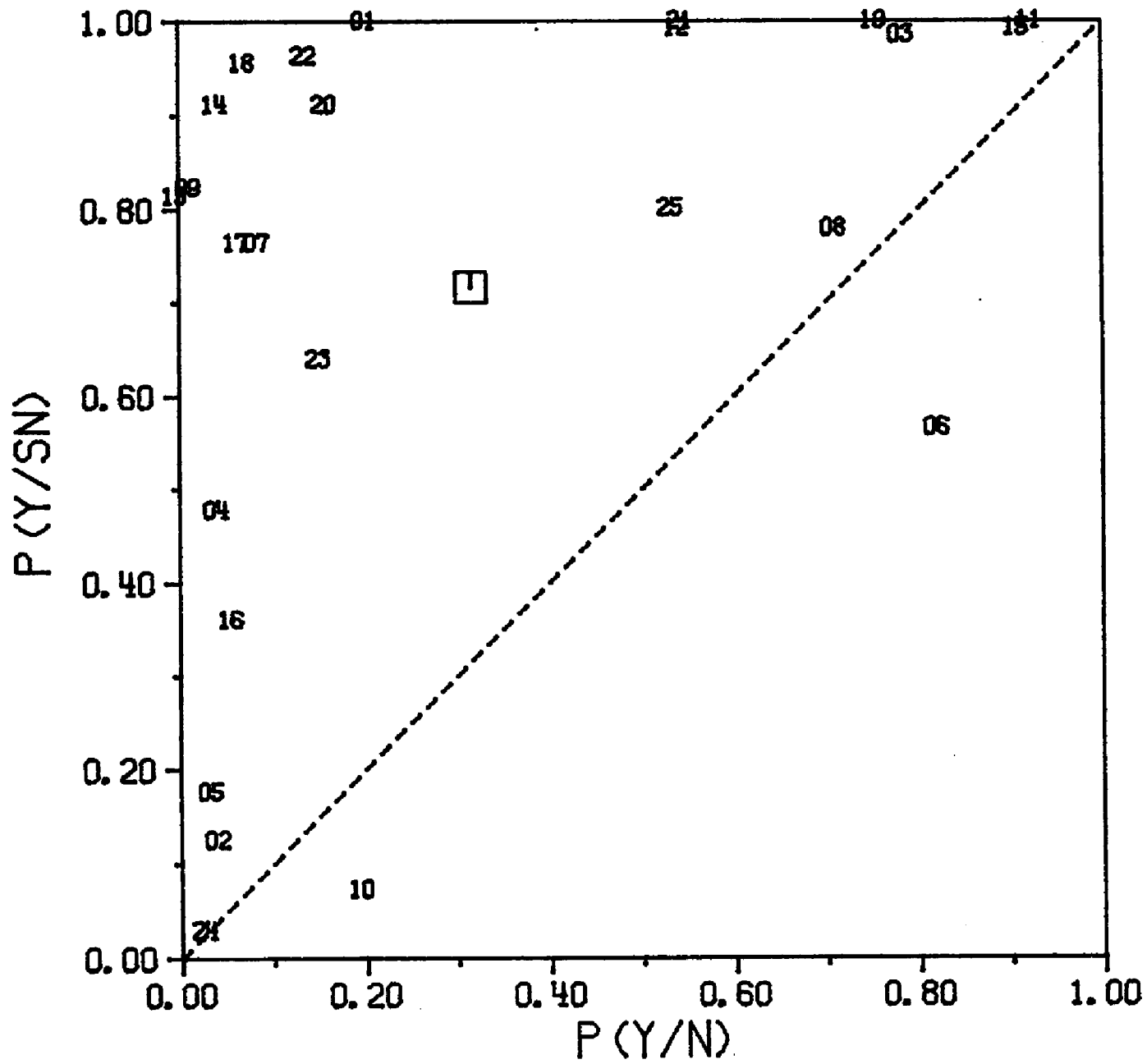


Figure A2.10. Hit and false-alarm rates obtained for individual samples are shown in ROC space. Each number plotted shows the data for the sample associated with that number. The square symbol shows the average hit rate and false alarm rate across all samples. The data shown are for subject TW and were collected with Alpha equal to 90.

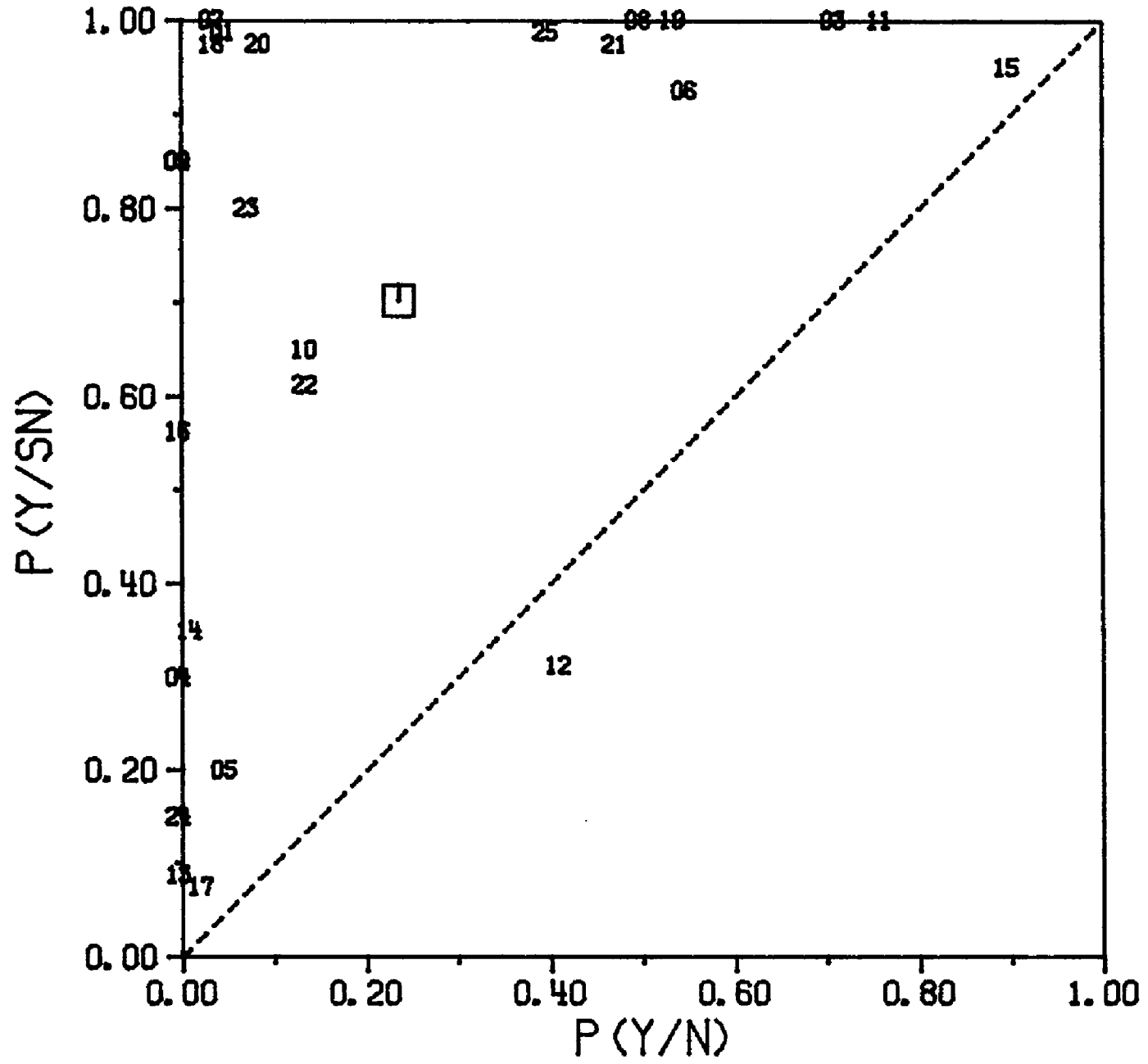


Figure A2.11. Hit and false-alarm rates obtained for individual samples are shown in ROC space. Each number plotted shows the data for the sample associated with that number. The square symbol shows the average hit rate and false alarm rate across all samples. The data shown are for subject TW and were collected with Alpha equal to 180.

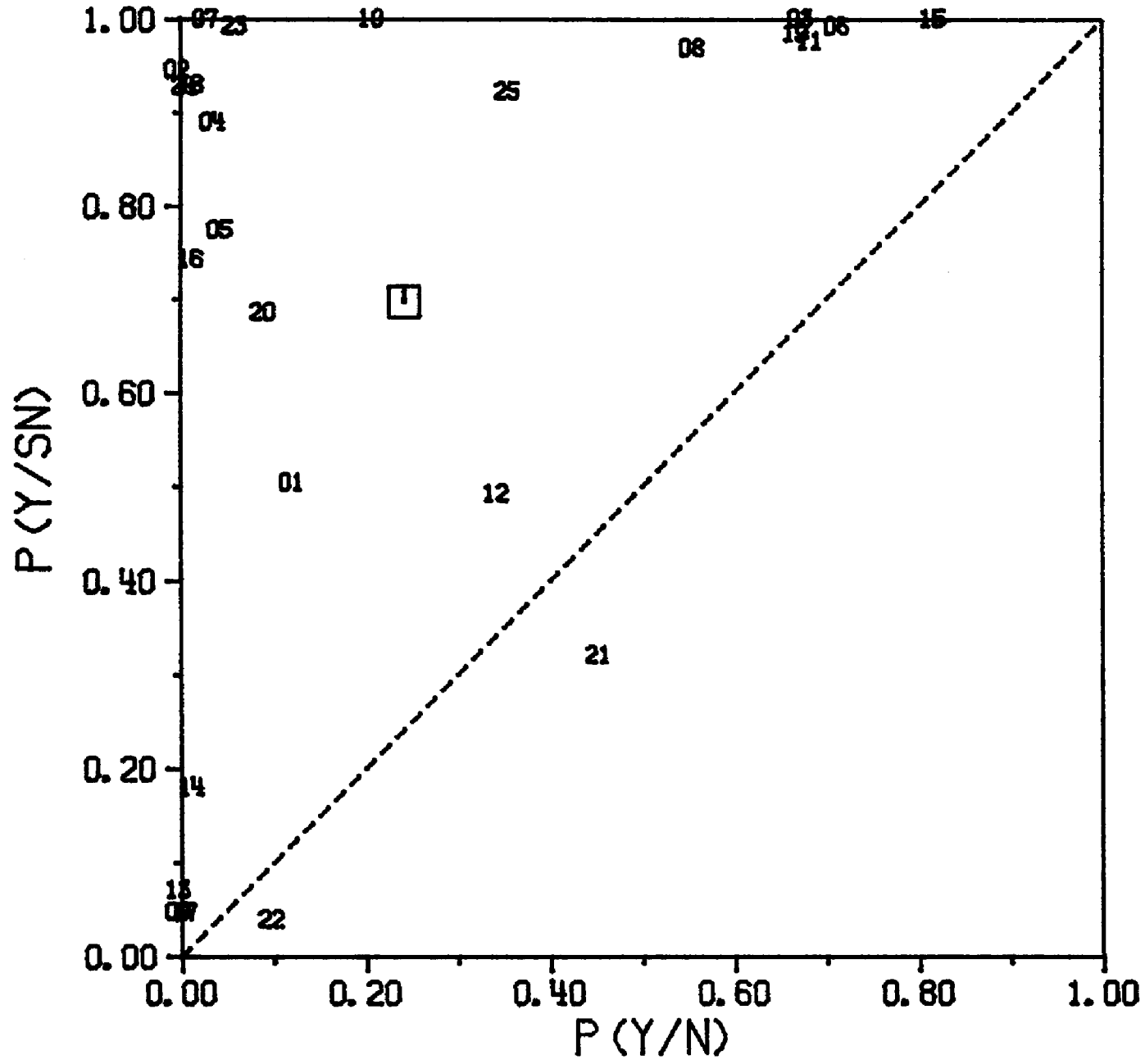


Figure A2.12. Hit and false-alarm rates obtained for individual samples are shown in ROC space. Each number plotted shows the data for the sample associated with that number. The square symbol shows the average hit rate and false alarm rate across all samples. The data shown are for subject TW and were collected with Alpha equal to 270.

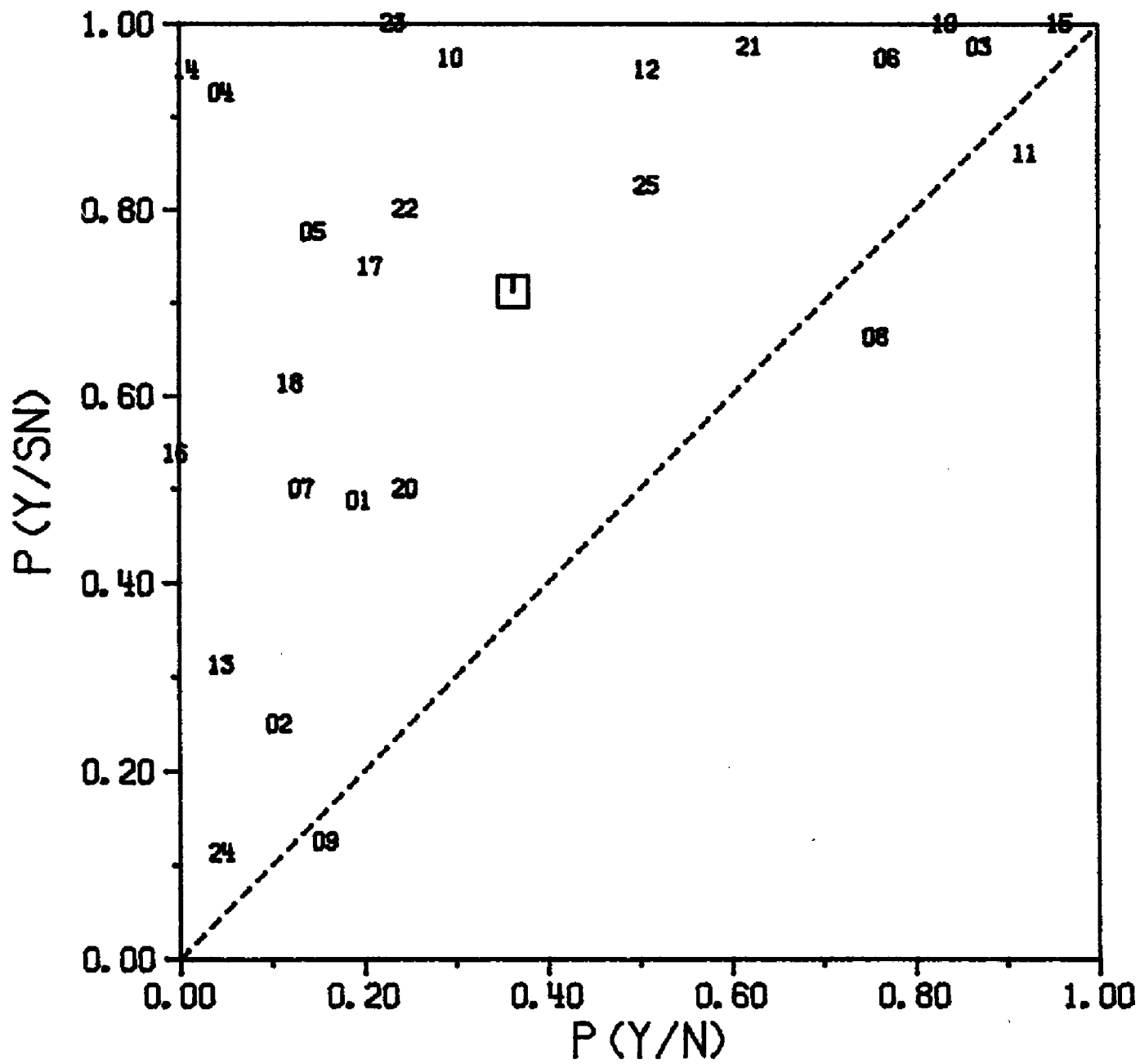


Figure A2.13. Hit and false-alarm rates obtained for individual samples are shown in ROC space. Each number plotted shows the data for the sample associated with that number. The square symbol shows the average hit rate and false alarm rate across all samples. The data shown are for subject JM and were collected with Alpha equal to 0.

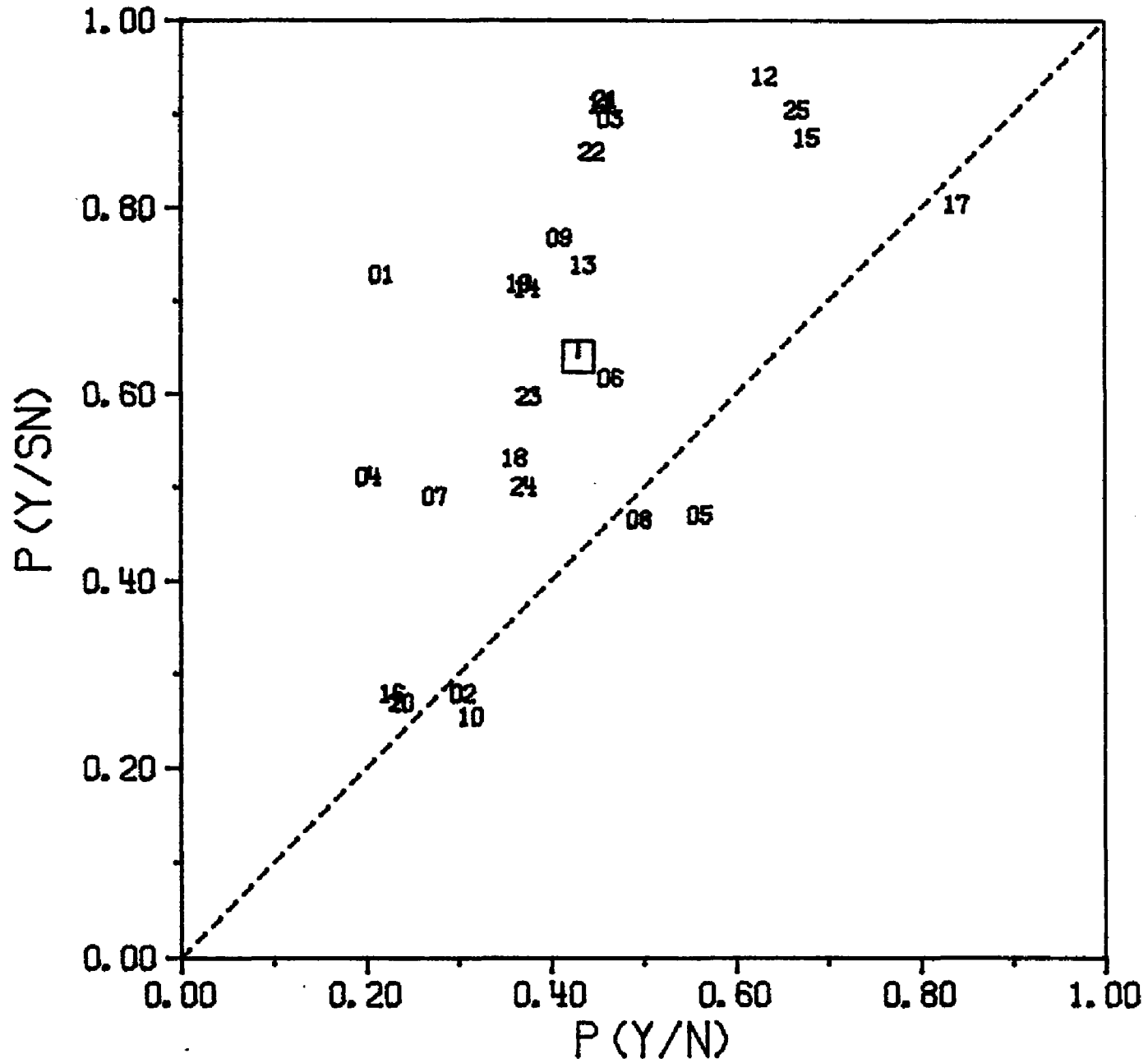


Figure A2.14. Hit and false-alarm rates obtained for individual samples are shown in ROC space. Each number plotted shows the data for the sample associated with that number. The square symbol shows the average hit rate and false alarm rate across all samples. The data shown are for subject JM and were collected with Alpha equal to 90.

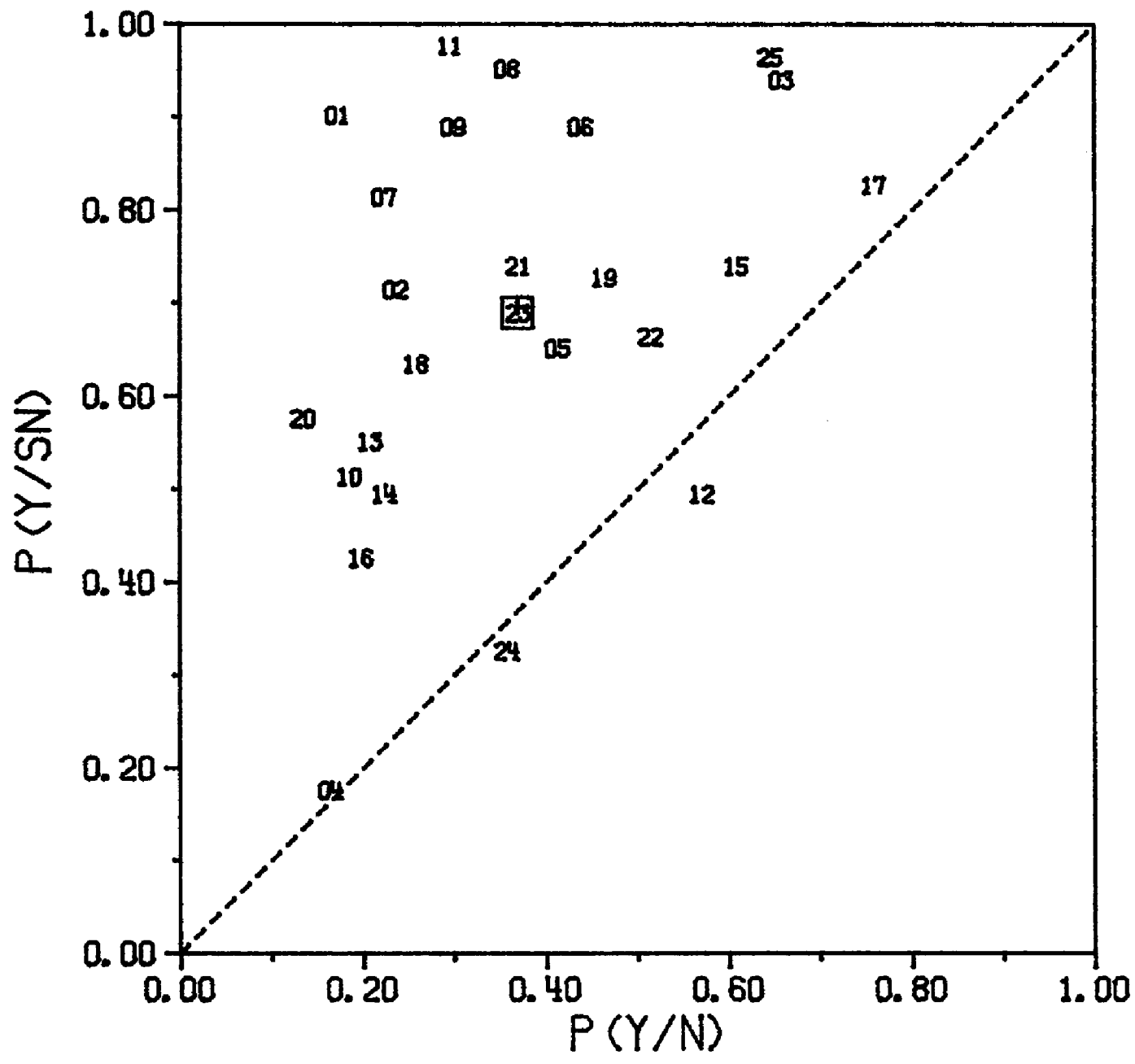


Figure A2.15. Hit and false-alarm rates obtained for individual samples are shown in ROC space. Each number plotted shows the data for the sample associated with that number. The square symbol shows the average hit rate and false alarm rate across all samples. The data shown are for subject JM and were collected with Alpha equal to 180.

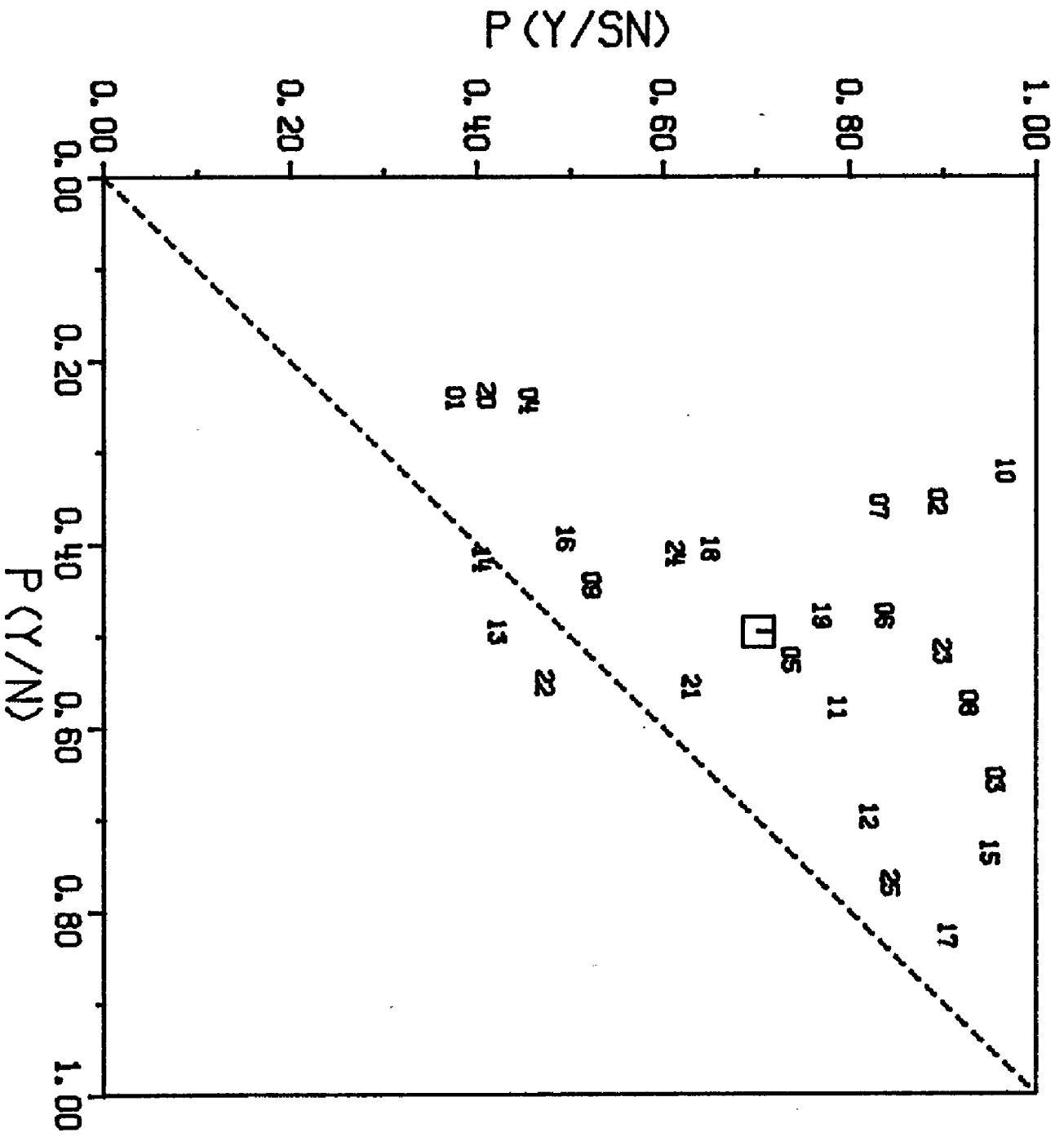


Figure A2.16. Hit and false-alarm rates obtained for individual samples are shown in ROC space. Each number plotted shows the data for the sample associated with that number. The square symbol shows the average hit rate and false alarm rate across all samples. The data shown are for subject JM and were collected with Alpha equal to 270.

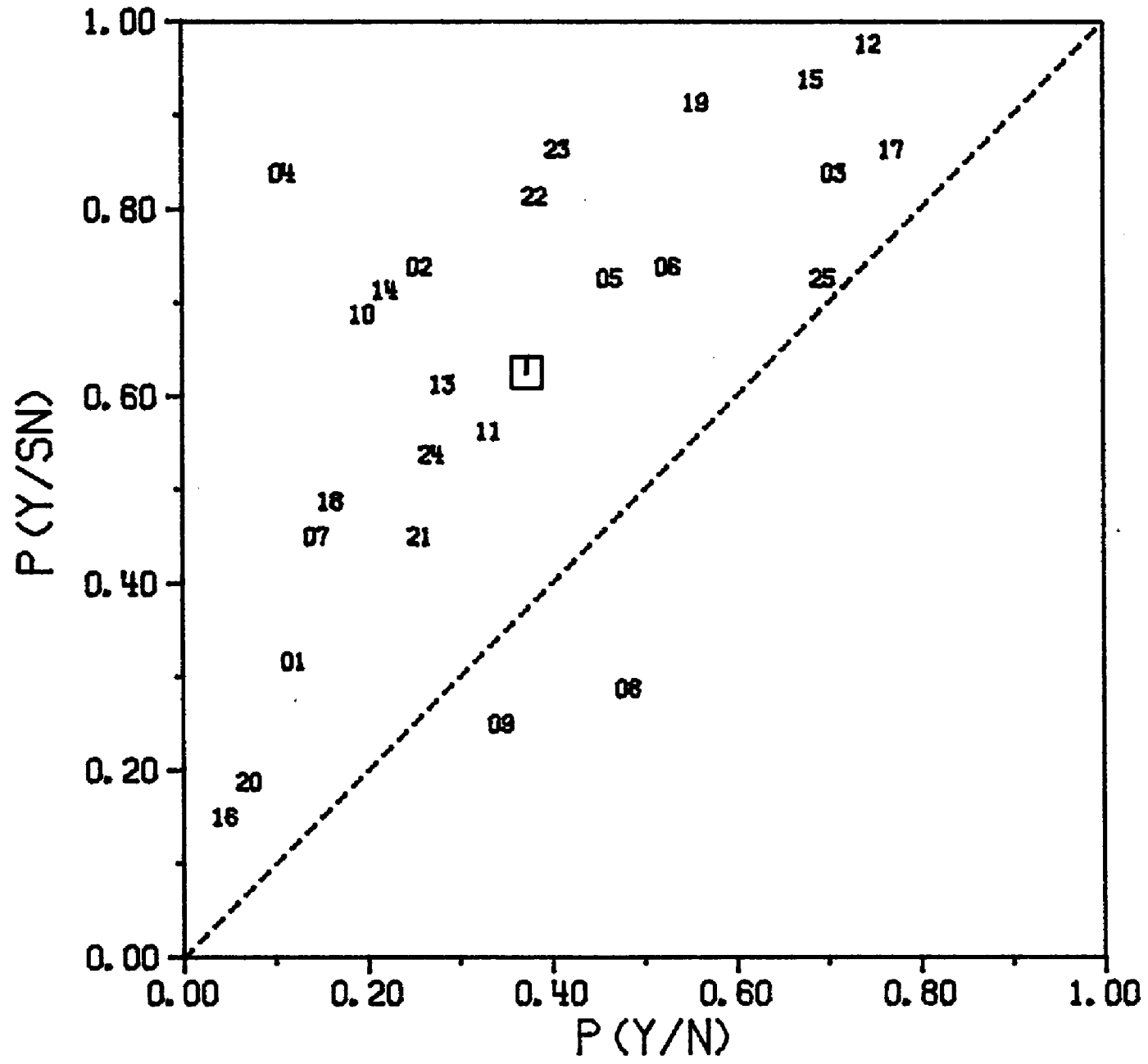
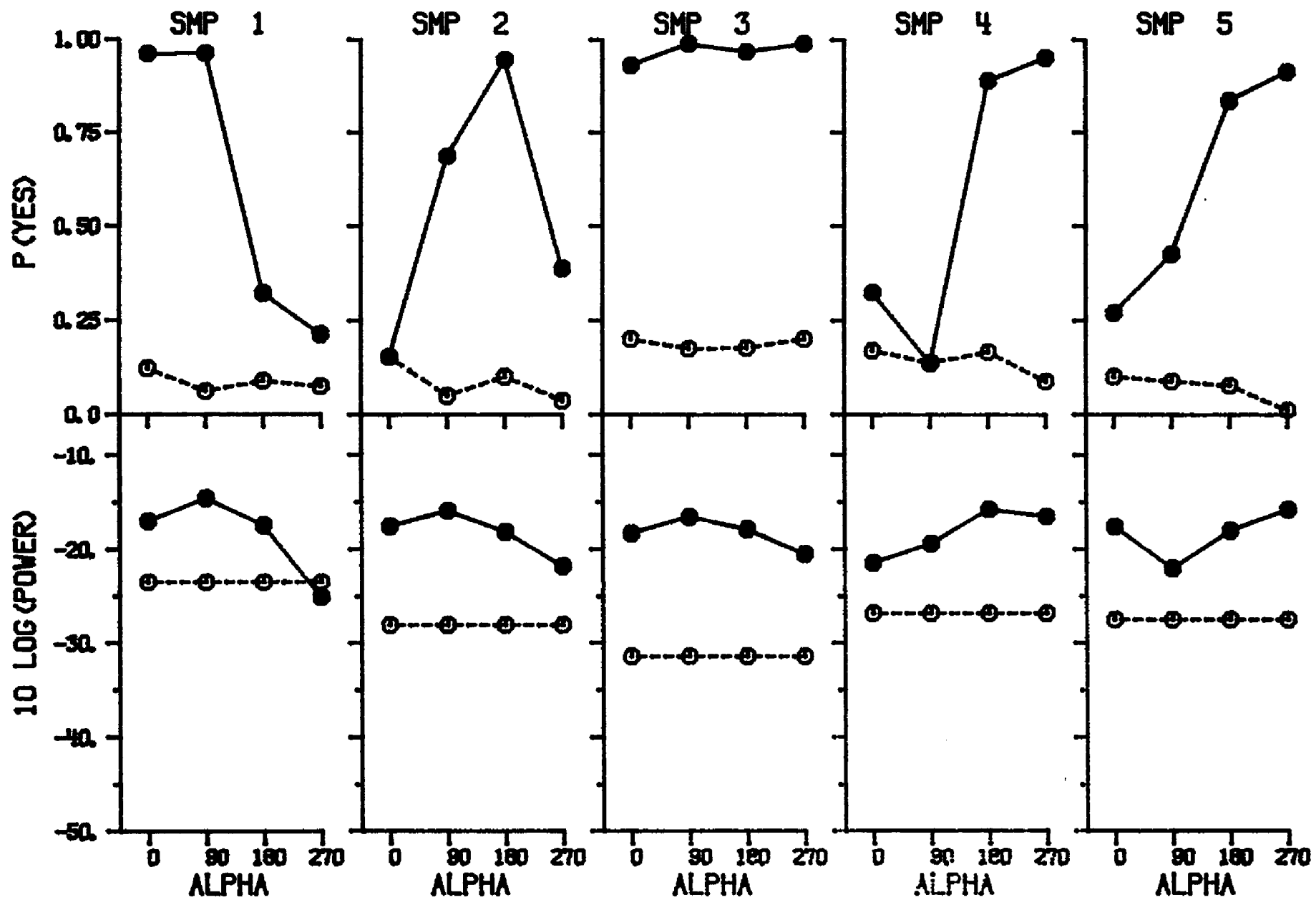
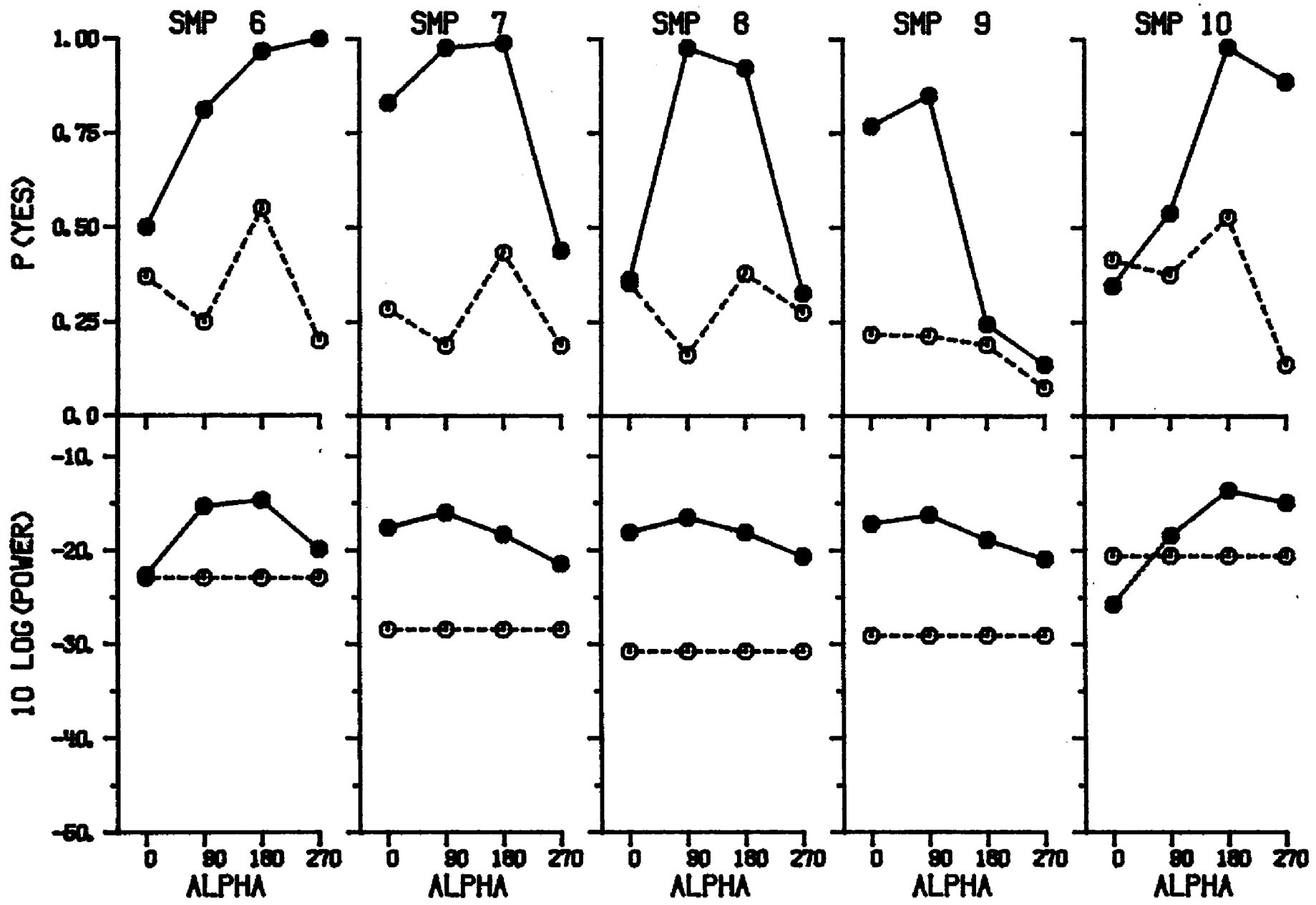
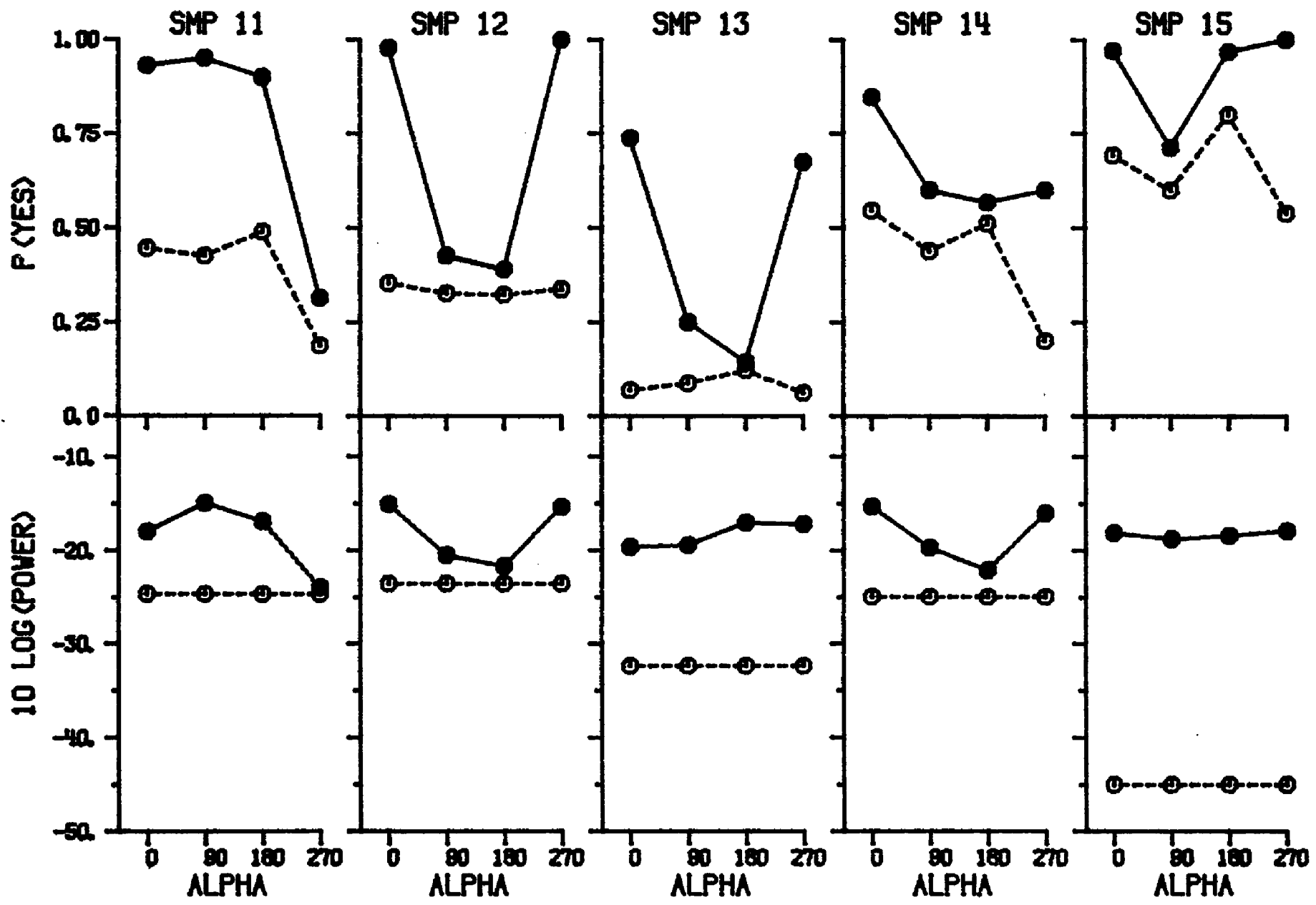
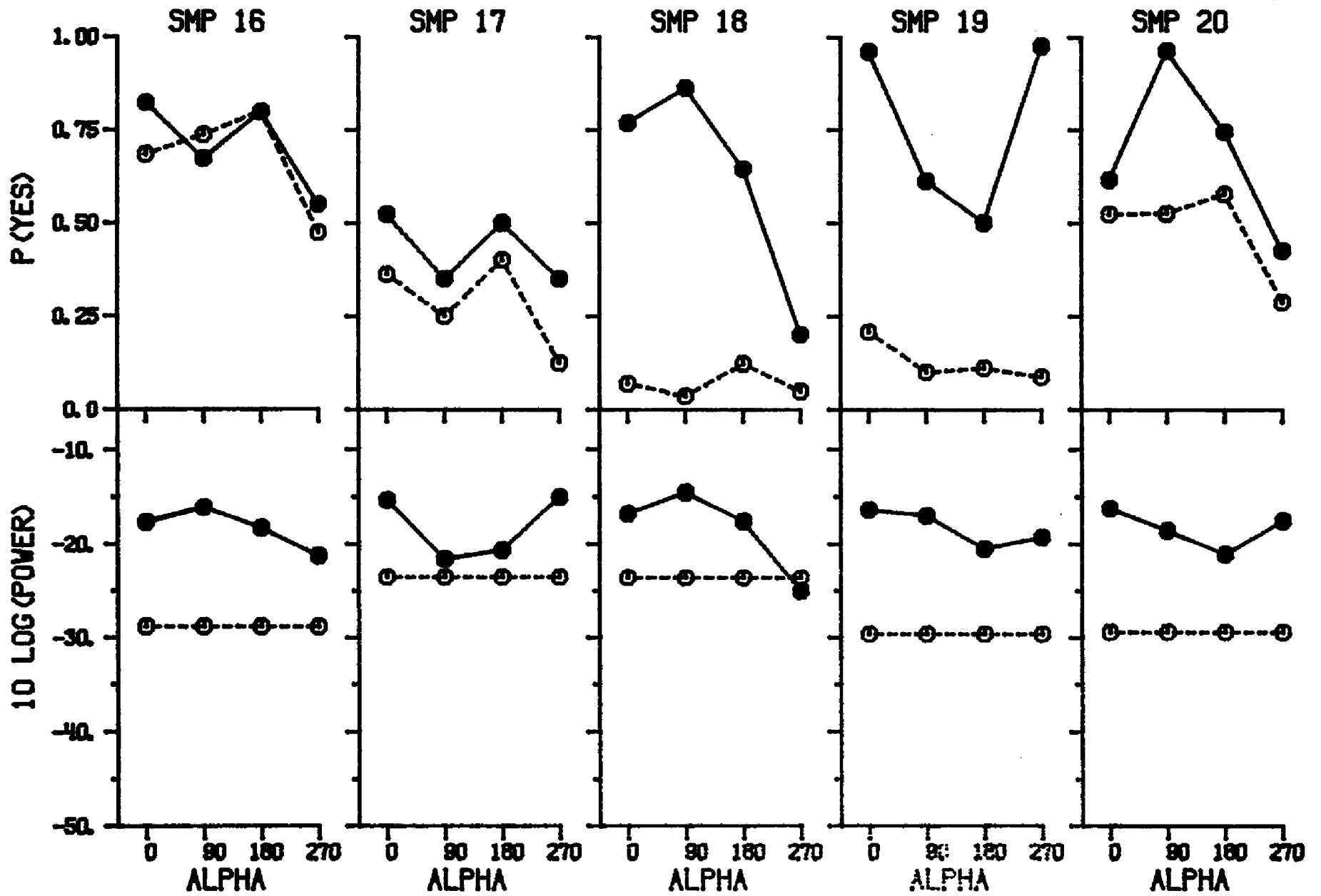


Figure A2.17. Performance and stimulus measures as a function of Alpha. Each panel shows the results for a particular sample. The upper half of each panel shows the obtained proportion of "Yes" responses as a function of Alpha. The lower half of each panel shows the power at the 500-Hz component of the Fourier spectrum of the stimulus. Filled symbols are for signal-plus-noise trials. Open symbols are for noise-alone trials. Performance data are for subject SG, and were collected at $10 \text{ Log}(E/No)$ equal to 8.5 dB. (The figure extends through five pages.)









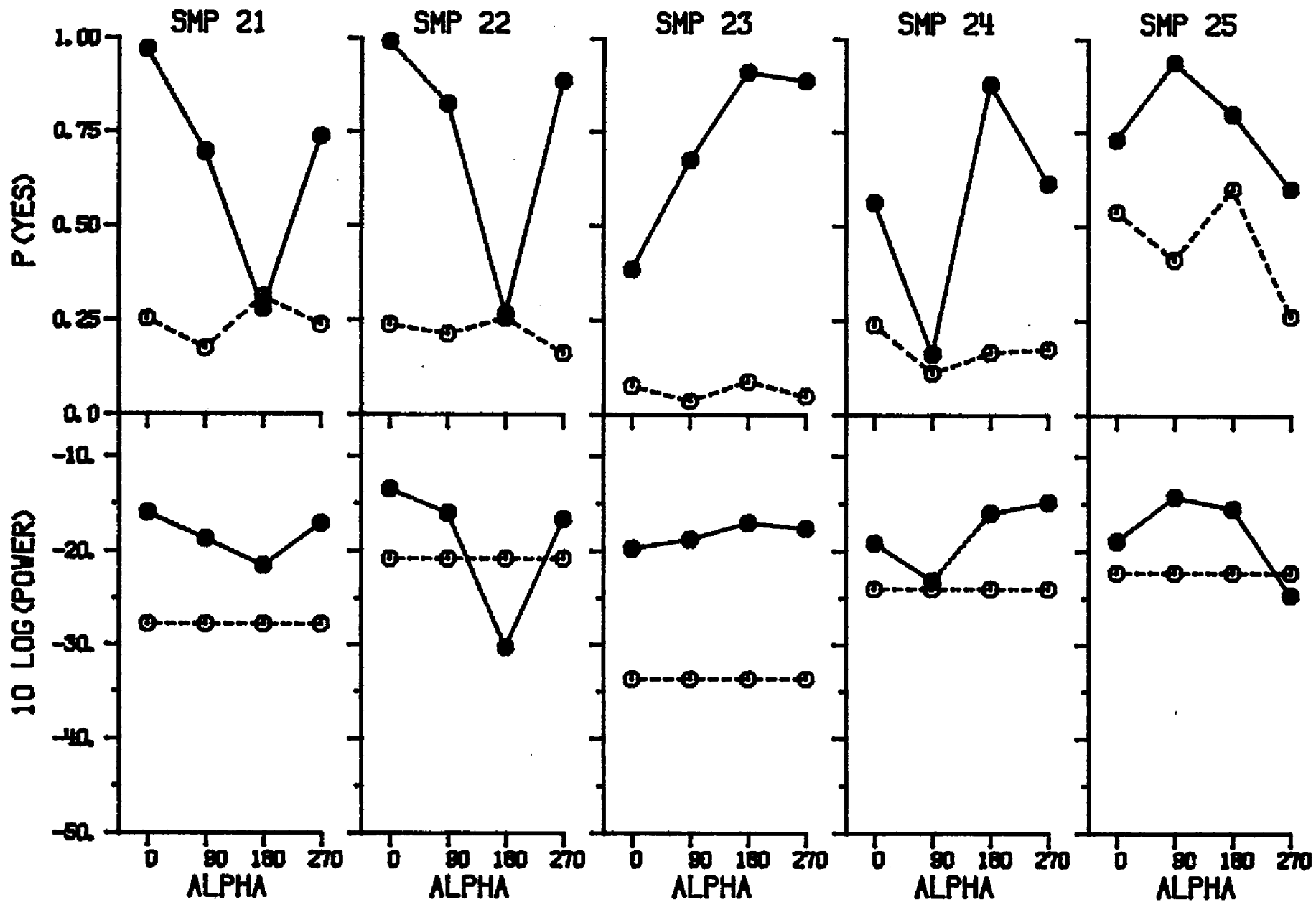
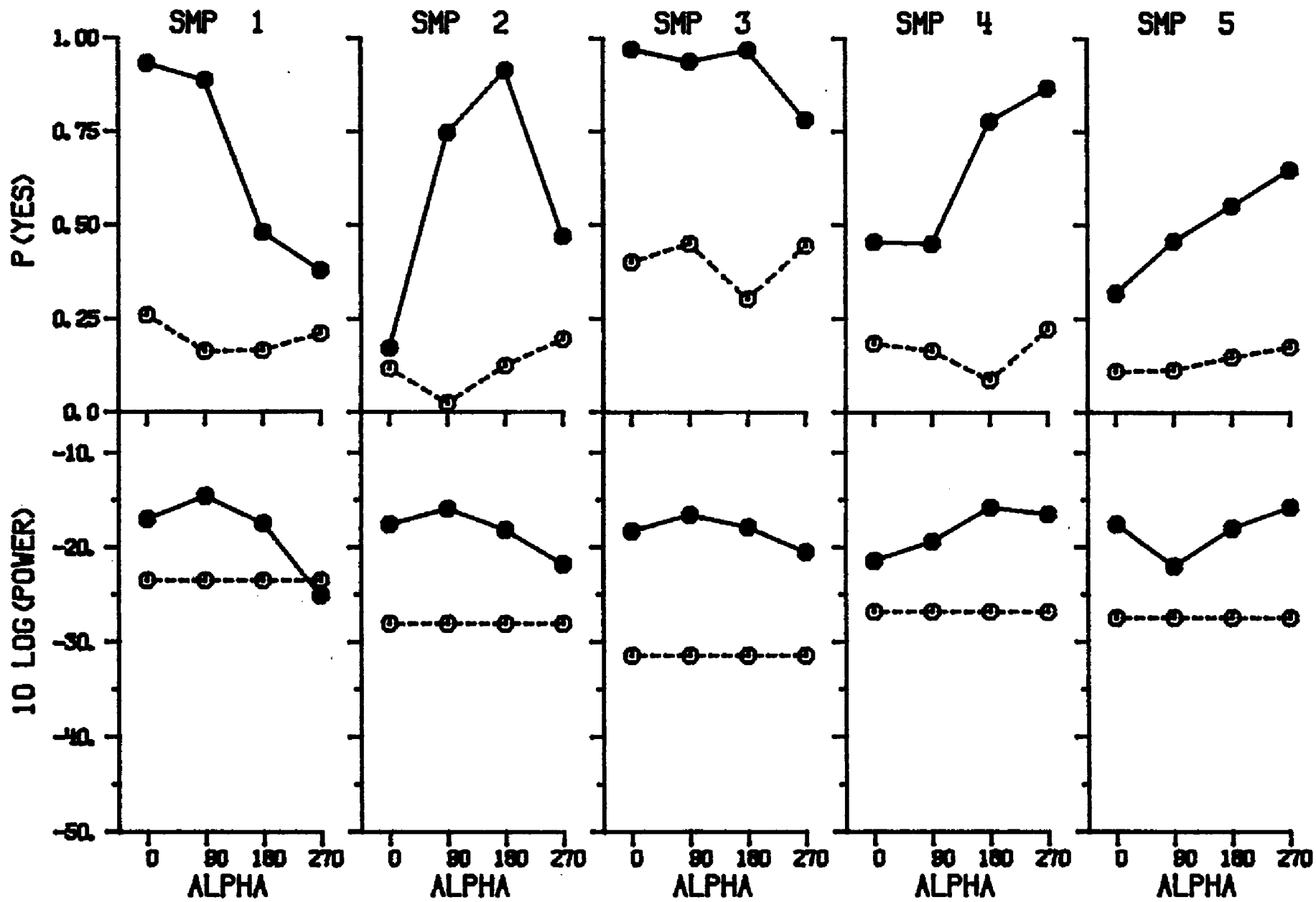
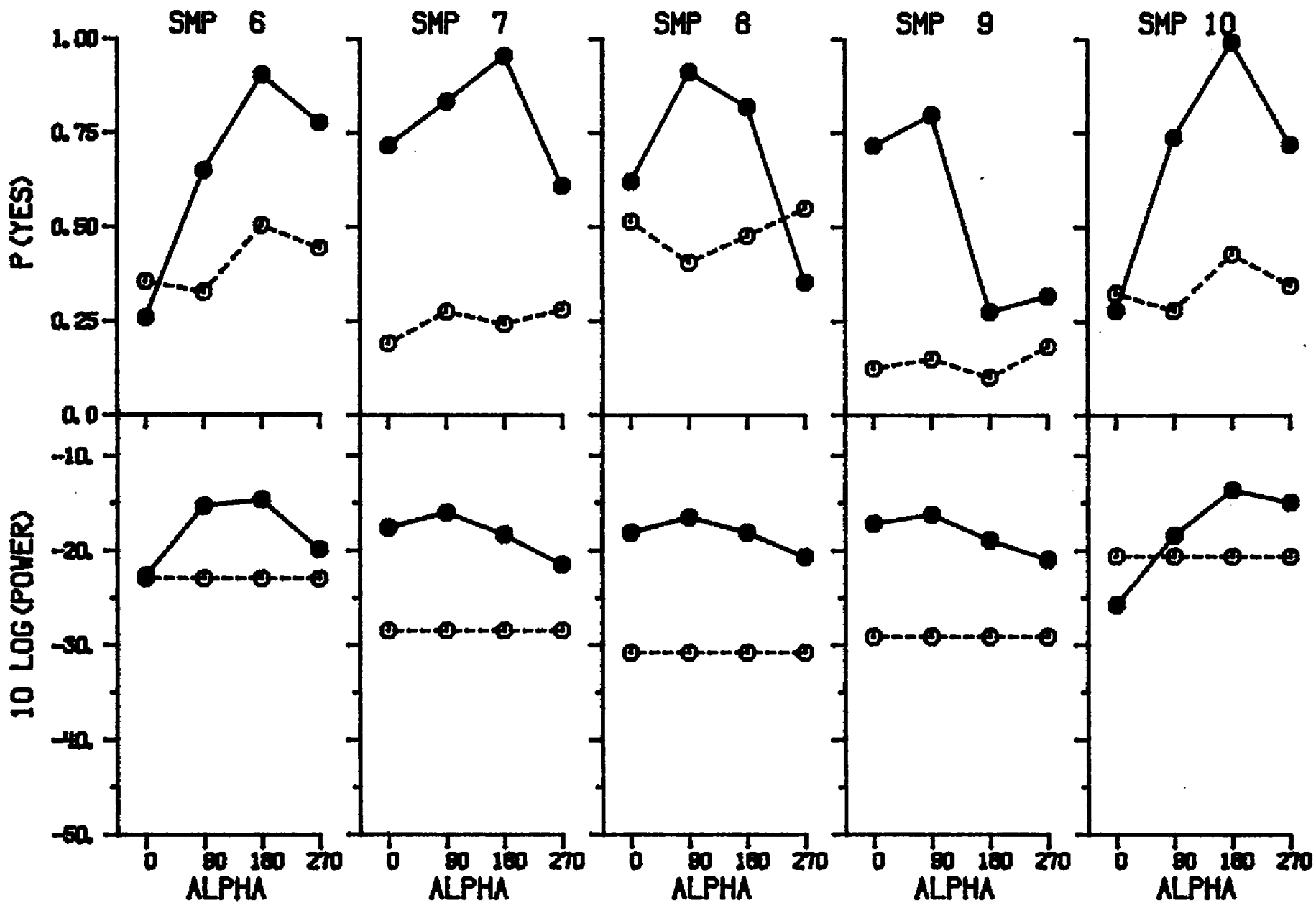
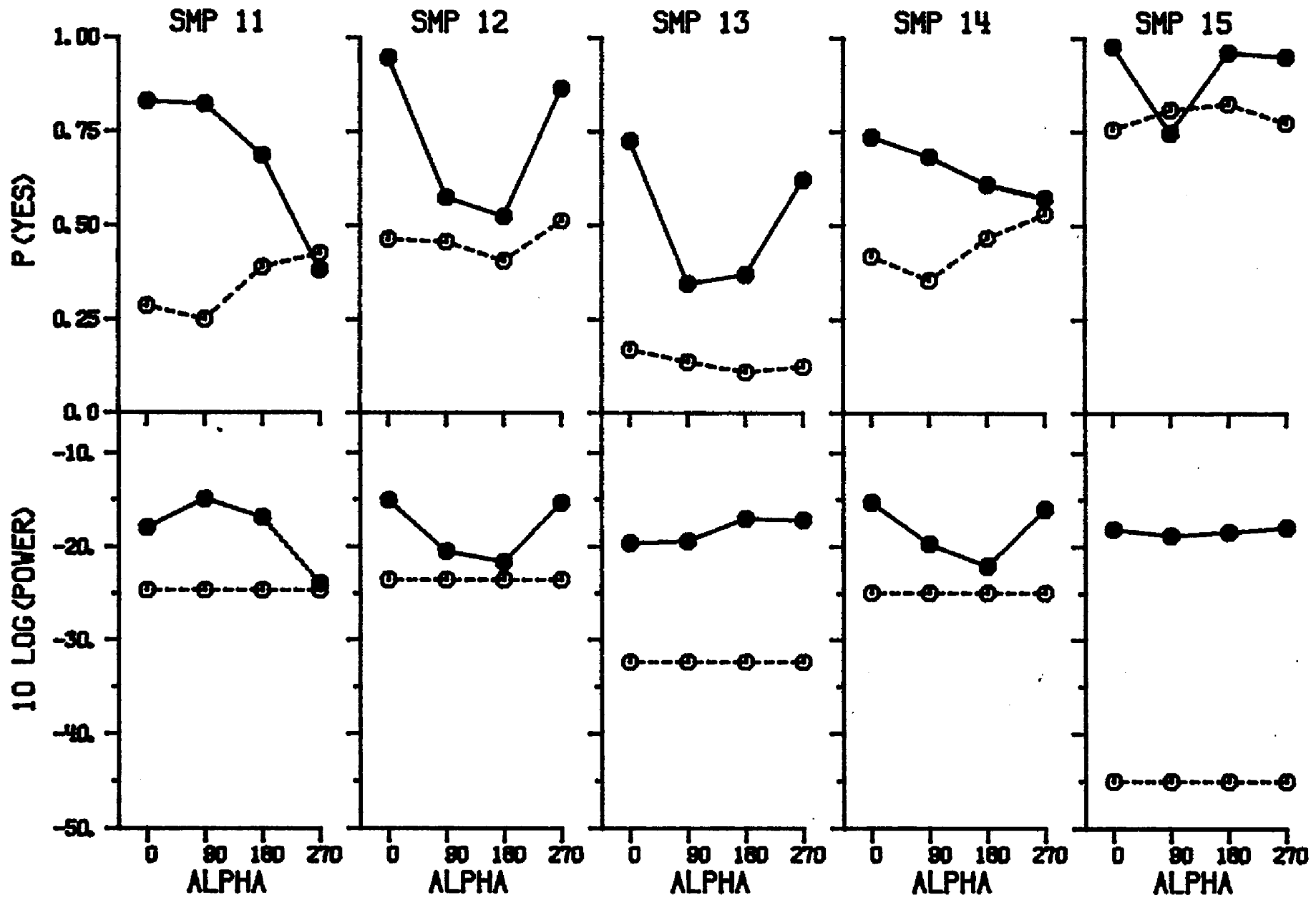
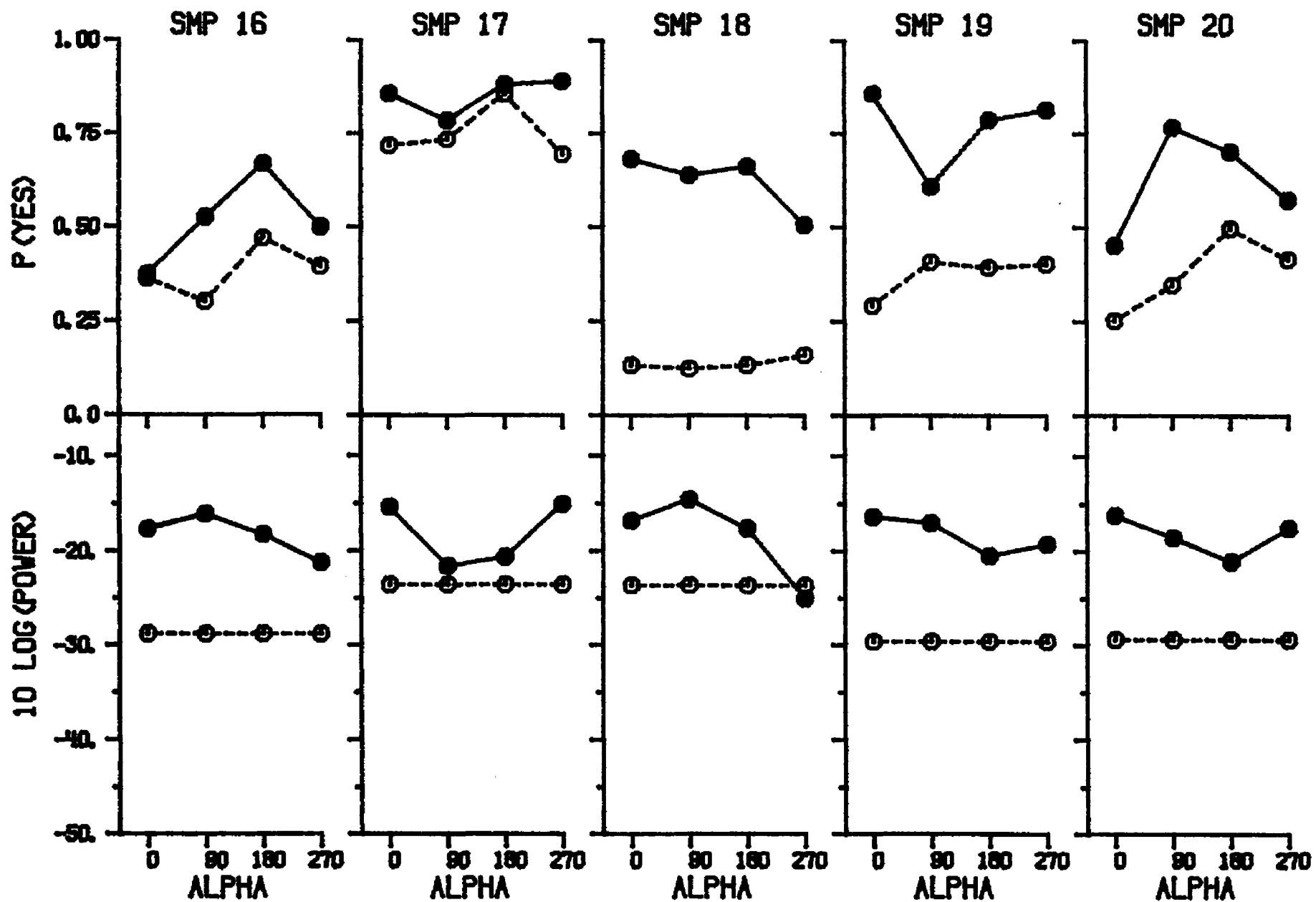


Figure A2.18. Performance and stimulus measures as a function of Alpha. Each panel shows the results for a particular sample. The upper half of each panel shows the obtained proportion of "Yes" responses as a function of Alpha. The lower half of each panel shows the power at the 500-Hz component of the Fourier spectrum of the stimulus. Filled symbols are for signal-plus-noise trials. Open symbols are for noise-alone trials. Performance data are for subject CV, and were collected at $10 \text{ Log}(E/No)$ equal to 8.5 dB. (The figure extends through five pages.)









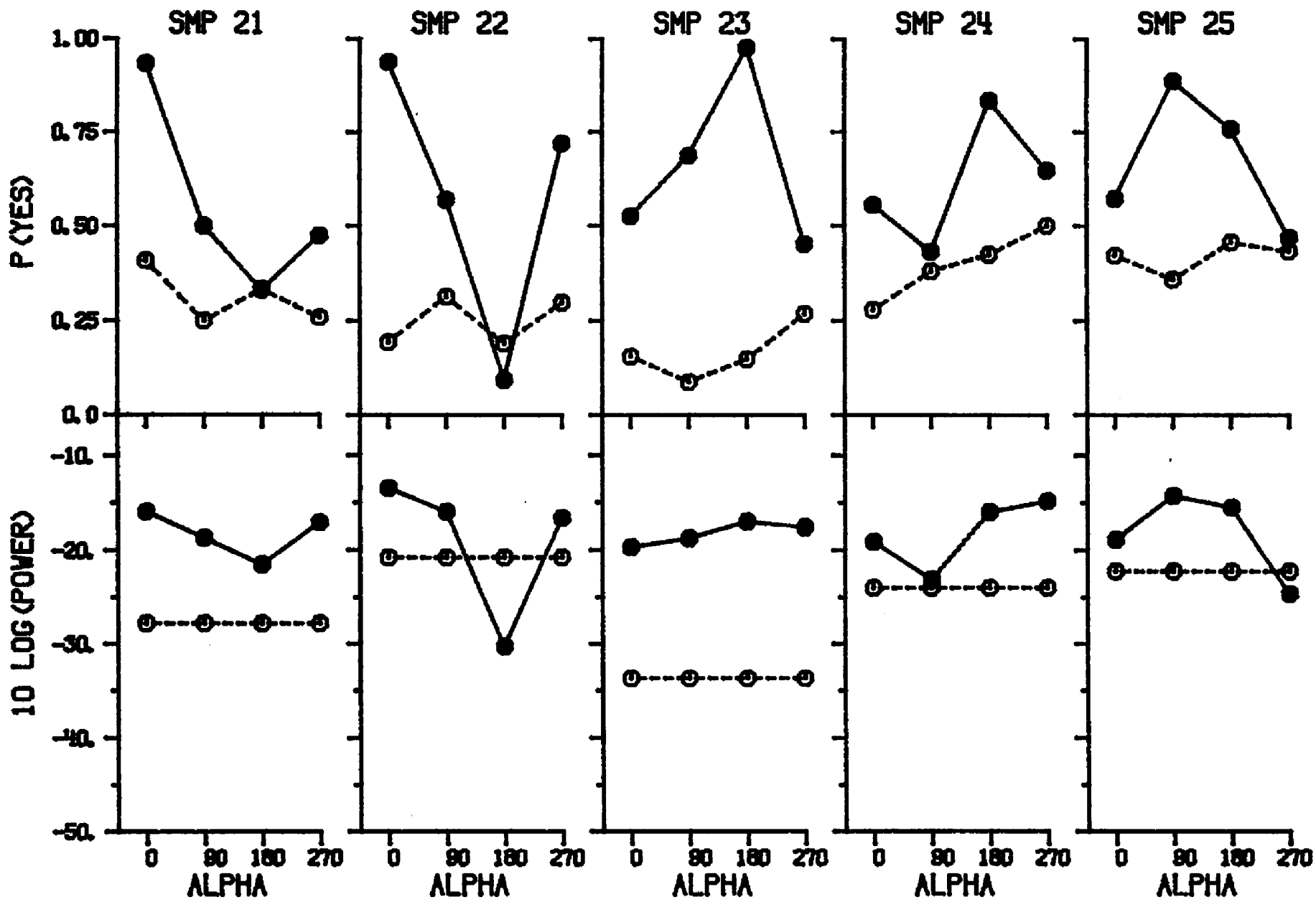
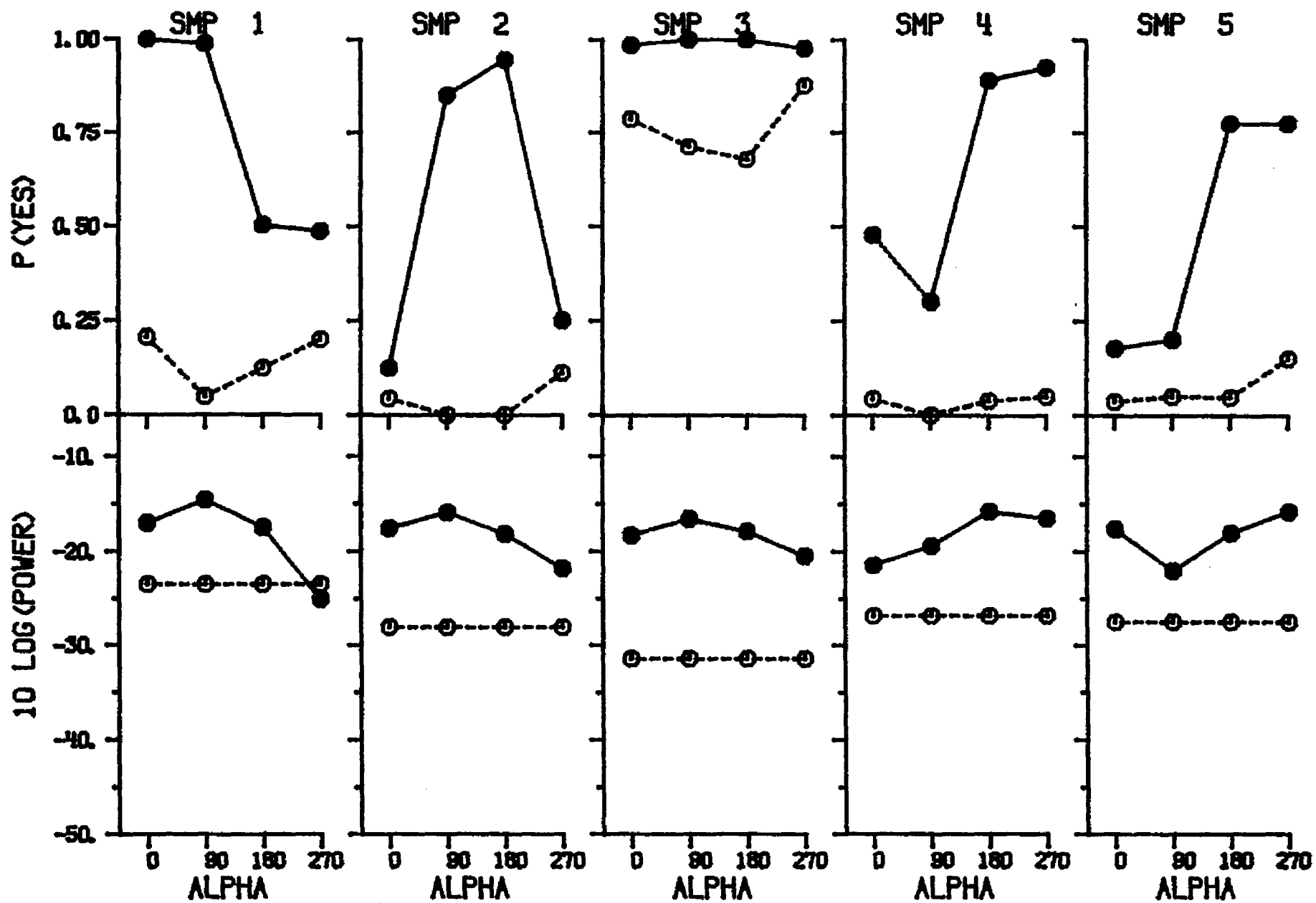
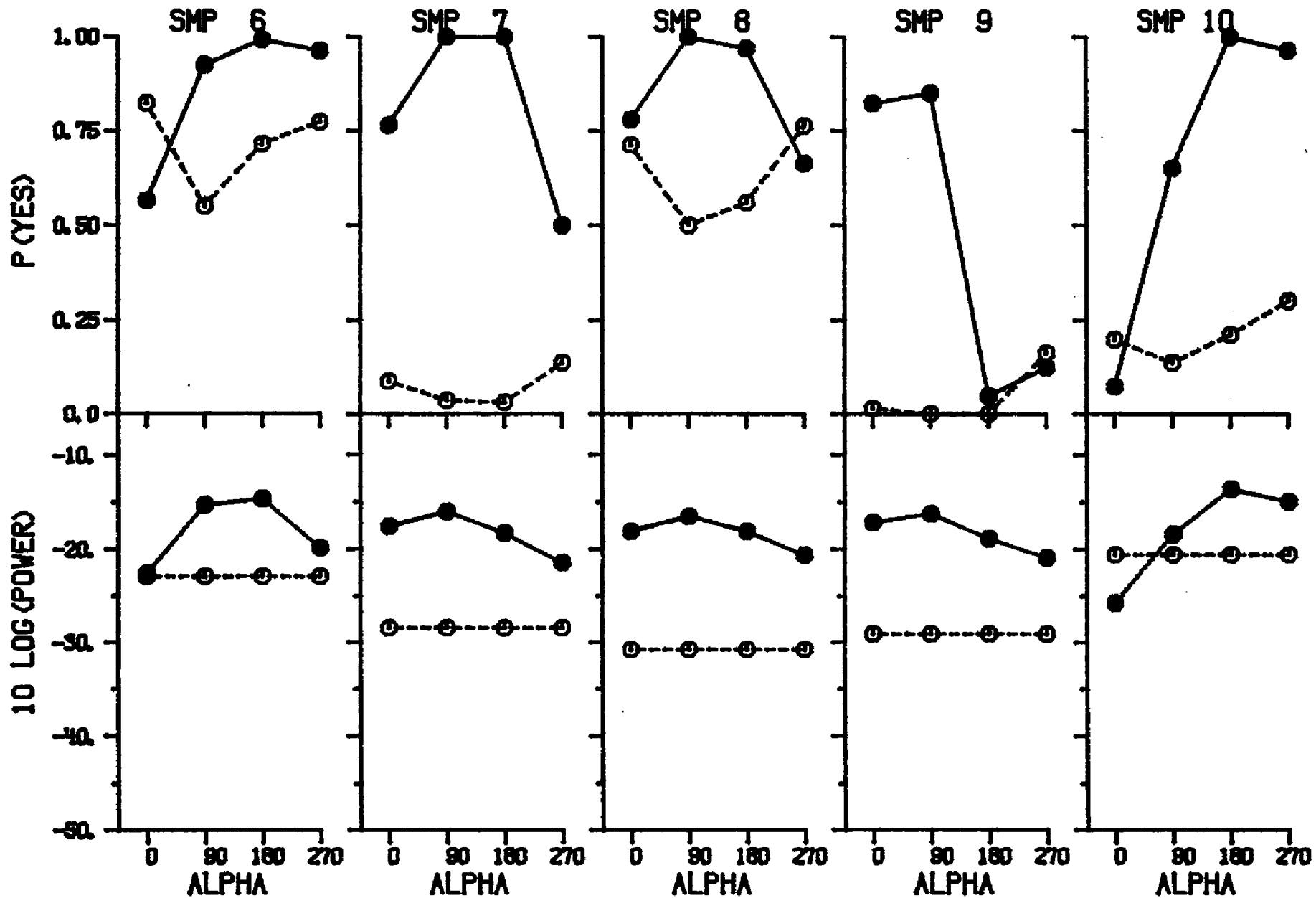
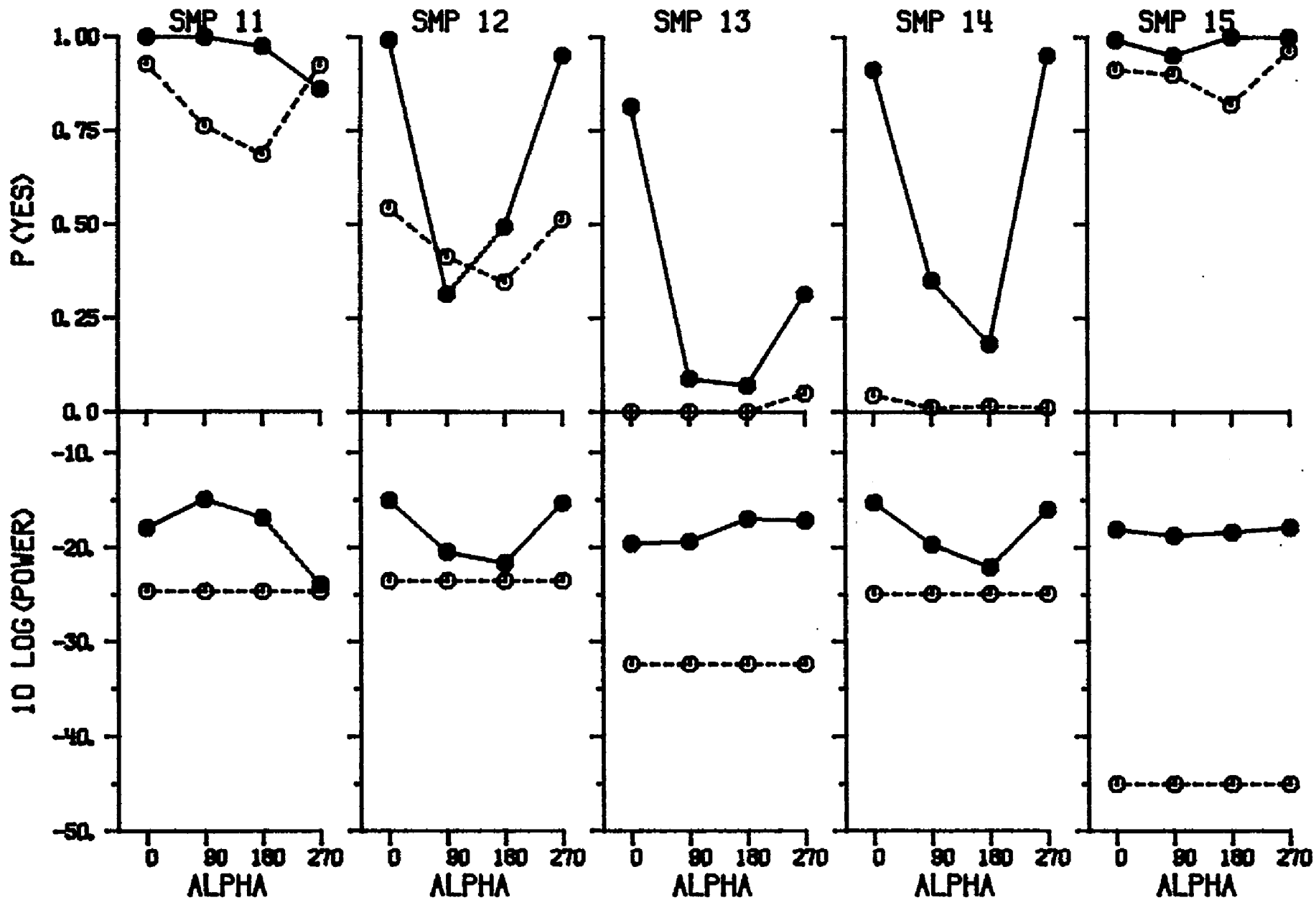
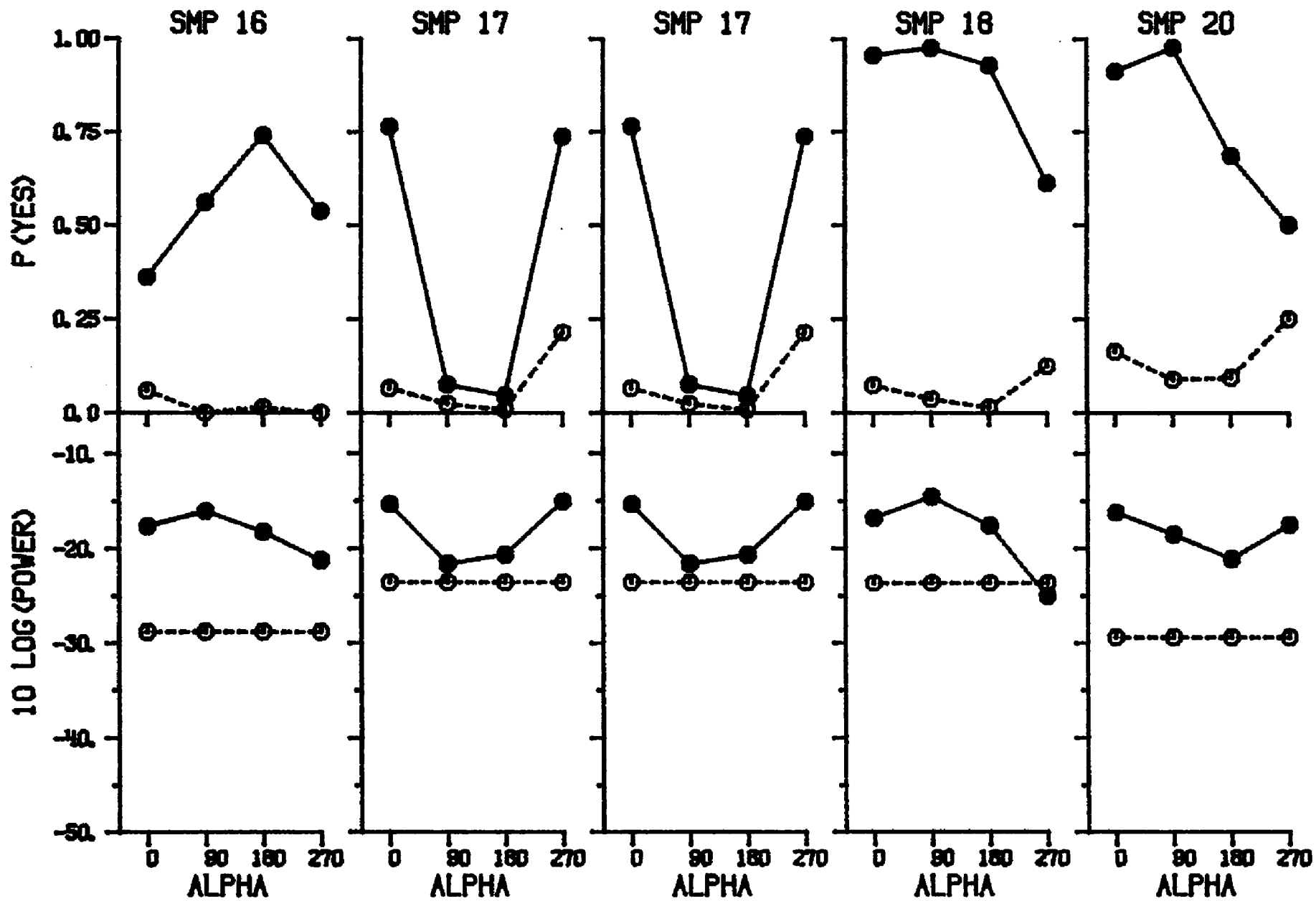


Figure A2.19. Performance and stimulus measures as a function of Alpha. Each panel shows the results for a particular sample. The upper half of each panel shows the obtained proportion of "Yes" responses as a function of Alpha. The lower half of each panel shows the power at the 500-Hz component of the Fourier spectrum of the stimulus. Filled symbols are for signal-plus-noise trials. Open symbols are for noise-alone trials. Performance data are for subject TW, and were collected at $10 \text{ Log}(E/No)$ equal to 8.5 dB. (The figure extends through five pages.)









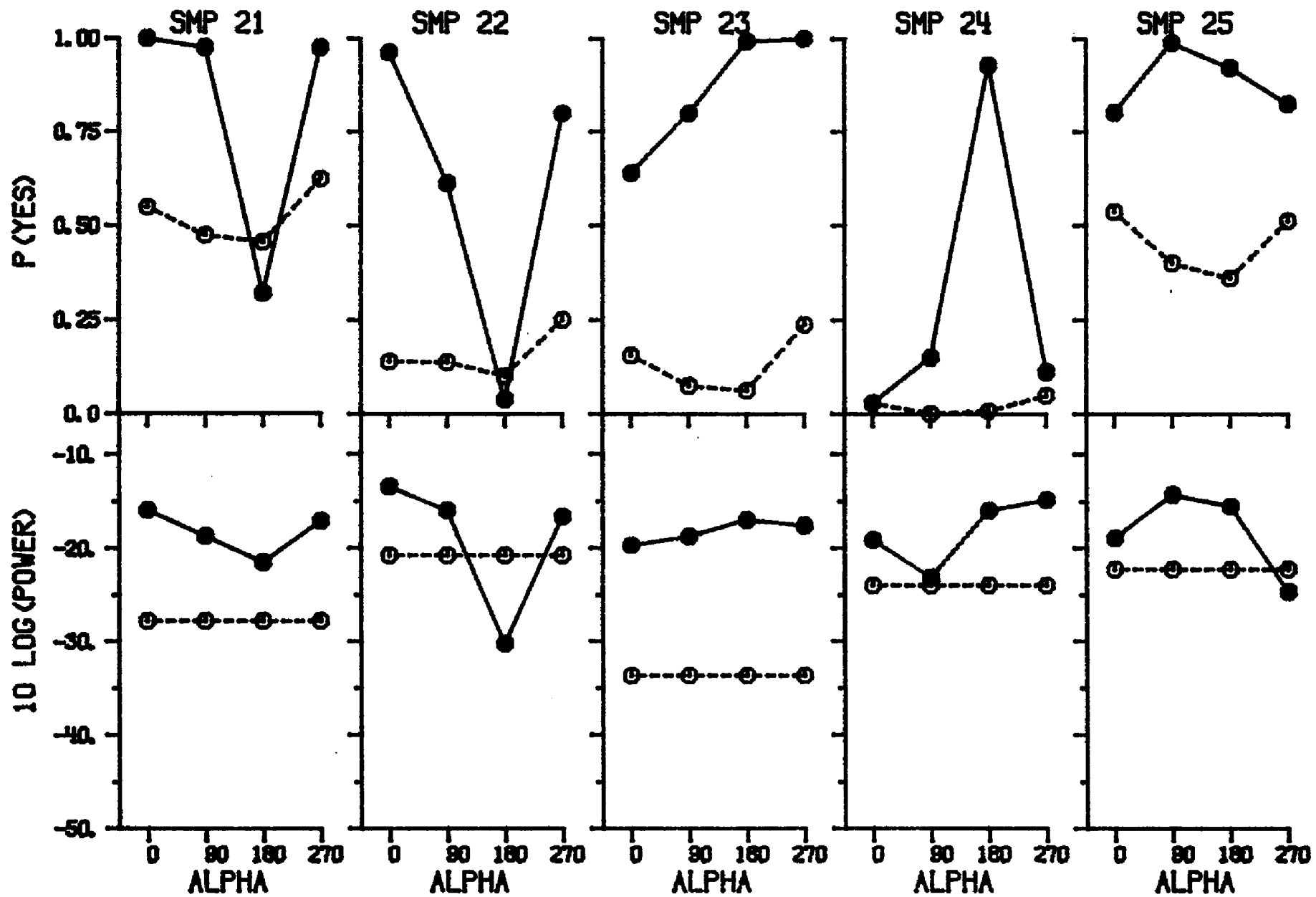
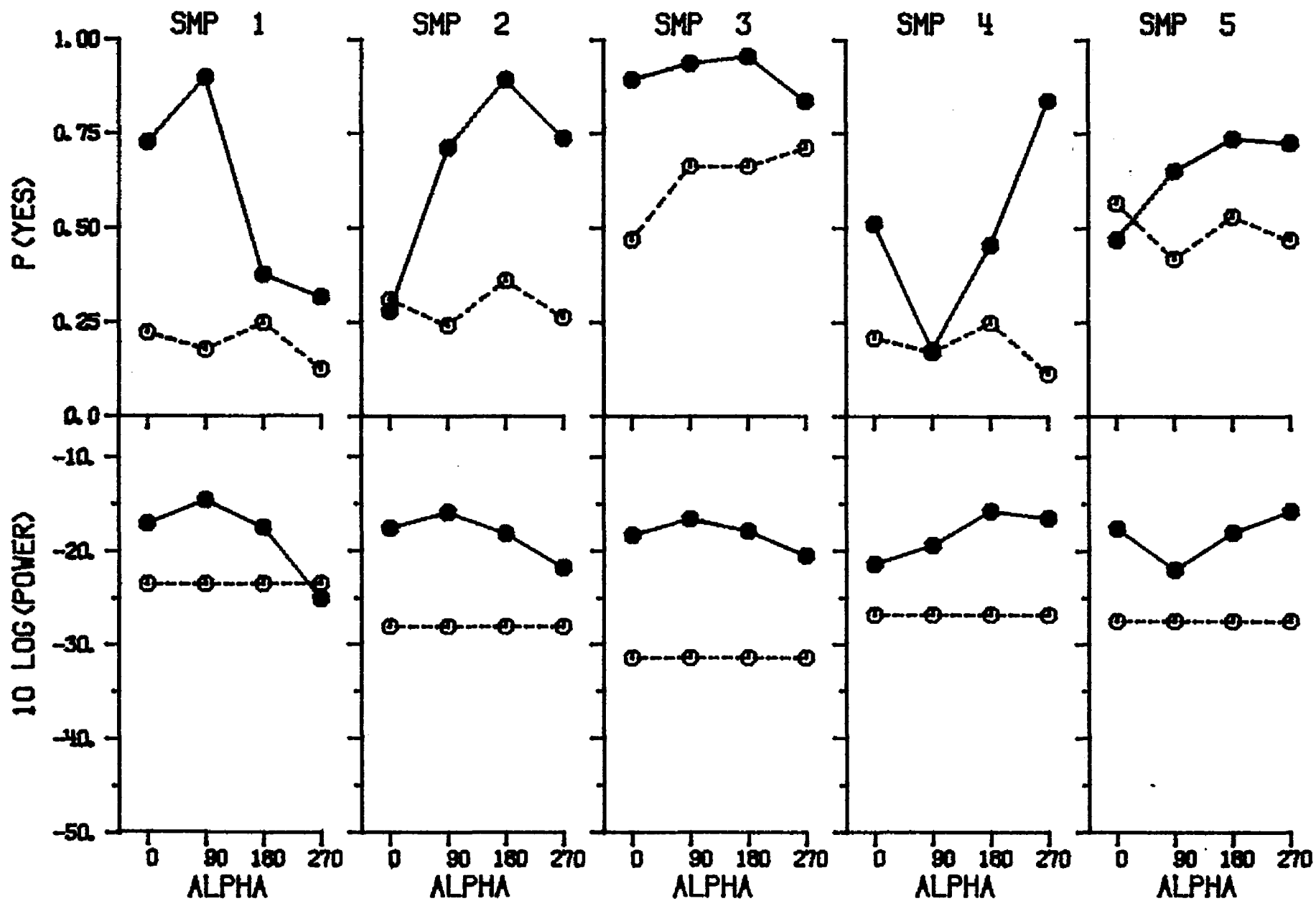
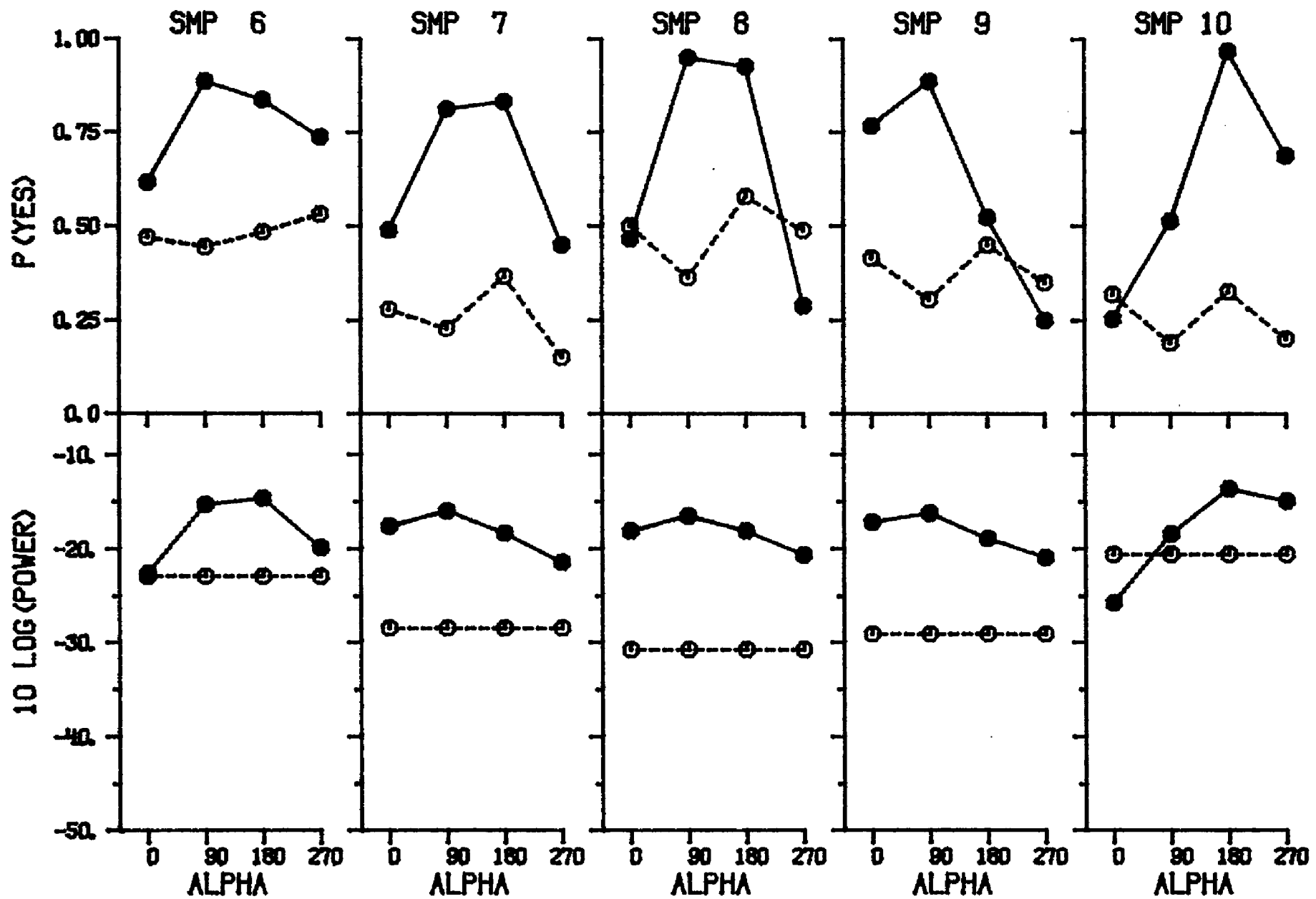
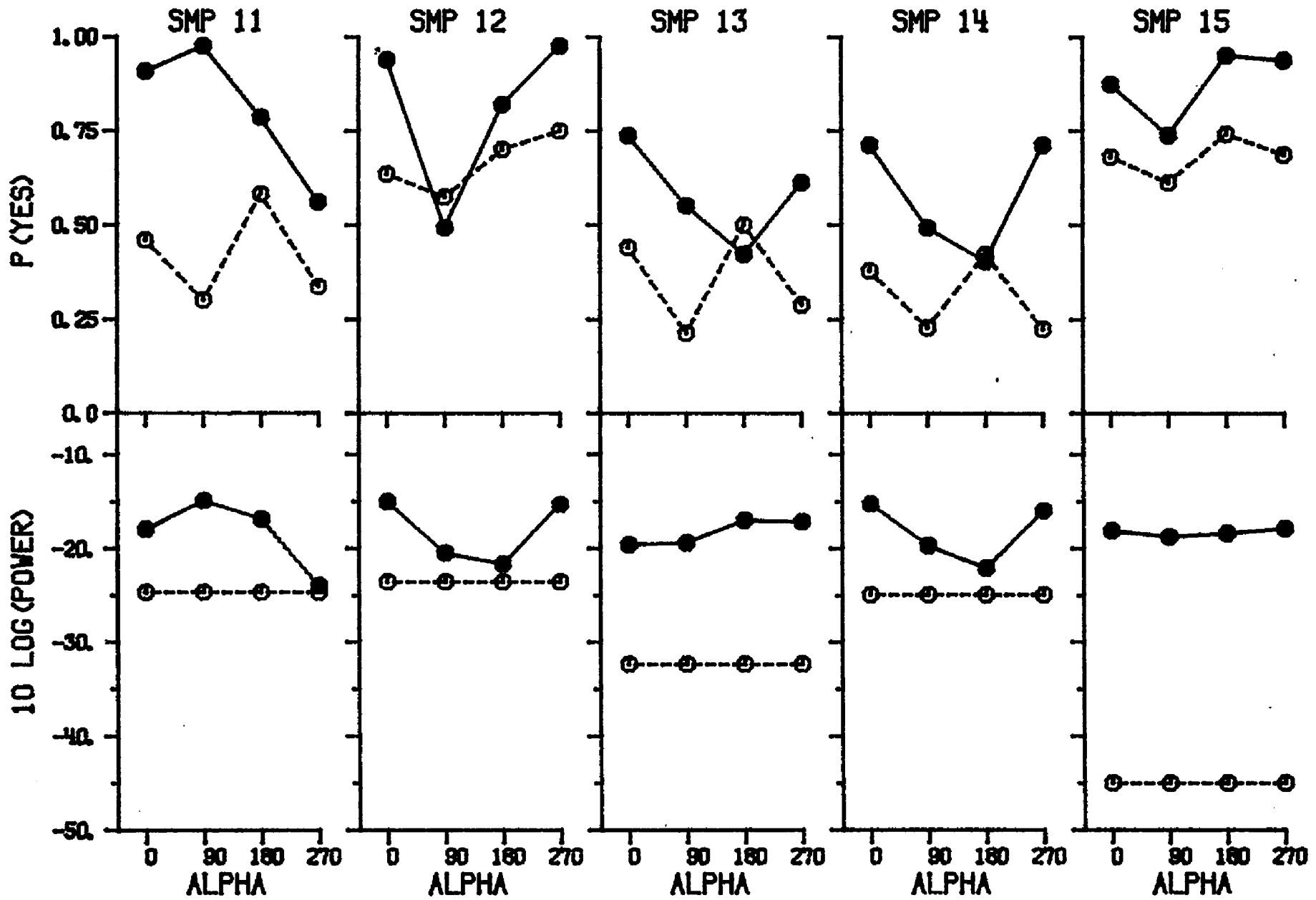
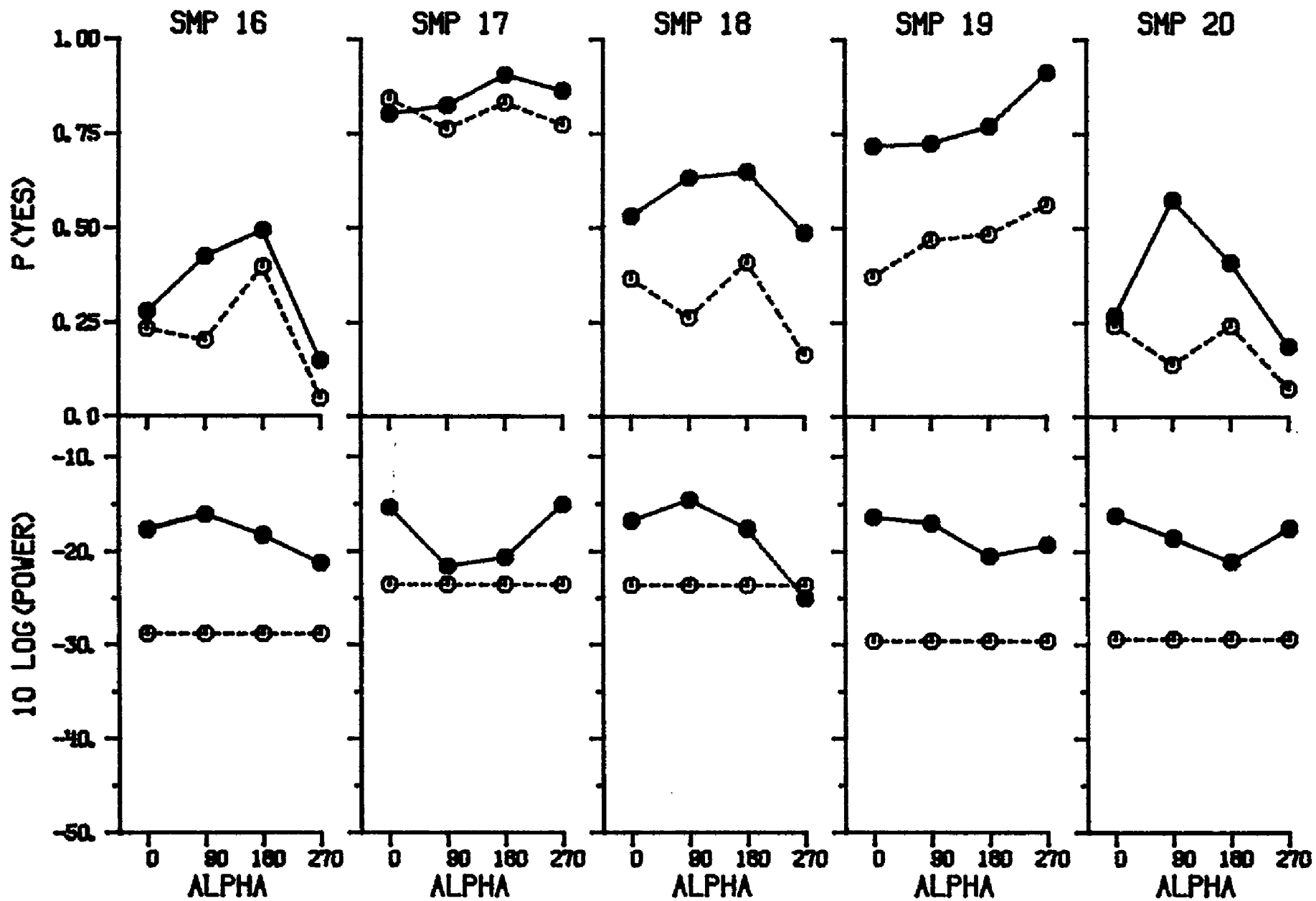


Figure A2.20. Performance and stimulus measures as a function of Alpha. Each panel shows the results for a particular sample. The upper half of each panel shows the obtained proportion of "Yes" responses as a function of Alpha. The lower half of each panel shows the power at the 500-Hz component of the Fourier spectrum of the stimulus. Filled symbols are for signal-plus-noise trials. Open symbols are for noise-alone trials. Performance data are for subject JM, and were collected at $10 \text{ Log}(E/No)$ equal to 8.5 dB. (The figure extends through five pages.)









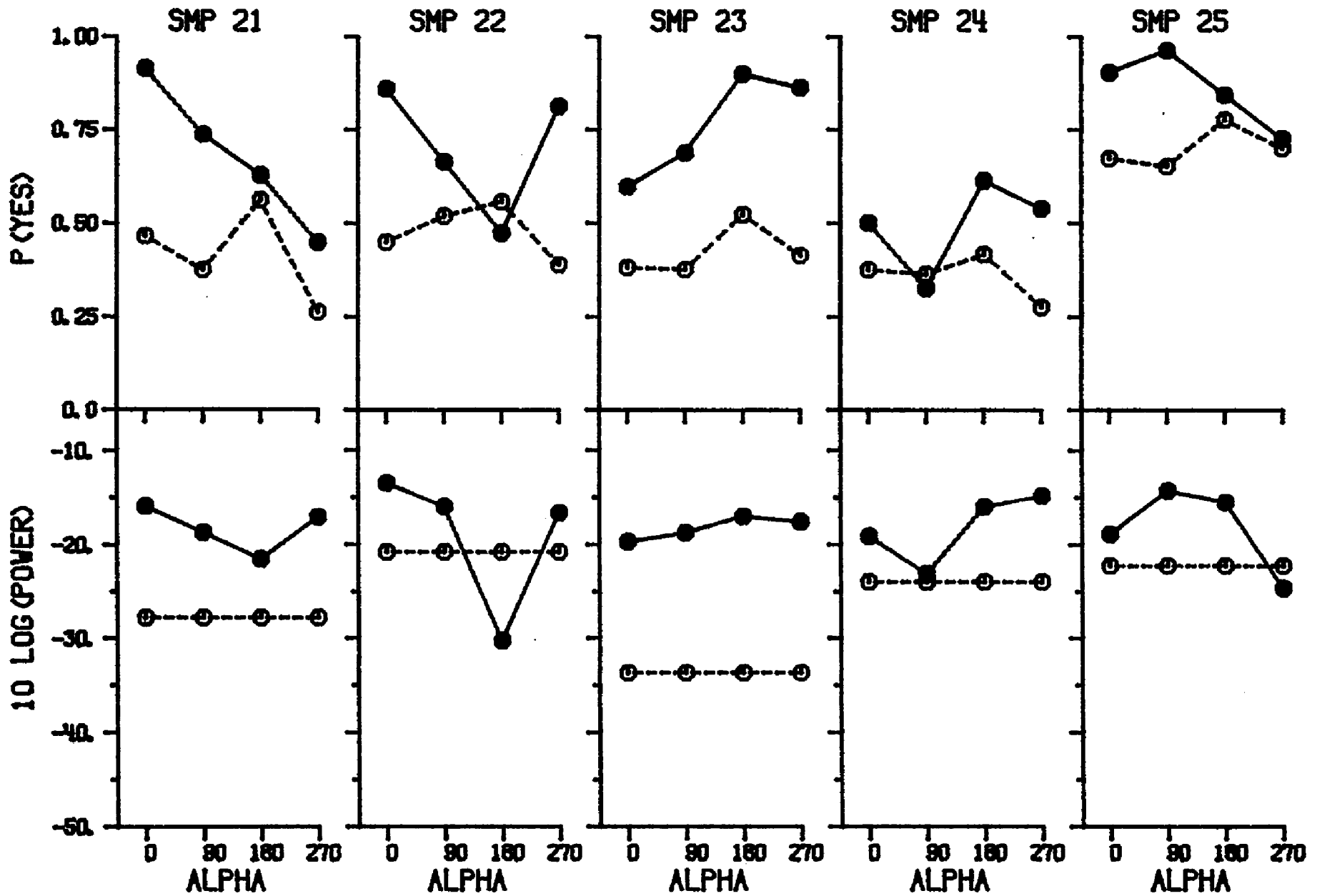
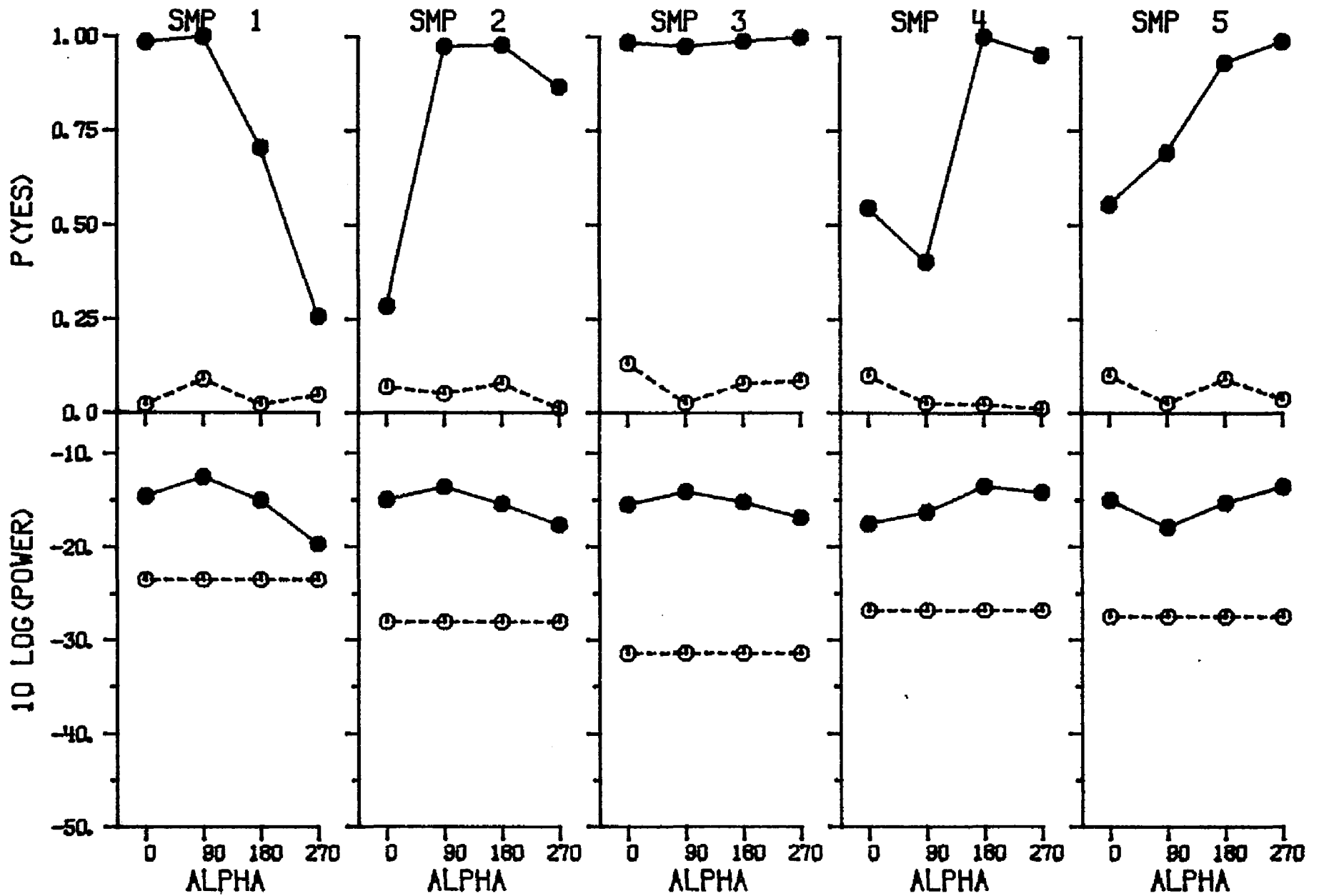
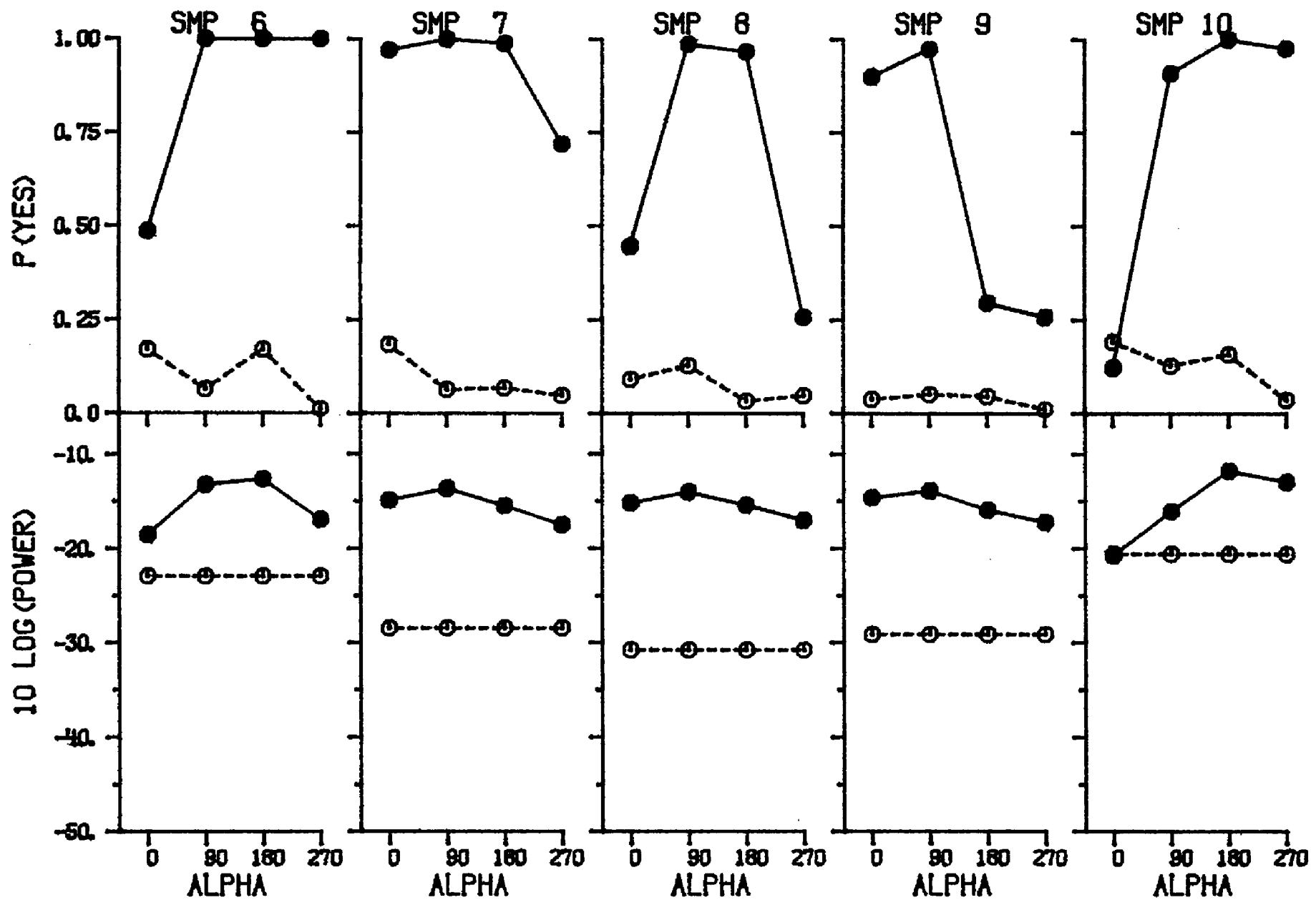
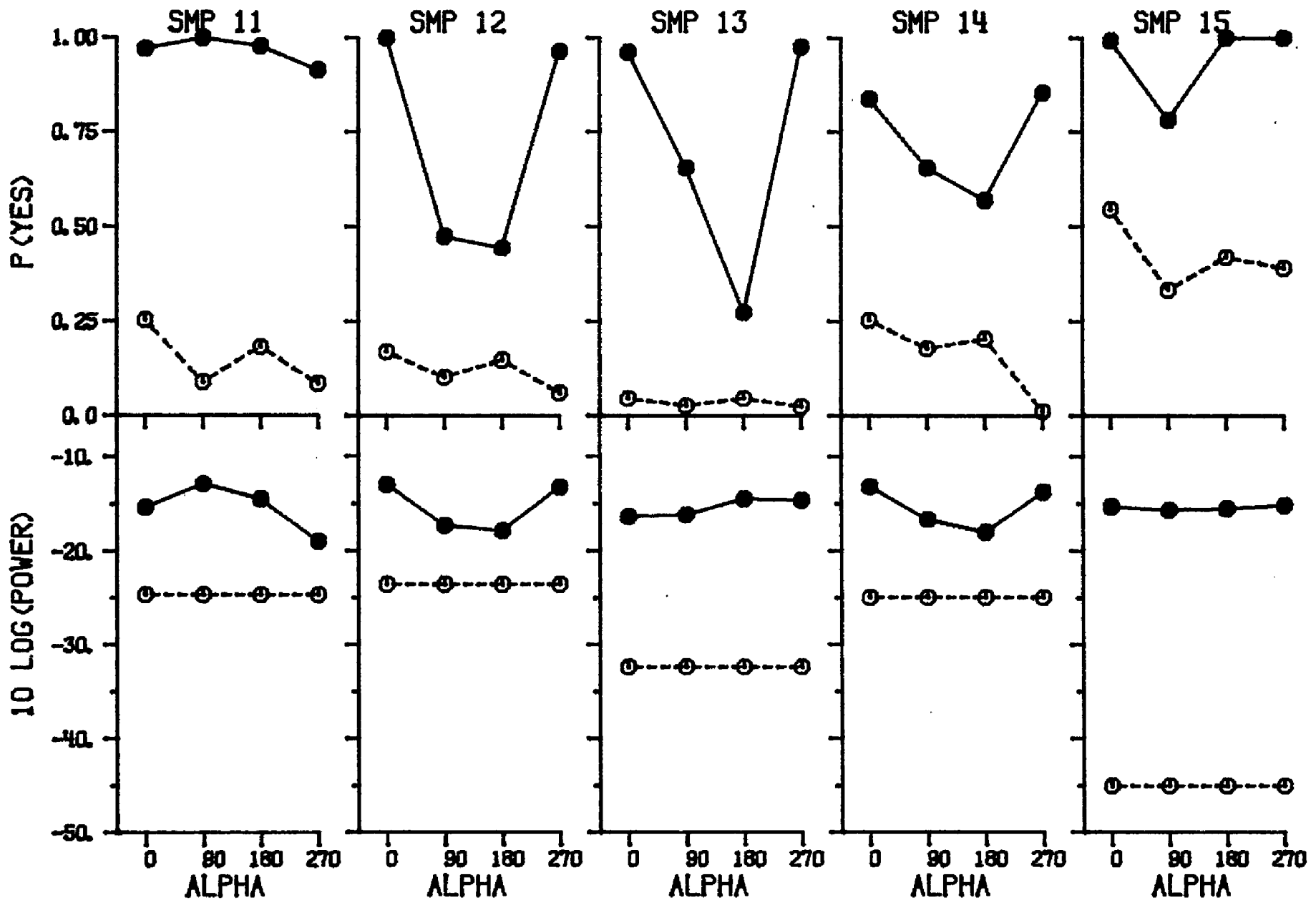
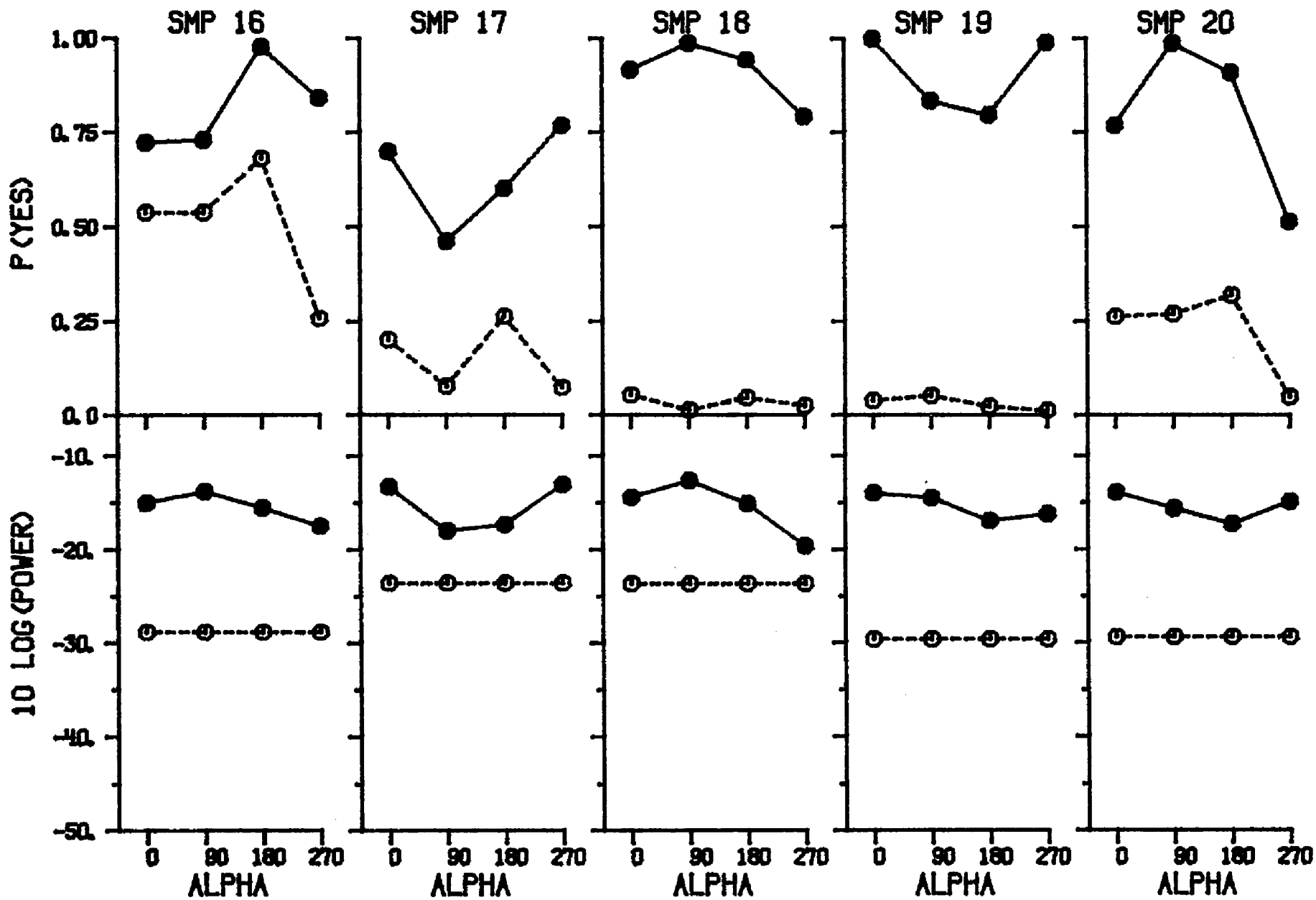


Figure A2.21. Performance and stimulus measures as a function of Alpha. Each panel shows the results for a particular sample. The upper half of each panel shows the obtained proportion of "Yes" responses as a function of Alpha. The lower half of each panel shows the power at the 500-Hz component of the Fourier spectrum of the stimulus. Filled symbols are for signal-plus-noise trials. Open symbols are for noise-alone trials. Performance data are for subject SG, and were collected at $10 \text{ Log}(E/No)$ equal to 11.5 dB. (The figure extends through five pages.)









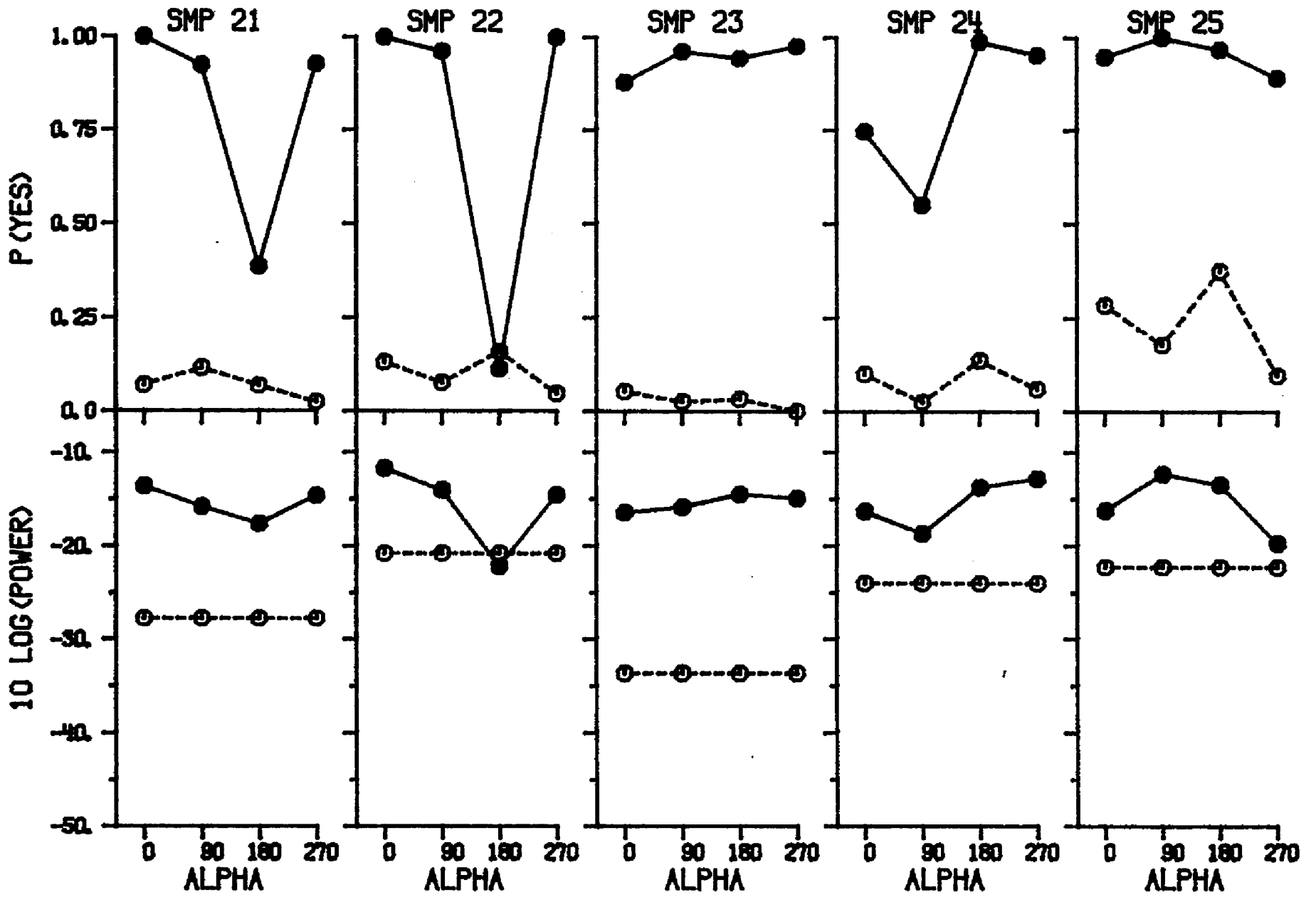
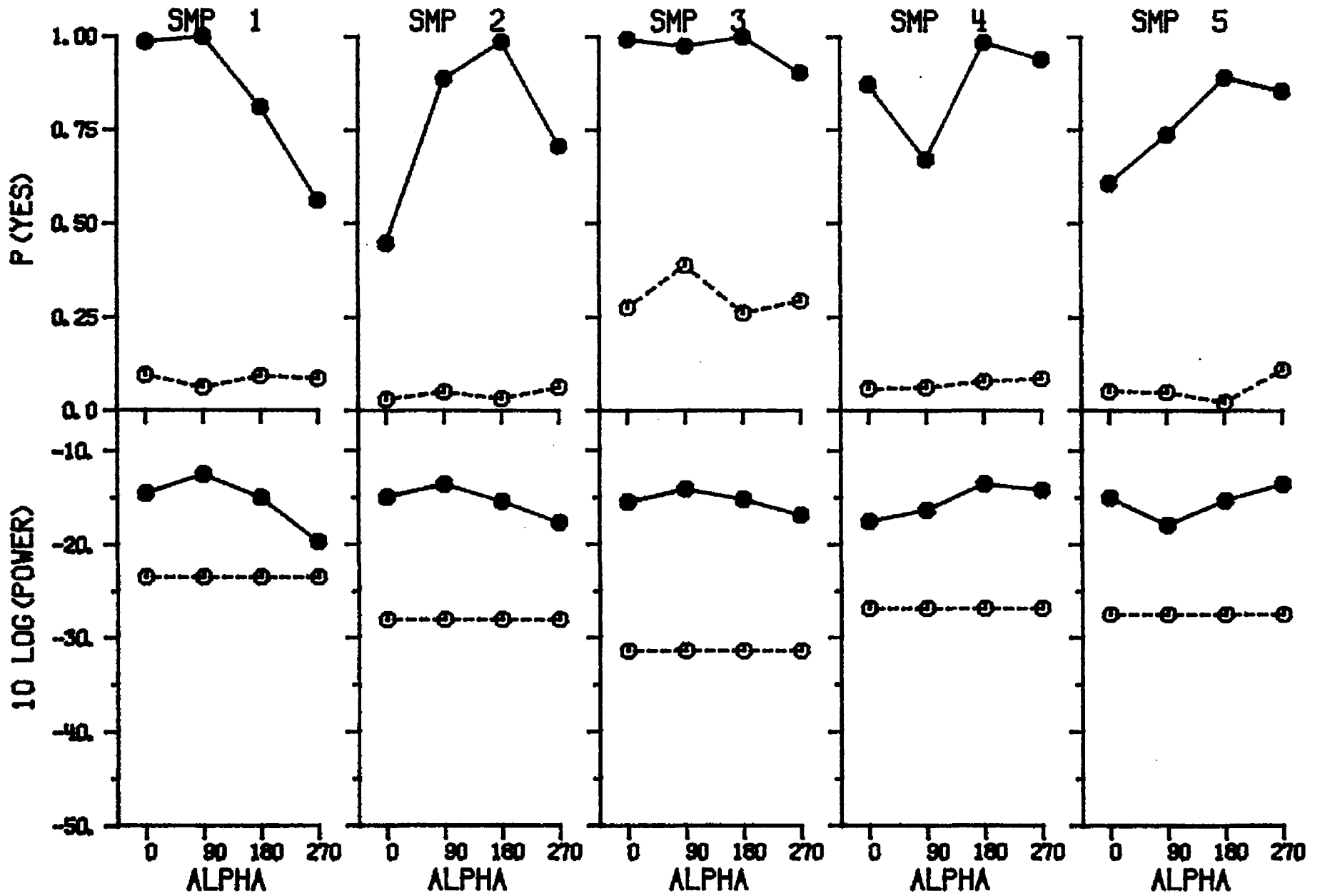
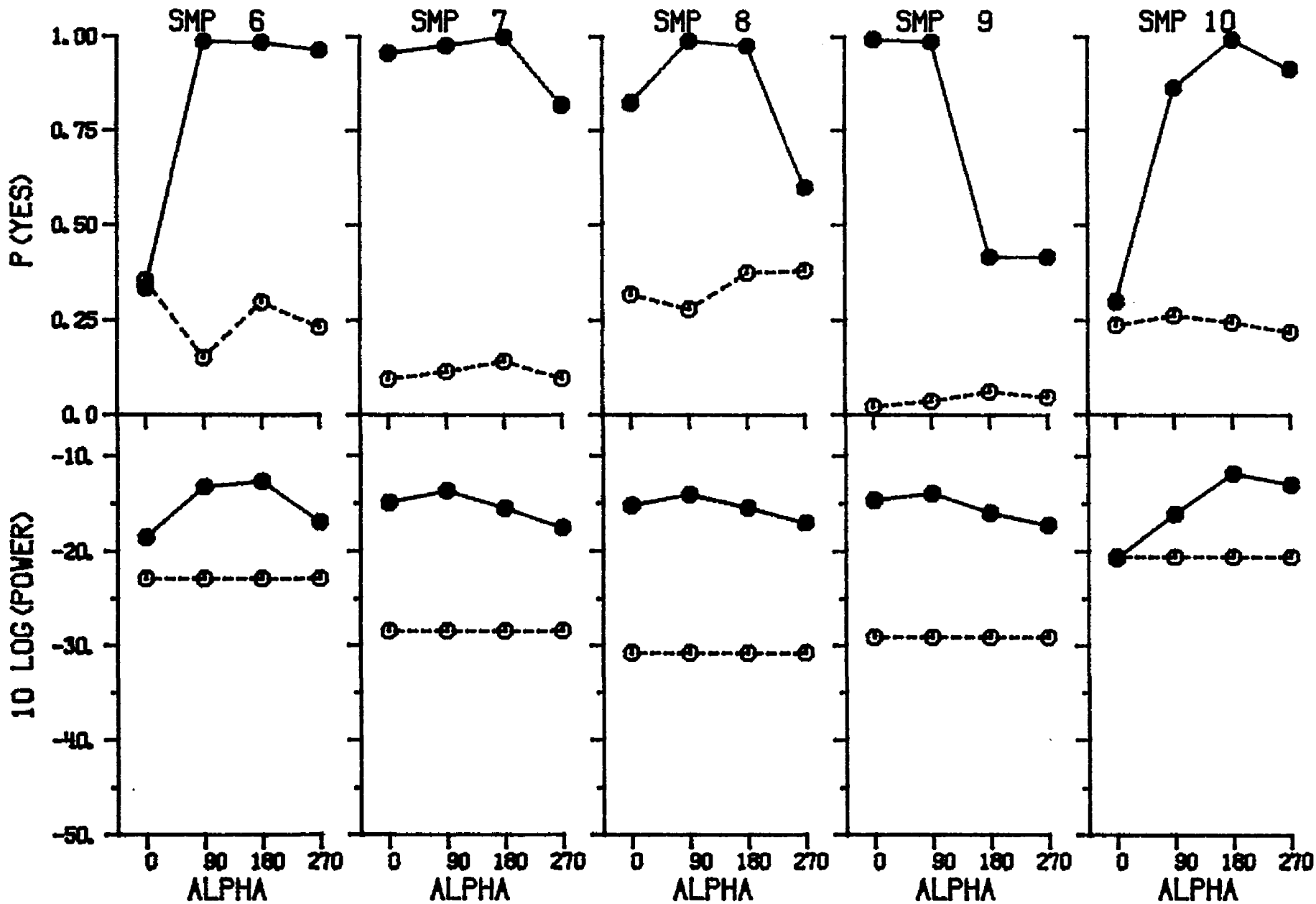
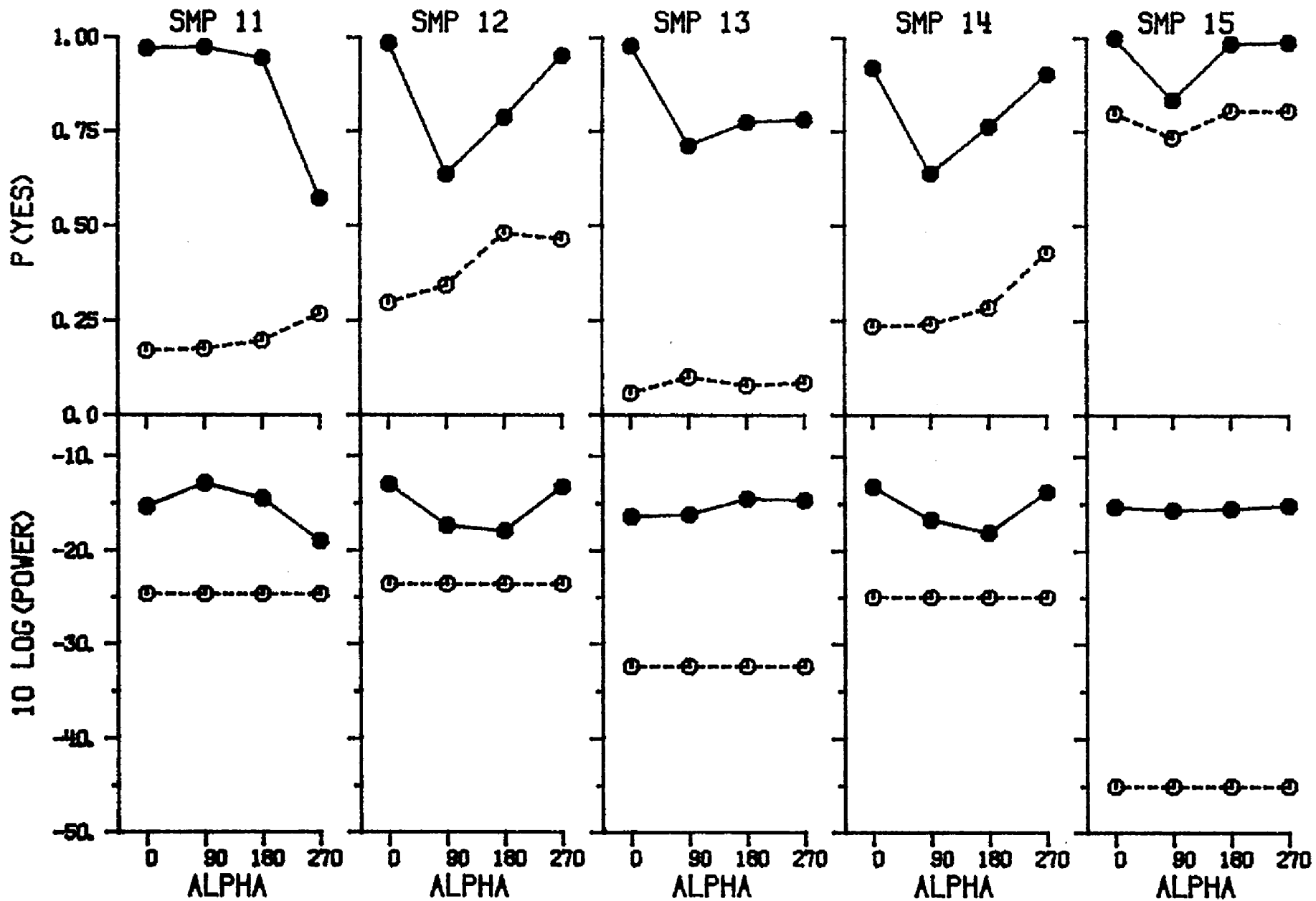
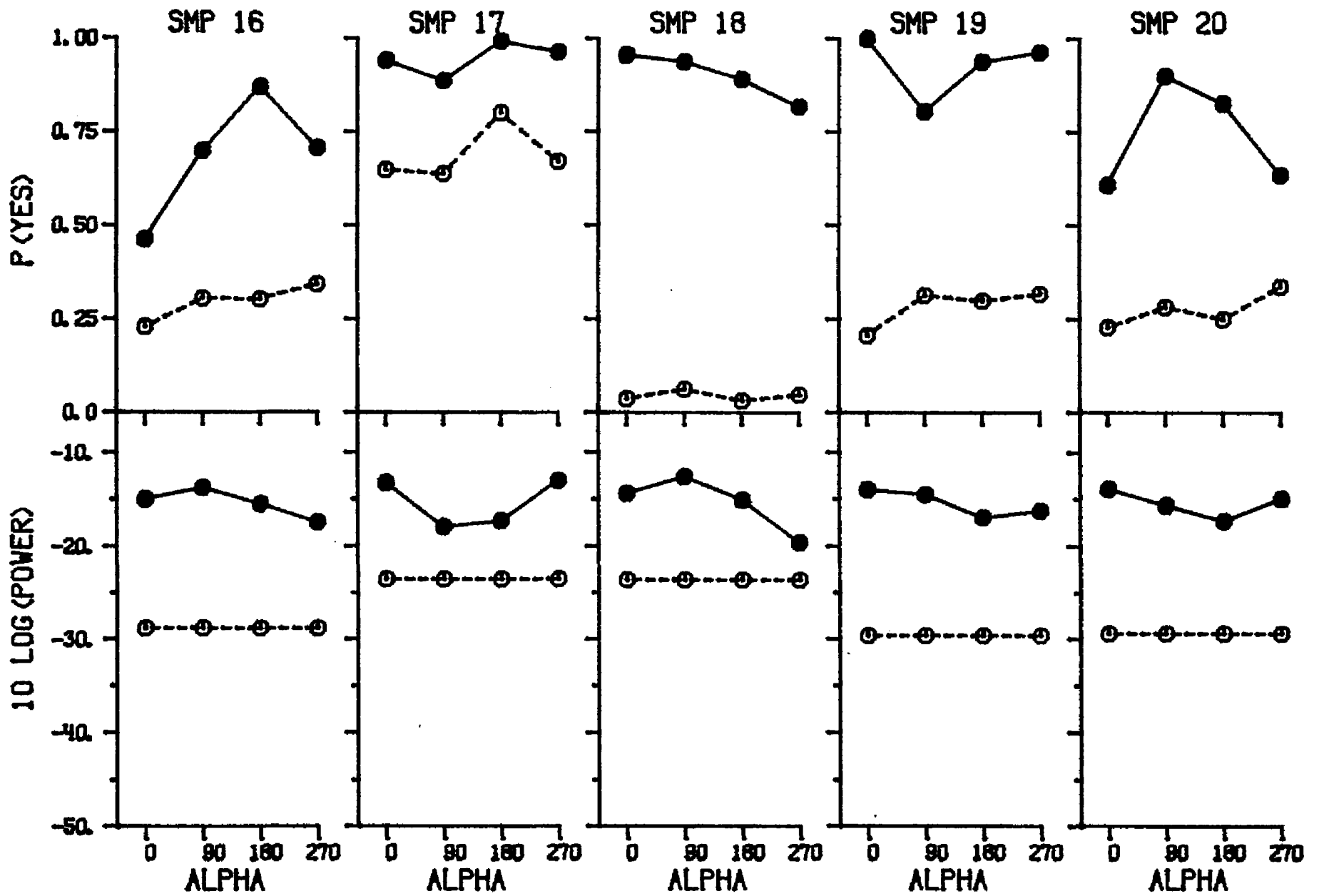


Figure A2.22. Performance and stimulus measures as a function of Alpha. Each panel shows the results for a particular sample. The upper half of each panel shows the obtained proportion of "Yes" responses as a function of Alpha. The lower half of each panel shows the power at the 500-Hz component of the Fourier spectrum of the stimulus. Filled symbols are for signal-plus-noise trials. Open symbols are for noise-alone trials. Performance data are for subject CV, and were collected at $10 \text{ Log}(E/No)$ equal to 11.5 dB. (The figure extends through five pages.)









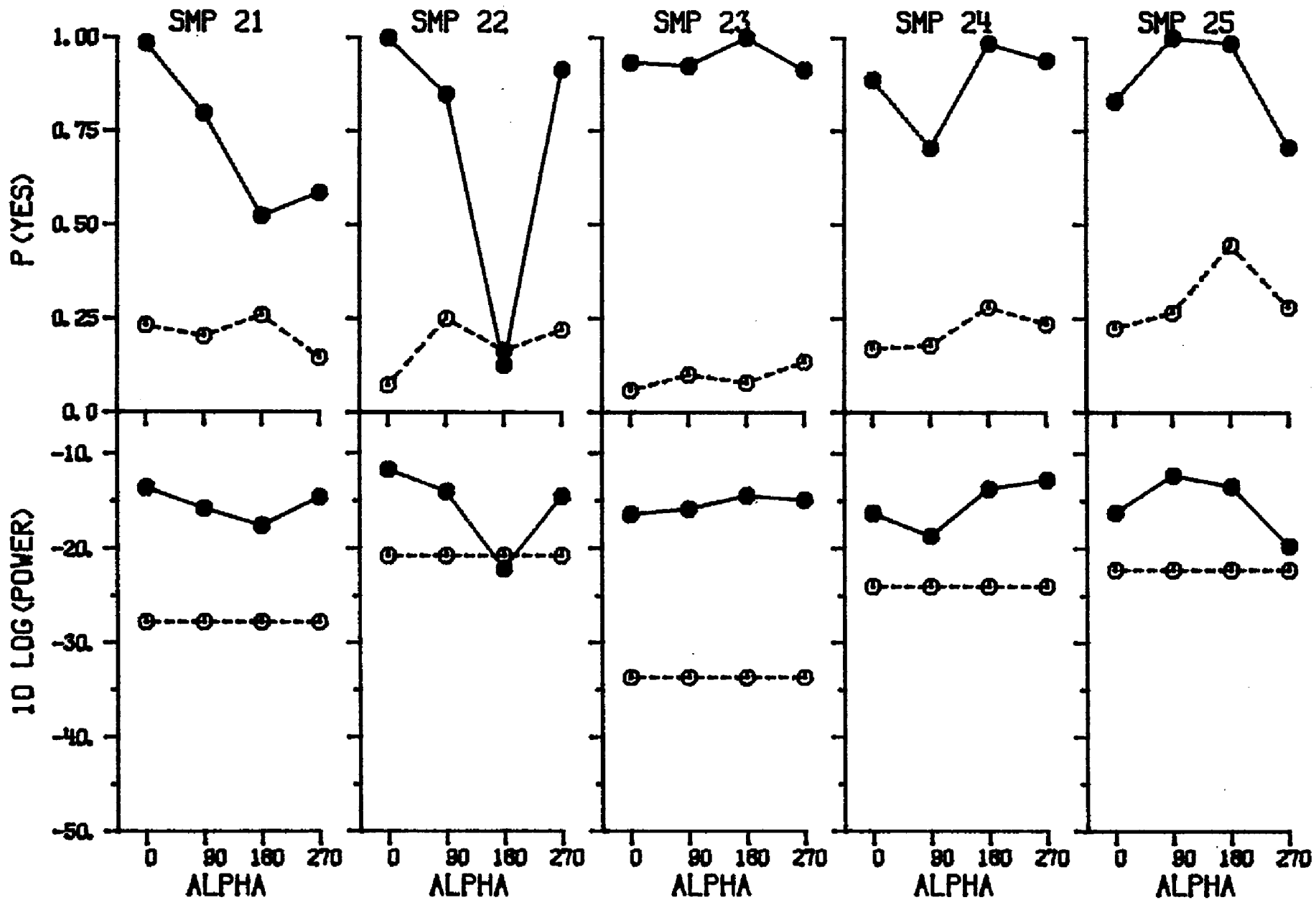
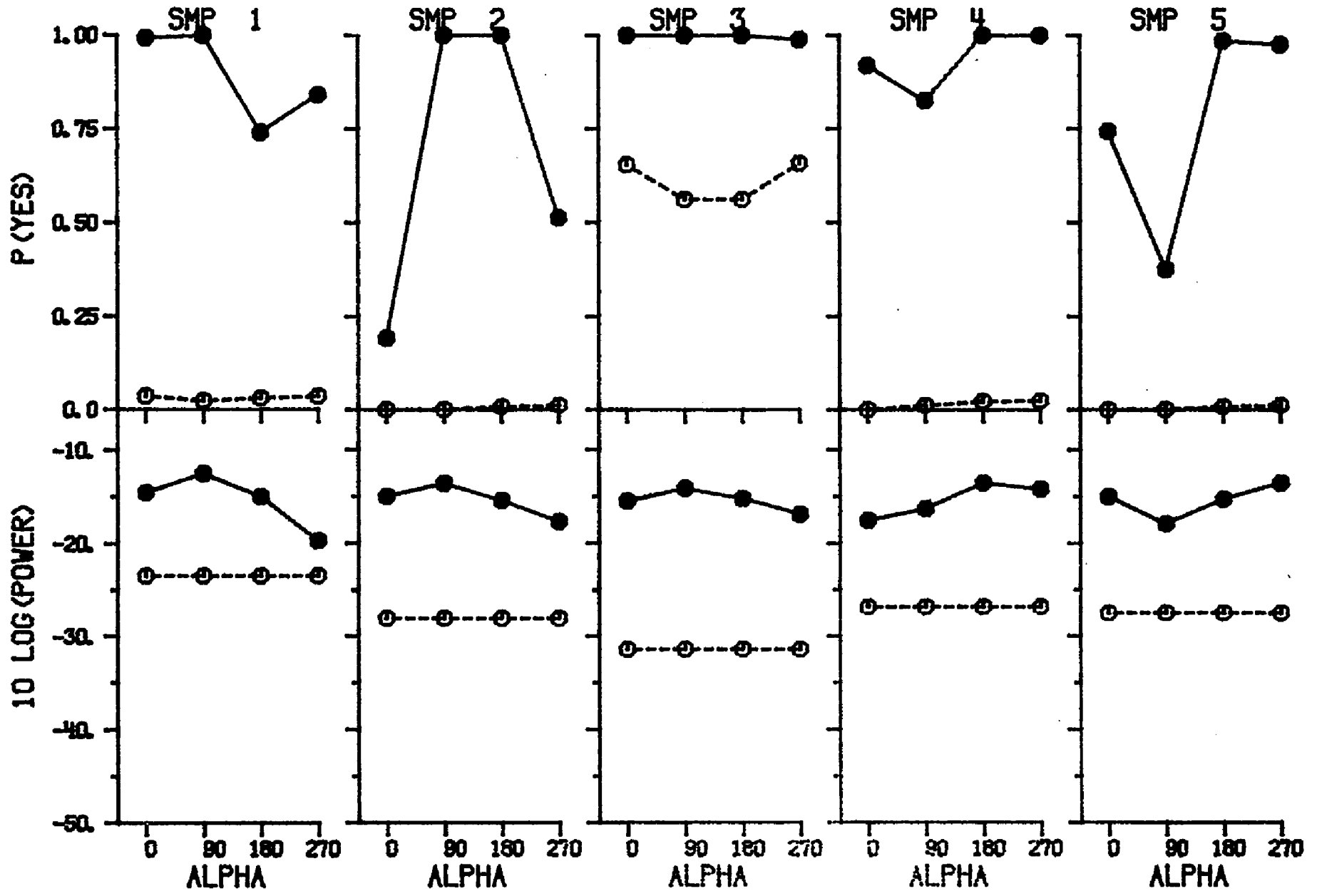
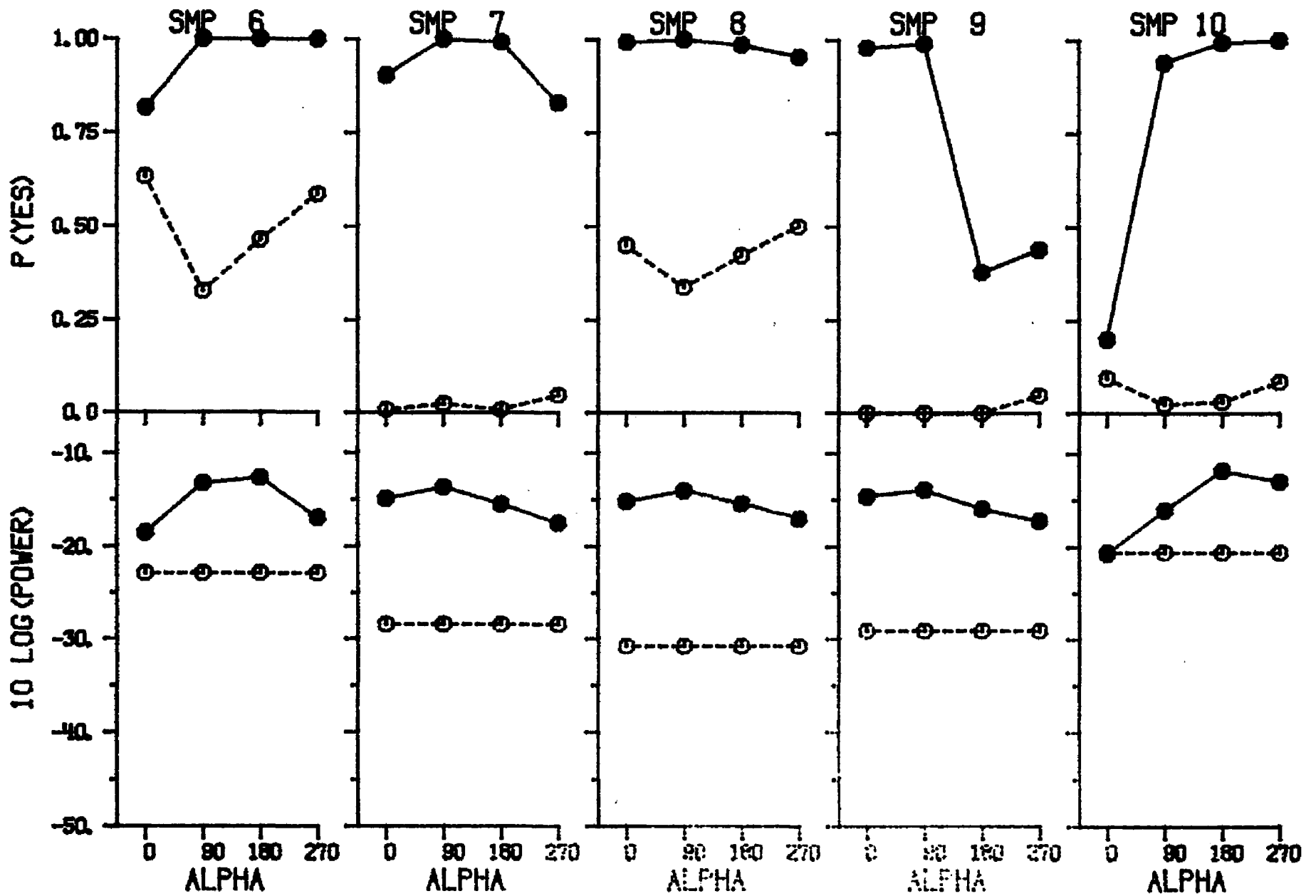
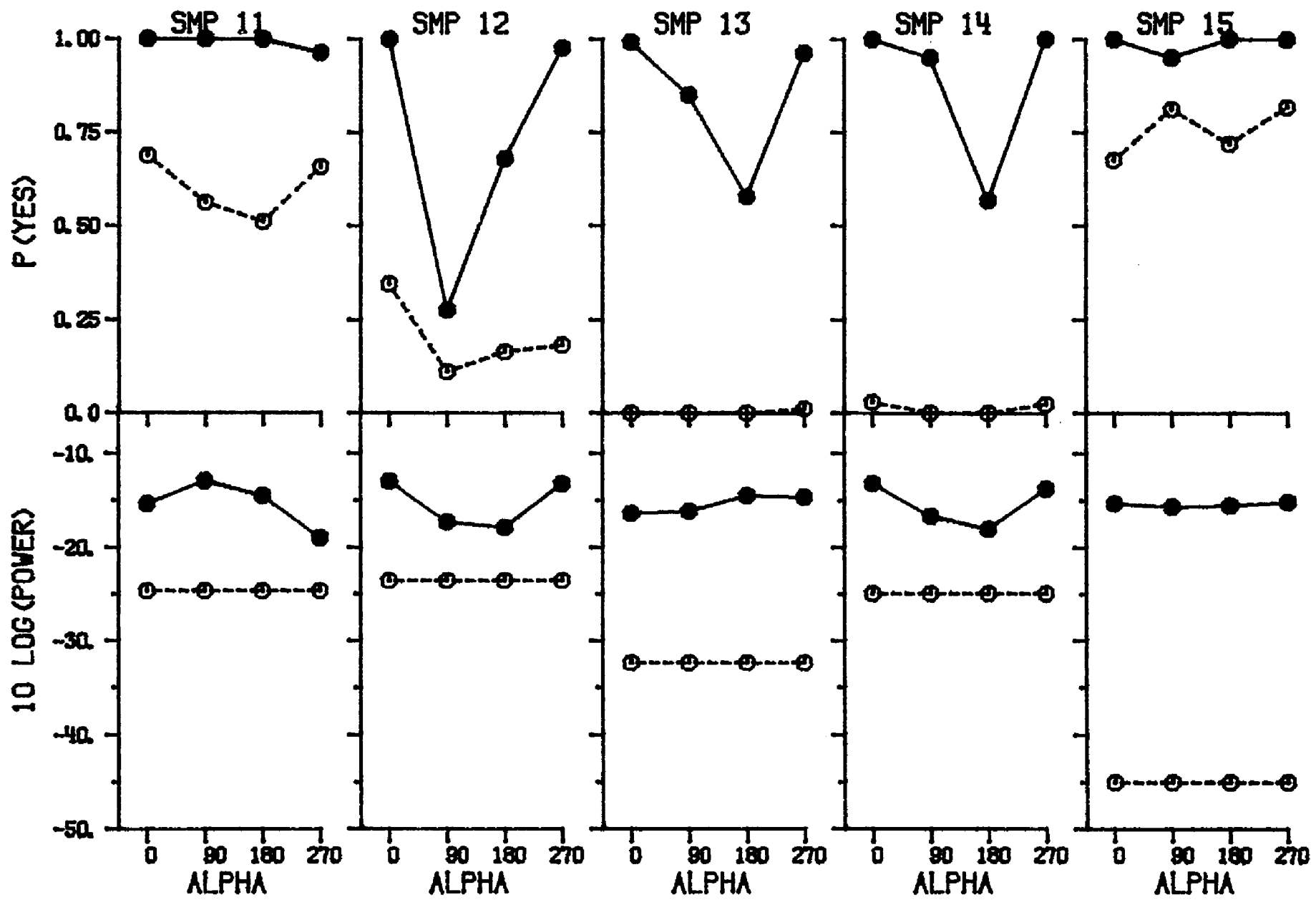
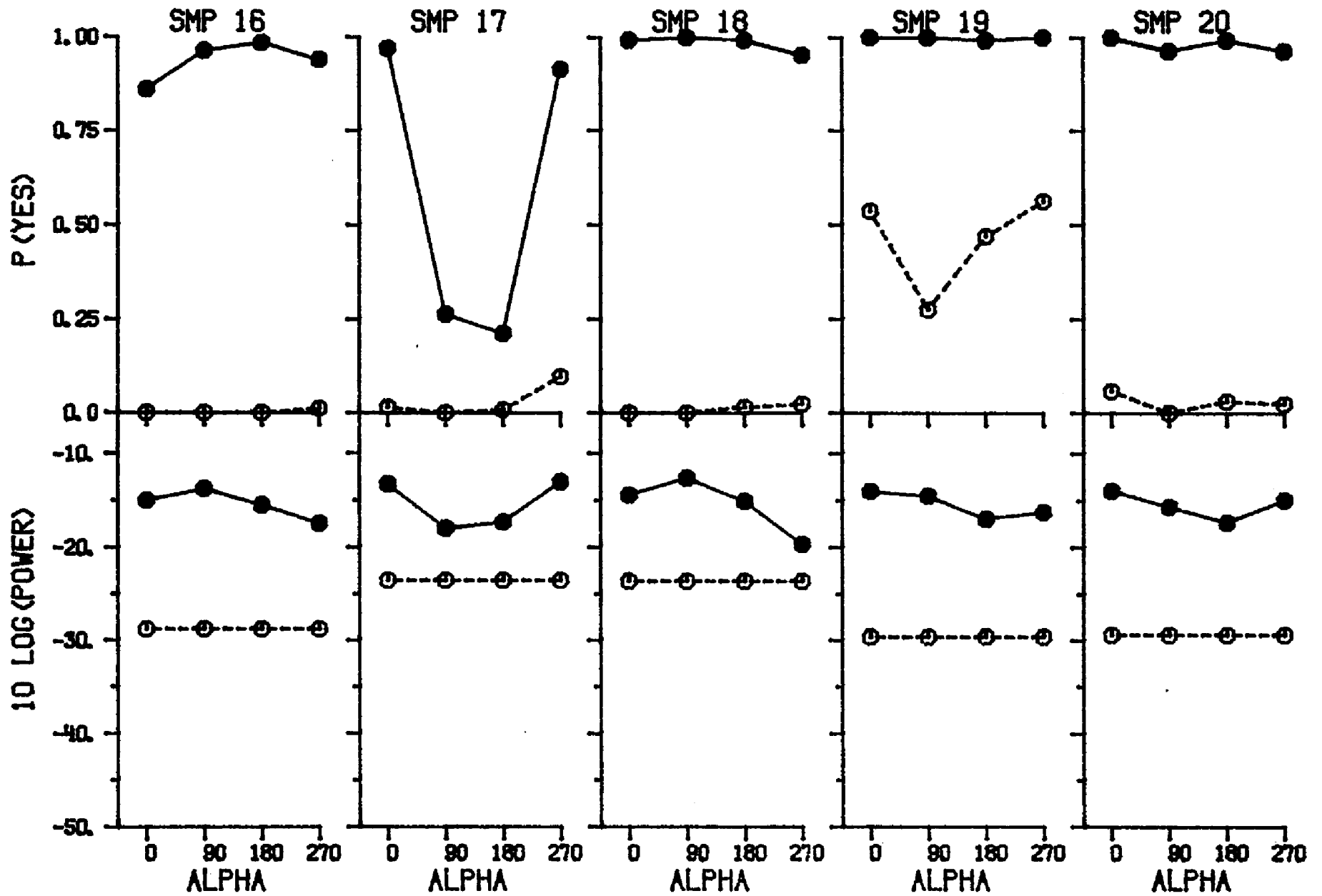


Figure A2.23. Performance and stimulus measures as a function of Alpha. Each panel shows the results for a particular sample. The upper half of each panel shows the obtained proportion of "Yes" responses as a function of Alpha. The lower half of each panel shows the power at the 500-Hz component of the Fourier spectrum of the stimulus. Filled symbols are for signal-plus-noise trials. Open symbols are for noise-alone trials. Performance data are for subject TW, and were collected at $10 \text{ Log}(E/No)$ equal to 11.5 dB. (The figure extends through five pages.)









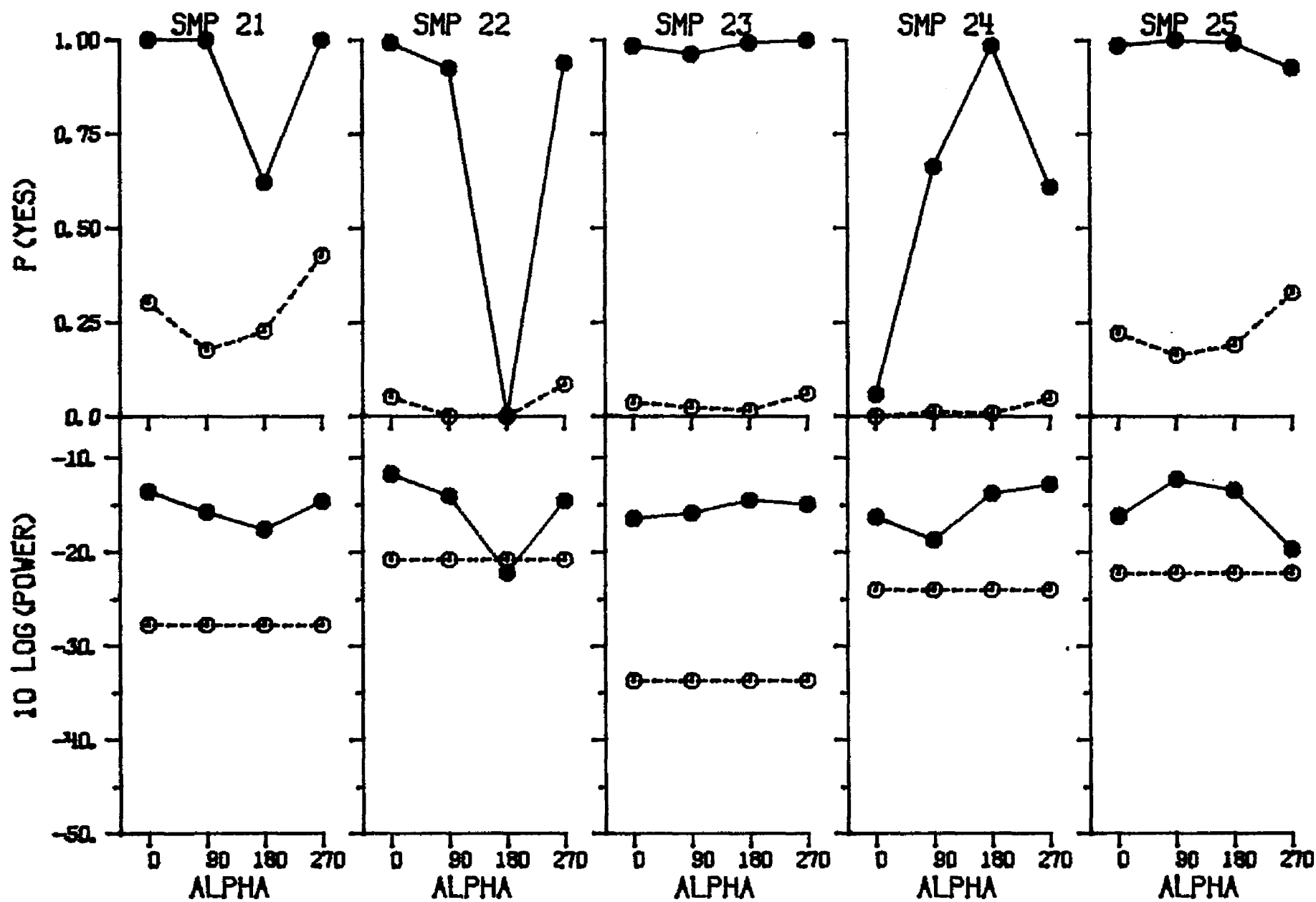
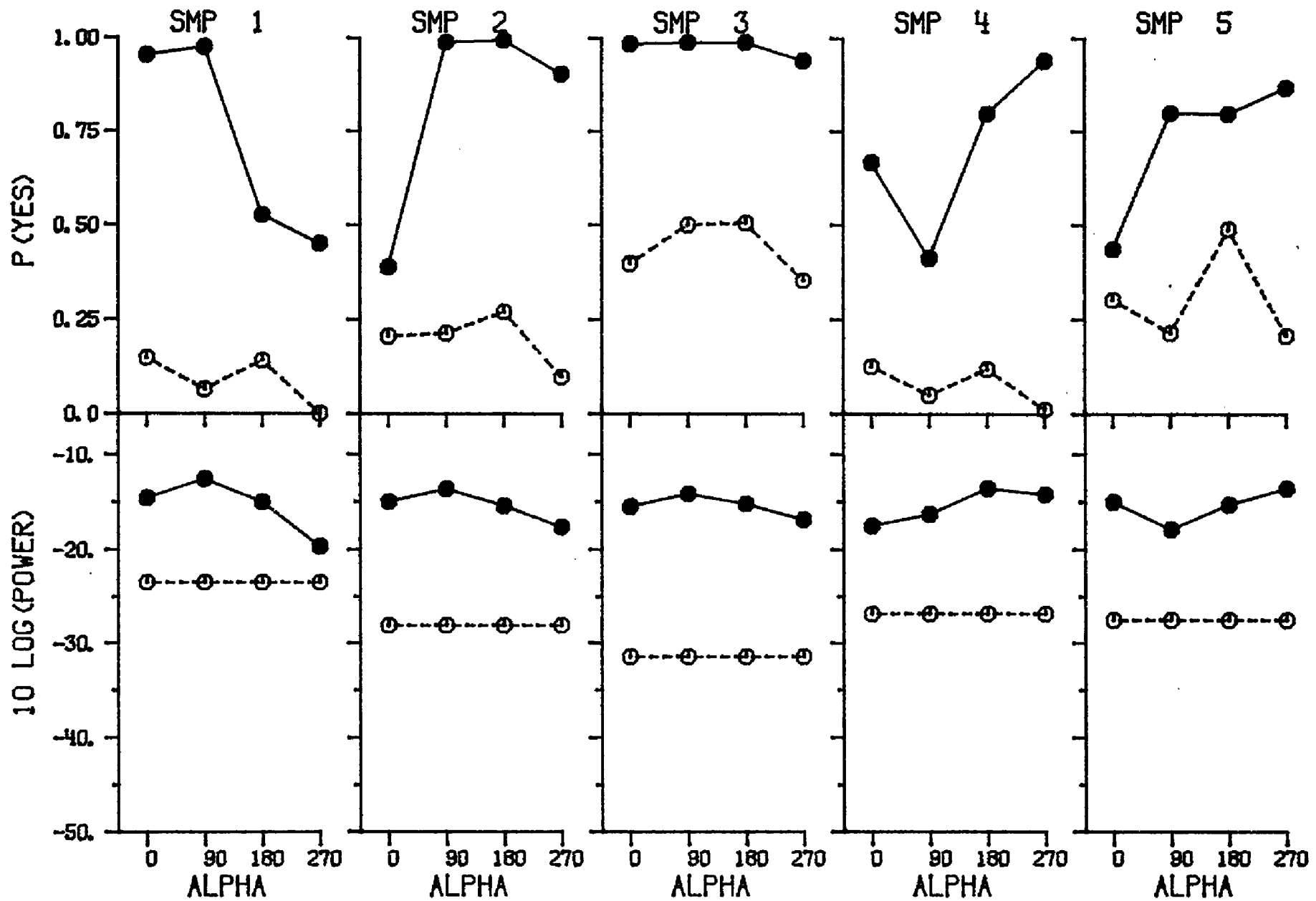
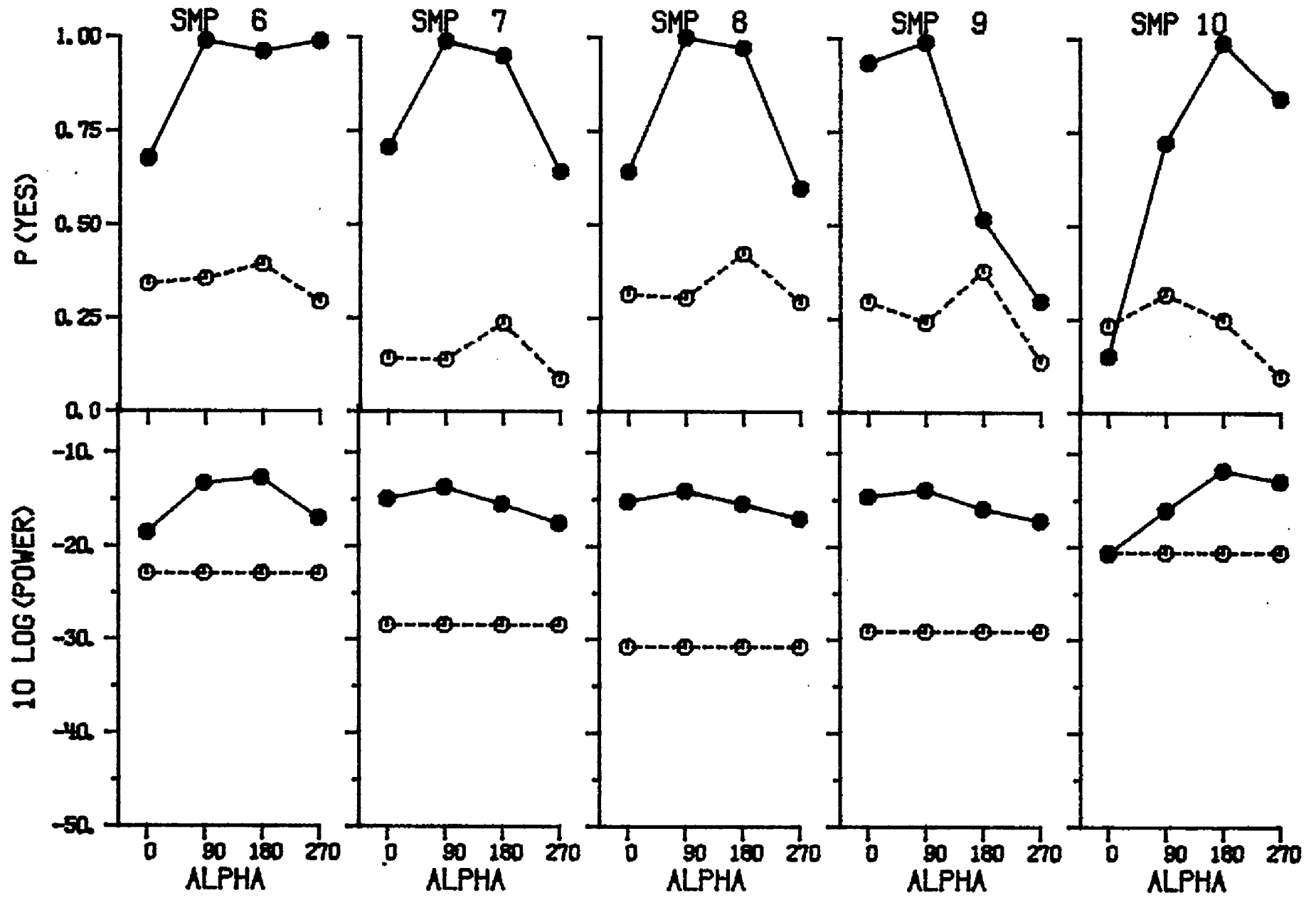
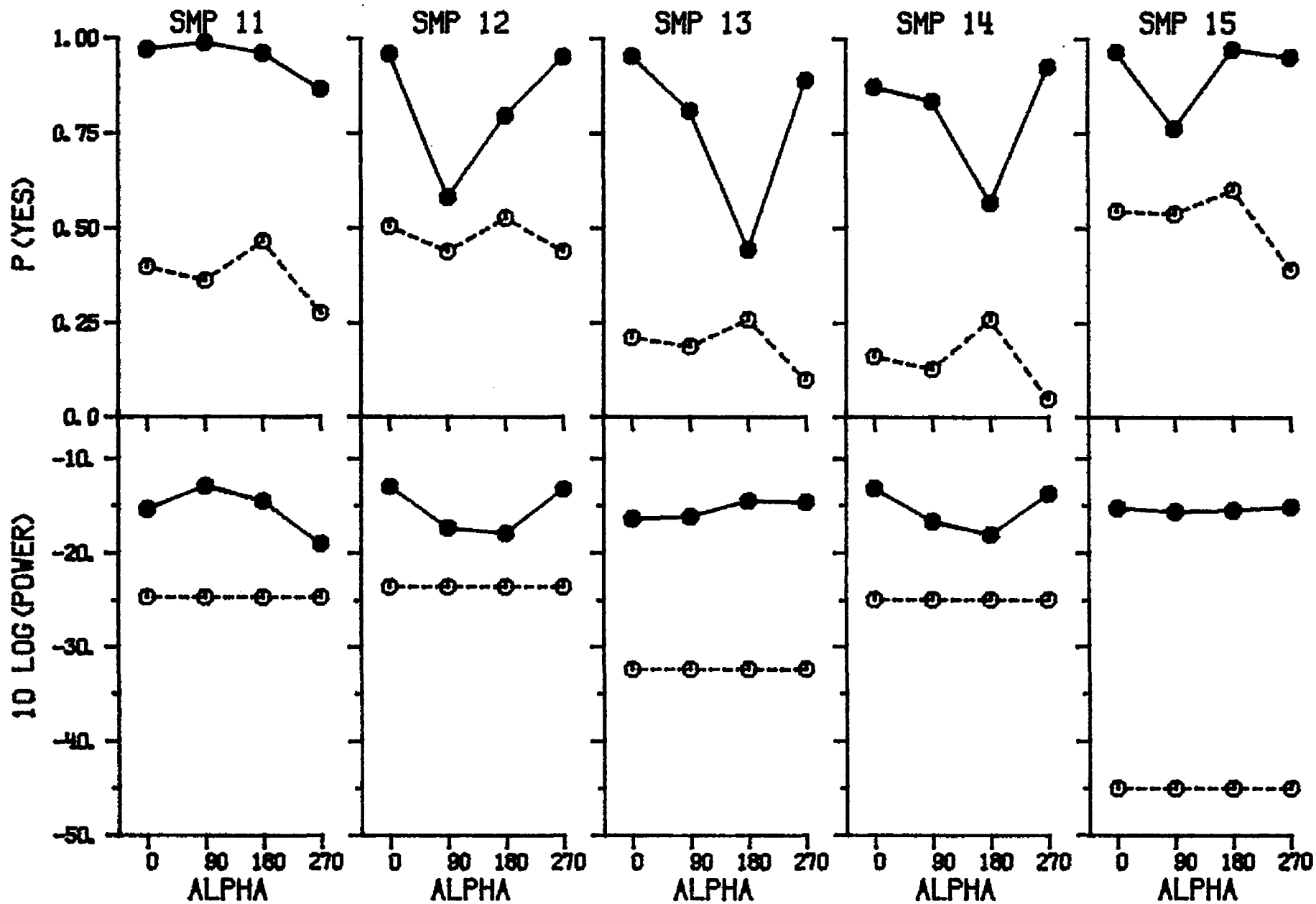
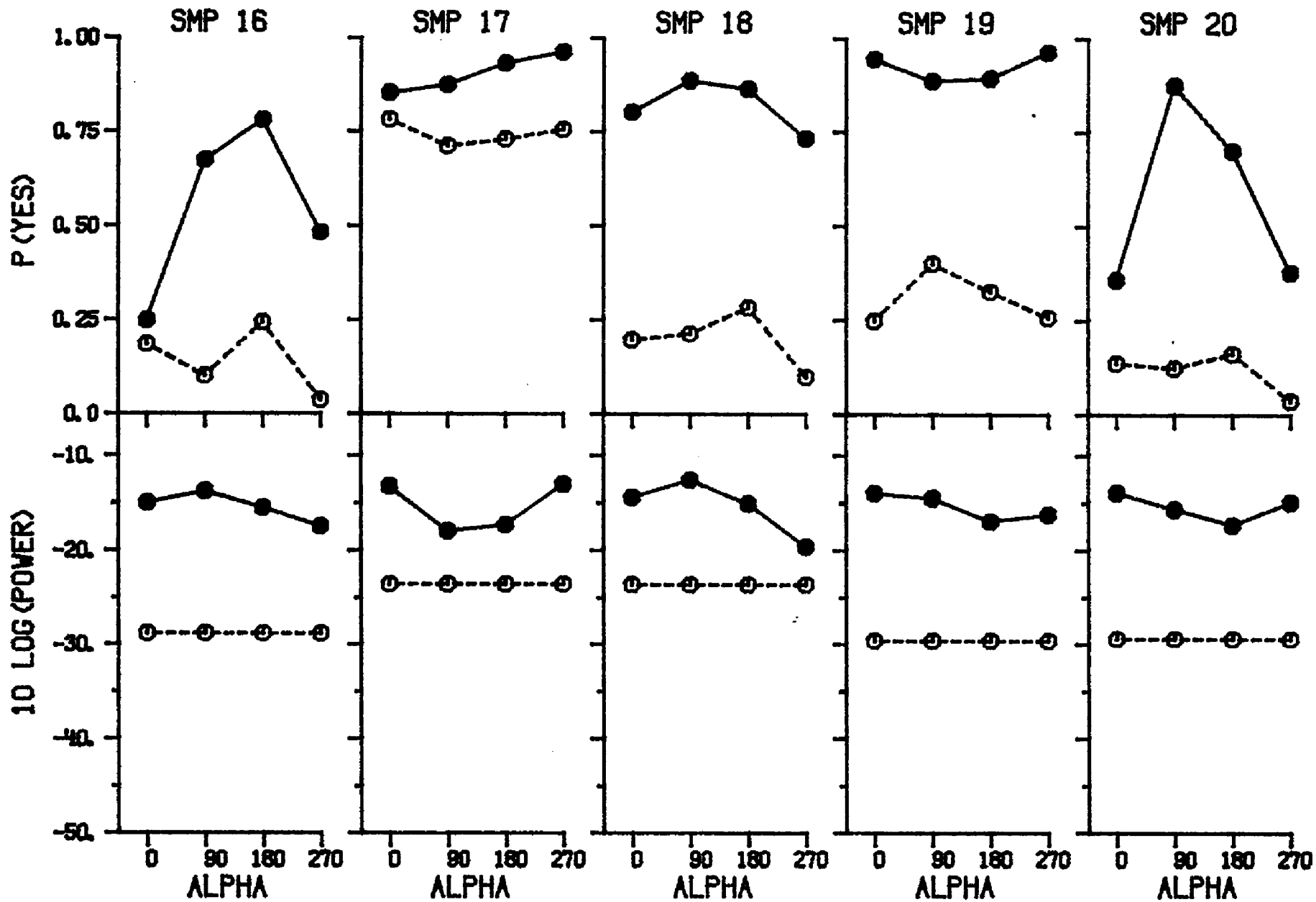


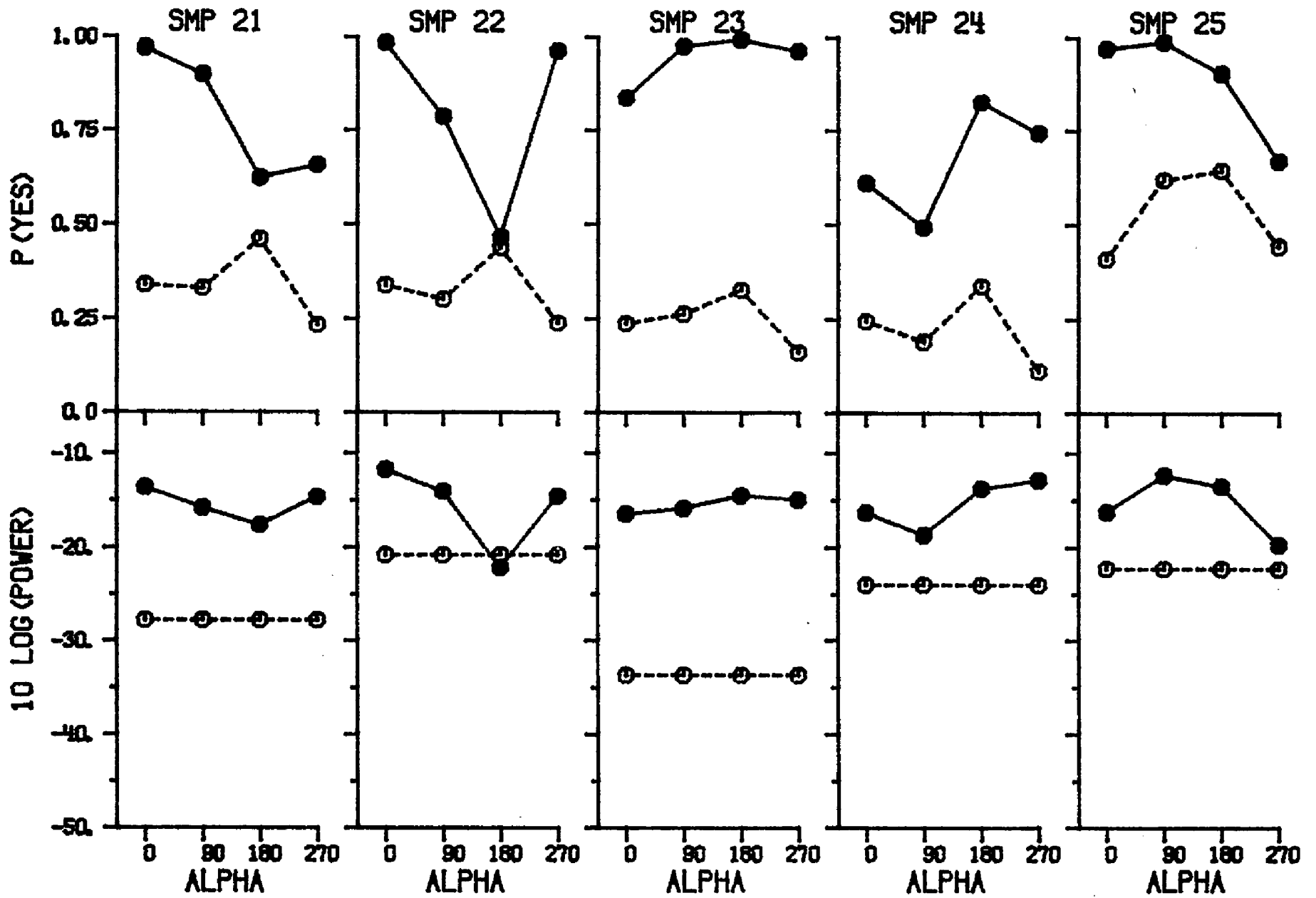
Figure A2.24. Performance and stimulus measures as a function of Alpha. Each panel shows the results for a particular sample. The upper half of each panel shows the obtained proportion of "Yes" responses as a function of Alpha. The lower half of each panel shows the power at the 500-Hz component of the Fourier spectrum of the stimulus. Filled symbols are for signal-plus-noise trials. Open symbols are for noise-alone trials. Performance data are for subject 1, and were collected at $10 \text{ Log}(E/No)$ equal to 11.5 dB. (The figure extends through five pages.)











VITA
Robert H. Gilkey
1981

Address:

Central Institute for the Deaf
818 S. Euclid
St. Louis, MO 63110
Ph: (314) 652-3200, ext. 336

Personal Data:

Born: December 18, 1951
San Mateo, California

Marital status: Single

Education:

De Anza College
Cupertino, California

University of California
Berkeley, California
B.A., Psychology, 1976

Indiana University
Bloomington, Indiana
Ph.D., Psychology, December 1981
Specialization: Sensory Psychology (Psychoacoustics)
Additional areas of Concentrated Study:
Physiological Psychology
Neurosciences
Speech and Hearing

Publications and Conference Papers:

Hafter, E. R., Gilkey, R. H., and Dye, R. H. (1976).
"Lateralization of signals without onsets," J. Acoust.
Soc. Am. 59, s22 (A).

Frank, A. S., Gilkey, R. H., and Robinson, D. E. (1978).
"Detection in diotic and dichotic conditions using
repeatable samples of noise." J. Acoust. Soc. Am. 64, s36
(A).

Gilkey, R. H., Frank, A. S., and Robinson, D. E. (1978).
"Estimates of internal noise," J. Acoust. Soc. Am. 64, s36
(A).

Haftner, E. R., Dye, R. H., Jr., and Gilkey, R. H. (1979).
"Lateralization of tonal signals which have neither onsets
nor offsets," J. Acoust. Soc. Am. 65, 471-477.

Gilkey, R. H., Hanna, T. E., and Robinson, D. E. (1980).
"Effects of signal phase on the detection of tonal signals
in the presence of repeatable noise maskers,"
J. Acoust. Soc. Am. 68, s59 (A).

Gilkey, R. H., Hanna, T. E., and Robinson, D. E. (1981).
"Estimates of the ratio of external to internal noise
obtained using repeatable samples of noise," In press (A).

Gilkey, R. H., and Frank, A. S. "A software pseudo-random
noise generator." Technical note, in preparation.

Gilkey, R. H., Hanna, T. E., and Robinson, D. E. "Estimates
of internal noise obtained under various diotic and dichotic
conditions." In preparation.

Gilkey, R. H., Hanna, T. E., and Robinson, D. E. "Detection
of tonal signals in the presence of repeatable noise
maskers." In preparation.